THE CHEMISTRY OF CH_4 ON Ni(111)

by

Qing-Yun Yang

B.S. Jilin University
(1982)

M.A. Columbia University
(1983)

SUBMITTED TO THE DEPARTMENT OF CHEMISTRY
IN PARTIAL FULFILLMENT OF THE REQUIREMENTS
FOR THE DEGREE OF
DOCTOR OF PHILOSOPHY

at the

MASSACHUSETTS INSTITUTE OF TECHNOLOGY

September 1989

Signature of Author_____
Department of Chemistry
September 8, 1989

Certified by_____
Sylvia T. Ceyer
Thesis Supervisor

Accepted by_____
Glenn A. Berchtold
Chairman, Department Committee

This thesis has been examined by a committee of the Department of Chemistry as follows:

Professor Sylvia T. Ceyer___ _____
Thesis Supervisor

Professor Robert W. Field___ _____
Chairman

Professor Robert J. Silbey___ _____

THE CHEMISTRY OF CH_4 ON Ni(111)

by

Qing-Yun Yang

Submitted to the Department of Chemistry
on September 8, 1989 in partial fulfillment of the
requirements for the Degree of Doctor of Philosophy in
Chemistry

ABSTRACT

The reactions of CH_4 on Ni(111) surface are studied using a surface vibrational spectroscopic technique, high resolution electron energy loss spectroscopy (HREELS). Molecular beam techniques are used to activate the dissociative chemisorption of CH_4, which normally occurs only under high pressure conditions (> 1 torr), in a UHV environment through direct translational activation and collisional activation. Coupled with vibrational spectra measured after activation of CD_4 and CH_3D, the products of the dissociative event is clearly identified as an adsorbed CH_3 group and an adsorbed H atom. The CH_3 species is determined to be adsorbed on a threefold site with C_{3v} symmetry. The "soft" symmetric C-H stretch mode and the overtone of the asymmetric deformation mode are observed to be in Fermi resonance. This study represents the first spectroscopic identification of an adsorbed CH_3 species.

The chemistry of the adsorbed CH_3 radical is studied by monitoring its vibrational spectrum as a function of surface temperature. At temperatures as low as 150 K, the adsorbed CH_3 decomposed to form an adsorbed CH species and more atomic hydrogen. Unambiguous identification of the CH species comes from the observation that the vibrational spectrum from the thermal decomposition of CH_2D is a superposition of those from the decomposition of CH_3 and CD_3. From the number and frequency of the vibrational modes, the CH species is determined to be adsorbed with a pyramidal geometry in a threefold site of C_{3v} symmetry. The relative stability of the C_1 species on Ni(111) is determined to be $CH_2 < CH_3 < CH$. At 250 K, carbon-carbon coupling occurs between the adsorbed species to form adsorbed C_2H_2. High coverages (0.25 ML) of C_2H_2 trimerize to form adsorbed molecular benzene. The synthesis of C_6H_6 from CH_4 is described in detail. The chemistry of CH_4 on Ni(111) is summarized as follows:

$$CH_4 \rightarrow CH_{3(a)} + H_{(a)} \rightarrow CH_{(a)} + 3H_{(a)} \rightarrow 1/2C_2H_{2(a)} + 3H_{(a)} \rightarrow 1/6C_6H_6 + 3H_{(a)}$$

The structure and adsorption site of benzene, one of the products of the reaction of CH_4 on Ni(111) is studied in detail by HREELS. At saturation coverage (1/7 ML), benzene forms a $(\sqrt{7} \times \sqrt{7})R19^o$ ordered phase below 300 K that has not been observed previously. The C_6H_6 molecule is determined to be adsorbed on the atop site with the ring parallel to the surface and with the C-H bonds pointing towards the bridge sites. The benzene in the ordered phase is determined to have $C_{3v}(\sigma_d)$ symmetry which differs only slightly from that of C_{6v} symmetry. This indicates that the C_6H_6 molecule experiences little Kekulé distortion and little interaction with the substrate beyond the first layer. At lower coverages, there are two C_6H_6 adsorption sites. The relative population of the two sites is a function of the surface temperature. The

symmetry point group for the lower binding energy site, either the atop or the threefold hollow site, is $C_{3v}(\sigma_v)$. The symmetry point group for the site with the higher binding energy is $C_s(\sigma_d)$. This adsorption site is undetermined. The C_6H_6 on both sites of the disordered phase are azimuthally rotated by 30° relative to the C_6H_6 in the ordered phase.

The structure and adsorption site of another product of CH_4 dissociative chemisorption on Ni(111), hydrogen is studied in detail. The vibrational spectra at a coverage of one half monolayer, $\theta(n_H/n_{Ni}) = 0.5$, indicate that two different hydrogen atoms exist on the surface, consistent with the previously proposed (2x2)2H structure. The two hydrogen atoms are adsorbed on both the fcc and the hcp threefold hollow sites. Four fundamentals are observed at 745, 790, 1080 and 1105 cm^{-1} along with three overtones at 1260, 1400 and 2180 cm^{-1}. The two lower frequency fundamentals are assigned as the modes polarized parallel to the surface and the two higher frequency fundamentals are assigned as the modes perpendicular to the surface based on the observed anharmonicity and angular distributions of the vibrational loss features. The splitting between each pair of loss features is explained by the difference between the potential energy surface for hydrogen adsorbed on the two different sites. This conclusion is based on the observation that the fundamental frequencies show no dispersion along $\overline{\Gamma M}$ of the two dimensional Brillouin zone of the substrate. The dramatically different impact energy dependence of the intensities of the two loss features of each pair is explained by dynamical coupling between H vibrations.

Thesis Supervisor: Sylvia T. Ceyer

Title: Associate Professor

Table of Contents

List of Tables

List of Figures Page

Chapter 2.

Chapter 3

Chapter 4

Acknowledgements

I would like to thank my research advisor Professor S. T. Ceyer for her guidance, encouragement and financial support throughout the past five years. She is highly admired for her scientific insight and persistence for excellence in science.

I would also like to thank Andy Johnson and Kevin Maynard who have helped a great deal to collect the data for the work of this thesis and with whom I enjoyed working. Andy's patience waiting for his turn to have the machine, while my experiment seemed to never end, is greatly appreciated. I am grateful for Kevin's willingness to provide help in collecting make-up data on many occasions and in proof-reading this thesis.

Past members of the group, Sau Lan Tang, John Beckerle and Myung Lee, are thanked for having built the machine on which this work was done. I am grateful to Sau Lan Tang for having constructed the HREEL spectrometer which is the workhorse for the work of this thesis. John's expertise and help in solving electronic and computer problems made life in the lab much easier.

Other members of the group, past and present, David Gladstone, Michelle T. Schulberg, Ken Laughlin, Marianne McGonigal and Joe Simonson are thanked for often providing needed help, particularly at night. Dave is thanked for helping to solve mechanical problems and to repair my long gone sports car. Michelle's help in correcting my English writing is appreciated. Her knowledge of the Red Sox and Celtics impresses me very much. I learned a great deal about molecular spectroscopy from Ken to whom I should also apologize about the missing Linda and Richard Thompson. Joe was always the one to provide good jokes in the lab.

I would also like to thank my family as well as my wife's family for their understanding and support. I am particularly thankful for my wife's love and support, especially during the writing of this thesis in the past several months. It is my wife and my parents to whom this thesis is dedicated.

Vera Spanos is thanked for expertly typing out the manuscript.

Chapter One

Introduction

One of the most important goals of modern surface science research is to understand the fundamental principles behind heterogeneous catalytic reactions. In order to reach this goal, it is first necessary to understand the reaction mechanisms and the detailed dynamics of each step of the reaction. This task is more tenable if the studies are carried out on well-defined surface such as single crystal surfaces [1,2] which serve as models for the surfaces of real catalysts. Well-defined single crystal surfaces allow the employment of modern surface science techniques that probe qualitatively and quantitatively the reactions of molecules incident on surfaces, the identification of surface adsorbates, the determination of adsorbate structures, and chemical reactions between adsorbates. Ultrahigh vacuum (UHV) conditions are required both for maintaining the cleanliness of the surface and operating most of the surface instruments.

A study of the microscopic details of a reaction on a single crystal surface consists of two overall steps. The first step is to understand the interaction of a gas molecule incident on the surface and the second step is to identify the species produced on the surface as a result of the initial collision of the gas molecule with the surface. In the first step [3], questions need to be answered such as the reaction rate or the probability for dissociative chemisorption of the incident molecule and the effects of the kinetic energy, the excitation of the internal degrees of freedom (rotations and vibrations), the incident angle of the molecules and the surface temperature. After the initial step, the species that are formed on the surface need to be identified [4] as the nascent product of the adsorption reaction or as the product of the subsequent reactions on the surface. Detailed information on the structures and adsorption sites of the species involved in the reactions on the surface helps to understand these reactions from a more fundamental point of view.

One of the experiments reported in this thesis is the CH_4 (methane) reaction on a Ni(111) surface. The motivation to study the reaction of CH_4 on a Ni surface is to understand an important industrial catalytic reaction, the steam reforming of natural gas over a

nickel catalyst [5]. The dissociation of CH_4 on a Ni surface is the first step of the reaction but the dissociation reaction has been observed only under relatively high pressure conditions (> 1 torr). No detectable hydrocarbon is left on the surface after the exposure of a Ni surface to CH_4 at a pressure below 10^{-4} torr. The lack of reactivity at low pressure is known loosely as the pressure gap in heterogeneous catalysis [6]. One proposed explanation for the apparent difference in the CH_4 dissociation reactivity under low and high pressure conditions is that the dissociation is an activated process. That is, there is an energy barrier that CH_4 molecules have to overcome in order to dissociate. Dissociation is observed only under high pressure conditions because there are a sufficient number of molecules in the energetic tail of the Boltzmann distribution to overcome the barrier and therefore dissociation is observed. In other words, dissociation is occurring under low pressure conditions but the rate is too slow for observation of dissociation within a reasonable time. The high pressure requirement can be bypassed by increasing the kinetic energy of the incident molecules through the use of supersonic molecular beam teachniques [7]. Molecular beam techniques allow kinetic energies to be accessed that are many times the average energy of a Boltzmann distribution at room temperature. The width of the kinetic energy distribution is also much narrower than a Boltzmann distribution at room temperature so that it is possible to study the dissociation probability as a function of energy with sufficient resolution. Other advantages of the technique, beneficial to the study of the dynamics of an activated dissociative chemisorption reaction, are that it allows control of the incident angle and, to some extent, the excitations of the internal degrees of freedom. A study using molecular beam techniques carried out in this lab provides a clear insight to the nature of the activation barrier to the CH_4 dissociation on Ni(111) [8,9]. The results demonstrate that the kinetic energy is very effective for CH_4 to overcome the dissociation barrier and that the dissociation probability increases exponentially with the kinetic energy. Using the same technique, a new dissociation mechanism has been observed which is the collision induced dissociation (CID) of physisorbed CH_4 by energetic inert gas atoms [10,11].

Another aspect of the CH_4 dissociation dynamics, the determination of the nascent dissociation product and the study of the subsequent surface reactions, are the subjects of Chapter II of this thesis. Both tasks require the use of a surface spectroscopic technique that can provide information on the molecular identity of surface adsorbates. The technique used in the experiment described in Chapter II, as well as the other two chapters, is high resolution electron energy loss spectroscopy (HREELS), a surface vibrational spectroscopy [12]. At the present stage, HREELS is by far more widely used than other surface vibrational spectroscopic technique such as IR or Raman because of its superior sensitivity to adsorbates. An important feature of HREELS is the dipole selection rule by which it is possible to distinguish a vibrational mode with a dynamical dipole moment perpendicular to the surface from other modes. Because the inelastic scattering occurs through the interaction between the primary electrons and the long range dynamical dipole field associated with a vibrational mode, the inelastically scattered electrons experience only a small momentum change parallel to the surface and as a result are scattered along the specular direction (forward scattering). Therefore, the intensity of a vibrational loss feature of a dipole active mode is narrowly peaked in the specular direction (dipole lobe) and is much more intense in the specular direction than a nondipole active mode, unless the associated dynamical dipole moment is very small. For a mode to be associated with a dynamical dipole moment perpendicular to the surface, the symmetry of the mode must belong to the totally symmetric representation of the point group of the adsorbate-surface complex. Other modes can also be observed but by a different mechanism, i.e., impact scattering. The inelastic scattering in this case is by the short range interaction between the primary electrons and the electron distribution of the adsorbate. Because the momentum change of the inelastically scattered electrons may be rather large these modes display no dipole lobes. There are selection rules for impact scattering as well, and modes of certain symmetry are forbidden [12], but situations are rarely encountered where they are applicable. It is another advantage of the technique that most modes of an adsorbate may be observed regardless of their symmetry, unlike, for example,

IR where the normal dipole selection rule strictly applies so that only totally symmetric modes may be observed. Knowledge of the symmetry of the vibrational modes is essential in vibrational analysis to determine the molecular identity and structure of an adsorbate.

In Chapter II, the detailed vibrational analysis of the nascent product of CH_4 dissociation on Ni(111) is reported. Because of the possibility of further reaction on the surface, it is necessary to keep the surface temperature low in order to trap the nascent product. The results show that CH_4 dissociates to produce, as the nascent product, a surface adsorbed CH_3 group on Ni(111), which reacts above 150 K. In the study of the subsequent surface reactions of the adsorbed CH_3, the disappearance and the appearance of surface species is monitored as the surface temperature is raised. It is also necessary to monitor the formation of molecules that desorb into the gas phase by a thermal desorption measurement. A series of surface reactions beginning with the CH_3 group have been observed which are discussed in Chapter II,

$$CH_3 \rightarrow CH \rightarrow C_2H_2 \rightarrow C_6H_6.$$

It is the unique combination of the molecular beam techniques and surface vibrational spectroscopy that makes possible the observation of novel adsorbed species such as CH_3 and CH, a C-C bond formation process ($CH \rightarrow C_2H_2$), and the synthesis of C_6H_6 from CH_4. This experimental technique will find wide application in the study of activated gas surface processes and the study of surface chemistry of species that can only be produced by an activated process.

Chapter III describes the study of C_6H_6 chemisorption on Ni(111). The interest in C_6H_6 chemisorption on Ni(111) arose during the study of the $C_2H_2 \rightarrow C_6H_6$ reaction from the observation that only a very small percentage (0.3%) of the hydrocarbon on the surface desorbs into the gas phase in the form of molecular C_6H_6. While the vibrational spectra of the hydrocarbon that remains on the surface are very complex, they resemble those previously assigned to a CH species by a different group [13]. Because a CH species is unambiguously observed in this study of the reaction of CH_4 on Ni(111) and because its vibrational spectra

are distinctly different from the previous assignments for CH, further study and the identification of the hydrocarbon remaining on the surface is needed. The important question of whether C_2H_2 trimerization to form C_6H_6 is only a minor surface reaction or whether the C_6H_6 reacts further on the surface to form another hydrocarbon cannot be answered until the identity of the remaining hydrocarbon has been determined and the relationship between the hydrocarbon and C_6H_6 on the surface is understood. Such information may be obtained from a study of C_6H_6 adsorption but, unfortunately, C_6H_6 chemisorption on Ni(111) is not well understood (particularly at higher temperatures) despite a few studies [14-17] involving HREELS. There are several issues that are not settled even for C_6H_6 adsorption at low temperatures, such as whether there are two adsorption sites for C_6H_6 on Ni(111). Another fundamental question is whether C_6H_6 on Ni(111) undergoes significant Kekulé distortion, whereby the C-C bonds are alternately shortened and lengthened upon adsorption on a surface. A change as much as +0.41 Å and -0.07 Å away from 1.4 Å for a free C_6H_6 molecule has been determined for C_6H_6 on Rh(111) by a dynamical LEED study [18]. Vibrational spectroscopy is a suitable technique to determine the presence of this distortion if it is noted that adsorbed C_6H_6 without Kekulé distortion can have a C_{6v} symmetry while C_6H_6 with significant distortion can have at most C_{3v} symmetry. As will be discussed in Chapter III, C_6H_6 experiences no significant Kekulé distortion on Ni(111). Results show that the same hydrocarbon species is observed when C_6H_6 is annealed to higher temperatures as the one observed during the study of the trimerization of C_2H_2, thus indicating that the formation of C_6H_6 from C_2H_2 is the main reaction pathway but only a small percentage of the product C_6H_6 desorbs.

In the final chapter of this thesis, Chapter IV, the vibrational spectroscopic study of H on Ni(111) is presented. In the course of the study of CH_4 reactions on Ni(111), it becomes necessary to distinguish H vibrational loss features from those of the hydrocarbons that are being considered. Unfortunately, there has been very little research on the vibrational spectroscopy of H on Ni(111) [19,20]. From a fundamental point of view, the importance of

H adsorption on metal surfaces lies in its simplicity and it serves as a model of adsorption [21]. A chemisorption theory has to be such that H vibrational frequencies extracted from a calculated potential energy surface based on the theory agree with the experimentally observed values. For this purpose accurate vibrational frequencies are needed. The vibrational spectra presented in Chapter IV are obtained with significantly higher resolution and intensity, due to the superior performance of the HREELS spectrometer, than previous studies and make it possible to correctly assign the vibrational modes of H on Ni(111). The results have been very useful in the identification of the CH group and the study of the hydrocarbon reactions discussed in Chapter II of this thesis.

References

1. *The Chemical Physics of Solid Surfaces and Heterogeneous Catalysis Vol. 4,* "Fundamental Studies of Heterogeneous Catalysis," ed. by D.A. King and D.P. Woodruff (Elsevier Scientific Publishing Company, Amsterdam, 1982).
2. K. Tamaru, *Dynamic Heterogeneous Catalysis* (Academic Press, London, 1978).
3. J. A. Barker and D.J. Auerbach, Surf. Sci. Reports **4** , 1 (1985).
4. See, for example, *The Nature of the Surface Chemical Bond*, ed. by T.N. Rhodin and G. Ertl (North-Holland, Amsterdam, 1979); M.W. Roberts and C.S. Mckee, *Chemistry of the Metal-Gas Interfaces"* (Oxford University Press, Oxford, 1978).
5. J.R. Rostrup-Nielson, "Catalytic Steam Reforming" in *Catalysis Science and Technology*, J.R. Anderson and M. Boudart, eds. (Springer-Verlag, Berlin, 1984) Vol. 5, p.1.
6. G.A. Somorjai, Surf. Sci. **89**, 496 (1979); G.A. Somorjai, *Chemistry in Two Dimensions: Surfaces* (Cornell University Press, Ithaca, 1981).
7. R.E. Smalley, L. Wharton and D.H. Levy, Acts. Chem. Res. **10**, 139 (1977); N. Abuaf, J.B. Anderson, R.P. Andres, T.B. Fenn and D.G.H. Marsden, Science **155**, 997 (1967).
8. M.B. Lee, Q.Y. Yang and S.T. Ceyer, J. Chem. Phys. **87**, 2724 (1987); M. B. Lee, Q. Y. Yang, S. L. Tang and S.T. Ceyer, J. Chem. Phys. **85**, 1693 (1986).
9. M.B. Lee, Ph.D. Thesis, Massachusetts Institute of Technology, 1987.
10. J.D. Beckerle, A.D. Johnson, Q.Y. Yang and S.T. Ceyer, to be published; J.D. Beckerle, Q.Y. Yang, A.D. Johnson and S.T. Ceyer, J. Chem. Phys. **86**, 7236 (1987).
11. J.D. Beckerle, Ph.D. Thesis, Massachusetts Institute of Technology, 1988.

12. H. Ibach and D.L. Mills, *Electron Energy Loss Spectroscopy and Surface Vibrations* (Academic Press, New York, 1982).

13. J.E. Demuth and H. Ibach, Surf. Sci. **78**, L747 (1978).

14. S. Lehwald, H. Ibach and J.E. Demuth, Surf. Sci. **78**, 577 (1978).

15. J. C. Bertolini and J. Rousseau, Surf. Sci. **89**, 467 (1979).

16. C.M. Friend and E.L. Muetterties, J. Am. Chem. Soc. **103**, 773 (1981).

17. A.K. Meyers, G.R. Schoofs and J. Benziger, J. Phys. Chem. **91**, 2230 (1987).

18. M.A. Van Hove, R.F. Lin and G. A. Somorjai, J. Am. Chem. Soc. **108**, 2532 (1986).

19. W. Ho, N.J. DeNardo and E.W. Plumer, J. Vac. Sci. Tech. **17** , 134 (1980).

20. R.R. Cavanagh, R. D. Kelley and J. J. Rush, J. Chem. Phys. **77**, 1540 (1982).

21. K. Christmann, Surf. Sci. Reports **9**, 1 (1988).

Chapter II

The Chemistry of Methyl Radicals Adsorbed on Ni(111)

I. Introduction

The enormous abundance of natural gas of which methane (CH_4) is the major constituent makes it a valuable resource for chemical industry. Steam reforming of natural gas over a Ni metal catalyst is one of the most important industrial chemical processes. In order to understand the mechanisms of the steam reforming reaction, it is necessary to study the fundamental interaction of CH_4 with clean Ni crystal surfaces using modern surface science techniques. It is also necessary to be able to define and control as many parameters as possible that are relevant to the CH_4 reaction with a Ni surface such as the surface temperature and the kinetic energy and internal excitations of the CH_4 molecules incident on the surface. There are three aspects to the study of the interaction of CH_4 reactions over a Ni catalyst. The first step of the reaction of CH_4 with a Ni surface is its dissociative chemisorption on the Ni surface. Consequently, one first wants to have the knowledge of the dissociation probability of CH_4 and its dependence on the kinetic energy and the internal excitations of the CH_4 molecules under reaction conditions. The second aspect is the identification of the nascent product of CH_4 dissociative chemisorption on the surface. This study along with the dissociation probability study constitute the two components of a study of the dynamics of CH_4 dissociative chemisorption. The third aspect is a study of the surface chemistry of the dissociative chemisorption product which is carried out by monitoring the formation of new adsorbed species or new gas phase species. This report is part of a series of studies [1-5] that encompass all three aspects of the interaction of CH_4 with a particular Ni single crystal surface, Ni(111).

The negligible dissociation probability of CH_4 at thermal energies [6,7,8] is an indication that CH_4 dissociation on Ni(111) may be an activated process. An activated process implies that in order for the dissociation of CH_4 to have appreciable probability, the incident CH_4 must have a kinetic energy much higher than that of a room temperature gas if the kinetic energy is effective in overcoming the activation barrier to dissociative

chemisorption. Supersonic molecular beam techniques [9] combined with a seeding technique are an excellent means of producing such energetic CH_4 molecules. In addition, the technique allows one to define and vary the kinetic energy as well as the internal excitations of the molecules in the beam, thereby enabling the dependence of the dissociation probability on the kinetic energy to be studied. The study carried out in this lab using this technique [1,2] shows that the activation barrier to CH_4 dissociation on Ni(111) indeed can be overcome by increasing the kinetic energy of the incident CH_4 molecules. The dissociation probability of CH_4 on Ni(111) increases drastically and shows an exponential dependence as the CH_4 kinetic energy is increased. The dissociation probability goes up by two orders of magnitude from about $2x10^{-5}$ to about $2x10^{-3}$ as the CH_4 kinetic energy is raised from 12 to 18 kcal/mole. The proposed mechanism of the dissociation involves the deformation of the CH_4 molecule upon impact onto the surface and H tunneling through the remaining barrier. The activation barrier is the energy needed to deform the CH_4 molecule. A seemingly different dissociation process of CH_4 on Ni(111) has also been discovered and studied in great detail [3-5]. This is the collision induced dissociation of physisorbed CH_4 by energetic inert gas atoms. The physisorbed CH_4 is condensed onto the surface with the surface temperature being held below the desorption temperature of a monolayer of physisorbed CH_4 but above the desorption temperature of a multilayer of CH_4. Bombardment of the physisorbed CH_4 with energetic inert gas atoms such as Ar, Kr and Xe from a supersonic beam of the inert gas seeded in He causes the dissociation of the physisorbed CH_4 molecules. A detailed analysis of the dependence of the dissociation probability on the kinetic energy of the inert gas atoms, which can be as high as 100 kcal/mole, indicates that the fundamental dynamics involved in the collision induced dissociation is the same as that involved in the direct dissociation of CH_4 incident on the surface from a molecular beam.

A complete understanding of the basic mechanism of CH_4 dissociation on Ni(111) requires the identification of the nascent products of the dissociative chemisorption event. High resolution electron energy loss spectroscopy (HREELS) [10] is a vibrational

spectroscopic technique ideal for this purpose. HREELS has been one of the most widely used surface spectroscopic techniques that provide information about the identity and structure of adsorbates. One advantage of HREELS in comparison to IR reflection-absorption techniques is its high sensitivity over a wide frequency range as low as 100 cm^{-1} to 6000 cm^{-1} [6]. The well known dipole selection rule makes it possible for one to distinguish modes of the totally symmetric represention from others if the modes have appreciable dynamical dipole moments. Information such as this is very useful to the appropriate assignment of vibrational modes which is necessary to correctly determine the identity and the structure of an adsorbate. By carefully analyzing the HREELS spectra measured after the dissociation of CH_4 on the surface, the nascent products of CH_4 dissociation on Ni(111) may be revealed. In addition, if it can be concluded from the HREELS study that the direct dissociation and the collision induced dissociation yield the same product for the dissociative chemisorption event, this would be proof from a different perspective that the two processes involve the same basic mechanism. The step-by-step study of the surface chemisty of CH_4 dissociation products can be accomplished using the same technique.

This experiment concerns the identification by HREELS of the dissociation product of CH_4 on Ni(111) and the surface chemistry of the dissociation product. Preliminary results of this work have been published before [1,11]. The vibrational spectra presented in this chapter were measured since then and are significantly improved. As will be discussed in detail, the nascent product of the dissociation of CH_4 on Ni(111) is a surface adsorbed CH_3, as expected if one of the C-H bonds is broken upon the dissociative chemisorption event. The surface chemistry of the CH_3 species is also discussed in this chapter. It includes the formation of a species identified as an adsorbed CH, the reaction of the CH species to form adsorbed C_2H_2 and the trimerization of C_2H_2 to form C_6H_6 as the surface temperature is raised. The experiment employs an apparatus that combines a molecular beam source and UHV chamber which is equipped with a HREELS spectrometer. The combination of

molecular beam techniques with a surface vibrational spectroscopy provides an opportunity to study the surface chemistry of species that cannot be produced by other means.

II. Experimental

Figure 1 is a schematic of the apparatus on which the experiments were carried out. The apparatus has been described in detail previously [5,12,13] and therefore only a brief description is provided here. The machine consists of a molecular beam source and UHV chamber. The UHV chamber, pumped by a 10" liquid nitrogen trapped diffusion pump, has a typical base pressure of $4x10^{-11}$ torr. The UHV chamber is equipped with a cylindrical mirror analyzer (CMA) with a coaxial electron gun for Auger spectroscopy, a rearview electron diffraction (LEED) apparatus, a high resolution electron energy loss spectrometer (HREELS), an ion sputter gun, a Bayard-Alpert type ionization gauge and a leak valve. In addition, there is a quadrupole mass spectrometer which is used for residual gas analysis, thermal desorption measurement and TOF characterization of the molecular beam.

The molecular beam source is a design [12] that consists of an inner and an outer tube welded to an end cap 0.020 inch thick into which a hole of about 25 μ diameter is spark-cut. The material used for the nozzle construction is inconel alloy. The nozzle can be heated resistively by passing a current through the end cap and between the inner and outer tubes. The temperature measurement is made by a chromel-alumel thermocouple spot-welded to the end cap. The remainder of the nozzle assembly is water-cooled. The nozzle can be heated to as high as 1400 K and can withstand a gas pressure up to 250 psig. The production of an atomic or molecular beam of high energy requires a high temperature and a high gas pressure, especially in the case of a heavy gas seeded in a much lighter gas. The source chamber is pumped by a 5000 l/s oil diffusion pump. There are two differential pumping stages between the source chamber and the UHV main chamber and they serve to minimize the gas load to the main UHV chamber from the source chamber whose pressure can rise as high as 10^{-4} torr when a gas is expanded through the nozzle. A skimmer of 1 mm diameter is mounted at a distance of 1 cm from the nozzle on the wall between the source and the first differential

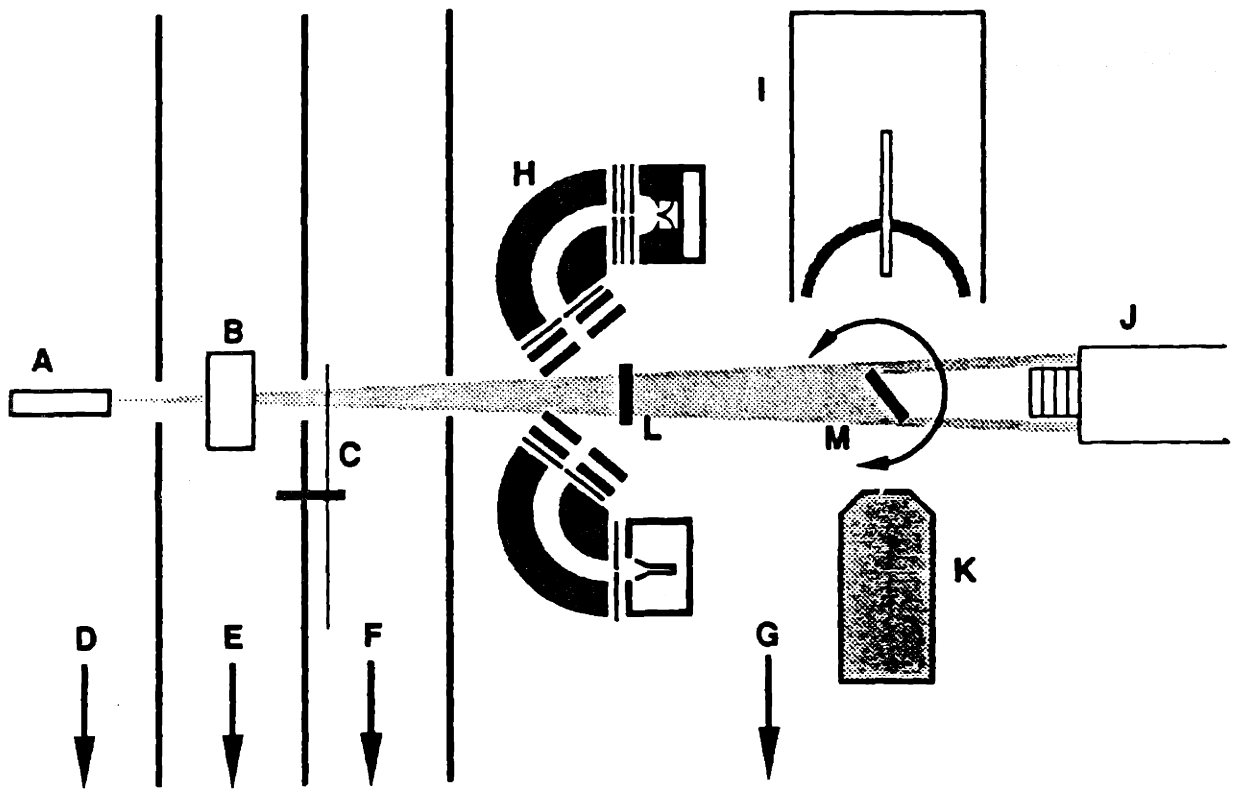

Figure 1. Schematic diagram of the molecular beam-UHV apparatus: A, nozzle molecular beam source; B, electronic shutter; C, rotating disk chopper; D, to source chamber 10-inch diffusion pump; E, to first differential stage 6-inch diffusion pump; F, to second differential stage 4-inch diffusion pump; G, to main chamber liquid N_2 trapped 10-inch diffusion pump; H, HREEL spectrometer; I, reverse view LEED; J, quadrupole mass spectrometer; K, single pass CMA Auger spectrometer; L,M, possible crystal positions and orientations for rotatable, liquid He cooled sample manipulator.

chamber. The molecular beam passes through a collimator on the wall between the first and the second differential pumping chambers before impinging onto the crystal in the UHV main chamber. A high speed electronic shutter, mounted in the beam path and located in the first differential chamber, is used to accurately control the time of exposure of the beam on the sample. Mounted in the beam path in the second differential chamber is a mechanical chopper which modulates the molecular beam during time-of-flight measurement. The chopper, which is a 127 μ thick stainless disk with four slots cut into the periphery, is clamped onto the shaft of an A.C. hysteresis synchronous motor. An arrangement of a LED and a photodiode which sandwich the chopper disk provides the trigger signal to the multichannel analyzer for the time-of-flight measurement. An O-ring sealed slide valve over the collimating slit isolates the UHV from the second differential chamber and is kept closed until a molecular beam is introduced into the main chamber.

The crystal is mounted on the end of a cryostat that can be cooled with cold air, liquid nitrogen or liquid helium. The cryostat is bolted to a manipulator composed of a rotatable feedthrough seated on an X-Y-Z translational stage. The manipulator is mounted eccentrically on a 36 cm diameter differentially pumped, Teflon sealed rotatable flange. The rotation of the flange provides the horizontal translation necessary to position the crystal in front of each surface analytical instrument. The crystal is spot-welded to two tungsten rods that are clamped into two copper rods extending from the base of the cryostat. The high thermal conductivity between the crystal and the bottom of the cryostat ensures a stable temperature of no higher than 80 K with liquid nitrogen as coolant and a cooling time of less than 5 minutes to reach 80 K after heating the crystal to 1100 K. The sample heating is by radiation or electron bombardment from a tungsten filament behind the crystal. In the case of electron beam heating, the sample is biased by a DC voltage variable between 0 and 600 volts. The temperature is monitored with a type E (chromel-constantan) thermocouple spot-welded to the top of the crystal. A heating rate of as high as 20 K/sec may be achieved by controlling the filament power supply. The description of the cryostat and the sample heating and cooling

can be found in Reference 12. The crystal is the same as has been used in the previous experiments. The absence of contaminants on the crystal surface is verified by Auger spectroscopy and EELS. The numerous previous cleaning cycles had removed most of the bulk impurities of the crystal and only occasional sputtering was necessary to remove small amounts of S, C and O contaminants.

The EELS spectrometer is composed of two single pass, 127 degree cylindrical deflector electron energy analyzers with a nominal incident and scattering angle of 60 degrees from the crystal normal. A typical count rate of 10^6 count/sec with a resolution of 50 cm^{-1} is achieved routinely for the beam elastically scattered from the clean crystal. The electron energy loss spectra can be measured at an off-specular angle by rotating the monochromator away from an incident angle of 60 degrees, although all the off-specular spectra in this report have been measured by rotating the crystal. The electron impact energy is varied by the bias on the crystal. The impact energy can be precisely determined by the difference between the bias at which current at the sample arising from the electrons incident normal to the surface drops to zero and the bias at which a spectrum is collected. The data acquisition is achieved through a dual timer/counter interfaced to a PDP-11/03 computer which also controls the DAC that supplies the linear ramp for scanning the voltage on the electron energy analyzer.

Gases and gas mixtures used in this work are handled in a bakeable gas manifold which is evacuated with a roots blower and a liquid nitrogen trapped diffusion pump. The gas mixtures (Kr/He, CH_4/He and CH_3D/He) are prepared in stainless steel mixing cylinders and are thoroughly mixed before use. The He, Kr and CH_4 gases are purchased with 99.9999%, 99.999% and 99.9995% chemical purity, respectively. The CD_4 and CH_3D gases are 99.0% isotopic purity (Cambridge Isotope Labs). To reduce the contribution of any condensible contaminants, all gases are passed through a liquid nitrogen trap or dry ice/acetone trap as vapor pressure allows before mixing or expansion from the nozzle or admission into the chamber through the leak valve. Special treatment of CD_4, CD_4/He and CH_3D/He are necessary to remove contaminants as they are not high purity. These gases are passed

through a trap that contains Nanochem resin provided by Hercules which is very effective in removing CO, O_2 and H_2O. The effectiveness of such a purification process is evidenced by the difference between the EEL spectra measured after the surface is exposed to CD_4/He that has and that has not passed through the Nanochem resin. The results show that the CD_4/He is as contamination free after passing through the Nanochem trap as CH_4/He. In contrast the EEL spectrum measured after the exposure of the surface to CD_4/He that did not pass through the Nanochem resin shows the presence of large amounts of CO and O on the surface.

The vibrational spectra presented in the next section are measured using a fixed nozzle temperature and gas mixture concentrations for CH_4 dissociative chemisorption. This is because the vibrational spectra measured after CH_4 dissociation do not appear to depend on the kinetic energy of the incident CH_4 molecules. The nozzle temperature is at about 850 K for all gas mixtures. The concentrations are, respectively, 2% for CH_3D, 0.5% for Kr/He and 3% for CH_4/He and CD_4/He.

III. The Nascent Products of CH_4 Dissociation

A. Results

The nascent products of the dissociative chemisorption of CH_4 on Ni(111) are identified from their high resolution electron energy loss spectra. These spectra, measured after exposure of the Ni(111) crystal at 80 K to a beam of CH_4 with a most probable translational energy of 17 kcal mol^{-1} and with an incident angle of 0°, are shown in Figure 2. The beam is generated by expansion of a 3% mixture of CH_4 in He from the nozzle held at 876 K. The translational energy distribution of the incident CH_4 is measured by a time-of-flight technique described previously [1]. The full width at half the maximum intensity of this distribution is about 12%. Since the nozzle temperature must be high to produce the energetic incident CH_4, it is necessary to eliminate the possibility that the observed spectrum is due to carbonaceous impurities such as C_2H_2 or C_2H_4 which may be produced in the hot nozzle. This is accomplished by measuring a vibrational spectrum after exposure of the surface to the beam

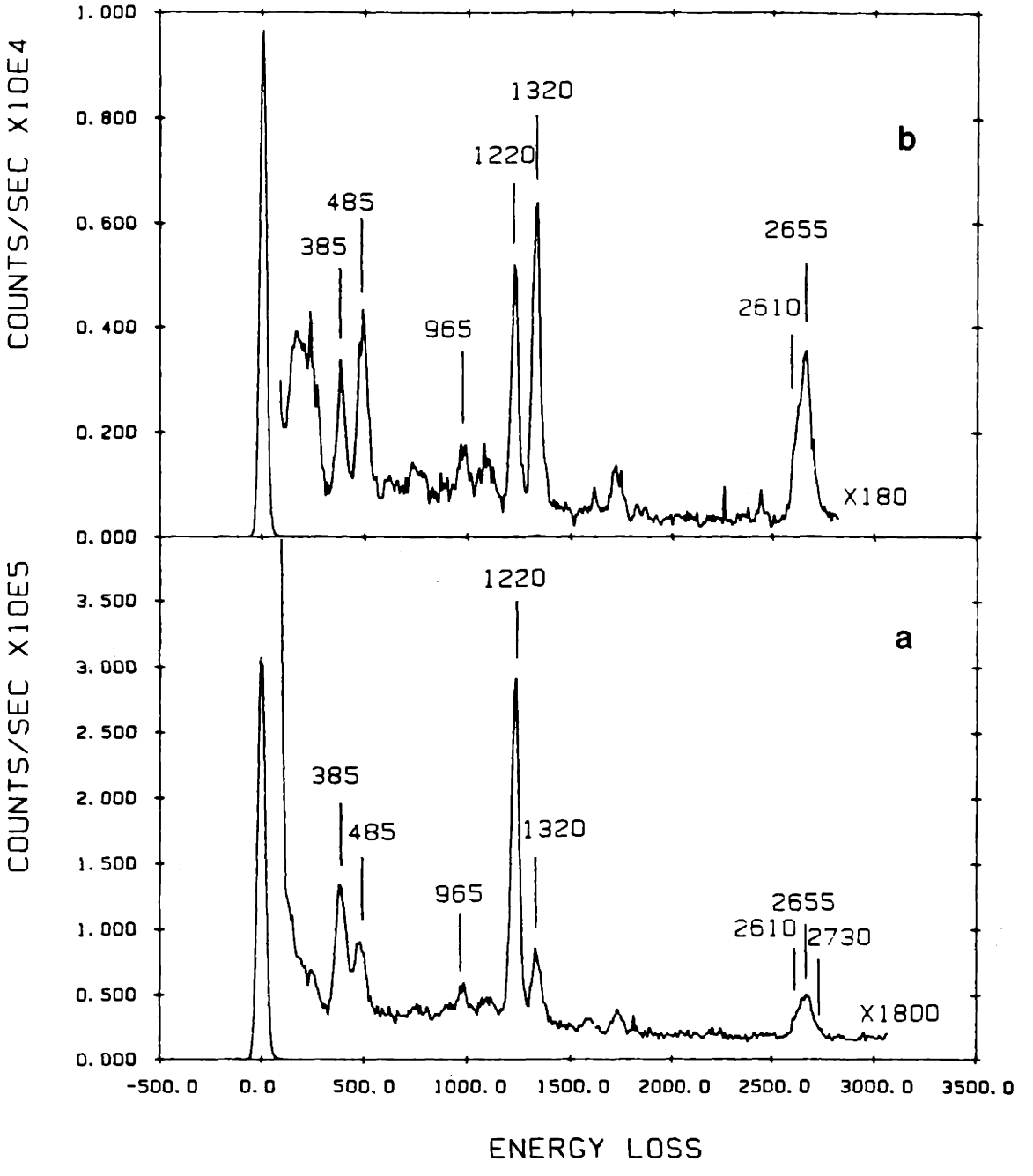

Figure 2. HREEL spectra after the dissociation of CH_4 incident on Ni(111) at 80 K with 17 kcal/mole kinetic energy. The coverage is 0.05 ML. The spectra were measured with a 4.5 eV impact energy at 80 K in the (a) specular and (b) 10^o off-specular direction. The ΔE_{FWHM} of the elastic feature is 45 cm^{-1} for 8 cm^{-1}/channel. The spectra are assigned to an adsorbed CH_3 on Ni(111).

incident at a 60° angle to the surface normal. Under this condition, the translational energy of the CH_4 normal to the surface is 4.3 kcal mol^{-1} which is too low for appreciable dissociation of CH_4. This is known from a previous study [1,2] in which the probability for dissociative chemisorption of CH_4 depends exponentially on the normal component of the incident translational energy and that at least 12 kcal mol^{-1} is necessary for a dissociation probability of 10^{-5}. However, the probability for adsorption of small amounts of C_2H_2 of C_2H_4 impurities remains high at glancing incidence. The spectra measured under these conditions show no loss features attributable to hydrocarbon species.

To ensure that the spectrum is that of the nascent product of the dissociative chemisorption event, the temperature of the surface during exposure to the beam and during the measurement of the spectrum must be sufficiently low to prevent the thermal decomposition of the nascent adsorbed product. The temperature below which the dissociation product is stable is not known apriori. The spectra shown in Fig. 2 are measured at 80 K after exposure of the surface at 80 K. These spectra are identical to those measured at 47 K after the dissociation at 47 K of physisorbed CH_4 induced by the collision of an incident inert gas atom which is a mechanism previously shown to be equivalent to translational activation of CH_4 [5]. Given that these spectra are identical and that 47 K is a low temperature for chemical change, it is assumed that the spectra in Fig. 2 represent the nascent product. This assumption is justified by the identification below of the product as an adsorbed CH_3 radical, a species that results from a single bond cleavage in the reactant CH_4.

It is also important to ensure that lateral interactions or surface reactions between the nascent dissociation product do not occur, thereby complicating the spectra and obscuring its identification. To this end, the spectra are measured at low coverage, most of them at a coverage of 0.05 carbon atoms per Ni or 0.05 ML. This coverage was calibrated by comparison of the ratio of the peak-to-peak intensities of the C(272 eV) to Ni(848 eV) Auger signal to the ratio measured from a (2x2) ordered overlayer (0.25 monolayer) of C_2H_4 on Ni(111) at 80 K. The coverage so calibrated agrees with that calculated from the time of

exposure of the surface to the beam (7 min.) and from the flux of the CH_4 beam ($2x10^{14}$ cm^{-2} sec^{-1}) and the dissociative chemisorption probability (~10^{-3} at 17 kcal mol^{-1}) determined previously [1].

Spectra are recorded at both the specular angle and at an off-specular angle, as shown in Figs. 2a and 2b, for the purpose of identifying the dipole active loss features. A total of eleven loss features, whose frequencies are marked in Fig. 2, are identified as being associated with the dissociation products. More loss features are observed here than in our preliminary spectra previously published [1-5] because the present spectra are measured at a higher electron impact energy (4.5 eV compared to previous measurements at 3.0 eV) where an electron-surface resonance occurs. This resonance enhances the intensity of the non-dipole loss features relative to the dipole active ones so much that the non-dipole features are clearly visible in the spectrum measured at the specular angle.

Two of the loss features arise from one of the products, adsorbed hydrogen. These features at 770 and 1100 cm^{-1} are the asymmetric and symmetric vibrations of H on Ni(111), respectively, as assigned and discussed previously [14,15]. The remaining nine features at 385, 485, 965, 1220, 1320, 2430, 2610, 2655 and 2730 cm^{-1} are assigned to the hydrocarbon product. The latter four loss features are more clearly seen in an expanded spectrum of the 2400-2800 cm^{-1} region shown in Fig. 3. The spectrum in Fig. 3a is measured at a higher electron energy of 5.5 eV and at a slightly lower coverage of 0.04 ML. The spectrum in Fig. 3b is measured at 4.5 eV electron energy but at a higher coverage that is no greater than 0.1 ML. Two unmarked loss features at 1580 and 1730 cm^{-1} are also present in spectra measured after exposure of the surface to a neat He beam expanded from the nozzle at 876 K. These features are attributed to small amounts of H_2O and CO, respectively. The unmarked features at 160 and 230 cm^{-1} are attributed to hindered translations parallel to the surface and to a surface phonon, respectively.

There are several features of the spectra in Fig. 2 that are immediately notable. First, the two most intense features at 385 and 1220 cm^{-1} represent dipole active modes because

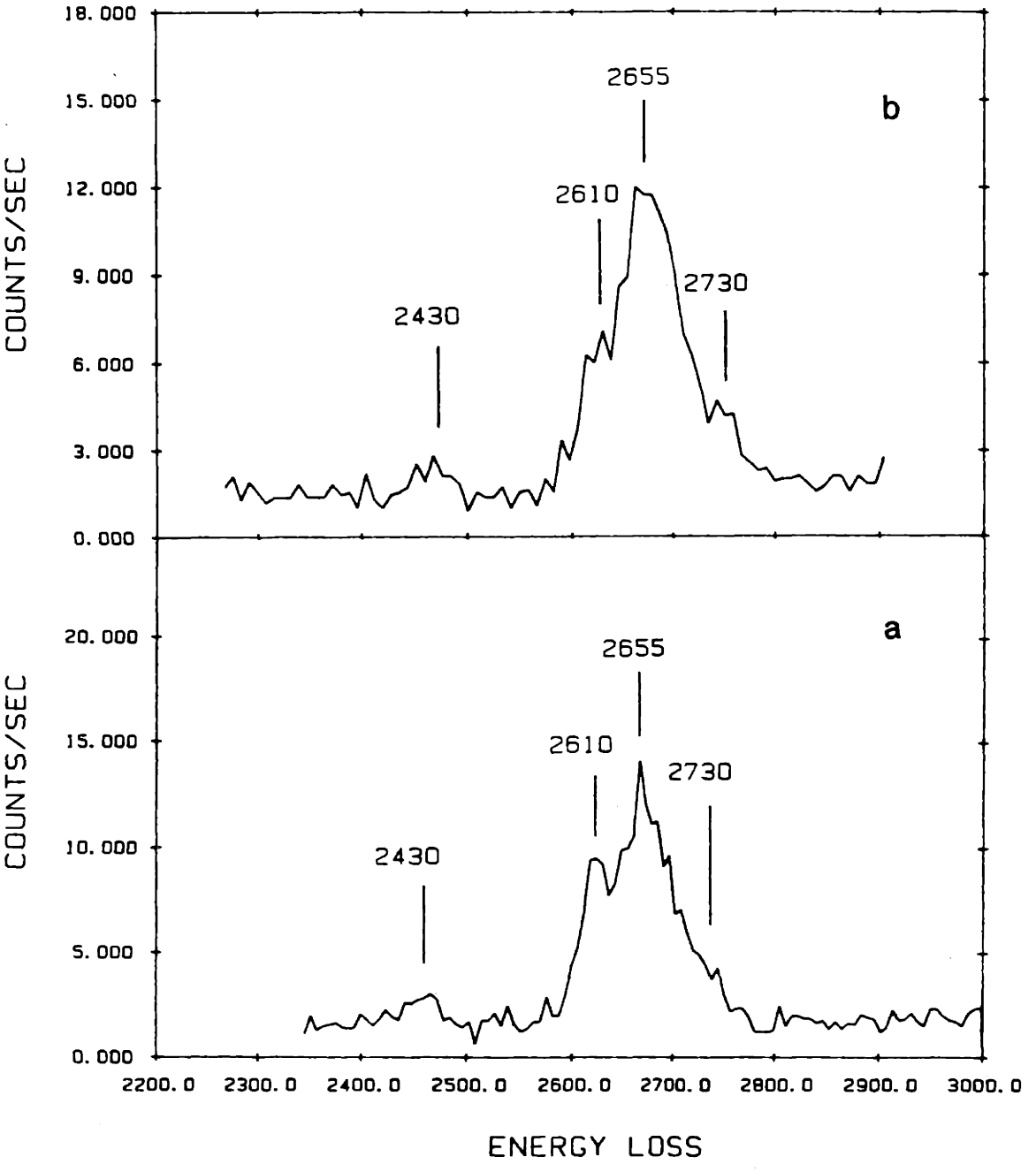

Figure 3. Expanded HREEL spectra of the region for C-H stretch modes and overtones of C-H deformation modes measured in the 10° off-specular direction under conditions similar to those in Figure 2 but with a higher resolution of ΔE_{FWHM}=35 cm^{-1} and 6 cm^{-1}/channel. (a) coverage is 0.04 ML; impact energy is 5.5 eV (b) coverage is no greater than 0.1 ML; impact energy is 4.5 eV. The loss features at 2610 and 2655 cm^{-1} are the symmetric C-H stretch mode and the overtone of the asymmetric C-H deformation mode of CH_3 in Fermi resonance.

their intensity decreases rapidly as the angle of detection of the scattered electrons is moved away from the specular angle in Fig. 2b. In addition, the intensity of these loss features increases relative to the other loss features for lower electron impact energy as they should for dipolar scattering [10]. These features are therefore assigned to modes of the totally symmetric representation of the point group to which the adsorbed species belongs.

A second interesting aspect of the spectra in Figs. 2 and 3 is the loss region between 2400-3000 cm^{-1} in which four loss features are observed. Some of these loss features arise from C-H stretching vibrations. However, the frequencies of these modes are 300-400 cm^{-1} lower than normal C-H stretching vibrations at about 3000 cm^{-1}. Such low frequency C-H modes have been observed previously, usually for large hydrocarbons adsorbed on transition metal surfaces, and are often referred to as "soft" C-H modes [6,16,17]. Some of the loss features in the 2400-3000 cm^{-1} region may also be overtones of lower frequency modes. Overtone excitations may complicate this region of the spectrum through a Fermi resonance such as a possible resonance between the 2610 and 2655 cm^{-1} modes and the overtone of the 1320 cm^{-1} vibrational mode. Assignment of the loss features and a detailed analysis are deferred to the discussion section.

Fig. 4 shows the corresponding spectra measured after exposure of the Ni(111) surface to an energetic beam of CD_4 under conditions similar to those for the spectra in Fig. 2. A total of 10 loss features are attributed to the dissociation products. The loss features at 570 and 800 cm^{-1} are the asymmetric and symmetric vibrations of D on Ni(111), respectively [14,15]. The remaining eight loss features at 365, 730, 915, 978, 1815, 1925 and 2030 cm^{-1} are associated with the hydrocarbon dissociation product. The loss features at 365 and 915 cm^{-1} are most intense at the specular angle and therefore correspond to the dipole active features at 385 and 1220 cm^{-1} in the corresponding CH_4 spectrum. The small isotope shift observed for the feature at 385(365) cm^{-1} indicates that this mode is predominantly associated with carbon motion while the large shift of the feature at 1220(915) cm^{-1} indicates that this mode is largely associated with H(D) motion. Of the loss features that result from non-dipole

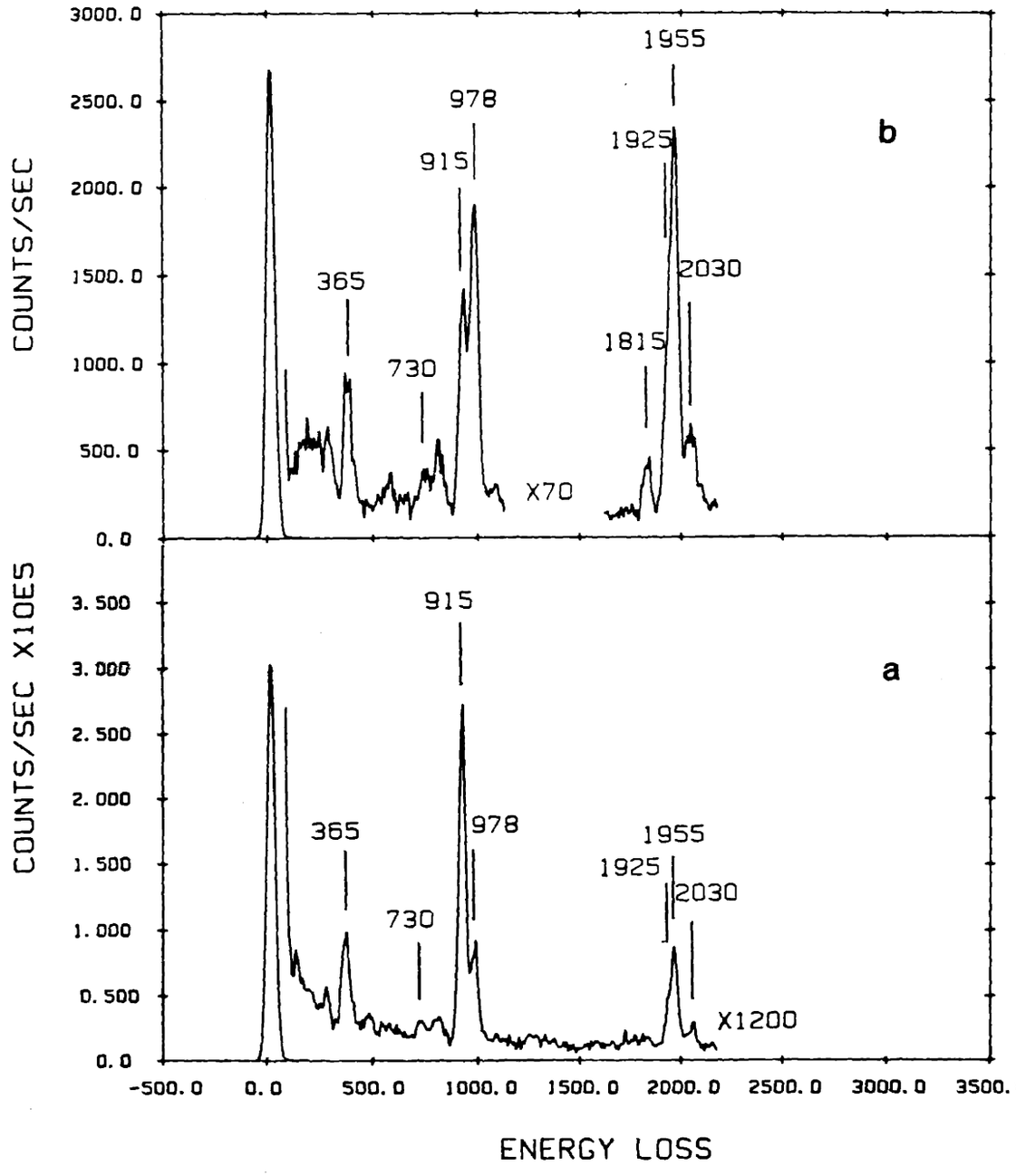

Figure 4. HREEL spectra after the dissociation of CD_4 under conditions similar to those for spectra in Figure 2 in the (a) specular and (b) 10^{o} off-specular direction. The coverage is 0.01 ML. The spectra are assigned to an adsorbed CD_3 and the two features at 1925 and 1955 cm^{-1} are assigned to the symmetric C-D stretch and the overtone of the asymmetric C-H deformation in Fermi resonance.

active modes, the loss at 978 cm^{-1} in Fig. 4b corresponds to the loss at 1320 cm^{-1} in Fig. 2b and the loss at 730 cm^{-1} corresponds to that at 965 cm^{-1} in Fig. 2b. The loss at 485 cm^{-1} in Fig. 2b is believed to be shifted to about 365 cm^{-1} in Fig. 4b such that it is superimposed onto the dipole active mode at 365 cm^{-1} in Fig. 4b. The loss features at 2030, 1955, 1925 and 1815 cm^{-1} correspond to the loss features at 2730, 2655, 2610 and 2430 cm^{-1} in Fig. 2b, respectively. This region of the C-D stretching vibrational modes is also likely to be complicated by a Fermi resonance.

Fig. 5 shows the corresponding spectra measured after exposure of the Ni(111) surface to an energetic beam of CH_3D under conditions similar to those for the spectra in Figs. 2 and 4. A total of eight loss features at 385, 485, 965, 1120, 1230, 1320, 2015 and 2680 cm^{-1} are attributed to the hydrocarbon product. The loss features at 385 and 1120 cm^{-1} represent the dipole active modes. The 1900-2800 cm^{-1} region of the spectra in Fig. 5 provide important information about the possible involvement of a Fermi resonance in the C-D and C-H vibrational modes of CD_3 and CH_3.

B. Discussion

1. Identification of Adsorbed CH_3

From an analysis of the spectra in Figs. 2-5, it is concluded that the nascent products of the dissociative chemisorption of CH_4 are an adsorbed CH_3 species and an adsorbed H atom. A structure in which the CH_3 species is adsorbed with C_{3v} symmetry at a threefold hollow site and with its C_3 axis normal to the surface provides an assignment most consistent with the spectra. The analysis leading to this identification for the dissociation products and for the symmetry and binding site is presented in this section.

The feature in the spectra that is key to the conclusion that the C_3 axis is normal to the surface is the dipole active feature at 385 cm^{-1} for the normal and 365 cm^{-1} for the deuterated methane. This feature is assigned to a Ni-C stretch because of the similarity of its frequency to other known Ni-C stretch frequencies [10] and because of its very small shift in frequency upon deuteration. The strong dynamical dipole moment associated with this loss feature is

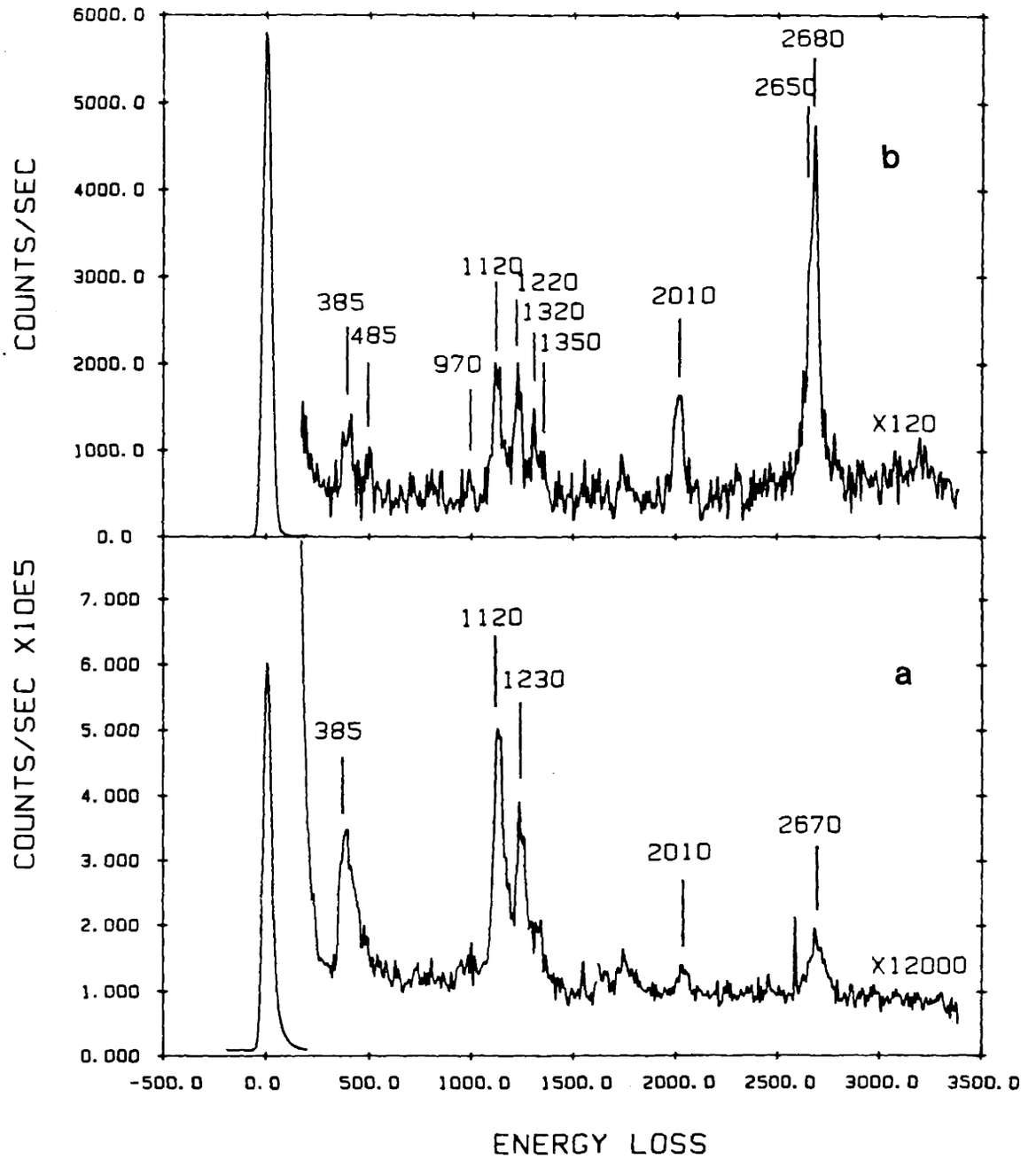

Figure 5. HREEL spectra after the dissociation of CH_3D under conditions similar to those for the spectra of Figure 2. The spectra were measured at 80 K in the (a) specular and (b) 12° off-specular direction. The spectra are assigned to the superposition of those of adsorbed CH_2D and CH_3.

consistent with a perpendicular orientation of the vibrational vector of this Ni-C mode and hence a perpendicular orientation of the C_3 axis.

There are an infinite number of sites to which an adsorbed CH_3 radical with its C_3 axis normal to the (111) surface may bind. However, there are a limited number of point groups to which the adsorbed CH_3 radical may belong. If the CH_3 is bound to the surface through the carbon at an on-top or threefold hollow site, it belongs to the C_{3v} point group as long as the hydrogens are pointed toward the twofold bridge sites or the on-top sites. If the hydrogens are not oriented toward either of those sites, the symmetry of the point group is lowered to C_3. A CH_3 radical adsorbed on a twofold bridge site with one of the hydrogens pointed toward the on-top site belongs to the C_s (σ_d) point group. All other binding sites or orientations result in a symmetry lower than C_s.

For the C_{3v} point group, there are three vibrational modes of the totally symmetric representation A_1. This implies that there should be three dipole active loss features: the Ni-C stretch vibration denoted z; the CH_3 symmetric deformation or umbrella mode, δ_s; and the symmetric C-H stretch vibration, ν_s. For the lower symmetry point group C_3, the same modes remain dipole active, but a fourth mode, the torsional mode R_z, which is of A_2 symmetry in the C_{3v} point group, acquires the totally symmetric representation and also becomes dipole active. For lower symmetry point groups such as C_s, at least eight modes are dipole active. Thus, in principle, the symmetry of the CH_3 species and its adsorption site are determinable from the number of dipole active modes.

As noted above, three dipole active loss features have been observed. Therefore, no structures for CH_3 of C_s symmetry will be considered further. The assignment of the feature at 385 cm^{-1} to a Ni-C stretching vibration and its dipole activity has already been discussed. A second dipole active mode at 2655 and at 1955 cm^{-1} for the deuterated species is here assigned to a C-H(C-D) symmetric stretching vibration, ν_s. Because this region of the spectrum is complicated by a Fermi resonance it will be discussed in a separate section. A third dipole active mode at 1220 cm^{-1} (915 cm^{-1}) is assigned as the symmetric deformation or

umbrella mode of $CH_3(CD_3)$, δ_s. This assignment is based both on the expected dipolar activity of this mode for a structure with C_{3v} or C_3 symmetry and from the magnitude of the frequency of this loss feature. A frequency of 1220 cm^{-1} is typical for a CH_3 symmetric deformation mode. This is clear from the list of frequencies of the symmetric deformation mode, δ_s, shown in Table I for several model organometallic and organohalide compounds. The identification of three dipole active modes whose frequencies are in the range expected for a Ni-C stretching vibration, a symmetric deformation vibrational mode and a C-H stretch mode seems to provide sufficient evidence for a C_{3v} symmetry for the adsorbed species. However, it is first necessary to assign the remaining loss features.

Besides the torsional mode (R_z) of A_1 or A_2 symmetry, depending on the point group, four doubly degenerate modes of the E representation are expected. The two degenerate hindered translations (x,y) parallel to the surface comprise one of the doubly degenerate modes. As is typical for hindered translations, the frequency of this mode is expected to be low [10]. The loss intensity at about 160 cm^{-1} is believed to arise from this mode although it is unresolvable from the loss feature due to the surface phonon at 230 cm^{-1} [18]. Further analysis of this spectral region was not carried out. Another doubly degenerate mode is the C-H asymmetric stretching vibration, ν_d, at 2730 cm^{-1} (2030 cm^{-1}). As mentioned in the discussion for the assignment of the C-H symmetric stretching vibration, this region of the spectrum is complicated by Fermi resonance and therefore is discussed in detail below.

The asymmetric deformation mode (δ_d) is another doubly degenerate mode of the E representation expected for an adsorbed CH_3 species. This mode is assigned to the loss feature at 1320 cm^{-1} and at 978 cm^{-1} for the deuterated species. This is a reasonable assignment because this feature clearly represents a non-dipole active mode predominantly involving hydrogen motion and because its frequency is slightly higher than the dipole active symmetric deformation mode (δ_s). The frequency of the asymmetric deformation mode is higher than that of the symmetric deformation mode in all molecules containing a -CH_3 group

Table I

Vibrational frequencies of molecules containing a CH_3 group

Vibrational Mode	CH_3Cl [a]	$CH_3Mn(CO)_5$ [b]	$CH_3Re(CO)_5$ [b]	CH_3TiCl_3 [c]	$CH_3CCo_3(CO)_9$ [d]
ν_d	3041	2898	2879	2980	2930
ν_s	2966			2898	2888
δ_d	1454			1375	1420
δ_s	1355	1191	1212	1052	1388
ρ_r	1015	755	775	580	1509

[a] Ref. 23
[b] Ref. 34
[c] Ref. 36
[d] Ref. 35

as shown in Table I. In addition, the magnitude of the frequency is very similar to those of the model compounds in Table I.

The fourth doubly degenerate mode is the rocking mode (ρ_d) which arises from the restriction of the rotational modes of CH_3 upon its binding to the surface. Rocking modes have been assigned to features in spectra of model compounds with frequencies as low as 580 cm^{-1} in $Ti(CH_3)Cl_3$, with a frequency in the intermediate range at 775 cm^{-1} in CH_3 $Re(CO)_5$ and as high as 1015 cm^{-1} in CH_3Cl as shown in Table I. Because the loss feature at 965 cm^{-1} and at 730 cm^{-1} in the deuterated species falls within this range and because this feature does not exhibit dipolar scattering, it is assigned as the doubly degenerate rocking mode.

There remains one loss feature, outside of the C-H stretch region shown in Fig. 2, to be assigned and one expected vibrational mode, the torsional mode, to be accounted for. This loss feature occurs at 485 cm^{-1} and is here assigned as the torsional mode (R_z). The torsional mode for the deuterated species is believed to be shifted to about 375 cm^{-1} and hence is unresolved from the Ni-CD_3 stretching vibration at 365 cm^{-1}. A close inspection of this loss feature indicates that a high frequency shoulder is present on the Ni-CD_3 loss feature. Unfortunately, the frequencies of torsional modes are not known from model compounds because the torsional frequency is presumably too low to be detectable. Accordingly, it may be argued that the frequency of this loss at 485 cm^{-1} is too high to be assigned to the torsional or hindered rotation about the C_3 axis. However, CH_3 adsorbed on Ni(111) may be peculiar because of the possible participation of the hydrogens in the bonding between the surface and the carbon atom as indicated by the very low C-H stretching frequencies. A substantial anisotropic interaction of the hydrogens with the surface may result in large a barrier or large force constant for torsional motion and hence in a high frequency for this motion.

Having now identified the torsional mode, which is clearly non-dipole active, it may be concluded that the symmetry of the adsorbed species is C_{3v} because only three modes are observed to be dipole active. However, some caution must be exercised here because it is possible that the torsional mode is indeed dipole active but that its dynamical dipole is too

Table II

Observed vibrational frequencies and mode assignments for $CH_{3(a)}$ and $CD_{3(a)}$

Vibrational Mode	Symmetry (C_{3v})	$CH_{3(a)}$	$CD_{3(a)}$
ν_d	E	2730	2030
ν_s	A_1	2655	1955
$2\delta_d$	A_1	2610	1925
$2\delta_s$	A_1	2430	1815
δ_d	E	1320	978
δ_s	A_1	1220	915
ρ_d	E	965	730
R_z	A_2	485	365
ν_s(Ni-C)	A_1	385	365

small to be observed as a dipole active loss feature. With this caveat in mind, it is concluded that the number of loss features corresponding to both dipole active and non-dipole active modes and the frequencies of these features are most consistent with an adsorbed CH_3 species with C_{3v} symmetry. The assignments of the loss features are listed in Table II.

The vibrational spectra resulting from the dissociative chemisorption of CH_3D shown in Fig. 5 are also consistent with the assignment of the spectra to an adsorbed methyl radical. If the C-D bond cleaves exclusively upon the dissociative chemisorption of CH_3D, the product would be an adsorbed CH_3 species and its vibrational spectrum should be identical to that measured after exposure to CH_4. A comparison of the spectra in Fig. 2 to that in Fig. 5 shows that this is clearly not the case. The spectra in Fig. 5 exhibit a larger number of loss features and significantly more congestion. The dissimilarity of the spectra is not surprising. Preferential cleavage of the C-D bond is not expected because the dissociation probability of CD_4 is known to be an order of magnitude below that of CH_4 [1]. Rather, it is more likely for C-H bond cleavage to occur, resulting in a mixed isotope, CH_2D species on the surface. The vibrational spectrum of adsorbed CH_2D is very different from that of adsorbed CH_3 or CD_3. The presence of the deuterium isotope lowers the symmetry of the point group from C_{3v} to C_s, resulting in a lifting of the double degeneracy of the asymmetric stretching vibration, ν_d, the asymmetric deformation vibrational mode, δ_d, and the rocking vibrational mode, ρ_d. Each of these modes now splits into a new kind of mode of a symmetric representation, a', and one of a non-symmetric representation, a", as shown in Table III. Therefore, six loss features are expected to exhibit dipolar scattering. However, even though C-D bond cleavage is significantly less probable, it does still occur. The two channels for dissociation result in two adsorbed products, CH_3 and CH_2D. The presence of two species with vibrations of similar frequencies produce a congested spectrum that is more difficult to assign than that of a single isotope. Therefore, some of the following assignments are considered tentative.

Table III

Correlation of vibrational frequencies of $CH_2D_{(a)}$ with those of $CH_{3(a)}$

$CH_{3(a)}$, C_{3v}			$CH_2D(a)$, C_s			CH_2DI,C_s
Vib. Mode	Symmetry	Frequency	Vib. Mode	Symmetry	Frequency	Frequency[a]
ν_d	E	2730	$\nu_a(CH_2)$ ν(C-D)	A" A'	2680 2012	3057 2241
ν_s	A_1	2655	$\nu_s(CH_2)$	A'	2650	3002
δ_d	E	1320	$\rho_t(CH_2)$ $\delta_b(N_i$-C-D)	A" A'		1240 710
δ_s	A_1	1220	$\delta_s(CH_2)$	A'	1350	1415
ρ_d	E	965	$\rho_\omega(CH_2)$ $\rho_r(CH_2)$	A' A"	1120 970	1175 862
R_z	A_2	485		A"	485	
ν_s(Ni-C)	A_1	385		A'	385	518

[a] Ref. 20,25

The most prominent new feature in the loss spectrum of Fig. 5a measured at the specular angle is a loss at 1120 cm^{-1}. This feature decreases substantially in intensity as the detection angle is moved away from the specular angle as shown in Fig. 5b. By analogy to the frequencies of the model compound CH_2DI also shown in Table III [20,25], this feature is assigned to the -CH_2 wag mode (ρ_ω) of a' symmetry. The feature at 1230 cm^{-1} is assigned to a superposition of the dipole active deformation mode δ_s of CH_3 and the non-dipole active twist mode (ρ_t) of -CH_2 in CH_2D. This assignment was made based on the increased width of this loss feature compared to the one at 1220 cm^{-1} in Fig. 2a and the smaller angular dependence of the intensity of this loss feature compared to that for the loss feature at 1220 cm^{-1} in Fig. 2b. The feature at 1320 cm^{-1} is the asymmetric deformation mode δ_d of -CH_3 while the feature at 1350 cm^{-1}, which is barely resolvable from the feature at 1320 cm^{-1}, is assigned to the dipole active scissors mode (δ_s) of CH_2 in CH_2D. The broad feature centered at 970 cm^{-1} is a superposition of the rocking mode ρ_d of CH_3, the dipole active D-C bending mode (δ_b) in CH_2D and the non-dipole active rocking mode (ρ_r) of CH_2 in CH_2D. The torsional modes R_z are at 485 cm^{-1} for CH_3 and at 440 cm^{-1} for CH_2D. The broad feature at about 2660 cm^{-1} is the superposition of the C-H symmetric ν_s and asymmetric stretching vibration ν_d or ν_a of CH_3 and CH_2D, while the new feature at 2015 cm^{-1} is the C-D stretching vibration ν(C-D).

Because the relative amounts of adsorbed CH_2D and CH_3 produced by CH_3D dissociation will be an important issue in the analysis of the thermal decomposition of the adsorbed methyl radical, a few words are appropriate here. The most intense feature in the spectrum in Fig. 5a is that belonging to the dipole active ρ_ω mode of the CH_2D species at 1120 cm^{-1}. The second most intense feature is that at 1230 cm^{-1} which is a superposition of the nondipole active ρ_t mode of CH_2D and the dipole active δ_s mode of CH_3. If it is assumed that the intensity of the feature at 1230 cm^{-1} is solely due to the dipole active δ_s mode of CH_3 and that the dynamical dipole moments of the ρ_ω mode of CH_2D and the δ_s mode of CH_3 are equal, then from the ratio of intensities of the loss features at 1120 cm^{-1} and 1230 cm^{-1} in Fig.

5a, there is twice as much CH_2D on the surface as there is adsorbed CH_3. In reality, the amount of CH_2D is much larger because the intensity of the feature at 1230 cm^{-1} does not solely arise from the CH_3 species and because the dynamical dipole moment of wag modes such as the ρ_ω mode in CH_2D is usually smaller than those of symmetric deformation modes such as ν_3 in adsorbed CH_3 [19,20]. Therefore, a value of 2 for the ratio of adsorbed CH_2D to adsorbed CH_3 produced by CH_3D dissociative chemisorption is a lower limit.

2. The C-H Stretching Region and Fermi Resonance

The C-H stretching region (2400-3300 cm^{-1}) of adsorbed CH_3 exhibits four loss features: 2430, 2610, 2655 and 2730 cm^{-1}. The lowest frequency and least intense feature at 2430 cm^{-1} is assigned as the overtone of the symmetric deformation mode δ_s at 1220 cm^{-1} because the intensity of this feature is low and because the anharmonicity is small as expected by analogy to methyl halides [21]. The remaining three loss features which are of comparable intensity cannot all be assigned as C-H stretches because only two C-H stretching vibrations are possible: a symmetric stretch mode ν_s and a degenerate asymmetric stretch mode ν_d. Instead, this region of the spectrum exhibits characteristics of a Fermi resonance which is a common interaction in molecules with CH_3 groups. The interaction occurs between the A_1 component of the overtone of $A_1 + E$ symmetry of the degenerate asymmetric deformation mode and the symmetric stretch mode which is of A_1 symmetry. The interaction is manifested by an increase in the intensity of the overtone because of intensity borrowing from the dipole allowed symmetric stretch and by frequency shifts in opposite directions of the two interacting vibrational states. For example, in CH_3Br(g), three vibrational transitions are observed in the 2850-3100 cm^{-1} region. Two of the transitions at 2862 and 2972 cm^{-1} are observed with comparable intensities both in the IR and Raman spectrum [22,23] and are assigned to the overtone of the asymmetric deformation mode δ_d and the fundamental of the C-H symmetric stretch mode ν_s in Fermi resonance, respectively. The frequency of the C-H symmetric stretch mode is shifted up from its frequency of 2935 cm^{-1} without resonance and the overtone is shifted down from twice (2886 cm^{-1}) the fundamental of the asymmetric

deformation mode ν_d at 1443 cm^{-1}. The C-H asymmetric stretch mode ν_d is observed as a transition at 3056 cm^{-1}.

Similar assignments can be made for CH_3 adsorbed on Ni(111). The loss features in Fermi resonance corresponding to those vibrational transitions in CH_3Br occur at 2610 and 2655 cm^{-1}. The degenerate asymmetric C-H stretch mode ν_d is assigned to the loss feature at 2730 cm^{-1}. The involvement of a Fermi resonance is supported by several observations. First, the frequency of the overtone of the asymmetric deformation mode δ_d without Fermi resonance, which is estimated as twice the fundamental frequency to be 2640 cm^{-1} with little anharmonicity, occurs at a frequency intermediate to the frequencies of the observed loss features. This observation indicates that the overtone is indeed shifted down in frequency by the repulsive interaction of a Fermi resonance. Secondly, the two loss features exhibit similar intensities and similar dependences on the incident electron energy and scattering angle as they should if intensity borrowing is occurring [23].

Isotopic substitution does not guarantee that a Fermi resonance remains operative. However, it is clear by comparison of the spectrum of adsorbed CH_3 to that of adsorbed CD_3 (Fig. 4) that the structure of the C-D stretch region is similar and that the involvement of a Fermi resonance is likely. Four loss features are again observed: 1815, 1925, 1955 and 2030 cm^{-1}. By analogy to the spectrum of adsorbed CH_3, the feature at 1815 cm^{-1} is assigned to the overtone of the symmetric deformation mode δ_s while the feature at 2030 cm^{-1} is assigned to the asymmetric C-D stretch mode ν_d. The vibrational transitions corresponding to the loss features at 1925 and 1955 cm^{-1} are in Fermi resonance and are assigned to the overtone of the asymmetric deformation mode δ_s and the symmetric C-D stretch mode ν_d, respectively.

Support for these assignments comes from the frequency (2015 cm^{-1}) of the feature assigned to the C-D stretching mode ν(C-D) in adsorbed CH_2D as shown in Fig. 5. When two deuterium atoms of a CD_3 group are replaced by hydrogen atoms, the frequency of the C-D stretching mode of the resulting CH_2D group is at a value intermediate between those of

the symmetric and asymmetric C-D stretching vibrations in a CD_3 group. More specifically, the C-D stretch frequency in CH_2D should be approximately the weighted average of the frequencies of the CD_3 symmetric and asymmetric stretch mode [20,24,25]. For example, in $CD_3Br(g)$ the symmetric and asymmetric C-D stretch modes have frequencies of 2160 and 2297 cm^{-1}, respectively, while the C-D stretch mode in $CH_2DBr(g)$ has a frequency of 2244 cm^{-1}. It is clear that the same situation is obtained for CD_3 adsorbed on Ni(111). Assuming that the frequency of the symmetric C-D stretch mode without perturbation by the Fermi resonance is the average frequency (1940 cm^{-1}) of the loss features at 1925 and 1955 cm^{-1} and given that the frequency of the asymmetric C-D stretch mode is 2030 cm^{-1}, then the frequency of 2015 cm^{-1} observed for the C-D stretch mode of adsorbed CH_2D is indeed an intermediate value as for the model compounds. A frequency of 2015 cm^{-1} is very close to the value of 2000 cm^{-1} predicted from the weighted average of the symmetric and asymmetric C-D stretch modes of adsorbed CD_3.

In summary, a Fermi resonance is responsible for the observation of three loss features of comparable intensity at 2730 (2030), 2655(1955), and 2610 (1925) in the C-H (C-D) stretch region of the spectra for $CH_3(CD_3)$ adsorbed on Ni(111). This observation of a Fermi resonance, which is a phenomenon common to molecules with CH_3 groups, is additional support for the identification of the nascent product of CH_4 dissociative chemisorption as an adsorbed methyl radical.

3. Why the Spectra are Inconsistent with CH_2, CH or C-C Bonded Species.

The above analysis has shown that the frequency and number of loss features in spectra of the nascent products of CH_4, CH_3D and CD_4 dissociation are consistent with adsorbed CH_3, CH_2D and CD_3, respectively. However, it is necessary to discuss briefly why other possible species, such as C-C bonded species, adsorbed CH and CH_2 are inconsistent with these data.

None of the loss features in Fig. 2 can be assigned as a C-C stretch vibration because all loss features with the exception of the feature at 385 cm^{-1} shift in frequency by a

Table IV

Vibrational frequencies of molecules containing CH_2 group.

Vib. Mode	CH_2Cl_2 [a]	CH_2CCl_2 [a]	CH_2 [b] / \ Fe–Fe	CH_2 [c] / \ Os–Os
ν_{as}	3040	3130	2976	2984
ν_s	2999	3035	2925	2935
δ_s	1467	1400	1379	1428
ρ_w	1268	875	978	961
ρ_r	898	1095	760	811
ρ_t	1153	686	936	869

[a] Ref. 22
[b] Ref. 37
[c] Ref. 38

substantial amount upon isotopic substitution. Although the loss feature at 385 cm^{-1} does exhibit only a small shift in frequency to 365 cm^{-1} upon isotopic substitution, the frequency of this mode is too low to be assigned to a C-C stretch mode which is expected to have a frequency above 900 cm^{-1}. Rather, it has been assigned to the Ni-CH_3(Ni-CD_3) stretch mode.

The possibility of an adsorbed CH species as the nascent product can also be excluded readily based on the large number of loss features observed in the spectra. An adsorbed CH species can have at most three vibrational loss features associated predominantly with hydrogen motion whereas at least six fundamental vibrational loss features are observed in Fig. 2. Another observation inconsistent with the assignment of the spectra to an adsorbed CH species are the vibrational spectra measured after exposure to energetic CH_3D (Fig. 5). These spectra would have to appear as a superposition of the spectrum of a CH species produced by exposure to energetic CH_4 and a spectrum of a CD species produced by exposure to CD_4. As discussed above, the spectrum measured after exposure to CH_3D is a completely new spectrum and is not a superposition of spectra resulting from CH_4 and CD_4 dissociative chemisorption. Clearly, the spectra in Figs. 2-5 are inconsistent with an adsorbed CH species. A spectrum which can be appropriately assigned to a CH species will be discussed below.

An adsorbed CH_2 species is the principal competition to the assignment of the spectra to an adsorbed CH_3 species. In the above discussion, it is concluded that because the Ni-C vibrational mode exhibits a strong dynamical dipole moment, the Ni-C bond is normal to the macroscopic plane of the Ni surface. If this is the case, then the scissors mode of an adsorbed CH_2 is a dipole active vibration, regardless of the adsorption site or orientation of the hydrogen atoms. The only loss feature in a reasonable frequency range which exhibits dipolar scattering and which mainly involves hydrogen motion is the feature at 1220 cm^{-1}. However, in comparison to the frequencies of the scissors mode of several model compounds which range from 1350-1500 cm^{-1} as shown in Table IV, a frequency of 1220 cm^{-1} is too

low for a reasonable assignment to a scissors mode to be made. In addition, for all known molecules containing a CH_2 group and those shown in Table IV, the scissors mode is the highest frequency vibration of the C-H bond bending modes. Yet the spectra in Fig. 2 clearly show a non-dipole active mode at 1320 cm^{-1}. Given that an adsorbed CH_2 species provides no reasonable assignment for this loss feature and that the frequency of the dipole active mode is too low to be assigned to a scissors mode, the assignment of the spectra to a CH_2 species with the Ni-C bond perpendicular to the surface is rejected.

It remains to consider structures of adsorbed CH_2 in which the Ni-C bond is not normal to the macroscopic plane of the surface. Tilting of the plane of the adsorbed CH_2 lowers the symmetry of the point group from C_{2v} or C_2 to C_s or C_1. The lower symmetry implies that at least six of the nine vibrational modes of the adsorbed CH_2 are dipole active. However, it is clear from the spectra in Fig. 2 that at most three modes are dipole active. Based on the small number of dipole active modes, a tilted CH_2 species as the nascent product of CH_4 dissociative chemisorption is also rejected.

4. The Structure of Adsorbed CH_3 on Ni(111)

As discussed above, the symmetry of the methyl radical adsorbed on Ni(111) was determined to be C_{3v}. Adsorption of CH_3 on either the on-top or threefold hollow sites satisfies the symmetry requirement. Adsorption of CH_3 on the on-top site might be expected because this site satisfies the carbon valence with the fewest bonds. If this is the case, then the frequency of the Ni-C stretch mode should be similar to that of these modes in Ni-organometallic complexes where the CH_3 ligand is bound to a single Ni atom. The frequencies of Ni-C stretch modes in organometallic compounds such as $L_2Ni(CH_3)_2$ and L_2NiCH_3X where L = $(CH_3)_3P$ and X=Cl, Br or I are approximately 500 cm^{-1} [26]. Based on this comparison, the frequency of the Ni-C stretch mode at 385 cm^{-1} is too low for CH_3 to be adsorbed at an on-top site. Therefore, a threefold hollow site is chosen as the adsorption site for CH_3 on Ni(111). This is in agreement with several recent calculations which have found that the threefold site is the most energetically favorable binding site for CH_3 on Ni(111) [27-

31]. Unfortunately, the vibrational spectra do not provide information about the orientation of the hydrogen atoms. The hydrogen atoms may point toward the three nearest on-top sites or they may point toward the bridge sites. Either configuration satisfies the C_{3v} symmetry requirement. A configuration where the hydrogen atoms point to the on-top sites has been calculated to be the more stable configuration [31].

An interesting aspect in the spectra of the adsorbed CH_3 radical is the very low frequency (~2650 cm^{-1}) of the C-H stretch modes compared to that expected (~3000 cm^{-1}) for sp^2 or sp^3 hybridization. Such low frequency or "soft" C-H modes have been observed previously for fairly large hydrocarbons adsorbed on transition metal surfaces [6,16,17]. They have also been observed as three center, two electron metal-H-C bonds in organometallic complexes and have been termed agostic bonds [33]. These bonds arise from interaction of the hydrogen with the metal, thereby resulting in a partial depletion of electron density in, and a weakening of, the C-H bond. Such a direct interaction between the hydrogens and the metal has been demonstrated in a Hückel molecular orbital calculation for CH_3 adsorbed on Ni(111) [27]. However, a more recent but identical calculation [29] as well as other more sophisticated calculations [31] have failed to show a sufficiently strong interaction between the hydrogens and the Ni atoms to account for the substantial lowering of the frequency of the C-H stretch modes. One theoretical study of the chemisorption of CH_3 on Ni clusters suggests that the low frequency of the C-H stretch mode arises from charge transfer from the metal into the C-H antibonding orbitals [30]. Whatever the exact origin of the low frequency C-H modes, it is clear from the spectra that the three hydrogen atoms are equivalent. The equivalency of the hydrogens provides further support for an adsorbed CH_3 with the C_3 axis normal to the surface.

IV. The Dissociation Product of Adsorbed CH_3

A. Results

The chemistry of the adsorbed CH_3 radical is determined by monitoring the vibrational spectrum of an adsorbed layer of CH_3, synthesized by the procedure described in the

previous section, as a function of surface temperature. The CH_3 dissociation product is produced by raising the temperature of the surface initially covered with 0.05 ML of CH_3 from 80 K to 220 K with a heating rate of 20 K s^{-1} and cooling it to 80 K. Heating of the crystal is generally carried out by bombardment of the back side of the crystal with 600 V electrons. In some cases, radiative heating of the back side of the crystal with no electron bombardment was used to raise the crystal temperature. The observation of the independence of the spectra on the heating method ensures that the dissociation of the adsorbate is not electron-beam induced. The vibrational spectra of the CH_3 dissociation product are measured without first measuring the spectrum of adsorbed CH_3 in order to minimize adsorption of contaminants from the ambient background pressure. The spectra measured at the specular angle and at 10^o away from the specular angle with an incident electron energy of 5 eV are shown in Fig. 6. Although these spectra were measured after heating the surface to 220 K, it should be noted that the dissociation of CH_3 takes place slowly at temperatures as low as 150K as evidenced by the disappearance of the characteristic loss features in Fig. 2 and the slow appearance of the features associated with the spectra in Fig. 6. No other spectra are detectable between the 150-220K range of temperature. What is immediately obvious from the spectra in Fig. 6 is that the intensities of the loss features measured at the specular angle are very weak. It appears that none of the vibrational modes associated with these loss features has an appreciable dynamical dipole moment. This fact will make the assignment of the spectra to a species with a well-defined structure difficult. At an off-specular angle, however, three intense loss features at 650, 1275 and 2970 cm^{-1} belonging to the hydrocarbon species and two loss features attributed to the Ni-H vibrational modes at 770 and 1100 cm^{-1} are clearly observed. The loss features associated with the Ni-H modes are significantly more intense in this spectrum than those in the spectrum of the CH_3 species indicating that there is a larger amount of atomically adsorbed hydrogen. By careful background measurements, it has been established that the loss features at 1750 cm^{-1}, 550 cm^{-1} and 400 cm^{-1}, which are most visible at the specular angle, are due to small amounts of

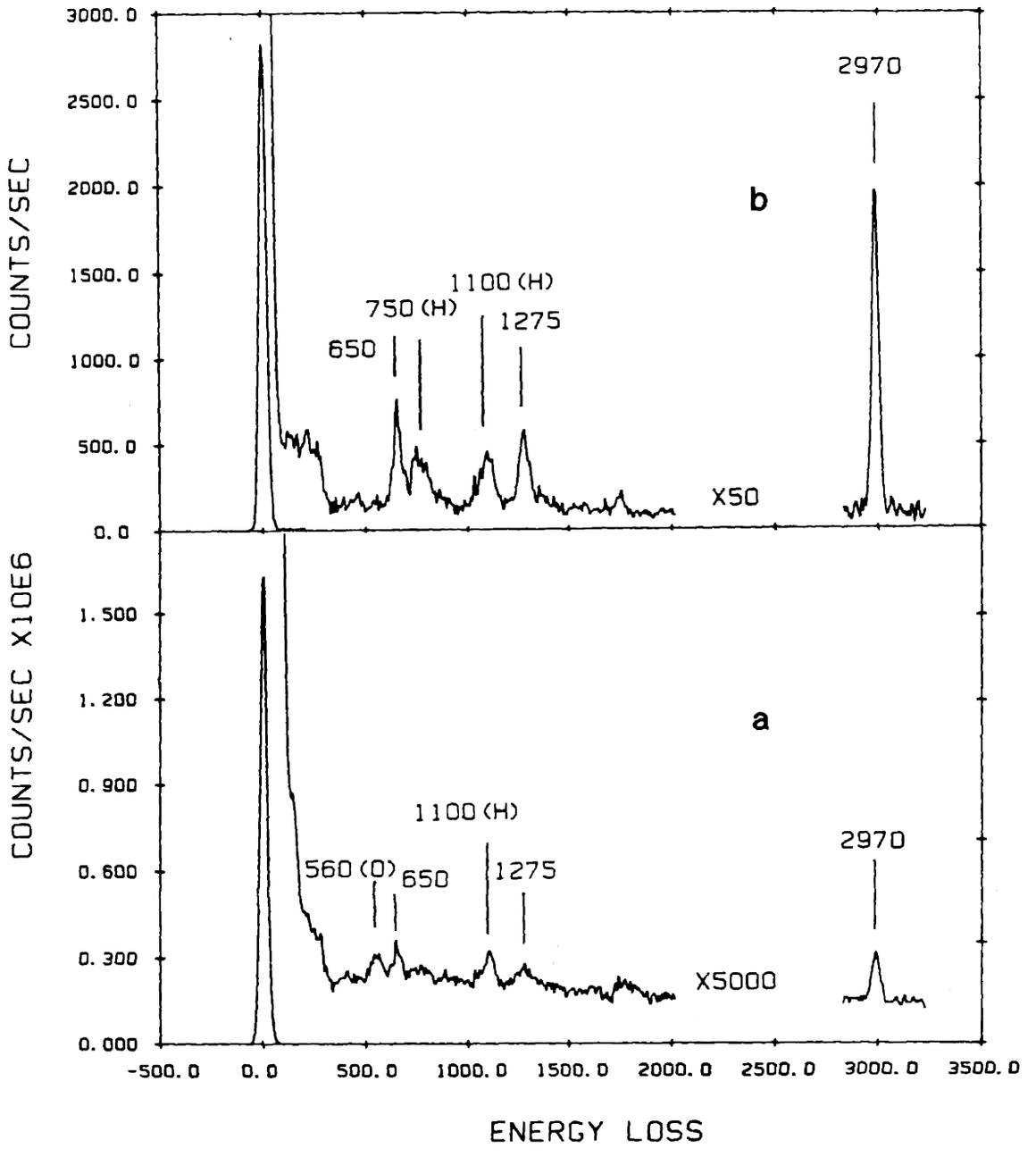

Figure 6. HREEL spectra after raising the surface temperature to 220 K following the dissociation of CH_4 under conditions similar to those for Figure 2. The coverage is 0.05 ML. The ΔE_{FWHM} of the elastic feature is 40 cm^{-1} with 8 cm^{-1}/channel. The spectra were measured at 80 K in the (a) specular and (b) 10° off-specular direction with 5.0 eV impact energy. The spectra are assigned to an adsorbed CH on Ni(111) that forms when the adsorbed CH_3 dissociates.

CO and O contaminants. The feature at 260 cm^{-1} is a surface phonon but no attempt to resolve it from the frustrated translations below 300 cm^{-1} is made here.

The corresponding spectra of the dissociation product of CD_3 are shown in Fig. 7. A substantial kinetic isotope effect associated with the thermal decomposition of CD_3 is clear from the higher temperature and longer time necessary to produce the dissociation products of CD_3. The procedure of ramping the temperature of the surface from 80 K to 240 K must be repeated 5-7 times before the loss features characteristic of CD_3 disappear and those of the dissociation product appear. The observed isotope effect is evidence that the conversion of CH_3 to its dissociation product involves C-H(C-D) bond breaking. There are three loss features associated with the deuterated hydrocarbon product: the feature at 2220 cm^{-1} corresponds to the feature at 2970 cm^{-1} in the spectrum of the hydrogen substituted species, the feature at 930 cm^{-1} corresponds to 1275 cm^{-1} and the feature at 630 cm^{-1} corresponds to the feature at 650 cm^{-1}. The features at 570 cm^{-1} and 800 cm^{-1} arise from the fundamental Ni-D vibrational modes while the features at 1030 cm^{-1} and 1075 cm^{-1} are the overtone modes of the Ni-D modes. The loss features at 400 cm^{-1} and 1800 cm^{-1} are again the result of small amounts of CO contamination.

The corresponding spectrum measured for the incident, energetic CH_3D isotopic variant is shown in Fig. 8. Only the spectrum measured in the off-specular direction is shown here. This spectrum is congested and complicated because it is a mixture of the dissociation products of adsorbed CH_2D and CH_3. However, upon careful inspection, it is clear that this spectrum is simply the superposition of the spectra of the CH_3 dissociation product in Fig. 6b and of the CD_3 dissociation product in Fig. 7b. The features at 2970, 1280 and 650 cm^{-1} are identical to those of the CH_3 dissociation product while the features at 2220, 930 and 630 cm^{-1} are identical to those of the CD_3 dissociation product. The feature of 550 cm^{-1} is the Ni-D vibrational mode, the broad feature at 750-800 cm^{-1} is the superposition of the Ni-D and Ni-H vibrational modes and the feature at 1030-1120 cm^{-1} is the superposition of the Ni-H vibrational mode and the overtone of the Ni-D vibrational mode.

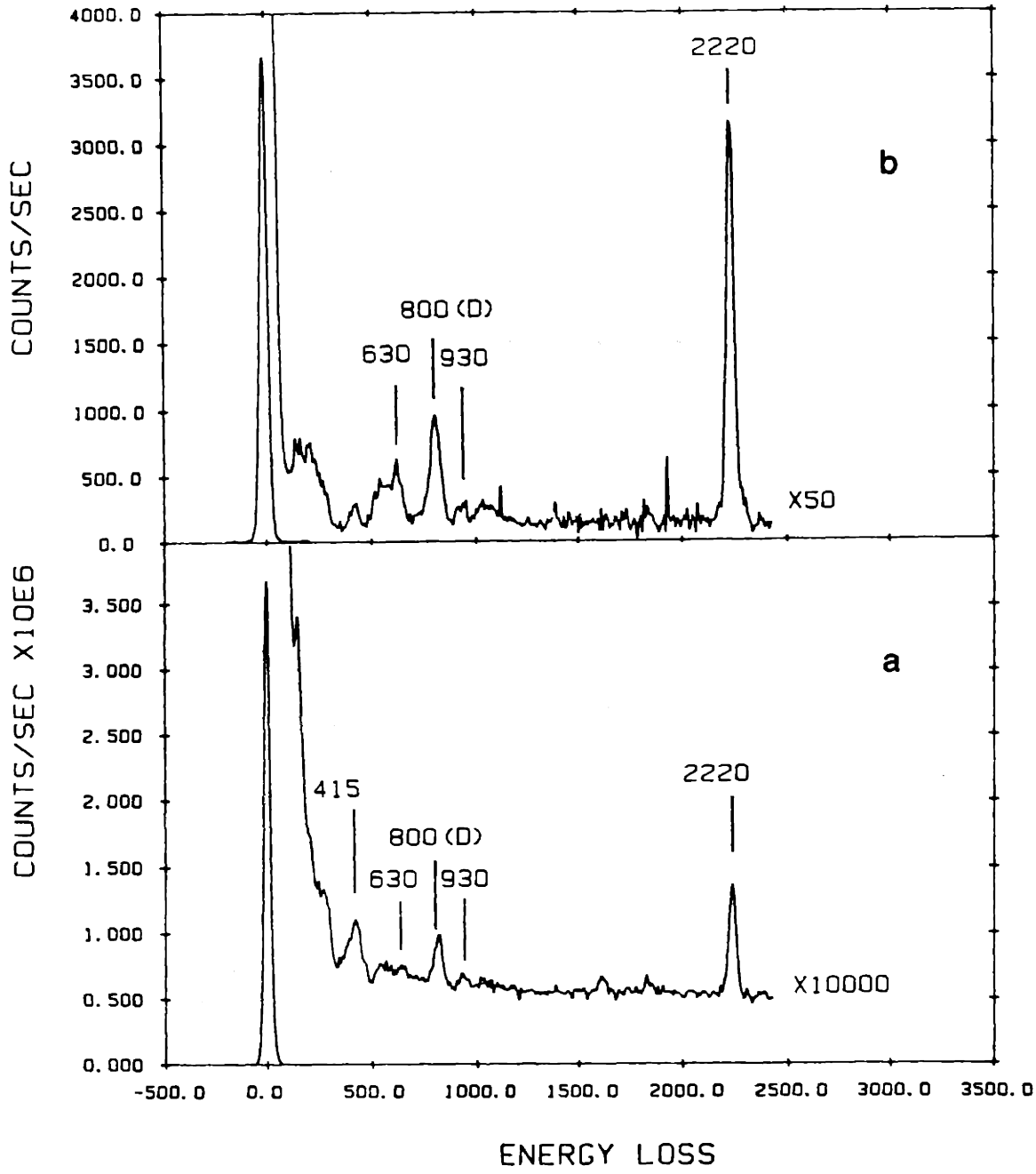

Figure 7. HREEL spectra after raising the surface temperature 5 times from 80 K to 240 K following the dissociation of CD_4 under conditions similar to those for Figure 4. The spectra were measured at 80 K in the (a) specular and (b) 10° off-specular direction. The spectra are assigned to those of an adsorbed CD on Ni(111) that forms when the adsorbed CD_3 dissociates. A kinetic isotope effect of the CH_3 and CD_3 dissociation requires the multiple annealing to 240 K.

The spectrum in Fig. 8 is crucial to the positive identification of the product of the thermal decomposition of adsorbed CH_3.

B. Discussion

1. Identification of Adsorbed CH

The vibrational spectrum of adsorbed CH_3 begins to disappear slowly as the surface temperature is increased to 150 K and is completely gone when the surface temperature is raised rapidly to 220 K. In its place is a new spectrum which will be assigned in this section to that of an adsorbed CH species.

The vibrational spectrum of the newly formed species is characterized by three loss features at 2970(2220), 1275(930) and 650(630) cm^{-1}. The identity of the species can easily be narrowed to that of a CH_2 or CH species because none of the loss features can be associated with a C-C stretch mode. Although the small frequency shift of the loss feature at 650 cm^{-1} to 630 cm^{-1} upon deuteration indicates that this vibrational mode predominantly involves carbon motion, the magnitude of the frequency is too low for assignment to a C-C stretch mode as discussed in the assignment of the CH_3 spectra.

There are two observations that unequivocally identify the dissociation products of CH_3 and CD_3 as adsorbed CH and CD, respectively. First, the loss feature assigned to the C-H(C-D) stretch mode at 2970(2220) cm^{-1} is as narrow in frequency as the incident electron beam whose full width at half maximum is about 35 cm^{-1}. Therefore, to within the 20 cm^{-1} capability of this experiment to distinguish two loss features of equal intensity, only one CH(C-D) stretch mode is present. This observation immediately rules out the presence of a CH_2 species because CH_2 has two C-H stretch modes, a symmetric and an asymmetric stretch mode. It may be argued that the difference in frequency of these two modes is smaller than the resolution of this experiment. However, the frequency difference between the symmetric and asymmetric C-H modes in CH_2 groups is typically appreciably greater than the resolution of this experiment. Regardless of the hybridization, the symmetric and antisymmetric C-H stretch modes are separated by 40-100 cm^{-1} as shown for a wide range of

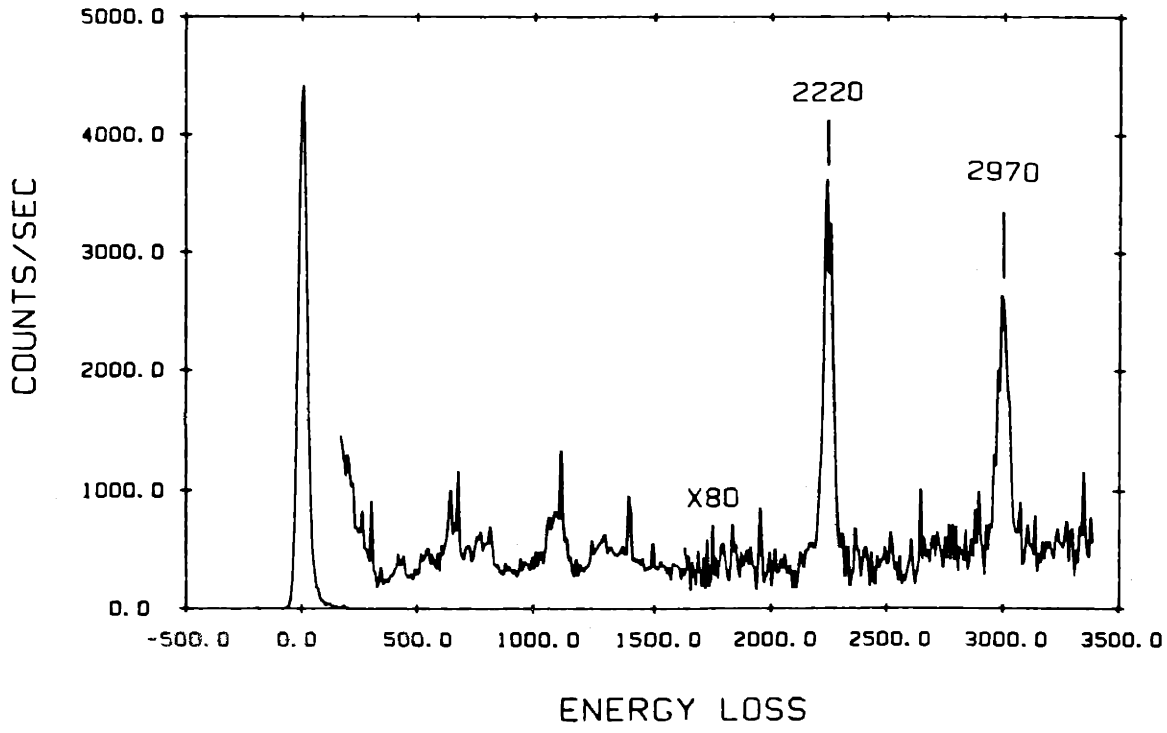

Figure 8. HREEL spectrum after annealing the surface for 50 sec at 240 K following the dissociation of CH_3D at a surface temperature of 80 K under conditions similar to those for Figure 5. Only the spectrum measured in the 12° off-specular direction is shown. The impact energy is 4.0 eV. The spectrum is a superposition of those of CH and CD adsorbed on Ni(111).

compounds in Table I and IV. The corresponding frequency difference for C-D stretch modes is greater than 100 cm^{-1} [22]. Consequently, the structure of the C-H stretch region of the spectra cannot be interpreted as that of a CH_2 species.

The second piece of very strong evidence against the assignment of the spectra to a CH_2 species is the identical frequency of the C-D stretch in the vibrational spectrum derived from CH_3D and shown in Fig. 8 to that derived from CD_4 shown in Fig. 7. If the mixture of adsorbed CH_3 and CH_2D thermally decomposed by loss of a single H or D, a mixed layer of CH_2 and CHD would be formed. Regardless of the relative population of the two isotopically different species, the C-D stretch mode would have to originate from the CHD species. It is known that the frequency of the C-D stretch mode in a CHD group is shifted from the frequency of the symmetric or asymmetric stretch mode of the corresponding CD_2 group [22]. In general, the frequency of a C-D stretch mode in CHD is approximately the average of the frequencies of the two C-D stretch modes in CD_2. For example, the frequencies of the symmetric and asymmetric C-D stretch modes in CD_2Cl_2 are 2205 and 2304 cm^{-1}, respectively, while the frequency of the C-D stretch mode in $CHDCl_2$ is 2249 cm^{-1} [22]. Therefore, if a CHD species were present, the frequency of this C-D stretch mode should be different from that observed for CD_2. Given that no frequency shift is observed between the species derived from CH_3D and that derived from CD_4, it is concluded that the species in Fig. 8 produced from the thermal decomposition of CH_2D and the species in Fig. 7 produced by the thermal decomposition of CD_3 are the same adsorbed species, CD. Similarly, the frequencies of the C-H stretch modes in the spectra resulting from the thermal decomposition of CH_3 and CH_2D are identical because they are due to the identical adsorbate, CH. The spectrum in Fig. 8 arises from an adsorbed layer of a mixture of CH and CD. It is simply the superposition of the spectra for CH in Fig. 6 and for CD in Fig. 7b.

The number of vibrational loss features that are observed is most consistent with the assignment of the spectrum to a CH species adsorbed at a site of C_{3v} symmetry with the C-H bond normal to the macroscopic plane of the surface. Such a species has four vibrational

modes: a C-H stretch mode of A_1 symmetry, a symmetric Ni-C stretch mode of A_1 symmetry, a doubly degenerate Ni-C-H bending mode of E symmetry and a doubly degenerate asymmetric Ni-C stretch of E symmetry. Three of the four modes are accounted for by the observed vibrational features. The vibrational loss features at 2970(2220) cm^{-1} and 1275(930) cm^{-1} are assigned as the C-H(C-D) stretch mode and the doubly degenerate Ni-C-H(Ni-C-D) bend mode, respectively. Based on the frequency, the vibrational loss feature at 650(630) cm^{-1} is assigned as the asymmetric Ni-C stretch mode.

Adsorption of CH at a site of lower symmetry, with a bent Ni-C-H geometry or with the Ni-C bond at a non-normal angle to the macroscopic surface would result in a breakdown of the degeneracy of the Ni-C-H bend mode and the asymmetric Ni-C stretch mode. Because only one Ni-C-H bend mode and one asymmetric Ni-C stretch mode are observed, it is concluded that the CH species is adsorbed with the Ni-C-H axis perpendicular to the surface at a site of C_{3v} symmetry.

2. The Structure of Adsorbed CH

On the basis of the number of observed loss features, it was concluded in the previous section that the linear Ni-C-H species has C_{3v} symmetry and that its axis is normal to the macroscopic surface. Adsorption on either the on-top or threefold hollow site satisfies the symmetry requirement. Adsorption on the on-top site requires that the hybridization of the carbon be almost of the sp type. This hybridization is inconsistent with the high frequency of the Ni-C-H bend mode at 1275 cm^{-1} and the low frequency of the C-H stretch mode at 2970 cm^{-1}. The frequencies of the C-H bend mode and C-H stretch mode for a sp hybridized carbon are more typically around 650 cm^{-1} and 3300 cm^{-1}, respectively. Therefore, on the basis of the incompatibility of the magnitude of these frequencies, an on-top adsorption site is rejected leaving the threefold hollow site as the adsorption site of choice. This conclusion for the bonding geometry is in agreement with the results of a recent calculation which showed that the most energetically favorable bonding configuration is a pyramidal Ni_3-C-H species adsorbed in a threefold hollow site [32].

The vibrational frequencies observed here are also in reasonable agreement with those of a CH ligand bound to three metal atoms in a trinuclear transition metal complex. In $H_3Ru_3(\mu_3\text{-}CH)(CO)_9$ [39] and $HCCo_3(CO)_9$ [40], the C-H stretch modes appear at 2990 and 3041 cm^{-1}, the M_3-C-H bend modes at 892 and 850 cm^{-1} and the two M_3-CH stretch modes at 425/670 and 420/715 cm^{-1}, respectively, as shown in Table V. The frequencies of the C-H bend mode in these complexes are significantly lower than those observed for CH adsorbed on Ni(111). However, it has been argued [40] that the low frequency of the C-H bend mode in $HCCo_3(CO)_9$ probably arises from the acute angle geometry at the apical carbon atom of $-CCo_3$. A more reasonable comparison may be one made to the frequencies of the modes of pyramidal molecules $CHCl_3$ or $CHBr_3$ also shown in Table V. The frequencies of the C-H bend modes in these molecules are 1216 cm^{-1} and 1142 cm^{-1}, respectively, which are in good agreement to the frequency of 1275 cm^{-1} observed for CH adsorbed on the threefold hollow site of Ni(111). The frequencies of the C-H stretch modes at 3019 and 3023 cm^{-1} in $CHCl_3$ and $CHBr_3$ and the halogen-carbon stretch modes at 550-760 cm^{-1} are also in reasonable agreement with the C-H stretch mode at 2970 cm^{-1} and the Ni-C stretch mode at 650 cm^{-1} for CH adsorbed on Ni(111).

This structure implies that two of the modes, the symmetric Ni-C stretch mode and the C-H stretch mode have A_1 symmetry and should be dipole active. However, it is clear that the intensities of the observed loss features do not decrease substantially as the detection angle is moved away from the specular angle. This does not necessarily imply that the proposed structure for CH is incorrect. Weak dipolar scattering can be the result of a small dynamical dipole moment as is very likely the case for the C-H stretch mode. The dynamical dipole moment of C-H stretch vibrations is known to be small [10]. However, a small dynamical dipole moment for a symmetric Ni-C stretch mode is not expected based on observations of intense and dipole active Ni-C loss features for many kinds of carbon containing adsorbates on Ni. A similar difficulty has been noted for NH_3 adsorbed on the threefold hollow sites on Pt(111) and Ni(111) [41,42] where no loss feature is observed that can be assigned as the

Table V

Comparison of vibrational frequency of $CH_{(a)}$ with molecules containing a CH group

Vib. Mode	Mode sym for C_{3v} group	$CH_{(a)}(CD_{(a)})$	$CHCl_3$ [a]	$CHBr_3$ [a]	$-Co_3CH$ [b]	$-Ru_3CH$ [c]
$\nu_{(C-H)}$	A_1	2970(2220)	3034	3042	3041	2988
$\delta_{(CH)}$	E	1275(930)	1220	1149	850	894
$\nu_a(M-C)$	E	650(630)	774	669	417	424
$\nu_s(M-C)$	A_1		680	541	715	670

[a] Ref. 22
[b] Ref.40
[c] Ref. 39

symmetric M-N stretch mode. It was argued that the nature of the threefold hollow site effectively screens the dynamical dipole resulting in little or no intensity in the M-N symmetric stretch loss feature. It is possible that the same effect is occurring for CH adsorbed in the threefold hollow site of Ni(111).

3. The Mechanism for the Dissociation of Adsorbed CH_3

The mechanism for the dissociation of adsorbed CH_3 to form adsorbed CH can be inferred from the data. The observation of a substantial kinetic isotope effect for the formation of adsorbed CH vs. CD from CH_3 or CD_3 implies a mechanism involving cleavage of the C-H bond such as in

$$Ni\text{-}CH_3 \rightarrow Ni\text{-}CH_2 + Ni\text{-}H \rightarrow Ni\text{-}CH + 2NiH$$

but the inability to detect the CH_2 species casts doubt on this mechanism. However, the dissociation of the isotopically substituted CH_2D species to equal amounts of CH and CD provides a straightforward rationale for the absence of a vibrational spectrum of CH_2.

Consider the dissociative chemisorption of CH_3D. In the previous section it was argued based on the measured isotope effect for CH_4/CD_4 dissociative chemisorption and on the relative intensities of the loss features associated with CH_2D to those of CH_3, that the dissociative chemisorption of CH_3D produces mostly adsorbed CH_2D. Because a large isotope effect is observed for the thermal decomposition of the adsorbed methyl radical, dissociation of CH_2D should produce predominantly CD if the dissociation mechanism were a one-step process with simultaneous cleavage of two C-H bonds. The same effect would be observed if the dissociation mechanism proceeded through a two-step process involving a CHD intermediate species that is more stable than the reactant CH_2D. It is clear however, from the similar intensities of the loss features arising from the C-H and C-D stretch modes that the amounts of adsorbed CH and CD are equivalent. The observation of an isotope effect in the rate of production of CH vs. CD and the observation of equivalent amounts of CH and CD are consistent only if the dissociation process occurs in two steps through a CHD intermediate that is either unstable to dissociation at the temperatures required to form CHD

from CH_2D or completely unbound. For example, the first step of the dissociation process, CH_2D to form CHD, gives rise to the kinetic isotope effect. However, because the CHD is unstable or unbound, the density of states of the newly formed CHD is so high that its dissociation to CH or CD occurs indiscriminately with respect to the isotope. Therefore, equal amounts of CH and CD are formed even though an isotope effect is observed in the rate of their formation.

This sequential, stepwise mechanism for the dehydrogenation of CH_3 to CH not only provides an explanation for what may seem contradictory observations but also provides an explanation for the inability to trap the CH_2 species. The CH_2 species is either unbound or unstable relative to the CH species at the temperatures required to form it from the dissociation of CH_3. This does not mean that CH_2 species can never be trapped on a Ni(111) surface but that CH_2 species must be adsorbed or synthesized on Ni in some way other than via the dissociation of CH_3. The relative stability of these C_1 hydrocarbon fragments is therefore concluded to be $CH_2 < CH_3 < CH$.

4. Comparison to Previous Results

A very different spectrum has been assigned to that of a CH species adsorbed on Ni(111) [43]. The CH species was reportedly produced by the annealing of a saturated layer of C_2H_2 to 450-500 K. Low coverages of C_2H_2 did not result in CH formation. A similar observation has been made on Pd [44]. The present study is in stark disagreement with the previous work. In fact, in the next section, the observation of the reaction of adsorbed CH to form C_2H_2 is discussed.

In an attempt to understand the previous results, a detailed study of the chemistry of C_2H_2 adsorbed on Ni(111) has been carried out [45] in this laboratory. This study showed that C_2H_2 at high coverage trimerizes to C_6H_6 and that the C_6H_6 then dehydrogenates and polymerizes to produce higher hydrocarbons in which the C_6 ring of benzene is preserved as the temperature is raised above 400 K. It was concluded that the spectrum previously attributed to CH on Ni(111) is actually due to the higher hydrocarbons produced when

benzene dehydrogenates and polymerizes [45,46]. A more recent study of the reactions of C_2H_2 on Pd also concluded that C_2H_2 does not dissociate by C=C bond cleavage to form CH [47].

V. Recombination of CH to Form C_2H_2

A. Results

When further annealing is carried out by raising the temperature above 300 K following the formation of CH on the surface, another species is observed which is represented by the vibrational spectra shown in Figure 9a and 9b. Figure 9c is a spectrum of C_2H_2 on Ni(111) which is measured after the surface is exposed to 1.5 L of C_2H_2 at room temperature. The coverage for the spectrum of Figure 9c determined by measurement of the carbon Auger signal is 0.2 ML which is the number of C_2H_2 molecules per Ni atom. The adsorption of C_2H_2 on Ni(111) has been studied extensively and C_2H_2 is known to be adsorbed on the surface molecularly forming a di-σ bond with the Ni atoms [48]. It is clear that adsorbed C_2H_2 is the newly formed species from the adsorbed CH species when a comparison is made between the vibrational spectra obtained after annealing CH on the surface and the C_2H_2 vibrational spectrum. The coverage for the spectrum of Figure 9b is about 0.2 ML which is the same as the one for Figure 9c. The coverage for the spectrum of Figure 9a is lower at 0.03 ML but the species is the same; an adsorbed C_2H_2 whose vibrational spectrum is characterized by a C-C stretch mode at about 1200 cm^{-1} [48]. It should be noted that while a vibrational loss feature for the Ni-H symmetric stretch at 1100 cm^{-1} is observed in the spectrum of Figure 9a, there is no longer atomic hydrogen on the surface when the spectrum of Figure 9b is measured. This is because the temperature is different at which the surface is annealed before the two spectra are measured. The spectrum of Figure 9a is measured after the surface is annealed for 30 sec at 320 K which is just below the hydrogen desorption temperature of about 370 K. The annealing temperature for the spectrum of Figure 9b is slightly higher at 380 K so that hydrogen desorption has already taken place. The disappearance of CH and the formation of C_2H_2 is also observed at

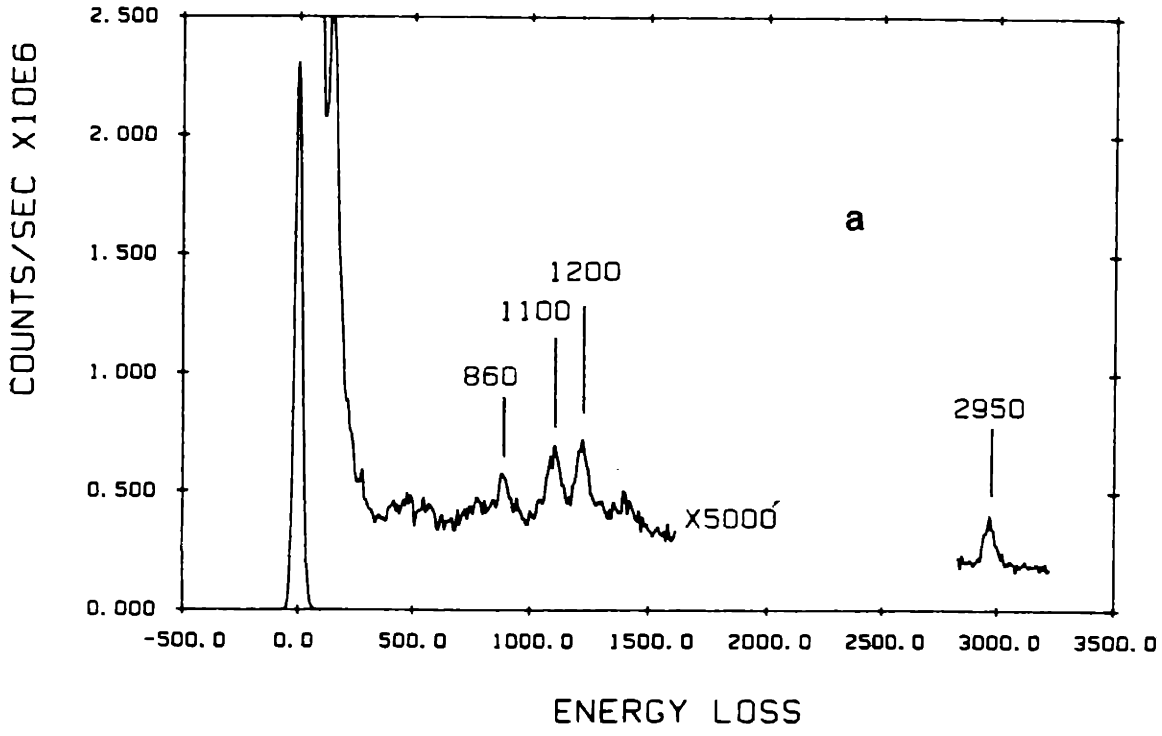

Figure 9. HREEL spectrum (a) after annealing the surface for 30 sec at 320 K following the dissociation of CH_4 under conditions similar to those for Figure 2. The coverage is 0.03 ML. The feature at 1100 cm^{-1} is due to a hydrogen vibrational mode on the surface; (b) after raising the surface temperature to 380 K following the dissociation of CH_4 by Kr incident with 80 kcal/mole kinetic energy. The coverage is 0.2 ML. The high coverage is achieved by a multiple exposure scheme describe in the text; (c) after the adsorption of 0.2 ML of C_2H_2. All three spectra were measured at 80 K in the specular direction with 4.0 eV impact energy. The spectra demonstrate the formation of C_2H_2 from adsorbed CH.

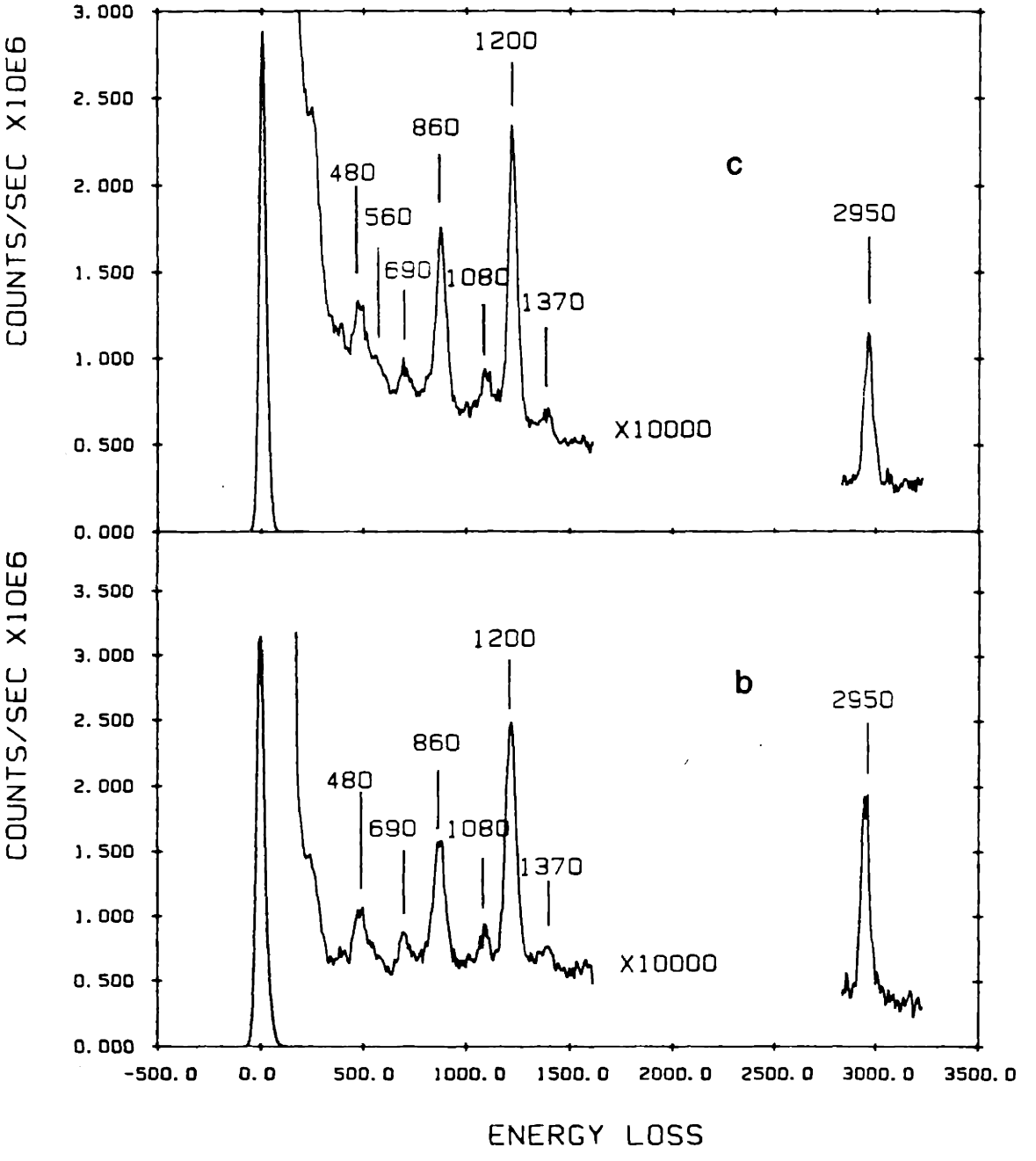
COUNTS/SEC X10E6
3.000
2.500
2.000
1.500
1.000
0.500
0.000
1200
860
480
560
690
1080
1370
c
2950
X10000
COUNTS/SEC X10E6
3.500
3.000
2.500
2.000
1.500
1.000
0.500
0.000
1200
b
2950
860
480
690
1080
1370
X10000
-500.0
0.0
500.0
1000.0
1500.0
2000.0
2500.0
3000.0
3500.0
ENERGY LOSS

temperatures as low as 250 K but the reaction is much slower. It is a significant observation that a C_2 species has been synthesized begining from CH_4, a C_1 species.

The C_2H_2 that gives rise to the spectrum in Figure 9a, is derived from CH_4 whose dissociative chemisorption has been effected by translational activation using a CH_4/He molecular beam as described above in the experimental section. The spectrum of Figure 9b is derived differently in that the initial dissociation of CH_4 is by the collision induced dissociation of physisorbed CH_4 by energetic inert gas atoms. The collision induced dissociation of physisorbed CH_4 is a new dissociation mechanism that was first observed in this lab [3-5]. The technique involves maintaining a monolayer of physisorbed CH_4 by keeping the surface temperature at 47 K and a CH_4 background pressure of $4x10^{-6}$ torr and bombarding the physisorbed CH_4 with energetic inert gas atoms of kinetic energy in the range of 20-120 kcal/mole. The energetic inert gas atoms are from a supersonic beam of a gas mixture of Ar, Kr, or Xe seeded in He. The impact of the energetic atoms on the physisorbed CH_4 causes the dissociation. It is necessary to maintain a background CH_4 pressure because a competing process, collision induced desorption [49], simultaneously takes place at a faster rate and depletes the physisorbed CH_4. The adsorption of molecular CH_4 from the $4x10^{-6}$ torr background pressure is sufficient to compensate for the depletion of physisorbed CH_4 due to the collision induced desorption so that a constant coverage of one monolayer can be maintained. Without this ambient pressure of CH_4 gas, it would not be possible to accumulate enough carbon on the surface to observe this dissociation mechanism. The inert gas atom used in the present experiment is Kr with a kinetic energy of about 80 kcal/mole produced from a 0.5% Kr/He beam expanded from a nozzle temperature at 900 K. A multiple exposure scheme is necessary to obtain the high carbon coverage 0.2 ML ($n_{C_2H_2}/n_{Ni}$) for the spectrum in Figure 9b because the dissociation of CH_4 on Ni(111) saturates at a fairly low coverage. The multiple exposure scheme involves dissociating CH_4 and then cycling the surface temperature to about 380 K and lowering the temperature back to 47 K for more dissociation.

This process is repeated until a desired coverage is reached. The 0.2 ML coverage for the spectrum of Figure 9b is obtained after four cycles of exposure. It is very likely that the accumulation of hydrogen on the surface causes the dissociation probability of CH_4 to decrease drastically and is thereby responsible for the low saturation coverage. The role of hydrogen may be to block the site on which CH_4 dissociates or increase the CH_4 dissociation barrier by changing the CH_4-surface potential energy surface. Raising the surface temperature to 380 K desorbs the hydrogen on the surface so that further dissociation of CH_4 on the surface can take place.

B. Discussion

It is clear that the surface chemistry of the adsorbed CH on Ni(111) is to combine to form an adsorbed C_2H_2 when the surface is raised to slightly higher than room temperature. It is known through extensive studies that C_2H_2 is adsorbed on Ni(111) molecularly and forms a di-σ bond with the surface. The vibrational assignment of C_2H_2 of Reference 48 is reproduced in Table VI. No desorption has been observed of species other than H_2 below 380 K. This along with the fact that only C_2H_2 is observed on the surface indicates that the formation of C_2H_2 is the sole pathway of CH reaction on Ni(111). The observation of the reaction of CH on the surface to form C_2H_2 at temperatures as low as 250 K and at coverages as low as 0.03 ML reflects the stability and reactivity of the CH species on Ni(111). It is an interesting and important finding that CH, a C_1 species combines to produce C_2H_2, a higher hydrocarbon instead of falling apart. All previous research of hydrocarbon reactions on well characaterized metal surfaces has been on the C-C bond breaking rather than C-C bond formation. Although C-C bond formation is the basis of Fisher-Tropsch synthesis of hydrocarbons over metal catalysts, this is the first time that a process of C-C bond formation has been identified by a spectroscopic technique. That C-C bond formation can take place at room temperature is important for our understanding of heterogeneous catalysis. The practical implication of the observation is in the utilization of natural gas to produce useful chemicals.

Table VI.

Assignment of modes for C_2H_2 on Ni(111)[a].

C_2H_2	C_2D_2	ν_H/ν_D	Mechanism	Mode
2920	2190	1.33	non dip	ν_{CH}
1370	1090	1.26	dip	δ_{CH}(as)
1220	1190	1.03	dip	ν_{CC}
1080	890	1.21	dip	δ_{CH}(s)
860	640	1.34	dip	γ_{CH}((as)
690	540	1.28	dip	γ_{CH}(s)
560	?		dip	ν_{Ni-C}
480	460	1.04	dip	ν_{Ni-C}

[a] Ref. 48

VI. Synthesis of C_6H_6

A. Results

Will the adsorbed C_2H_2 react to form higher hydroacarbons, now that the adsorbed CH is observed to form C_2H_2 in a C-C bond linking process? Different from the reaction of CH to form C_2H_2, the surface chemistry of C_2H_2 depends very much on the coverage when the surface is annealed to a higher temperature. At low coverage of C_2H_2 complete dehydrogenation takes place when the surface is annealed to 400 K. This is shown in Figure 10 which is a vibrational spectrum measured after the formation of 0.03 ML of C_2H_2, whose vibrational spectrum is shown in Figure 9a, and annealing at 400 K for 30 sec. No hydrocarbon is left on the surface and no desorption of any molecule other than H_2 is observed, indicating that C_2H_2 dehydrogenates completely.

However, a completely different vibrational spectrum is observed at higher C_2H_2 coverages. Figure 11a is a vibrational spectrum obtained after about 0.25 ML of C_2H_2 formed from the adsorbed CH is annealed at 395 K. This spectrum is very similar to the one shown in Figure 11b which is measured after adsorption of 0.10 ML of C_6H_6 on the surface at room temperature and annealing the surface at 400 K for 120 sec. In a study of C_6H_6 chemisorption reported in the next chapter, it is shown that C_6H_6 adsorption on Ni(111) is partially reversible. The annealing of the surface at 400 K for 120 sec causes partial desorption so that the coverage of C_6H_6 remaining on the surface is 0.08 ML when the spectrum of Figure 11b is measured. The hydrocarbon coverages for the two spectra of Figure 11a and 11b are the same if it is noted that the 0.08 ML coverage of C_6H_6 is equivalent to 0.24 ML coverage of C_2H_2. It is clear from the similarity of the spectra that C_2H_2 trimerizes to form C_6H_6 on the surface when the temperature is raised. Indeed the trend to form higher hydrocarbon continues with C_2H_2 but only at higher coverages. The trimerization fo C_2H_2, to form C_6H_6 on Ni(111), where the surface was exposed to molecular C_2H_2, has been proposed previously but the evidence was not conclusive [50].

The conclusive evidence for C_6H_6 formation and the important result is the

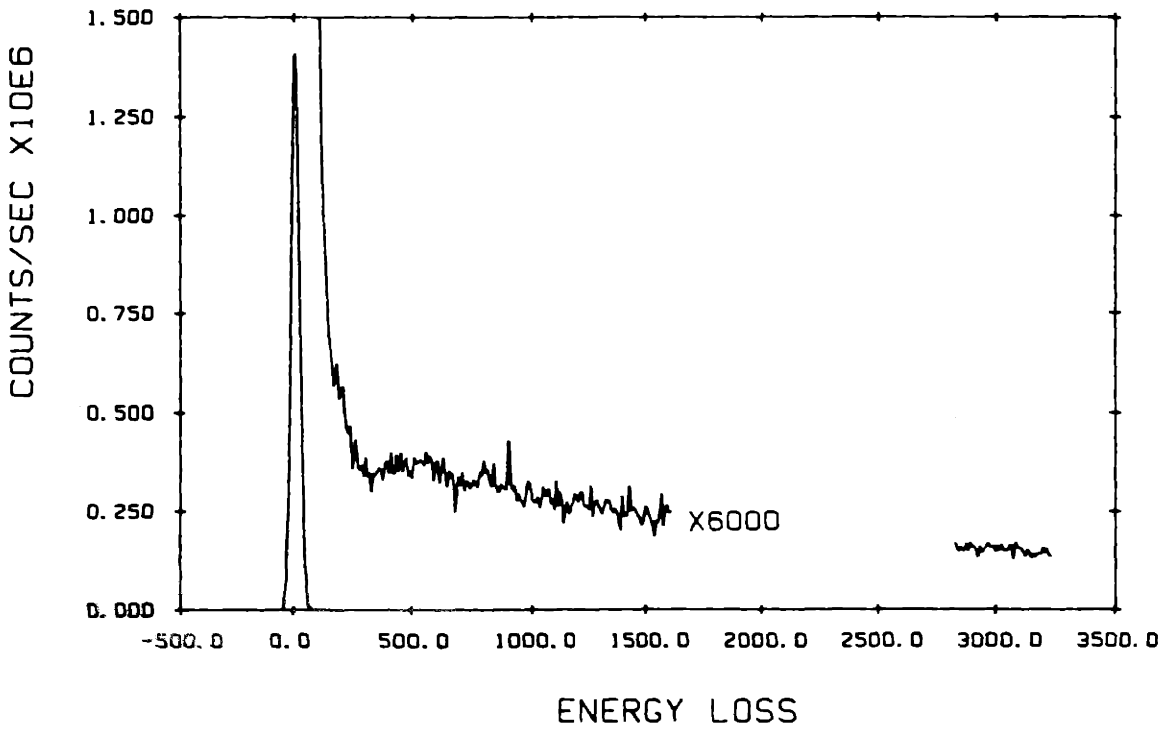

Figure 10. HREEL spectrum after annealing the surface for 30 sec at 400 K after the measurement of the spectrum in Figure 9a. The spectrum was measured at 80 K in the specular direction with 4.5 eV impact energy. The spectrum shows that C_2H_2 dissociates completely at low coverages.

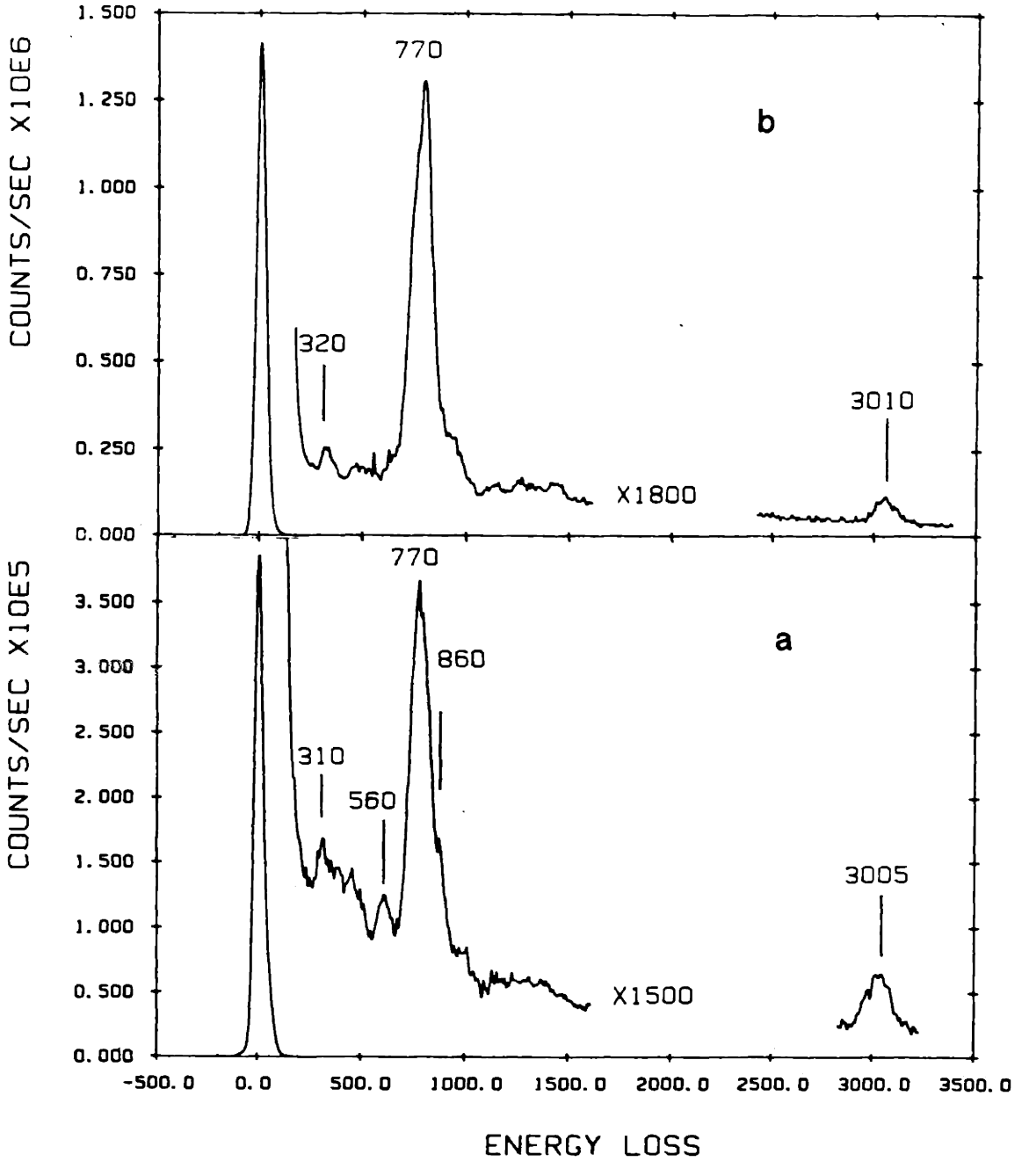

Figure 11. HREEL spectrum (a) after 12 cycles of dissociation of CH_4 and annealing the surface at 395 K as described in the text. The spectrum was measured at 40 K in the 8° off-specular direction. The coverage is 0.25 ML; (b) after annealing the surface for 120 sec at 400 K following the adsorption of 0.14 ML C_6H_6. The coverage of C_6H_6 is 0.08 ML (=0.24 ML C_2H_2) after partial desorption. The spectrum was measured at 80 K in the specular direction with 4.5 eV impact energy.

observation of desorption of molecular C_6H_6. Figure 12 shows two thermal desorption spectra measured at 78 and 51 AMU when the surface is heated at a rate of 17 K/sec after the formation of 0.25 ML of C_2H_2 from the adsorbed CH and annealing to 395 K. The thermal desorption measurement shows that some of the C_6H_6 formed from C_2H_2 desorbs at 425 K. The amount of desorption is determined to be 0.2% based on a calibration of the number of C_6H_6 molecules for a given TDS peak area from a study of C_6H_6 chemisorption on Ni(111) reported in Chapter III of this thesis. The observed desorption temperature of 425 K for the C_6H_6 formed beginning with CH_4 dissociation is the same as that when a similar coverage of C_6H_6 is adsorbed on the surface. No desorption of other hydrocarbons is observed.

The 0.25 ML coverage of C_2H_2 is obtained using the collision induced dissociation of physisorbed CH_4 by energetic Kr atoms and the multiple exposure procedure described in the previous section. The number of cycles of exposure is 12 to produce the 0.25 ML coverage of C_2H_2. The key to the observation of C_6H_6 formation and desorption is the attainment of a sufficiently high C_2H_2 coverage, which is the reason why 12 cycles of exposure were used to obtain the thermal desorption spectra shown in Figure 12. The surface is annealed at 395 K for 45 sec in order for the recombinative desorption of H_2 and the formation of C_2H_2 to occur. The actual yield of C_6H_6 is higher than the 0.2% calculated from the measured thermal desorption peak area because the trimerization of C_2H_2 and the desorption of C_6H_6 takes place during the multiple annealing to 395 K. The upper limit for the desorption yield is estimated at 1.5%.

The composition of the remaining hydrocarbon on the surface is no longer molecular C_6H_6 . Thermal desorption of H_2 from a C_6H_6 layer starts at 380 K and extends up to 700 K for a heating rate of 17 K/sec. This indicates that partial dehydrogenation of C_6H_6 has already taken place at 380 K. The extent of dehydrogenation is quite large for the annealing procedure used to obtain the spectra of Figure 11a and 11b. The dehydrogenation of C_6H_6 on Ni(111) at higher temperatures is complicated and will be discussed elsewhere [45]. The

reaction can be summarized as the formation of large cyclic hydrocarbons produced by polymerization of partially dehydrogenated C_6 rings.

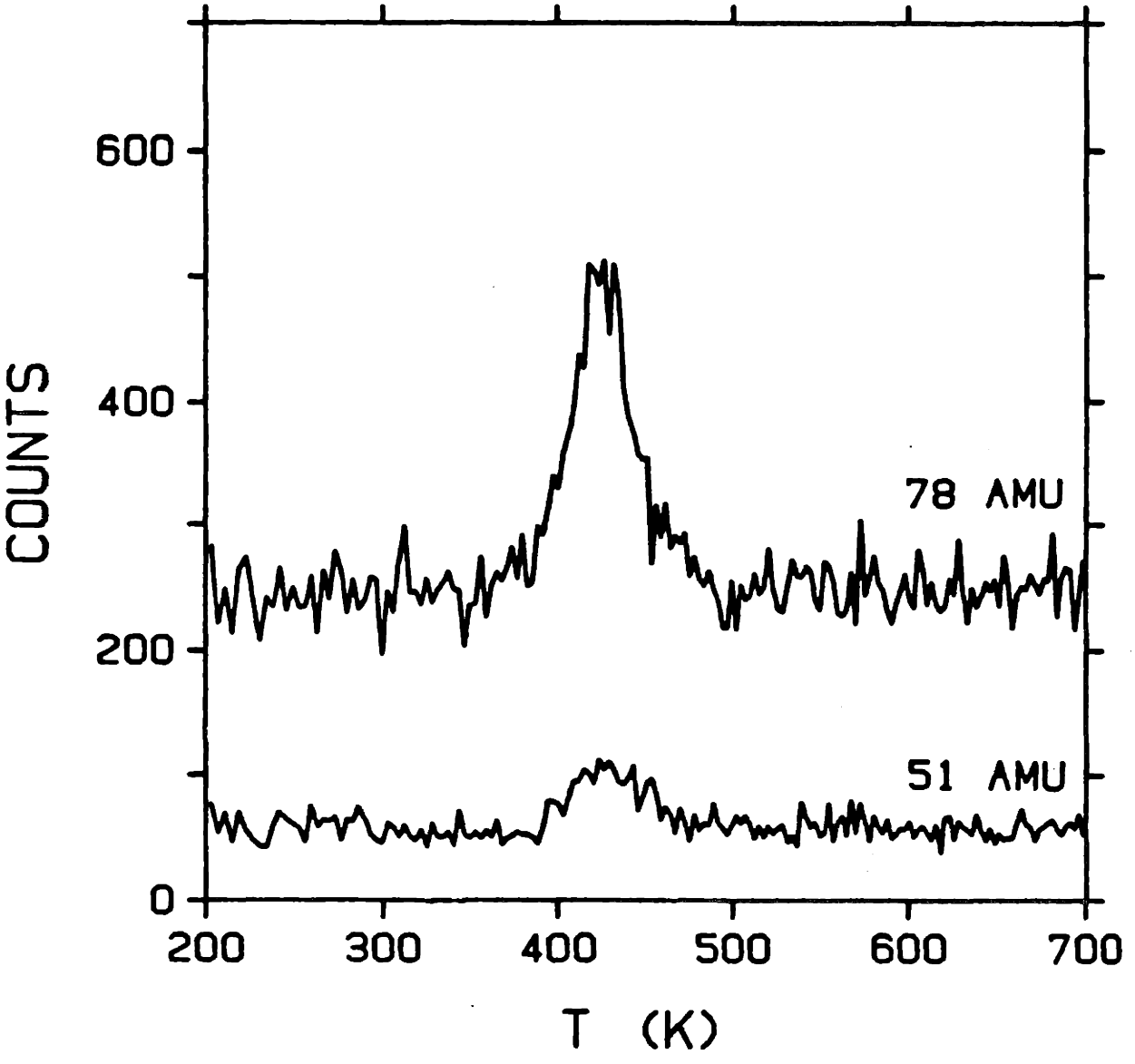

Figure 12. Thermal desorption spectrum after 12 cycles of dissociation of CH_4 and annealing the surface at 395 K as described in the text. The curves are partial pressures at masses 78 and 51 as a function of surface temperature measured by a mass spectrometer. The heating rate is 17 K/sec. The feature at 425 K corresponds to the desorption of benzene.

The vibrational spectra of these hydrocarbon molecules are characterized by an intense vibrational loss feature at about 770 cm^{-1}. This vibrational loss feature is due to the C-H bending vibration of hydrogen that still remains bonded to the C_6 ring. The vibration is the equivalent of the C-H out of plane bending mode of C_6H_6 on Ni(111), which is why the intensity and the frequency of the vibrational loss features is similar to those of the symmetric C-H out of plane bending mode of C_6H_6 on the surface. The vibrational assignment and the identification of the surface species will be discussed in detail in another report [45,46]. The composition of the surface species for the vibrational spectra of Figure 10a and 10b include molecular C_6H_6, C_4 species, C_8 species and large cyclic hydrocarbons.

The observed surface reaction of C_2H_2 formed from CH is identical to C_2H_2 that is adsorbed on the surface directly from ambient C_2H_2 gas. In separate studies [45] using C_2H_2 as the initial reactant, C_2H_2 below 0.1 ML is observed to dehydrogenate at 400 K without undergoing the trimerization and desorption as C_6H_6. The C_2H_2 coverage must be high, in order for trimerization to occur at low temperature where there is no C_2H_2 dehydrogenation. Desorption of C_6H_6 is only observed when the coverage of C_2H_2 is close to 0.25 ML and takes place at the same temperature as for the thermal desorption spectra shown in Figure 12. The composition of the surface layer is the same as that represented by the vibrational spectra in Figrues 11a and 11b when similar thermal annealing is carried out.

B. Discussion

The vibrational and thermal desorption measurement results clearly show that C_6H_6 is produced from CH_4 on a Ni(111) surface and desorbs at 425 K. The above results indicate that the trend of C-C bond formation continues with C_2H_2 which is formed in another C-C bond formation reaction of CH. The reaction of C_2H_2 on Ni(111), however, depends on the coverage. The trimerization reaction of C_2H_2 to form C_6H_6 dominates at high coverages upon thermal annealing to 400 K. In contrast, complete dehydrogenation of C_2H_2 is observed at low coverages. The different reaction behavior at low and high coverages can be explained by the fact that at low coverages, a C_2H_2 molecule has to diffuse over a large

distance in order to react with other C_2H_2 molecules to form C_6H_6. The observation of similar vibrational spectra after annealing a C_2H_2 layer adsorbed directly from C_2H_2 gas and a C_2H_2 layer formed from adsorbed CH indicates that the reaction of CH to form C_2H_2 discussed in the previous section is the main pathway of CH reaction on Ni(111). The trimerization of C_2H_2 to form C_6H_6 at high coverages is the main pathway of C_2H_2 reaction on Ni(111). Only a small amount of C_6H_6 desorption is observed because of a competing reaction of polymerization and dehydrogenation of C_6H_6 on the surface [46]. The key to the benzene formation is the attainment of a sufficiently high C_2H_2 coverage. This is the first observation of a reaction of CH_4 to form a gas phase, higher hydrocarbon over a metallic catalyst at low pressures ($<10^{-4}$ torr) commensurate with a UHV environment. The results may provide mechanistic information useful to possible extrapolation of this synthesis from molecular beam-UHV environments to more practical conditions.

VII. Summary of CH_4 Chemistry on Ni(111)

This study shows that the chemistry of CH_4 on Ni(111) can be summarized as follows:

$$CH_4 \rightarrow CH_{3(a)} + H_{(a)} \rightarrow CH_{(a)} + 3H_{(a)} \rightarrow 1/2C_2H_{2(a)} + 3H_{(a)} \rightarrow 1/6C_6H_6 + 3H_{(a)}$$

The dissociation of CH_4 on Ni(111) produces an adsorbed CH_3 and H atom on the surface. The adsorbed CH_3 is identified and its structure is determined by detailed vibrational analysis. The adsorbed CH_3 is adsorbed on a threefold hollow site with C_{3v} symmetry. The symmetric and the asymemtric C-H stretch modes of the adsorbed CH_3 are observed, as "soft" modes, at frequencies between 2600 and 2750 cm^{-1}. The symmetric C-H stretch and the first overtone of the asymmetric deformation mode are observed to be in Fermi resonance. This is the first time that an adsorbed CH_3 has been identified by a surface spectroscopic technique. The observation of the formation of the same nascent product, adsorbed CH_3, on Ni(111) from both the direct translationally activated dissociation of CH_4 and the collision induced dissociation of physisorbed CH_4 supports the conclusion that the microscopic mechanism is the same for the two processes [5]. The dissociation of the adsorbed CH_3 above 150 K

produces, via a CH_2 intermediate, an adsorbed CH species. Unambiguous identification of the CH species comes from the observation that the vibrational spectrum from the thermal decomposition of an adsorbed CH_2D is a superposition of those from the decomposition of adsorbed CH_3 and CD_3. From the number and frequency of the observed vibrational modes, the CH species is determined to be adsorbed with a pyramidal geometry in a threefold site of C_{3v} symmetry. The determined relative stability of C_1 species on Ni(111) is $CH_2<CH_3<CH$. The adsorbed CH species combines to form an adsorbed C_2H_2 above 250 K. Although it is the basis of Fischer Tropsh synthesis of hydrocarbons over metal catalysts, the formation of a C_2 species from a C_1 species on a well characterized metal surface has not been observed before by a spectroscopic technique. At low coverages C_2H_2 dehydrogenates completely above 400 K. At high coverages trimerization of C_2H_2 to form C_6H_6 takes place at temperatures about 400 K. A small percentage of the C_6H_6 synthesized from CH_4 desorbs at 425 K. This is the first observation of a reaction of CH_4 to form a gas phase, higher hydrocarbon over a metallic catalyst at the low pressures ($>10^{-4}$ torr) commensurate with a UHV environment.

References Chapter II

1. M.B. Lee, Q. Y. Yang and S.T. Ceyer, J. Chem. Phys. **87**, 2724 (1987).
2. M.B. Lee, Q.Y. Yang and S.T. Ceyer, J. Chem. Phys. **85**, 1693 (1986).
3. J.D. Beckerle, Q. Y. Yang, A.D. Johnson and S. T. Ceyer, J. Chem. Phys. **87**, 7236 (1987).
4. J.D. Beckerle, A.D. Johnson, Q. Y. Yang and S. T. Ceyer, J. Vac. Sci. Tech. **A6**, 903 (1988).
5. J. D. Beckerle, A. D. Johnson, Q. Y. Yang and S. T. Ceyer, J. Chem. Phys. **91**, 000 (1989).
6. N. A. Gaidai, L. Babernich and L. Guczi, Kin. Catal. **15**, 868 (1974).
7. A. Frennet and G. Lienard, J. Chem. Phys. **67**, 598 (1970); **68**, 1526 (1971); Catal. Rev. Sci. Eng. **10**, 37 (1974).
8. F. C. Schouten, O. L. J. Gijzeman and G. A. Bootsma, Bull. Soc. Chim. Belg. **88**, 541 (1979); Surf. Sci. **87**, 1 (1979).
9. R. E. Smalley, L. Wharton, D. H. Levy, Accts. Chem. Res. **10**, 139 (1977).
10. H. Ibach and D.L. Mills, *Electron Energy Loss Spectroscopy and Surface Vibrations* (Academic Press, New York, 1982).
11. Q. Y. Yang and S. T. Ceyer, J. Vac. Sci. Tech. **A6**, 851 (1988).
12. M. B. Lee, Ph.D. Thesis, Massachusetts Institute of Technology, 1987.
13. J. D. Beckerle, Q. Y. Yang, A. D. Johnson and S. T. Ceyer, Surf. Sci. **195**, 77 (1988).
14. Q. Y. Yang, A.D. Johnson, K. J. Maynard and S. T. Ceyer, to be published.
15. W. Ho, N. J. DeNardo and E. W. Plummer, J. Vac. Sci. Tech. **17**, 134 (1980).
16. J. E. Demuth, H. Ibach and S. Lehwald, Phys. Rev. Lett. **40**, 1044 (1978).
17. F. M. Hoffmann and T. H. Upton, J. Phys. Chem. **88**, 6209 (1984).
18. H. Ibach and D. Bruchmann, Phys. Rev. Lett. **44**, 36 (1980).

19. A. D. Dickson, J. M. Mills and B. C. Crawford, Jr., J. Chem. Phys. **27**, 445 (1957).

20. J. R. Riter, Jr., and D. F. Eggers, Jr., J. Chem. Phys. **44**, 745 (1966).

21. H. B. Weissman, R. B. Bernstein, S. E. Rossev, A. G. Meister and F. F. Cleveland, J. Chem. Phys. **23**, 544 (1955).

22. T. Shimanouchi, Natl. Stand. Ref. Data Serv., Natl. Bur. Stand., No. **39**; J. Chem. Ref. Data **6**, 993 (1977).

23. G. Herzberg, *Molecular Spectra and Molecular Structure, II, Infrared and Raman Sepctra of Polyatomic Molecules*. Van Nostrand-Reinhold, New York, 1945.

24. J. C. Whittmer and B. D. Lewis, J. Mol. Struct. **24**, 317 (1975).

25. J. S. Weaving and T. A. Ford, J. Mol. Struct. **161**, 245 (1987).

26. H.-F. Klein and H. H. Karsch, Chem. Ber. **105**, 2628 (1972).

27. R. M. Gavin, Jr., J. Reutt and E. L. Meutterties, Proc. Natl. Acad. Sci. **78**, 3981 (1981).

28. C. Minot, M. A. Hove and G. A. Somorjai, Surf. Sci. **127**, 441 (1982).

29. C. Zheng, Y. Apeloig and R. Hoffmann, J. Am. Chem. Soc. **110**, 749 (1988).

30. J. Schule, P. Siegbahn and U. Wahlgren, J. Chem. Phys. **89**, 6982 (1988).

31. H. Yang and J. L. Whitten, *The Challenge of d and f Electrons, Theory and Computation*, D. R. Salahub and M. C. Zerner, Eds., ACS Symposium Series No. 394 (1989).

32. H. Yang and J. L. Whitten, J. Chem. Phys. **91**, 126 (1989).

33. M. Brookhart and M. L. H. Green, J. Organomet. Chem. **250**, 395 (1983).

34. G. P. McQuillan, D. C. McKean, C. Long, A. R. Anderson and I. Torto, J. Am. Chem. Soc. **108**, 863 (1986).

35. P. Skinner, M. W. Howard, I. A. Oxton, S. F. Kettle, D. P. Powell and N. Shepperd, J. Chem. Soc., Faraday Trans. A2, **77**, 1203 (1981).

36. A. Berry, Z. Dawoodi, A. E. Dermoe, D. M. Dickinson, A. J. Downs, J. C. Green, M. L. H. Green, P. M. Hare, M. P. Payne, D. W. H. Rankin and H. E. Robertson, J. Chem. Soc., Chem. Comm. **520** (1986).

37. Sou-Chan Chang, Zakya H. Kafafi, Robert H. Hauge, Kenton H. Whitmire, W. Edward Billups and John L. Margrave, Inorg. Chem. **25**, 4530 (1986).

38. I. A. Oxton, D. B. Powell, N. Sheppard, K. Burgess, B. F. G. Johnson and J. Lewis, J. Chem. Soc., Chem. Commun. **719** (1982).

39. I. A. Oxton, Spectrochim. Acta **38A**, 181 (1982).

40. M. W. Howard, S. F. Kettle, I. A. Oxton, D. B. Powell, N. Shepperd and P. Skinner, J. Chem. Soc. Faraday Trans II, **77**, 397 (1981).

41. B. A. Sexton and G. E. Mitchell, Surf. Sci. **99**, 523 (1980).

42. G. E. Fisher and G. E. Mitchell, J. Elect. Spec. Rel. Phenom. **29**, 253 (1983).

43. J. E. Demuth and H. Ibach, Surf. Sci. **78**, L238 (1978).

44. J. A. Gates and L. L. Kesmodel, Surf. Sci. **124**, 68 (1983).

45. K.J. Maynard, A.D. Johnson, Q. Y. Yang and S.T. Ceyer, to be published.

46. Q. Y. Yang, Chapter 3, Ph.D. Thesis, Massachusetts Institute of Technology, 1989.

47. L.L.Kesmodel, G.D. Waddill and J.A. Gates, Surf. Sci. **38**, 464 (1984).

48. H. Ibach and S. Lehwald, J. Vac. Sci. Tech. **18**, 625 (1981).

49. J.D. Beckerle, A.D. Johnson and S.T. Ceyer, Phys. Rev. Lett. **62**, 685 (1989).

50. J.C. Bertolini, J. Massardier and G. Dalmai-Imelik, J. Chem. Soc. Faraday Trans. I **74**, 1720 (1978).

Chapter III

The Chemisorption of Benzene on Ni(111)

I. Introduction

The chemisorption of C_6H_6 (benzene) on transition metal surfaces has been the concern of many studies [1-15] using different techniques including high resolution electron energy loss spectroscopy (HREELS) [16], a surface vibrational spectroscopic technique. Below room temperature, C_6H_6 is generally found to be molecularly adsorbed on the surface and retains a structure very similar to that of the gas phase molecule [3-11]. Benzene has been consistently observed to be adsorbed with the ring parallel or nearly parallel to the surface. Various kinds of adsorption sites and symmetry point groups have been proposed but these questions are not well resolved in most cases. An interesting observation about the structure of C_6H_6 on some metal surfaces is that the molecule shows significant Kekulé distortion, in which the C-C bonds are alternatively shortened and lengthened. An example is C_6H_6 on Rh(111) for which the two C-C bond lengths are determined to be 1.33 and 1.81 Å by a dynamical LEED calculation [3]. Benzene tends to form ordered phases and some ordered phases are only stable if a small amount of CO is coadsorbed on the surface [1,2,4,8,9]. Benzene adsorption on transition metal surfaces is also generally found to be partially reversible. Some molecular C_6H_6 desorption is observed to take place at slightly higher than room temperature [8,9,12,13]. In addition to desorption of C_6H_6, H_2 desorption takes place above room temperature indicating that the C_6H_6 remaining on the surface dehydrogenates [8-10,12-15]. Details of the decomposition reactions of adsorbed C_6H_6 are not well understood, though formation of adsorbed CH or C_2H groups has been proposed [15].

Benzene on Ni(111) behaves similarly to other transition metal surfaces. There have been two previous studies using HREELS. In one of the studies, it is proposed that C_6H_6 adsorbs on two different sites on the surface [5]. The proposal is made on the basis of two intense vibrational loss features at 730 and 820 cm^{-1}, assigned as the ν_4 (Herzberg notation is used throughout this report) mode of the C_6H_6 molecule adsorbed on two different sites, which show a strong temperature dependence in their relative intensity. The temperature dependence is explained by site conversion due to the difference in the binding energy of the

two adsorption sites. It is suggested that both C_6H_6 have the same symmetry point group $C_{3v}(\sigma_d)$, so that two of the three sites of threefold symmetry on Ni(111) (the atop, the fcc threefold or the hcp threefold site) must be involved as the adsorption sites. This is also thought to be true for the $(2\sqrt{3}x2\sqrt{3})R30°$ ordered phase that has been observed previously [17]. Since it is not possible for the unit cell of the $(2\sqrt{3}x2\sqrt{3})R30°$ ordered phase to accommodate two C_6H_6 molecules given that the ring is parallel to the surface, the two molecules are suggested to be in separate phases. A quite different picture is drawn by the study of another group [6]. No evidence is presented to indicate that there are two different C_6H_6 adsorption sites on the surface, even though the coverage is believed to be the same. The C_6H_6 was first suggested to be on the bridge site. Later, the assignment of the bridge site as the adsorption site was revised based on vibrational results obtained with a better resolution and in conjunction with a force field calculation [7]. Again, a single benzene species was proposed, but the symmetry point group and the adsorption site were undetermined. The number of different C_6H_6 sites is consequently an unsettled issue. The certainty of the assignments of the symmetry point groups and the adsorption sites is also questionable because, in both studies, no measurement of the dependence of the intensities of the vibrational loss features on scattering angle was made. Such a measurement is necessary in order to define the scattering mechanism (dipole, impact or both) by which a vibrational loss feature is observed, so that it can be determined whether a mode belongs to a totally symmetric representation. Unless the dipole activity of a sufficient number of modes is known, it is difficult to know with certainty the symmetry point group and the adsorption site of an adsorbate.

For the purpose of resolving the issues of the number of different C_6H_6 sites on the surface and the symmetry point group(s) and the adsorption site(s), the chemisorption of C_6H_6 on Ni(111) was studied by a combination of techniques, HREELS, low energy electron diffraction (LEED) and thermal desorption spectroscopy (TDS). The dependence of the intensities of the C_6H_6 vibrational loss features in HREELS spectra was carefully measured in

order to determine the symmetry of each vibrational mode so that the symmetry and adsorption site could be determined. The vibrational spectra of partially deuterated benzene (1,2-$C_6H_4D_2$ and 1,2,4,5-$C_6H_2D_4$) were measured in order to answer the question whether C_6H_6 on Ni(111) shows any significant Kekulé distortion. While it is possible for the point group to be C_{6v} without the distortion, the highest symmetry is C_{3v} with the distortion. With a significant Kekulé distortion, two different $C_6H_4D_2$ species should be observed depending whether the bond between the two deuterated carbon atoms is shortened or lengthened while without a significant distortion there should be only one. The symmetry point group of an undistorted $C_6H_2D_4$ on the surface is C_{2v}, the common subgroup of the C_{6v} group and the C_{2v} group, while the point group of a significantly distorted $C_6H_2D_4$ is C_s, the common subgroup of C_{3v} and C_{2v}. A detailed analysis of the vibrational spectra of $C_6H_4D_2$ and $C_6H_2D_4$ on the surface, therefore, provides information on whether the C_6H_6 point group is C_{6v} or C_{3v}. In addition, the surface chemistry of benzene on Ni(111) at higher temperatures was studied.

II. Experimental

The description of the experimental apparatus is omitted here because it can be found in other chapters of this thesis and in previous publications [18-21]. The low energy electron diffraction (LEED) apparatus which is not involved in the previous experiments is a VG Scientific model 640-2 RVL, two grid, reverse view LEED with a coaxial electron gun. The sample cleaning procedure has been described previously [21]. The occasional cleaning is accomplished by sputtering the surface with 0.5 or 1.0 KeV Ar ions and the sample cleanliness is monitored with Auger electron spectroscopy and HREELS. The off-specular HREELS spectra were measured after rotating the crystal away from the 60° angle of nominal incidence.

The C_6H_6 used in the experiments was Mallinckrodt spectrAR grade which was purged of air by repeated freeze and thaw cycles with a dry ice/acetone bath. The C_6D_6 is obtained from Cambridge Isotope Laboratories with a 99.6% deuterium isotope purity and was also freeze/thaw degassed prior to use. The isotopically substituted benzenes, $^{13}C_6H_6$, 1,2-

$C_6H_4D_2$ and 1,2,4,5-$C_6H_2D_4$ are from MSD Isotopes with the isotope purity no less than 99%.

The exposure of the Ni(111) surface to benzene was performed with one of the following methods. One method is to expose the surface to an ambient background C_6H_6 pressure by introducing the gas into the UHV chamber through a leak valve. The advantage of this method is that it is easy to control the exposure to the surface. However, it should be kept in mind that the high sticking probability of C_6H_6 on most exposed metal surfaces may lower the local pressure at some parts of the UHV chamber considerably. This is particularly a problem if a lower exposure is used. The problem can be avoided by consistently positioning the sample face at the same location for each exposure. Another way to expose the surface is to use a pure benzene molecular beam since the apparatus is equipped with a molecular beam source coupled to the UHV chamber. In practice, it is difficult to maintain a stable beam flux for a condensible liquid like benzene, so this method is only employed to form a saturated layer beacause it is not critical whether the exposure is higher than required. It is much easier to monitor the surface saturation with the beam because the sticking probability of C_6H_6, on an unsaturated surface is close to unity, but drops to zero at saturation coverage, leading to a distinct background pressure rise when the surface is saturated, as shown in Figure 1.

The coverage is determined by measurement of the carbon Auger signal or calculated, for coverages below saturation, from the exposure and the sticking probability which has been accurately determined using the moelcular beam source. Measurement of the carbon Auger signal yields a relative coverage which is converted to an absolute coverage by calibration against the Auger signal from the known saturation coverage of $2.7 \times 10^{14}/cm^2$ at which a $(\sqrt{7} \times \sqrt{7})R19°$ ordered phase forms. The background benzene pressures before and after saturation when the surface is exposed to a pure C_6H_6 molecular beam and measured by a mass spectrometer, shown in Figure 1, shows a constant sticking probability for C_6H_6 on Ni(111) before reaching saturation. The ratio of the background benzene pressures before and

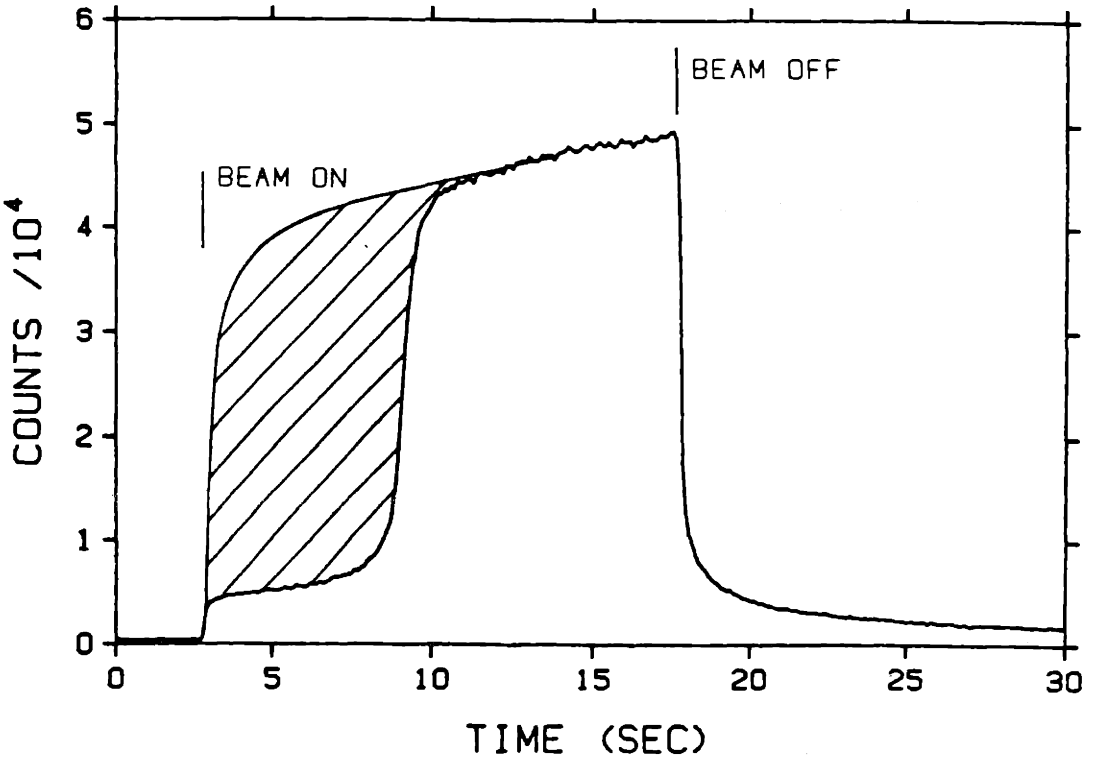

Figure 1. Benzene partial pressure when a pure benzene molecular beam is introduced into the chamber and onto the Ni(111) surface at 260 K measured at mass 78 by the quadrupole mass spectrometer. The shaded area is the amount of adsorption leading to a saturation coverage of 0.14 ML at which the $(\sqrt{7} \times \sqrt{7})R19°$ ordered phase forms.

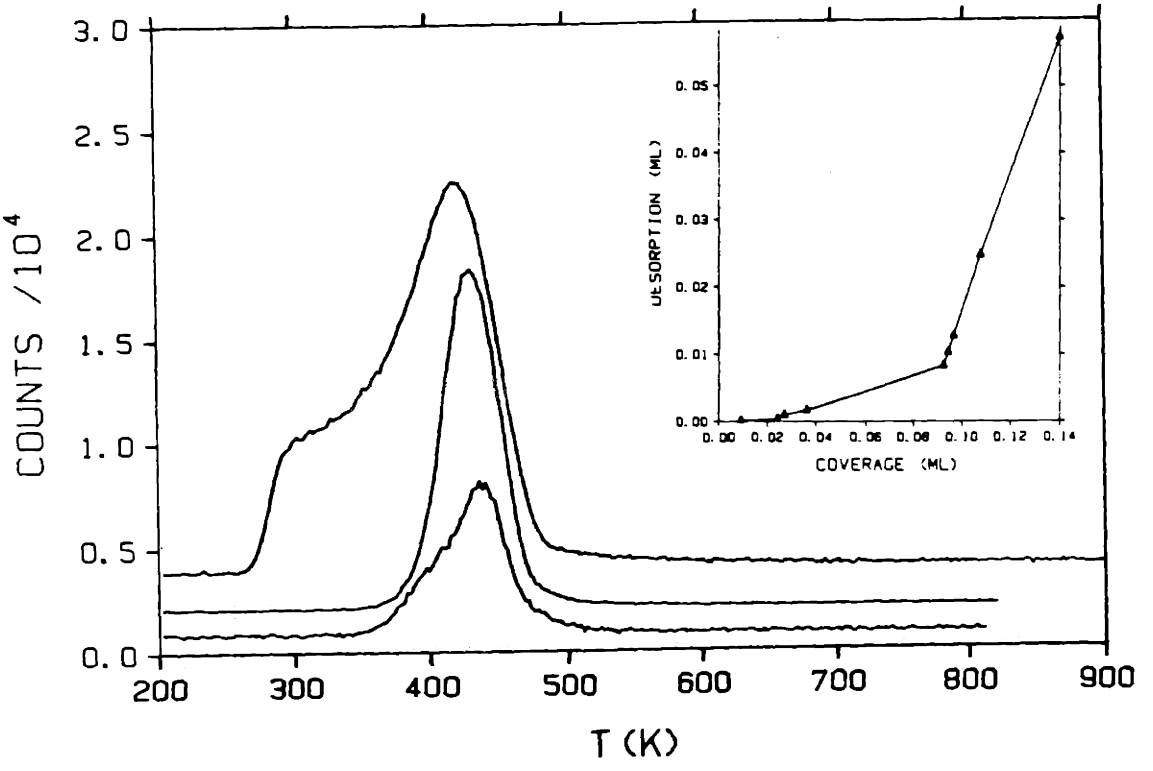

Figure 2. Thermal desorption spectra of benzene after the exposure of the surface to benzene at 260 K measured at mass 78 with a heating rate 17 K/sec. The coverage is (a) 0.036 ML, (b) 0.095 ML and (c) 0.14 ML. The insert shows the amount of desorption as a function of coverage in ML.

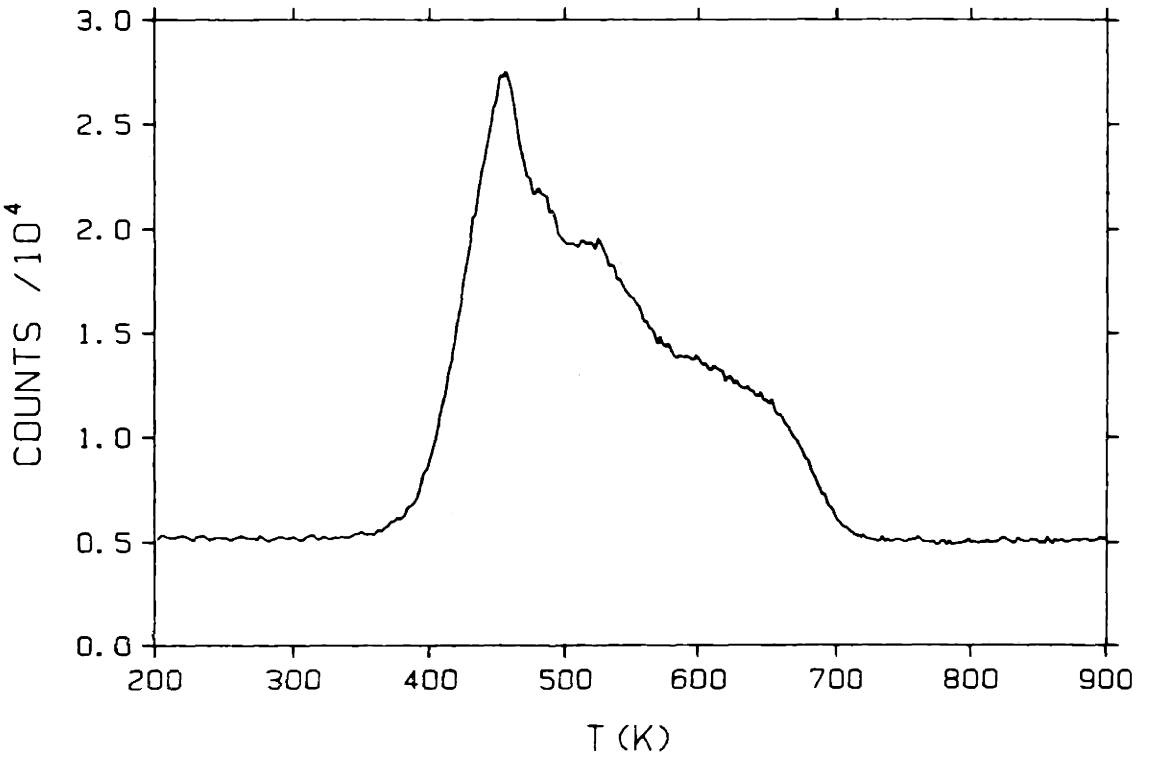

Figure 3. Thermal desorption spectrum of hydrogen from a saturation coverage of 0.14 ML benzene measured at mass 2 with a heating rate of 17 K/sec. Spectrum shows that benzene dehydrogenates to produce H_2 between 400 and 700 K.

after the saturation gives directly the sticking probability (0.85) which can be used to calculate the coverage for a known exposure.

The shaded area in Figure 1 represents the amount of benzene that forms a saturated layer as measured by the mass spectrometer. Since the number of benzene molecules in a saturated layer is known, this shaded area can be used to calibrate the thermal desorption signal for the number of benzene molecules desorbed.

III. Results

The adsorption of C_6H_6 on Ni(111) appears to occur with a near unity sticking probability (0.85). This is shown in Figure 1 which is the mass 78 signal level in the UHV chamber measured by the mass spectrometer when the surface is exposed to a pure C_6H_6 molecular beam. The difference before and after the saturation is used to determine the sticking probability which is calculated to be 0.85. The measurement is carried out while the surface temperature is held at 260 K in order to avoid multilayer adsorption which is shown not to occur by HREELS spectra measured after the surface is exposed to C_6H_6 under these conditions. The high sticking probability of C_6H_6 on Ni(111) is not unique. On other transition metal surfaces, a low exposure of only a few Langmuirs is sufficient to reach saturation coverage [8,9,17].

If the absolute saturation coverage is known, this provides a calibration method by which a C_6H_6 thermal desorption peak can be converted into an absolute number of desorbing C_6H_6 molecules. As will be shown later, a $(\sqrt{7}x\sqrt{7})R19°$ ordered phase is formed at saturation coverage which corresponds to $2.7x10^{14}/cm^2$ or 0.14 monolayer.

A. Thermal Desorption Spectroscopy

Similar to adsorption on other transition metal surfaces, C_6H_6 on Ni(111) appears to be partially reversible [8-10,12,13]. Figure 2 shows a series of C_6H_6 TDS spectra measured at a heating of 17 K/sec at different benzene coverages. The insert in Fig. 2 shows the absolute amount of C_6H_6 desorption as a function of the coverage determined as described in the experimental section. The peak area of each thermal desorption spectrum is converted into an

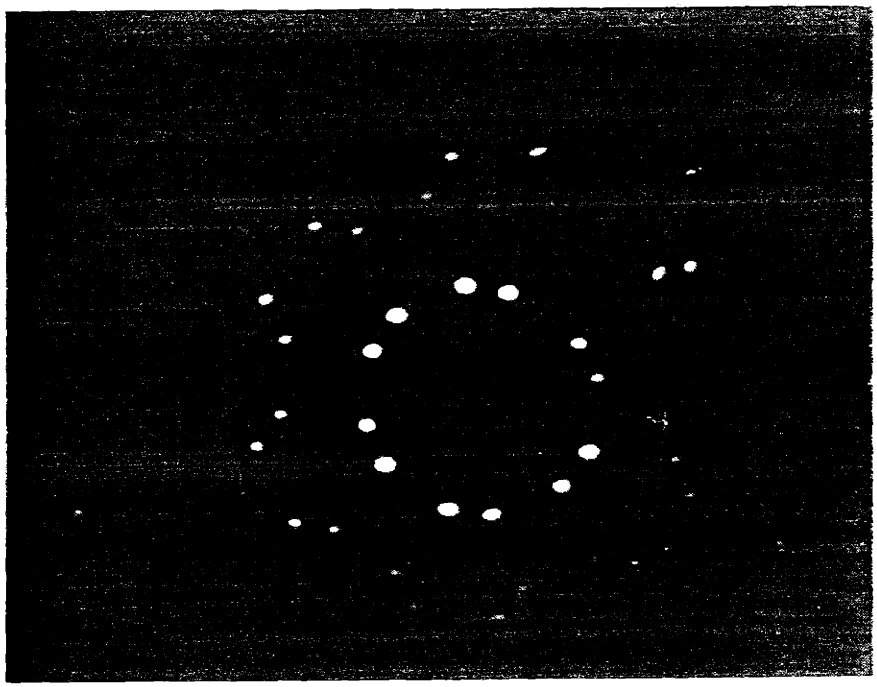

Figure 4. The $(\sqrt{7} \times \sqrt{7})R19°$ LEED pattern formed after exposure of the surface at 260 K to 10 L (not corrected for ionization cross section) of benzene. The ordered phase forms at the saturation coverage of 0.14 ML or $2.7 \times 10^{14}/cm^2$ below 280 K.

absolute amount of desorption by comparing to the amount of adsorption to form a saturation layer, of $2.7 \times 10^{14}/cm^2$ which produces the $(\sqrt{7} \times \sqrt{7})R19^o$ ordered phase, measured by the mass spectrometer as discussed in the experimental section. For the saturation coverage of the $(\sqrt{7} \times \sqrt{7})R19^o$ ordered phase, Figure 2 shows that $1.1 \times 10^{14}/cm^2$ C_6H_6 desorbs between 260 and 480 K. This amounts to about 40% desorption of the saturated layer. There are two different regimes of desorption depending on whether the coverage is above or below 60% of saturation. While in the low coverage regime the amount of desorption is very small, in the high coverage regime the amount of desorption is such that the amount of irreverisble adsorption stays constant at 60% of the saturation. The coverage at which the high coverage regime begins is calculated from the exposure and the sticking probability of 0.85 which is determined as described earlier. The present result is similar to a previous study [12] on Ni(111) in which a C_6H_6 desorption peak maximum at about 400 K is observed. The thermal desorption spectrum of a saturated layer published by another group [13] shows a broad peak similar to the one in Figure 2. Unlike Figure 2, however, where the desorption is peaked at about 400 K with a broad shoulder on the low temperature side, the previously measured thermal desorption maximizes at 300 K with a broad shoulder on the high temperature side. The origin of the difference is not known although the adsorption temperature in the previous study is slightly lower than the one for Figure 2, so multilayer adsorption is a possibility.

The thermal desorption spectrum at mass 2 of an initially saturated layer shows a broad peak extending from about 400 to 700 K as shown in Figure 3. This is an indication that dehydrogenation of the irreversibly adsorbed C_6H_6 has taken place.

B. Low Energy Electron Diffraction.

When the surface is saturated with C_6H_6 (10 L withouth correction for the ionization cross section) at 260 K, a sharp $(\sqrt{7} \times \sqrt{7})R19^\circ$ LEED pattern, shown in Figure 4, is observed after the surface temperature is lowered to 80 K following the exposure. The sharp LEED pattern is also observed at 260 K after exposure under the same condition. Only a faint ring is observed when it is attempted to saturate the surface at 80 K. The low mobility of C_6H_6 on the

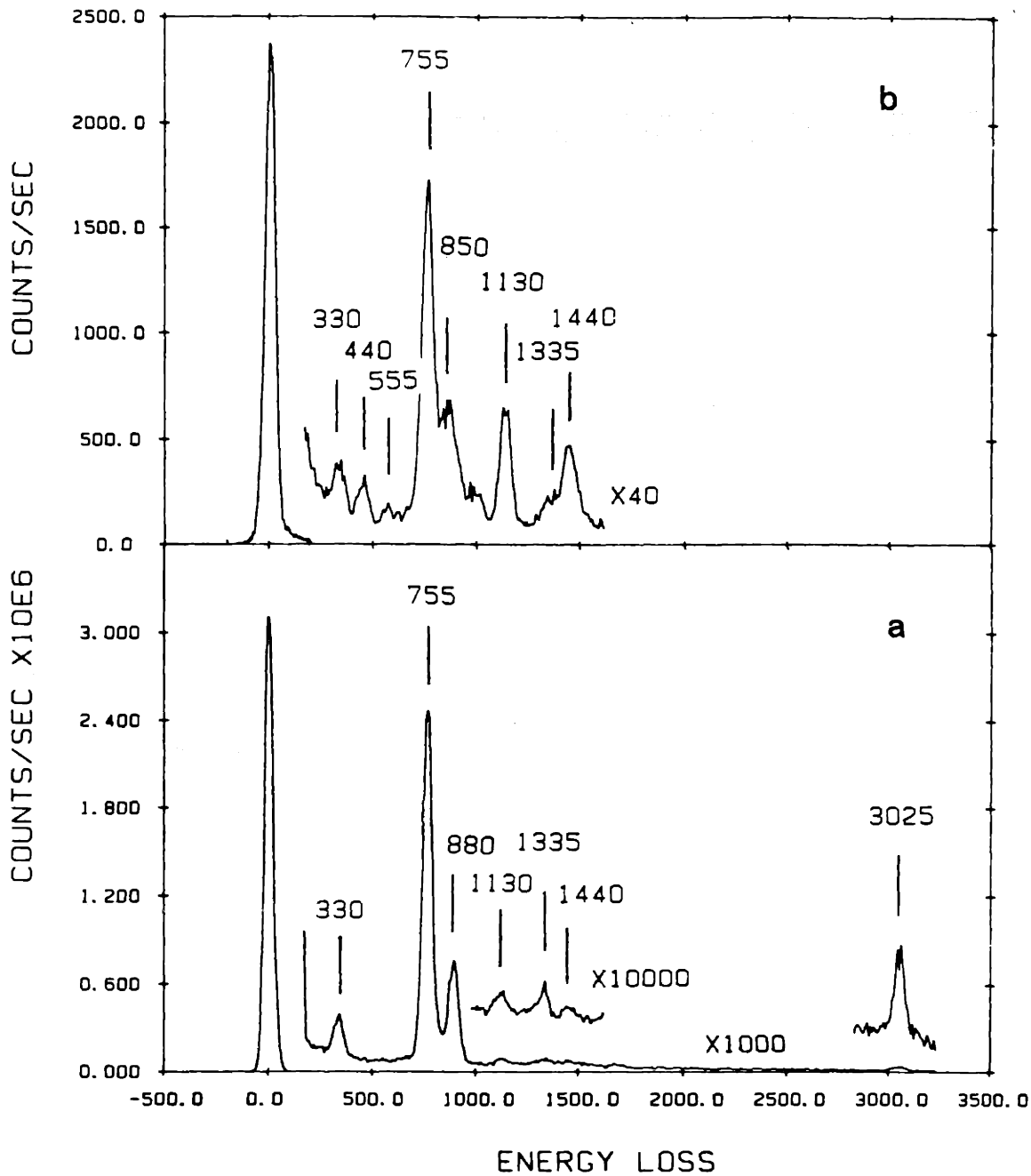

Figure 5. HREEL spectra of the $(\sqrt{7} \times \sqrt{7})R19°$ ordered phase of benzene after exposure of the surface at 260 K to a benzene molecular beam. The spectra were measured with an impact energy of 4.0 eV at 80 K in the (a) specular and (b) 10° off-specular direction.

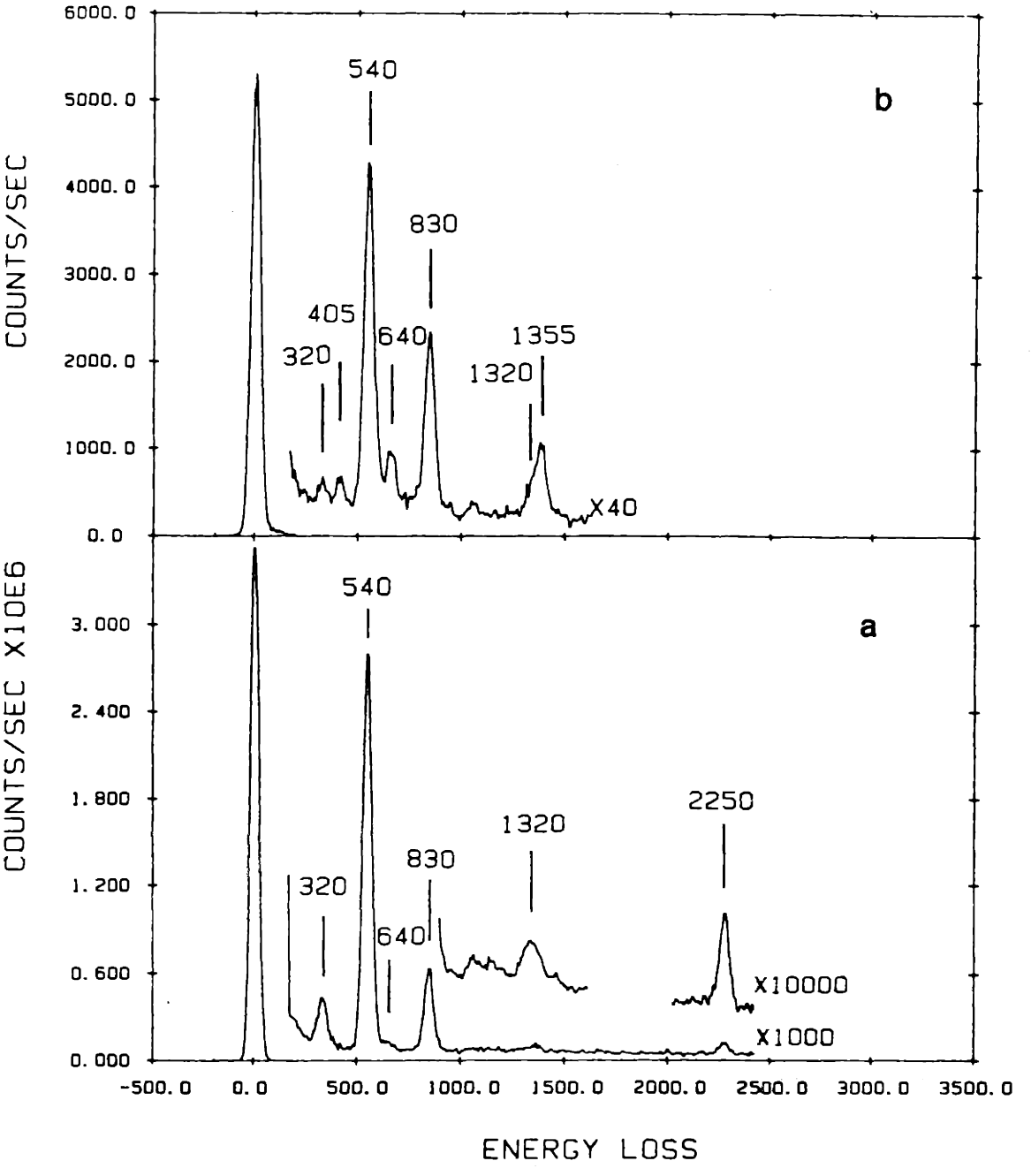

Figure 6. HREEL spectra of the $(\sqrt{7} \times \sqrt{7})R19°$ ordered phase of deuterated benzene after the exposure of the surface at 260 K to a deuterated benzene molecular beam under conditions similar to those for the spectra in Figure 5. The spectra were measured with an impact energy of 4.0 eV at 80 K in the (a) specular and (b) 10^{o} off-specular direction.

surface at 80 K probably prevents the formation of a well ordered layer. The same behavior is also observed when C_6H_6 is substituted with C_6D_6. The LEED pattern becomes a defuse ring when the surface temperature is raised to 300 K following the exposure. Examination of the thermal desorption measurement shown in Figure 3 indicates that partial desorption of C_6H_6 is responsible for the deterioration of the LEED pattern.

A different ordered phase on Ni(111) with a $(2\sqrt{3}x2\sqrt{3})R30°$ LEED pattern has been reported [17] after exposure of the surface at 300 K to 3 L of C_6H_6. The coverage of this ordered phase is $1.58x10^{14}/cm^2$. In the present experiment, a LEED pattern corresponding to this phase is not observed even though the exposure is controlled so that the coverage corresponds to the $(2\sqrt{3}x2\sqrt{3})R30°$ ordered phase. The coverage in this case is determined by the C/Ni Auger peak ratio relative to that for the $(\sqrt{7}x\sqrt{7})R19°$ ordered phase. On some transition metal surfaces, more than one ordered C_6H_6 phase has been observed by LEED. However, it has been shown that the coadsorption of CO is essential to the stabilization of some ordered phases, particularly the lower density ones [1,3,4,8]. The possibility can not be ruled out that the previously observed $(2\sqrt{3}x2\sqrt{3})R30°$ ordered phase which has lower density than the $(\sqrt{7}x\sqrt{7})R19°$ phase is only stable in the presence of a small amount of coadsorbed CO. As will be detailed in the discussion section, the $(\sqrt{7}x\sqrt{7})R19°$ ordered phase possesses the highest density of any ordered phase of C_6H_6 on Ni(111). However, it is not clear why the spectra in the same previous report [17] do not show vibrational loss features due to adsorbed CO. No attempt was made to deliberately dose the surface with CO in order to verify whether CO coadsorption might be the reason for the previous observation of the $(2\sqrt{3}x2\sqrt{3})R30°$ ordered phase.

C. HREELS of the Ordered Phase

Figures 5 and 6, respectively, are the high resolution electron energy loss spectra (HREELS) of the $(\sqrt{7}x\sqrt{7})R19°$ ordered phase of C_6H_6 measured at 4.0 eV impact energy in both the specular (a) and 10° off-specular (b) directions at 80 K. That the intensities of the C_6H_6 vibrational loss features at 330, 755, 880 and 3025 cm^{-1} measured in the 10° off

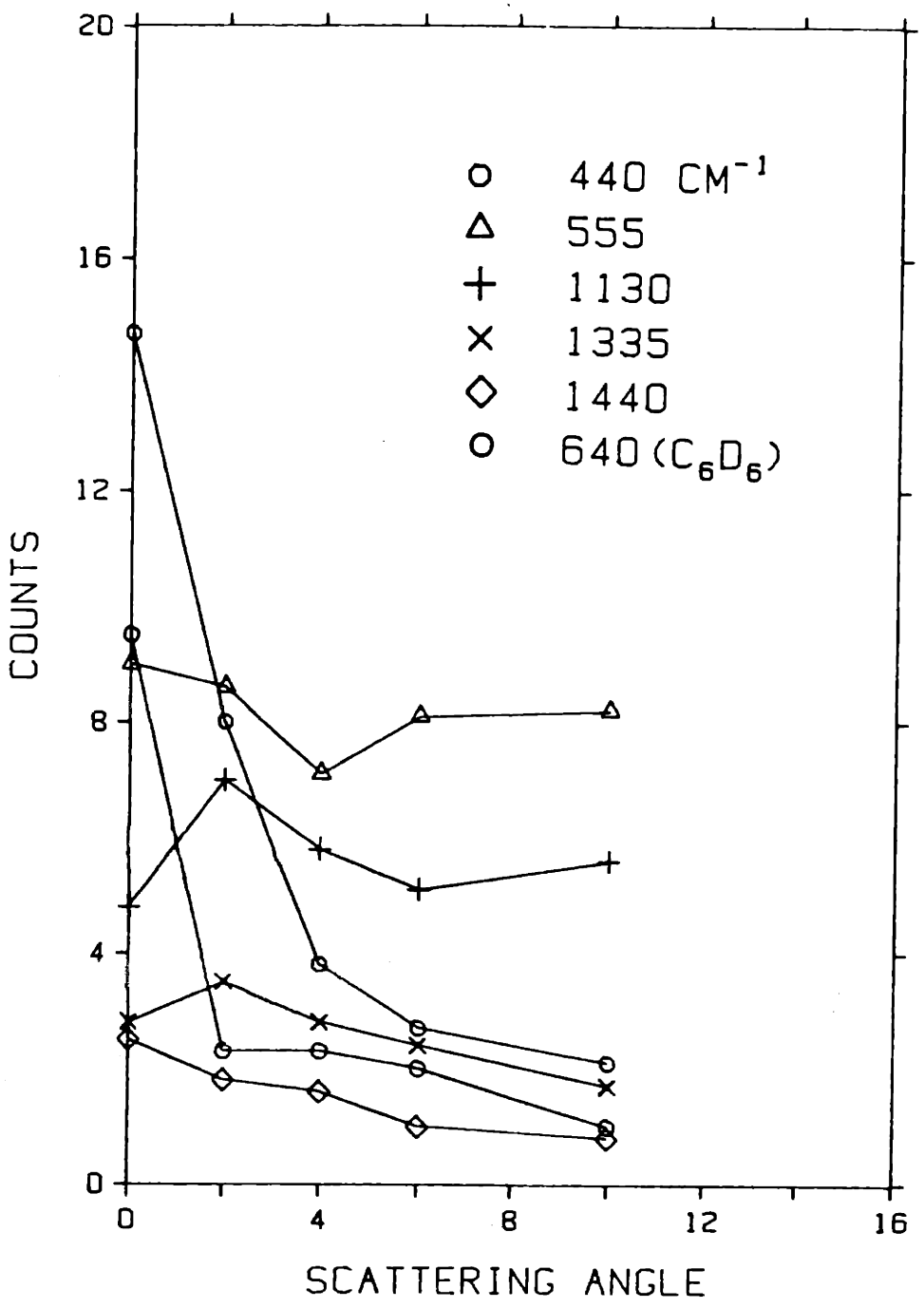

Figure 7. Intensities of the vibrational loss features of benzene at 440, 555, 1130, 1335 and 1440 cm^{-1} and deuterated benzene at 640 cm^{-1} as a function of scattering angle for the $(\sqrt{7} \times \sqrt{7})$R19° ordered phase measured at 80 K and at 4.0 eV impact energy.

specular direction are much lower than those measured in the specular direction indicate that these loss features are due to dipole active modes. Their frequencies are shifted to 320, 540, 830 and 2250 cm^{-1} for C_6H_6, respectively. Vibrational loss features for C_6H_6(C_6D_6) are also observed at 440(405), 555(?), 850(640), 1130(830), 1335(1320) and 1440(1355) cm^{-1} which are weak in the specular direction. There is no C_6H_6 loss feature that can be assigned to the corresponding C_6H_6 loss feature at 555 cm^{-1}. This can be explained by the fact that the 555 cm^{-1} C_6H_6 loss feature is due to a mode of C motion because the lowest frequency mode of H motion is at 673 cm^{-1} for the gas phase C_6H_6 molecule and therefore the corresponding C_6D_6 mode frequency is only slightly lower than the frequency of the C_6H_6 mode at 555 cm^{-1} so that the loss feature for this C_6D_6 mode is obscured by the 540 cm^{-1} feature. The correlation of two C_6H_6 loss features at 880 and 1130 cm^{-1} to one C_6D_6 loss feature at 830 cm^{-1} is made based on a comparison of the intensities of these loss features [8-10]. That the intensities of the C_6H_6 loss feature at 880 cm^{-1} and the C_6D_6 loss feature at 830 cm^{-1} in the spectra of Figures 5a and 6a measured in the specular direction are comparable indicates that the two loss features of C_6H_6 and C_6D_6 are due to the same vibrational mode. The same C_6D_6 loss feature at 830 cm^{-1} is also assigned to be due to the same mode as another C_6H_6 loss feature at 1130 cm^{-1} because the C_6D_6 loss feature is the only one whose intensity is comparable to that of the C_6H_6 loss feature in HREELS spectra measured at the 10° off-specular angle, shown in Figure 5b and 6b. There are also some other weak loss features observed in the off-specular direction that will not be discussed because of the difficulty of unambigiously correlating C_6H_6 and C_6D_6 loss features.

In order to determine the dipole activity of the modes that give rise to the C_6H_6 loss features at 440, 555, 850, 1130, 1335 and 1440 cm^{-1}, the dependence of the intensities of these loss features on the scattering angle is measured and is shown in Figure 7. The small separation of 30 cm^{-1} between the C_6H_6 loss features at 850 and 880 cm^{-1} makes it impossible to measure accurately the intensity of the 850 cm^{-1} feature, and therefore the angular distribution of the corresponding C_6D_6 loss feature at 640 cm^{-1} is measured instead. The result

indicates that of the six loss features only the one at 1335 cm^{-1} is clearly due to a dipole active mode and the ones at 440, 555, 1130 and 1445 cm^{-1} are due to nondipole active modes.

The dipole activity of the mode that gives rise to the loss feature at 850 cm^{-1} for C_6H_6 and at 640 cm^{-1} for C_6D_6 is more difficult to determine. The C_6D_6 loss feature at 640 cm^{-1} appears to show dipole scattering because the angular distribution, shown in Figure 7, is peaked in the specular direction. However, the angular distribution places the high limit of the dipole moment associated with the observed dipole lobe at 2% of that of the C_6D_6 540 cm^{-1} loss feature. The high limit of 2% is the ratio of the loss intensities of the two C_6D_6 loss features at 640 and 540 cm^{-1} which is proportional to the ratio of the dipole moments that gives rise to the loss features, because the intensities of the two loss features are due to dipole scattering predominantly. The contribution of dipole scattering to a loss feature is the intensity of the feature in the specular direction minus the intensity of the feature in an off-specular direction measured at a scattering angle at which dipole scattering is negligible. As will be detailed in the discussion, the small dipole lobe is likely to be the result of a small amount of disordering in the adsorbed layer. If this is the case, then the dipole scattering may arise from those molecules adsorbed at sites populated in the disordered phase. The loss feature at 640 cm^{-1} in the disordered phase is observed to be strongly dipole active as discussed in the following section. The small amount of disordering in the adsorbed layer is due to the fact that the coverage is slightly lower than the saturation coverage of a perfect ordered phase because the temperature, 260 K, at which the surface is exposed to benzene, is where the desorption of molecular benzene starts to take place as shown by the thermal desorption spectrum of a saturated layer in Figure 2.

The vibrational spectra of C_6H_6 on Ni(111) are very similar to those on other transition metal surfaces [5-10], Rh(111) in particular [8]. In the cases studied so far C_6H_6 appears to be adsorbed molecularly with the ring parallel or nearly parallel to the surface below room temperature. A consequence of such a structure is that the symmetric C-H out-of-plane bending mode ν_4, has the strongest dynamical dipole moment and the corresponding loss

feature is the most intense in the HREELS spectra of C_6H_6 . As will be discussed below, these characteristics are shared by C_6H_6 on Ni(111) and the 755 cm^{-1} loss feature, which will be assigned as the ν_4 mode.

As will be shown in the discussion section, the results presented so far can be explained by C_6H_6 of $C_{3v}(\sigma_d)$ symmetry so that the adsorption must be on the atop site or one of the two threefold sites. With the intention to determine which of these sites is occupied, a vibrational study of two partially deuterated benzene isomers was performed. Figure 8 and 9 show the vibrational spectra of 1,2-$C_6H_4D_2$ (1,2-dideuterobenzene) and 1,2,4,5-$C_6H_2D_4$ (tetradeuterobenzene), respectively, in the ordered phase measured in the specular direction and at 4 eV impact energy. For the $C_6H_4D_2$ spectrum, the interest is in the two loss features at 575 and 755 cm^{-1} which are due to C-D and C-H out-of-plane bending modes [22-24]. As explained below, each of the two loss features should be split into two bands if the adsorption is on a threefold hollow site while such would not be the case on the atop site. Neither of the two loss features shows an observable splitting in the $C_6H_4D_2$ vibrational spectrum of Figure 8. The linewidth of the loss feature (37 cm^{-1}) at 755 cm^{-1} is comparable to that of the elastic peak (30 cm^{-1}) which indicates that the feature is due to a single mode. The situation is somewhat more complicated for the loss feature at 575 cm^{-1}. The feature is slightly broader with a 50 cm^{-1} linewidth and appears to be asymmetric with a shoulder to lower frequency. This is likely due to the fact that there should be a mode at about 550 cm^{-1}, which corresponds to the C_6H_6 mode at 555 cm^{-1}. The loss feature due to this $C_6H_4D_2$ mode, which is dipole active because the molecular symmetry is lower is more intense than the corresponding C_6H_6 feature and appears as a shoulder to the one at 575 cm^{-1}.

Other prominent loss features observed at 330, 430 and 870 cm^{-1} are correlated with the C_6H_6 loss features at 330, 440 and 880 cm^{-1}. The intensity of the loss feature at 430 cm^{-1} indicates that the mode for the partially deuterated benzene is dipole active whereas the corresponding C_6H_6 mode is nondipole active. For $C_6H_2D_4$ the concern is the dipole activity

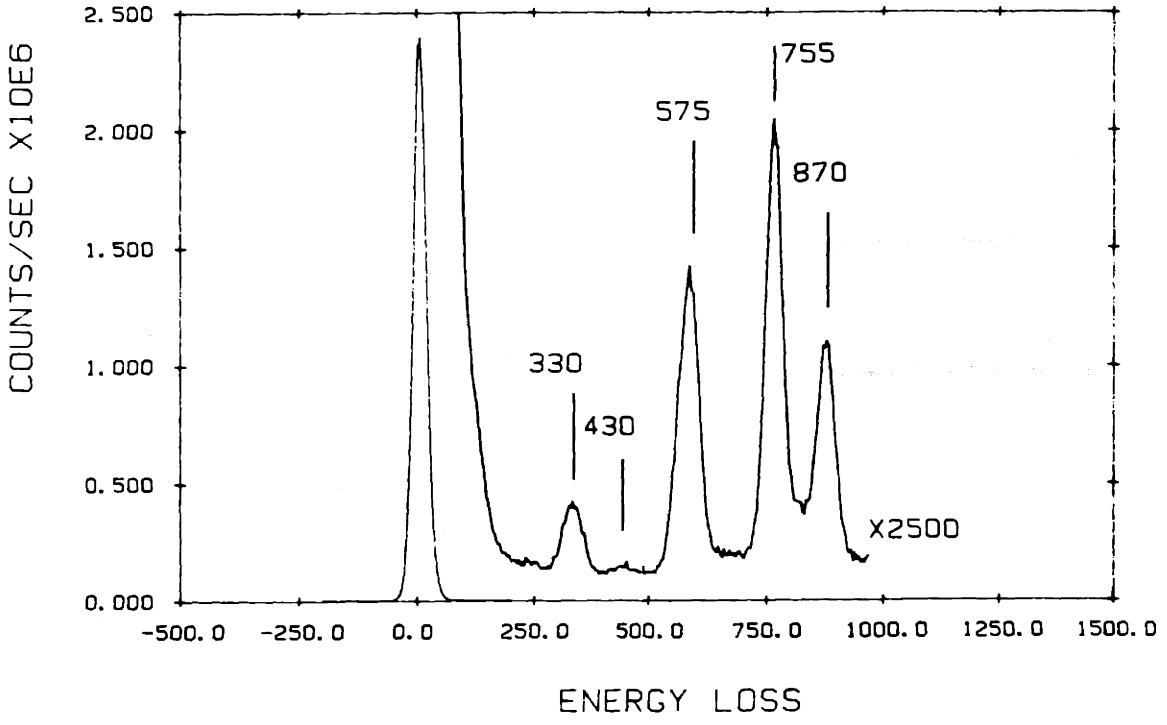

Figure 8. HREEL spectrum of the ($\sqrt{7}$ x$\sqrt{7}$)R19° ordered phase of 1,2-$C_6H_4D_2$ measured at 80 K in the specular direction at 4.0 eV impact energy. The full width at half maximum is 30 cm^{-1} for the elastic feature, 37 cm^{-1} for the feature at 775 cm^{-1} and 50 cm^{-1} for the feature at 575 cm^{-1}.

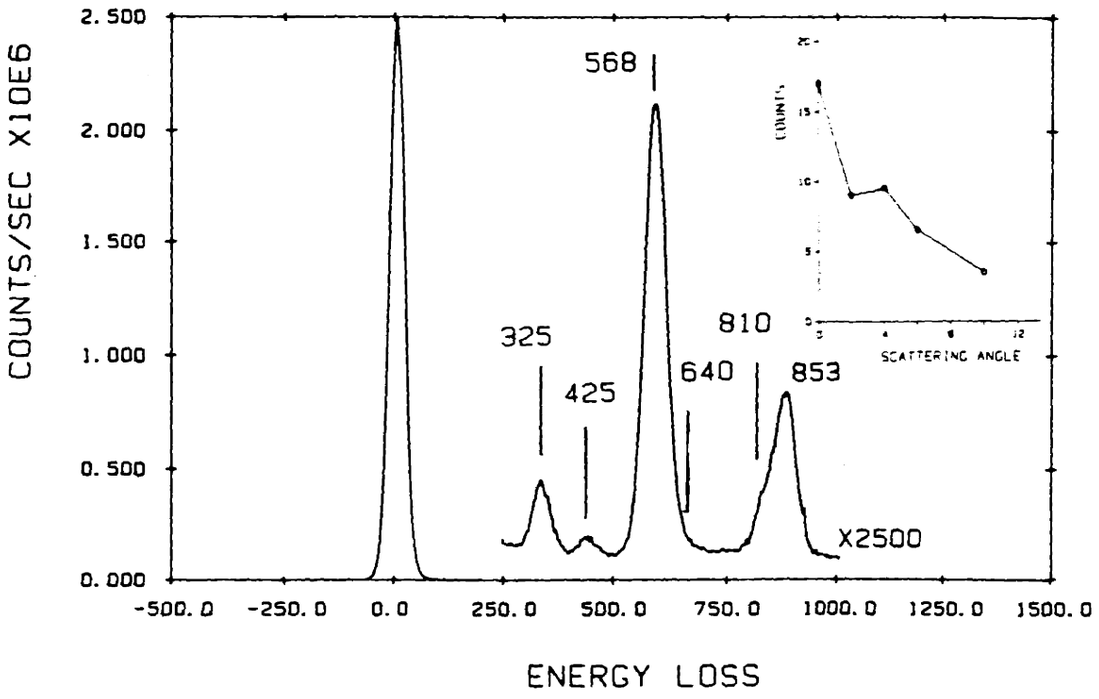

Figure 9. HREEL spectrum of the $(\sqrt{7}x\sqrt{7})R19°$ ordered phase of 1,2,4,5-$C_6H_2D_4$ measured at 80 K in the specular direction at 4.0 eV impact energy. The insert is the intensity of the feature at 640 cm^{-1} as a function of the scattering angle. The intensity of the feature in the specular direction is 2% of that of the loss feature at 565 cm^{-1}. The dipole lobe is due to the slight disordering in the ordered layer as discussed in the text.

of the C-D out-of-plane bending mode at 640 cm^{-1} in the spectrum shown in Figure 9. This mode occurs at 660 cm^{-1} in the free gas phase molecule [22-25] and at 640 cm^{-1} in adsorbed C_6D_6. The insert in Figure 9 shows a weak dipole lobe in the angular distribution of the loss feature which seems to indicate that the corresponding mode is dipole active. Similar to the C_6D_6, however, the dipole moment associated with the dipole lobe is no higher than 2% of the mode that gives rise to the 565 cm^{-1} loss in the $C_6H_2D_4$ spectrum of Figure 9. As in the case of C_6D_6, the loss feature is observed to show dipole scattering likely because of a slight disordering in the ordered layer. The corresponding out-of-plane bending mode for the disordered phase, which is not shown in this report, is observed to be dipole active as is the 640 cm^{-1} C_6D_6 loss feature of the disordered phase. That the $C_6H_2D_4$ and C_6D_6 losses show a similar dipole lobe indicates that the same origin is probably responsible for the observation of dipole activity. As will be discussed in the discussion section, the observation is significant to the question of the adsorption site and the extent of Kekulé distortion. Other loss features at 325, 425, 810 and 855 cm^{-1} are apparently due to dipole active modes as indicated by the intensities of these features in the spectrum measured in the specular direction shown in Figure 9. Except for the loss feature at 810 cm^{-1}, correlation of the 325, 425 and 855 cm^{-1} loss features of $C_6H_2D_4$ to the 330, 440 and 880 cm^{-1} C_6H_6 losses can easily be established. As will be shown in the discussion, the loss feature at 810 cm^{-1} is due to a mode whose corresponding mode for C_6H_6 is not observed.

D. HREELS of the Disordered Phase.

As the coverage is lowered below the saturation coverage of the $(\sqrt{7} \times \sqrt{7})R19°$ ordered phase, the vibrational spectra change dramatically. The lower coverage is obtained by either subjecting the surface to a lower exposure or raising the surface temperature to desorb some of the adsorbed C_6H_6 molecules of the saturated layer. Figure 10 shows the HREELS spectra of C_6H_6 at 0.07 ML coverage, which is one half of the saturation coverage, measured in both the specular and the 10° off-specular directions and at 80 K. One dramatic change in the vibrational spectrum measured in the specular direction is the appearance of two intense loss

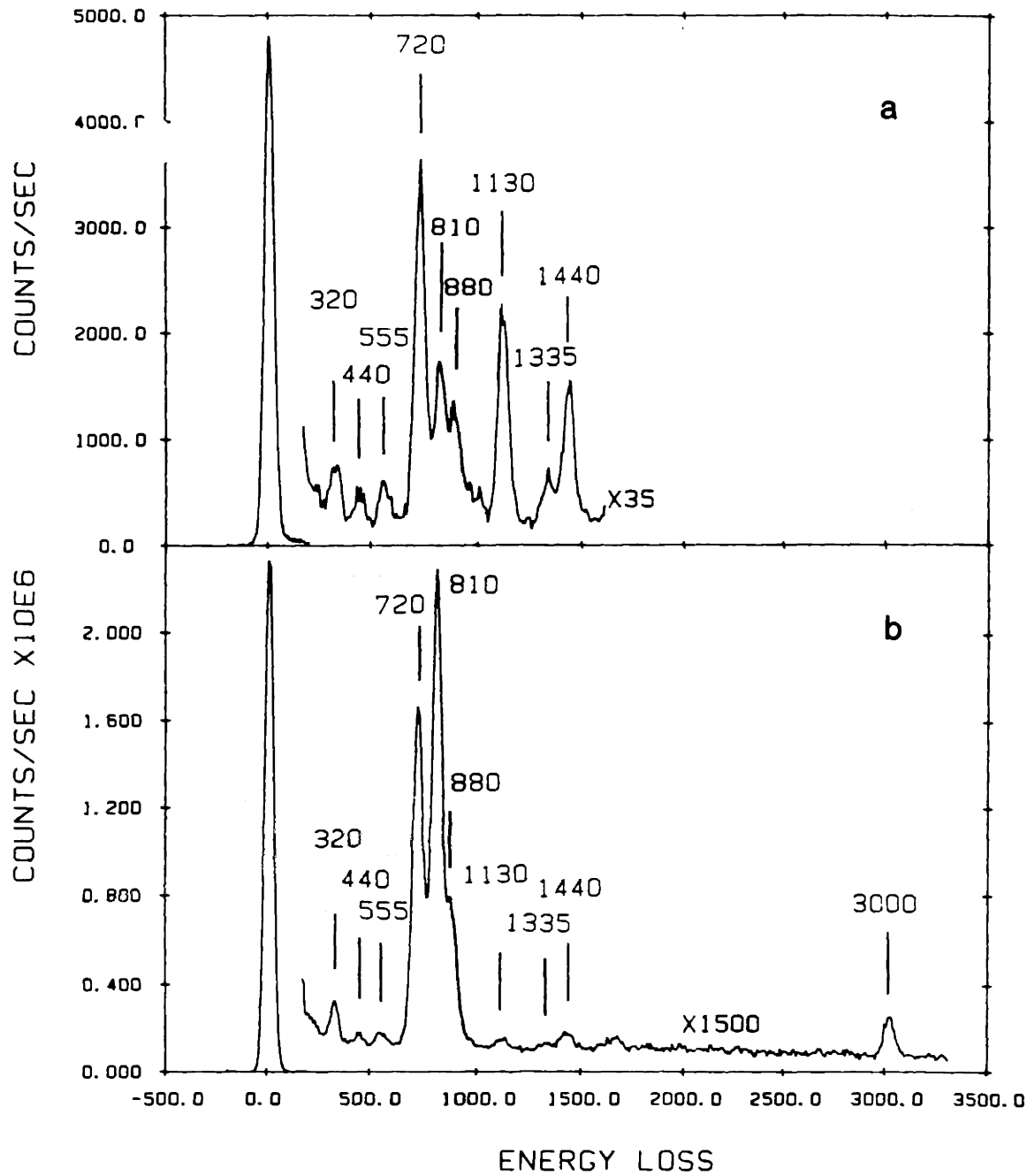

Figure 10. HREEL spectra of the disordered phase of benzene at 0.07 ML coverage measured at 80 K in the (a) specular and (b) 10° off-specular direction at 4.0 eV impact energy.

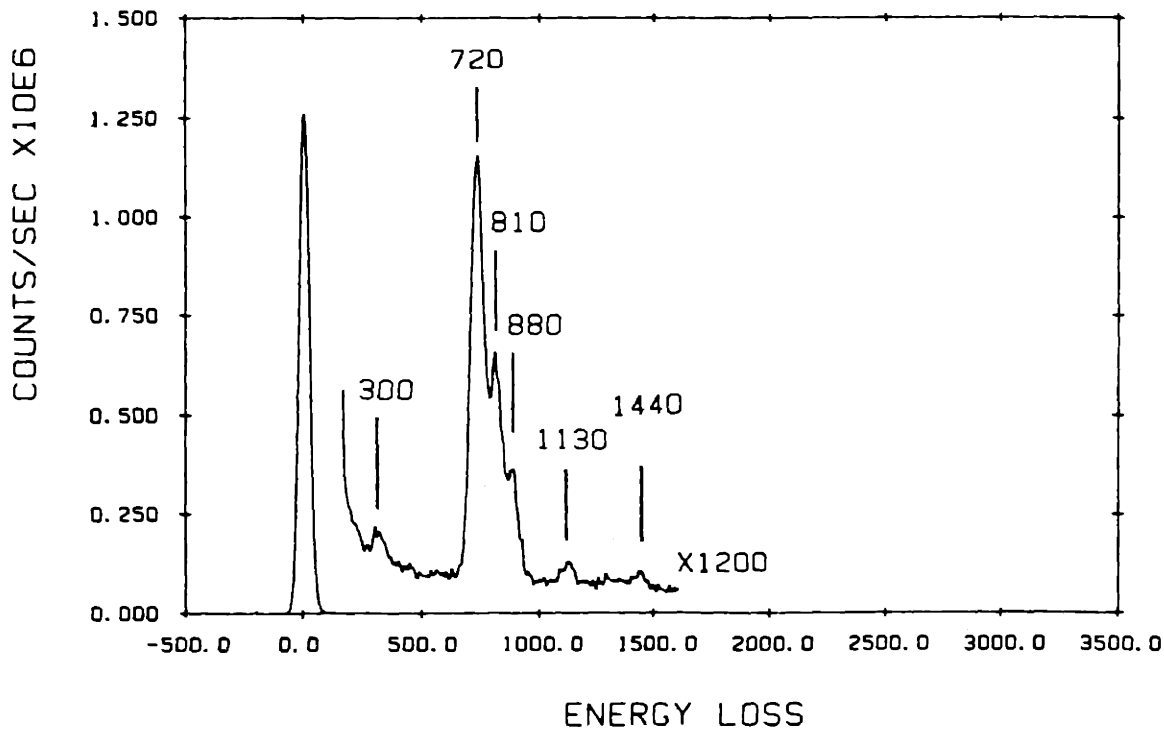

Figure 11. HREEL spectrum of the disordered phase of benzene at 0.07 ML coverage, same as for the spectra in Figure 10, measured at 300 K in the specular direction at 4.0 eV impact energy.

features at 720 and 810 cm^{-1} where a single intense feature at 755 cm^{-1} is observed for the ordered phase. Similar observation of two intense loss features at 730 and 820 cm^{-1} has been made previously [5] and the two loss features have been assigned to ν_4, the symmetric C-H out-of-plane bending mode, of C_6H_6 on two different sites. This is largely based on the observation that the two loss features show a temperature dependence in their relative intensity. This is interpreted as an indication that the populations of C_6H_6 on the two sites are a function of the surface temperature as a result of the binding energy difference.

Figure 11 shows a C_6H_6 vibrational spectrum measured in the specular direction at the same coverage as for Figure 10 but at room temperature. The observed temperature dependence of relative intensity of the two most intense loss features is consistent with the previous observation. While at 80 K the 810 cm^{-1} loss is slightly more intense than the 720 cm^{-1} loss, at room temperature the former is much less intense than the latter. The only reasonable explanation for such a daramtic change is to assume that there are two different binding sites and their relative population changes as a function of the surface temperature due to the difference in the binding energies.

Further examination of the spectra of Figure 10 and 11 also reveals a frequency shift from 320 cm^{-1} at 80 K to 300 cm^{-1} at room temperature of a loss to be assigned as the symmetric Ni-C stretch. The frequency shift of the symmetric Ni-C stretch is additional evidence that support the two site proposal. The shift can be explained by assuming the frequencies of the symmetric Ni-C stretches of the C_6H_6 adsorbed in two different sites are slightly different. The change in the relative intensity of the loss features of the symmetric Ni-C stretch modes of C_6H_6 in the two different sites results in the observation of a single peak, as a superposition of the two loss features, that shifts in frequency as a function of temperature.

In the C_6D_6 spectra shown in Figure 12 measured at 80 K and at a coverage similar to that for the spectra of C_6H_6 shown in Figures 10 and 11, three loss features at 515, 560 and

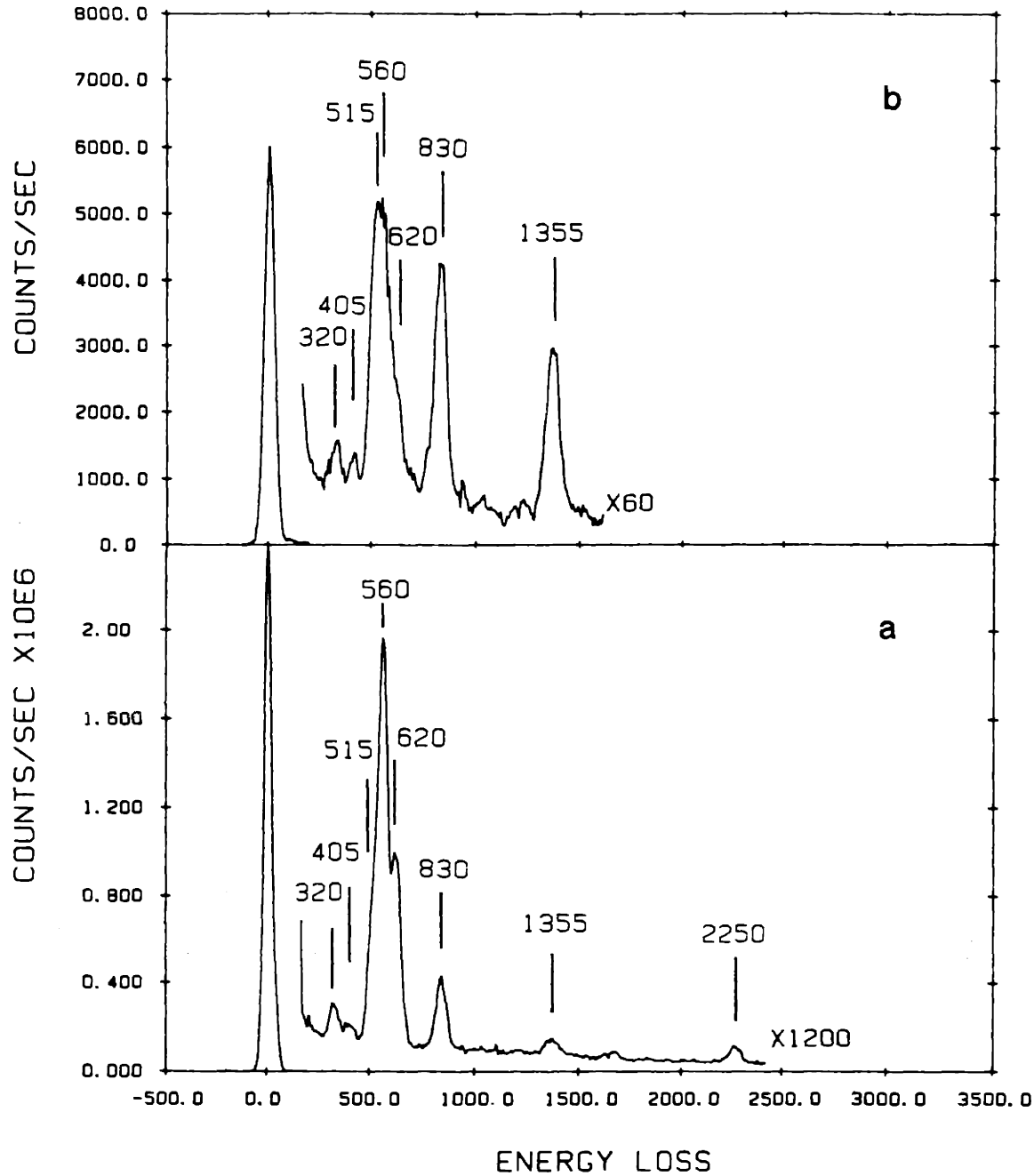

Figure 12. HREEL spectra of the disordered phase of deuterated benzene at a coverage similar to that for the spectra in Figure 10 measured at 80 K in the (a) specular and (b) 10° off-specular direction at 4.0 eV impact energy.

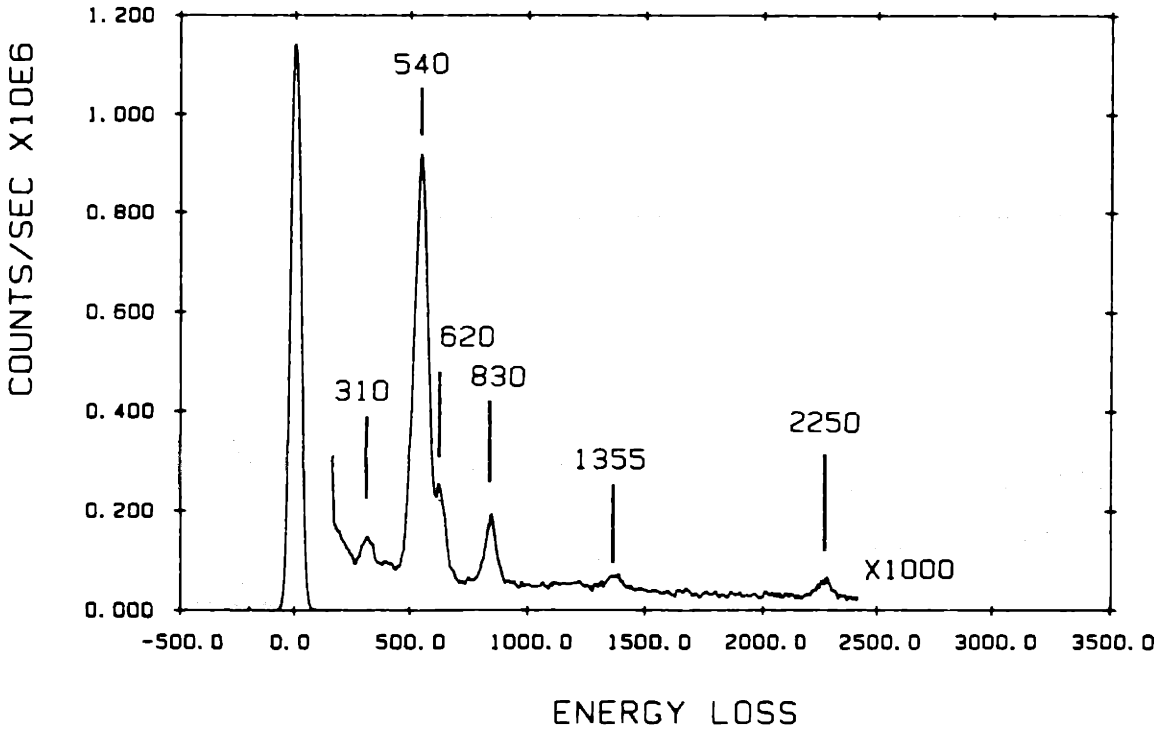

Figure 13. HREEL spectrum of the disordered phase of deuterated benzene at the same coverage as for the spectra in Figure 12 measure at 300 K in the specular direction at 4.0 eV impact energy.

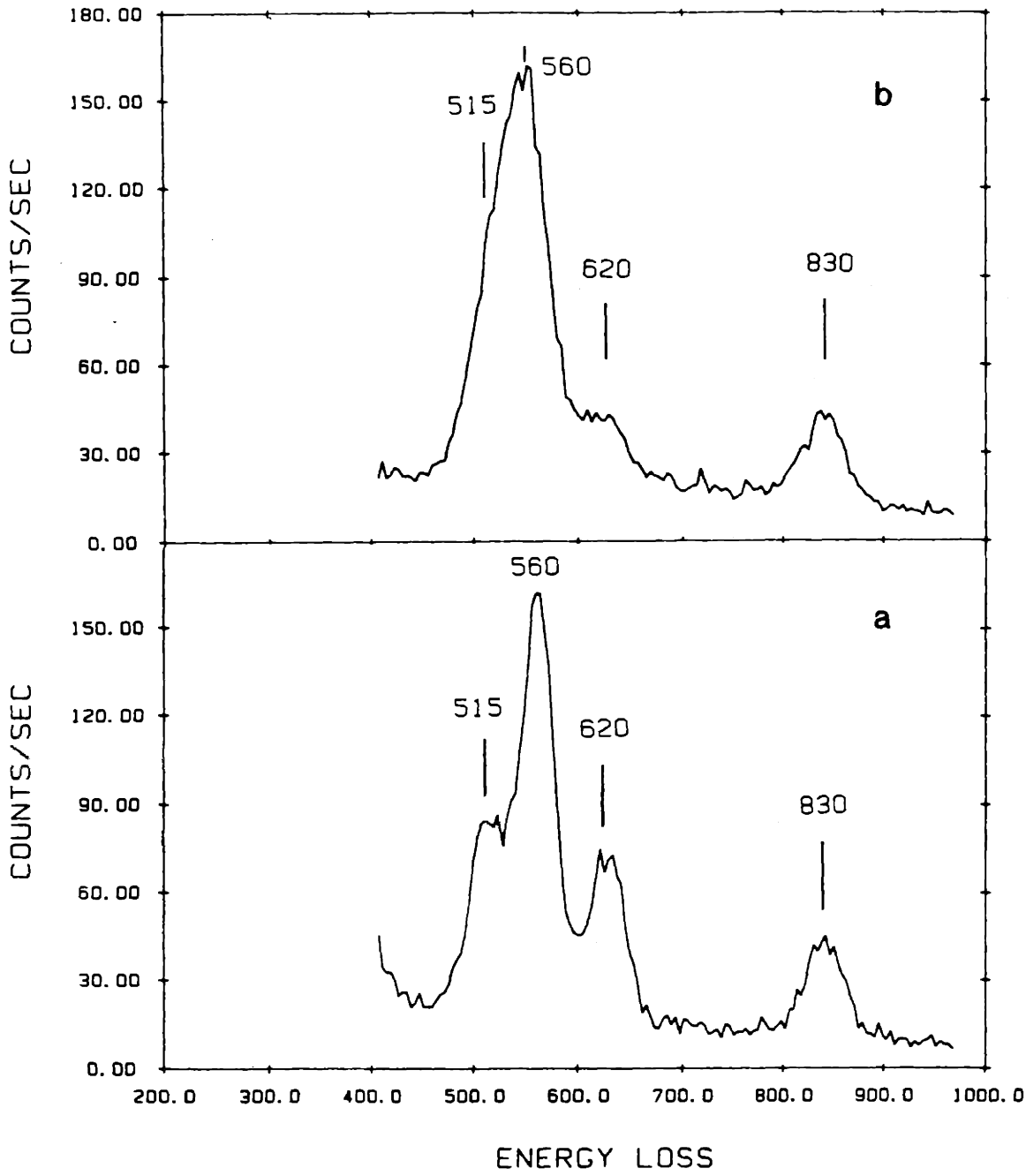

Figure 14. HREEL spectra of the disordered phase of deuterated benzene at the same coverage as for the spectra in Figure 12 measured at (a) 80 K and (b) 300 K in the specular direction at 2.0 eV impact energy.

620 cm^{-1} are observed where there is only one at 540 cm^{-1} for the ordered phase C_6D_6. Figure 13, shows a C_6D_6 spectrum measured in the specular direction at room temperature. Figure4a and 14b are two spectra of C_6D_6 at 80 K and at room temperature measured in the specular direction at a higher resolution (ΔE_{FWHM}=35 cm^{-1} for the elastic peak). At 80 K, while the loss feature at 515 cm^{-1} appears as a shoulder of the feature at 560 cm^{-1} in the spectrum measured in the specular direction shown in Figure 12, the feature is clearly resolved in the spectrum measured at a higher resolution shown in Figure 14a. It is not apparent from the C_6D_6 spectrum at 80 K alone which two of the three loss features are correlated with the 720 and 810 cm^{-1} C_6H_6 features. A comparison between the spectra at 80 K in Figure 12 and that at room temperature in Figure 13 indicates that the 515 cm^{-1} loss feature increases in intensity relative to the 560 and 620 cm^{-1} losses as the temperature is raised. This is clearly shown by the two spectra at 80 K and at room temeprature measured at the higher resolution in Figure 14. It follows that the 515 cm^{-1} C_6D_6 loss should be correlated with the 720 cm^{-1} C_6H_6 loss. The isotope ratio of 1.4 is the same as for the C_6H_6 (C_6D_6) 755(540) cm^{-1} loss feature of the ordered phase indicating that they are due to the same mode. The 560 cm^{-1} C_6D_6 loss must be related to the 810 cm^{-1} C_6H_6 loss, although the isotope ratio of 1.45 is unusually high. Alternative correlation of the loss feature at 620 cm^{-1} for C_6D_6 to the feature at 810 cm^{-1} for C_6H_6 would leave the feature at 560 cm^{-1} for C_6D_6 with no C_6H_6 feature of comparable intensity to correlate with. The C_6D_6 spectrum at 80 K in Figure 14 shows that the 620 cm^{-1} feature is one third of the intensity of the 560 cm^{-1} loss feature. As a result, the C_6H_6 loss feature associated with the 620 cm^{-1} C_6D_6 loss feature may have been obscured by others for its intensity would be only about one third of the 810 cm^{-1} loss feature. From the change of the intensities of the three C_6D_6 loss features as a function of the surface temperature it can also be concluded that the two C_6D_6 loss features at 560 and 620 cm^{-1} are associated with a molecule on one of the two sites while the 515 cm^{-1} loss feature with a moelcule on the other site.

The change in the relative intensity as a function of the surface temperature indicates that of the two C_6H_6 sites, the one associated with the 720 cm^{-1} loss feature is the lower binding energy site and the one associated with the 810 cm^{-1} loss feature is the higher binding energy site. In the discussion that follows they will be referred to as the lower and the higher binding energy sites. It has been mentioned that the 720 cm^{-1} C_6H_6 loss feature of the disordered phase and the 745 cm^{-1} loss feature of the ordered phase are due to the same mode. It will be shown in the discussion section that the mode is ν_4, the symmetric C-H out-of-plane bending mode because none of the other modes is capable of displaying a dipole moment as intense as observed. The 810 cm^{-1} loss feature will be similarly assigned.

The difference between the three C_6H_6 species, one for the ordered phase and two for the disordered phase, in terms of adsorption site and structure is a more difficult question to answer. The starting point is to define the symmetry point group for each of the three adsorption sites by determining the dipole activity of each vibrational mode [16]. For the disordered phase most of the loss features appear at the same frequencies as in the ordered phase exccept for the ones that have already been discussed. The C_6H_6 loss features at 440, 555, 1130 and 1440 cm^{-1} in the specular direction are more prominent for the disordered phase than the ordered phase. This may mean that the corresponding modes have changed to be dipole active. Caution, however, should be taken before drawing such a conclusion because there is a dramatic decrease in the surface reflectivity with respect to the incident electron beam, measured by the intensity of the elastic peak, from the ordered phase to the disordered phase. The trend continues as the coverage is lowered further. The consequence of the lower reflectivity is that in a HREELS spectrum, a loss observed by impact scattering may appear to be more prominent relative to one by dipole scattering because the intensity of the former is proportional to the reflected beam, the elastic peak [16]. It is thus necessary to measure the angular distribution of the loss intensities, in the case of weak loss features, in order to determine the dipole activity. Figure 15 shows the angular distributions of the loss features of the disordered C_6H_6 phase at 440, 555, 1130, 1335 and 1440 cm^{-1} measured at 80 K. The

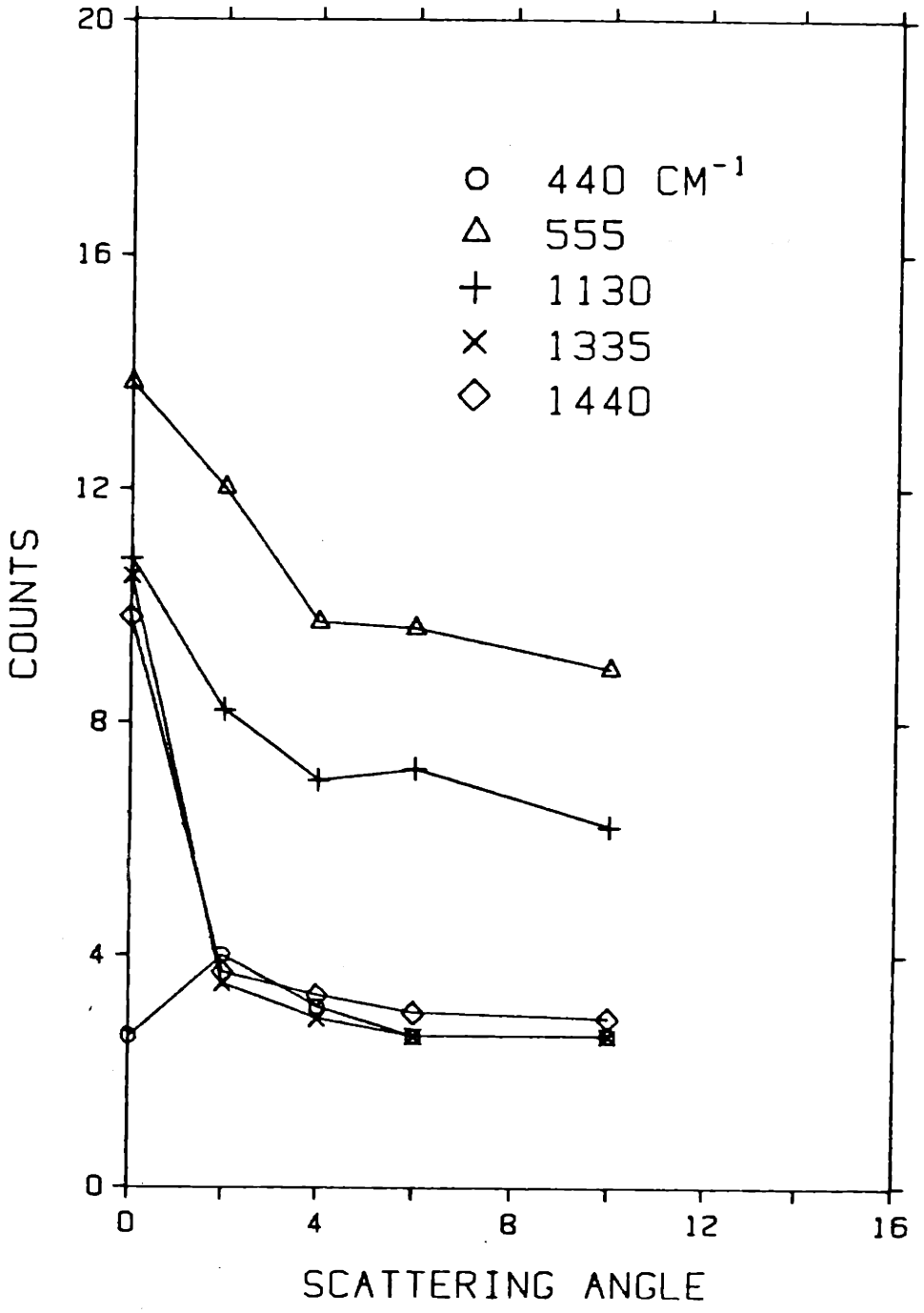

Figure 15. The intensities of the vibrational loss features of the disordered phase benzene at 440, 555, 1130, 1335 and 1440 cm^{-1} as a function of the scattering angle measured at 80 K and at 4.0 eV impact energy.

data clearly show that except for the 1335 cm^{-1} loss feature, all loss features are due to dipole active modes. The angular distribution of the 620 cm^{-1} C_6D_6 loss feature is not measured since it can be concluded that the mode has also changed to be dipole active based on the fact the loss feature is as intense as one third of the feature at 560 cm^{-1} which is due to a mode (ν_4) with a large dynamical dipole moment. It is an interesting observation that all six of the loss features have reversed their dipole activity from the ordered phase.

Because there are two different C_6H_6 sites, it becomes necessary to determine for each of them the dipole activity of each mode. The 620 cm^{-1} C_6D_6 loss feature decreases in intensity proportionally to the 560 cm^{-1} loss feature from 80 K to room temperature. This observation shows that the two losses are associated with the same molecule, the one on the higher binding energy site. In addition, the observation indicates that the loss feature for the C_6D_6 on the lower binding energy site, that corresponds to the 620 cm^{-1} feature of the C_6D_6 on the higher binding energy site and should also be at about 620 cm^{-1}, is much less intense. The assumption that this mode should appear at 620 cm^{-1} for C_6D_6 in both the lower and higher binding energy sites is reasonable because the frequencies of $C_6H_6(C_6D_6)$ vibrational modes have been shown to be very similar on different transition metal surfaces except for the symmetric out-of-plane bending mode (ν_4). Consequently, the mode for the lower binding energy site that corresponds to the mode at 620 cm^{-1} for the higher binding energy site is concluded to be nondipole active.

The two loss featires at 440 and 555 cm^{-1} are much weaker at room temperature. It seems that the modes for the two loss features are dipole active only for C_6H_6 adsorbed on the higher binding energy site and are nondipole active for the C_6H_6 on the lower binding energy site. The angular distributions measured at room temperature shown in Figure 16 confirm the observation that the dipole lobes of the two loss features decrease significantly from 80 K to room temperature.

The dipole lobes of the loss features at 1130 and 1440 cm^{-1} also decrease in intensity as the temperature is increased but not as dramatically as for the 440 and 555 cm^{-1} loss features

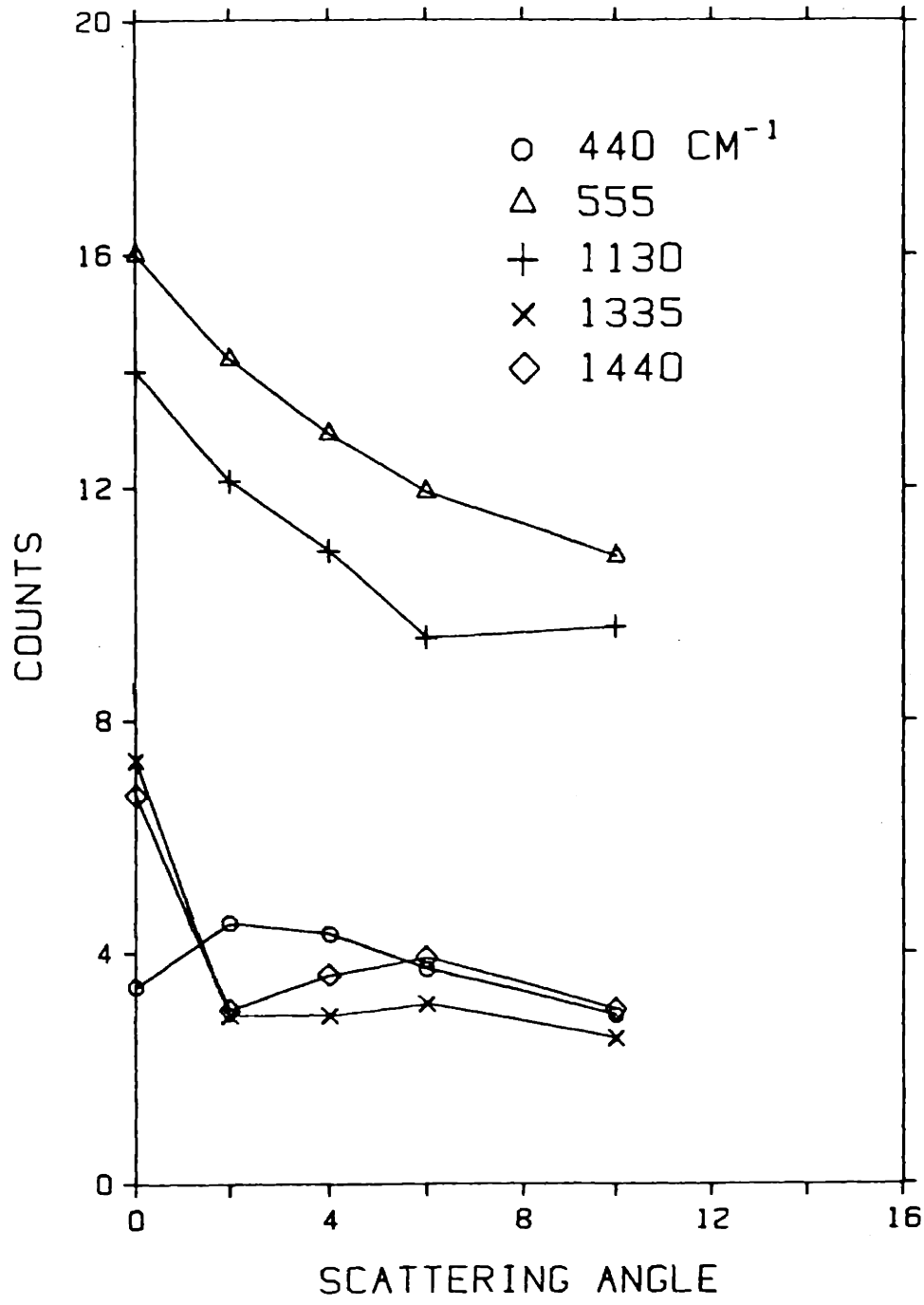

Figure 16. The intensities of the vibrational loss features of the disordered phase benzene at 440, 555, 1130, 1335 and 1440 cm^{-1} as a function of the scattering angle measured at 300 K and at 4.0 eV impact energy.

However, as will be shown in the discussion section, the modes at 1130 and 1430 cm^{-1} are necessarily nondipole active if the two modes giving rise to the 440 and 555 cm^{-1} loss features are nondipole active. The mode that gives rise to the remaining weak loss feature at 1335 cm^{-1} appears to be nondipole active for both the higher and the lower binding energy C_6H_6 because no dipole lobe is observed at any surface temperature.

The results on the disordered phase can be summed up as follows. Benzene is adsorbed on two different sites. The benzene adsorbed on the lower binding energy site is characterized by an intense loss feature at 720 cm^{-1} and the C_6H_6 adsorbed on the higher binding energy site is characterized by an intense loss feature at 810 cm^{-1}. Five of the loss features associated with the C_6H_6 on the higher binding energy site are observed to have reversed their dipole activity from C_6H_6 of the ordered phase. The modes that correspond to the loss features at 440, 555, 1130 and 1440 cm^{-1} change to dipole active, while the one at 1335 cm^{-1} change to be nondipole active. The reversal in the dipole activity is also observed for another mode that gives rise to the 620 cm^{-1} C_6D_6 loss feature. For the C_6H_6 on the lower binding energy site, these six modes are nondipole active. The symmetry point groups for the three kinds of C_6H_6 sites, two kinds of C_6H_6 in the disordered and one in the ordered phase, must be different.

For the correlation made earlier between the 810 cm^{-1} C_6H_6 and 560 cm^{-1} C_6D_6 loss features, the isotope ratio of 1.45 is much higher than a normal mode of H motion. It is probably not a coincidence that the C_6H_6 molecule involved in this anomalous ratio also happens to be the one of lower symmetry indicated by the larger number of dipole active modes. If the C_6H_6 or the C_6D_6 mode is in Fermi resonance with another mode, the frequency of the C_6H_6 or the C_6D_6 mode would be shifted upwards or downwards and consequently the isotope ratio would be anomalously high. This possibility is made more probable because the lower symmetry of the higher binding energy C_6H_6 molecule means that more modes have the same symmetry and are dipole active. An experiment was carried out, to verify whether the C_6H_6 mode is in Fermi resonance with the combination band of the 320 and 440 cm^{-1} modes.

The frequency of the C_6H_6 mode without Fermi resonance can be estimated to be at 785 cm^{-1} from the frequency of the corresponding C_6D_6 mode at 560 cm^{-1} using the isotope ratio of 1.4, which is the ratio observed for the other two kinds of C_6H_6 . The mode, at 785 cm^{-1} without Fermi resonance, would be in a position to be in Fermi resonance with the combination band at about 770 cm^{-1} of the 320 and 440 cm^{-1} modes. It should be noted that the symmetric Ni-C stretch of the higher binding energy C_6H_6 may be slightly higher than 320 cm^{-1}, the observed loss frequency because the loss is an overlap of two features. Should this be true, $^{13}C_6H_6$ would be free of such an effect and the corresponding mode should be observed at a frequency lower by about 30 cm^{-1} than the $^{12}C_6H_6$ loss at 810 cm^{-1}. The vibrational spectrum for $^{13}C_6H_6$ along with a spectrum for C_6H_6 measured under the same conditions are shown in Figure 17 of the disordered phase at 80 K. The mode under consideration does not show a 30 cm^{-1} frequency shift as expected. The frequency of the mode does shift from 810 to 800 cm^{-1} but this shift is too small to support the possibility of Fermi resonance between the 810 cm^{-1} C_6H_6 mode and the combination band.

E. Higher Temperature Species

Benzene adsorption on Ni(111) is only partially reversible [12,13]. After raising the surface temperature above 500 K about 40% of the saturation layer desorbs into the gas phase in the form of molecular C_6H_6 . It is important to know what happens to the remaining C_6H_6 . The broad H_2 thermal desorption curve extending from 400 to 700 K indicates that the remaining C_6H_6 dehydrogenates completely in this temperature range. Auger measurement after annealing the surface to 700 K shows no C presence on the surface indicating that C has dissolved into the bulk.

However, the dehydrogenation of a molecule as complex as C_6H_6 is unlikely to be a one-step process. This is shown in the broadness and the irregular appearance of the H_2 thermal desorption curve shown in Figure 3. The curve consists of several peaks which probably corresponds to the different steps of benzene dehydrogenation. It should be noted that H_2 desorption is at about 375 K on Ni(111) without the presence of a coadsorbate, so that the

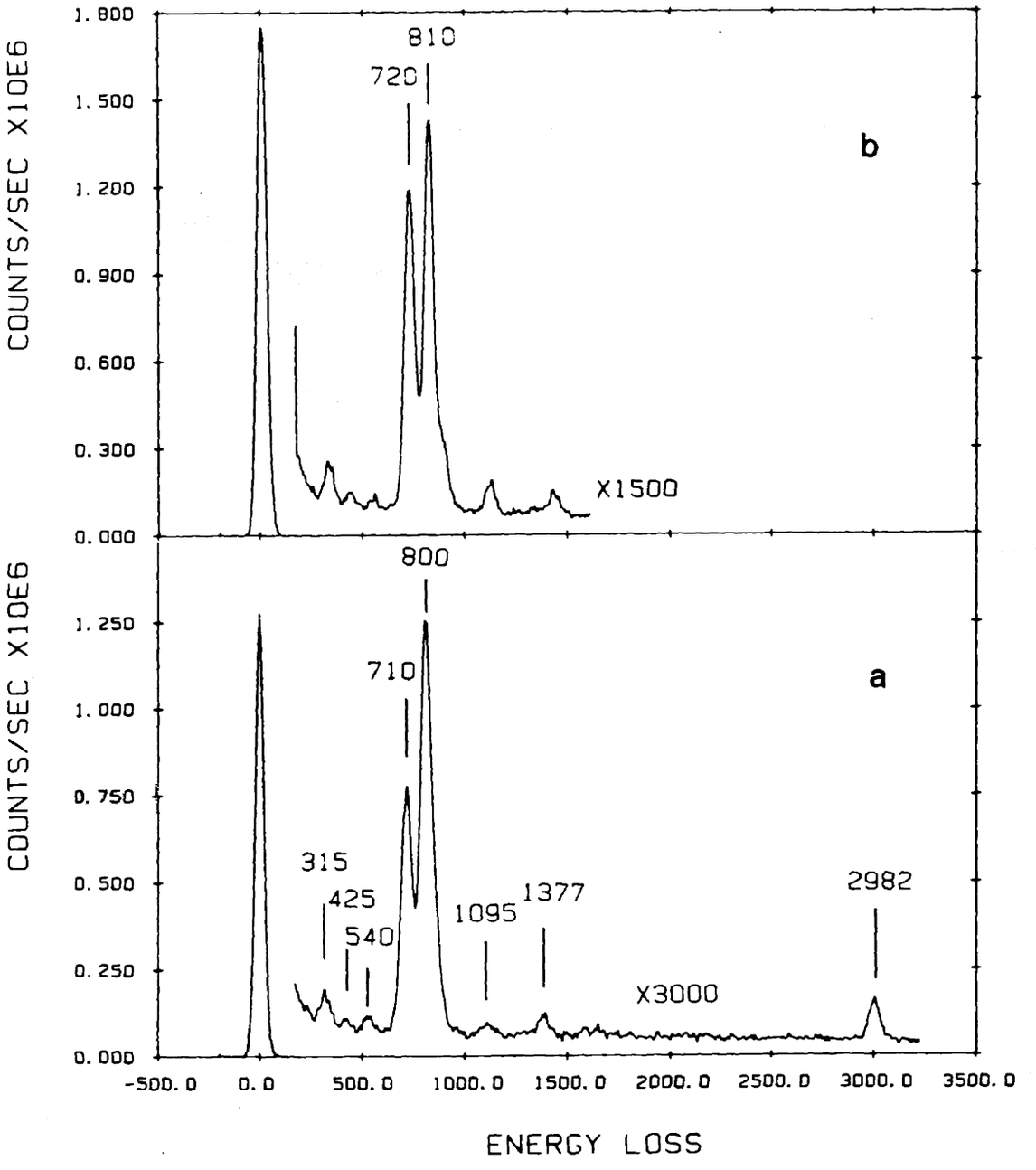

Figure 17. HREEL spectrum of the disordered phase of (a) $^{13}C_6H_6$ and (b)$^{12}C_6H_6$ at 0.07 ML coverage measured at 80 K in the specular direction at 4.0 eV impact energy.

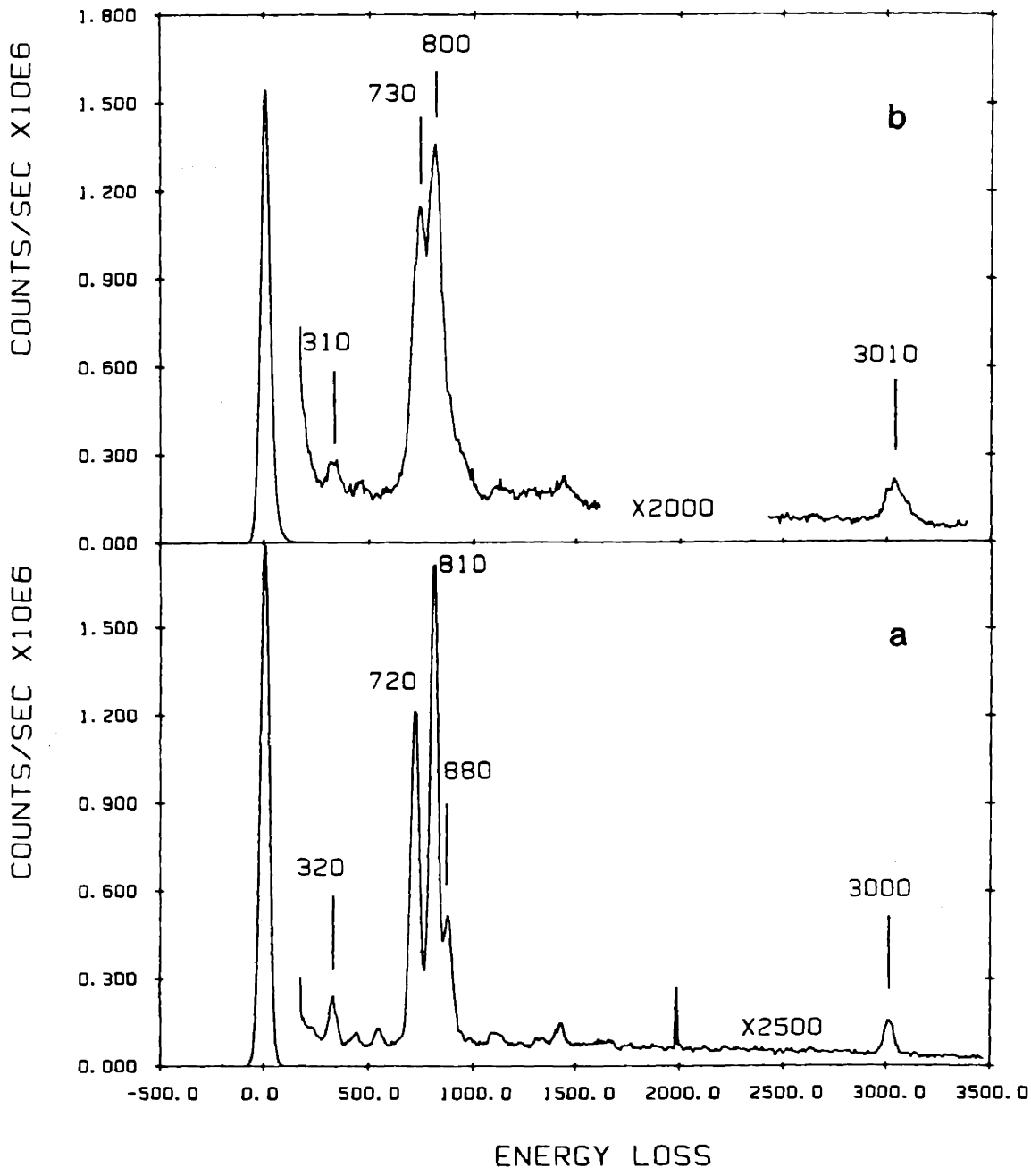

Figure 18. HREEL spectra after annealing to (a) 320 K, (b) 400 K, (c) 505 K and (d) 560 K following the adsorption of benzene and the formation of the $(\sqrt{7} \times \sqrt{7})R19°$ ordered phase at 260 K. The dehydrogenation takes place between 400 and 700 K as indicated by the thermal desorption spectrum in Figure 3.

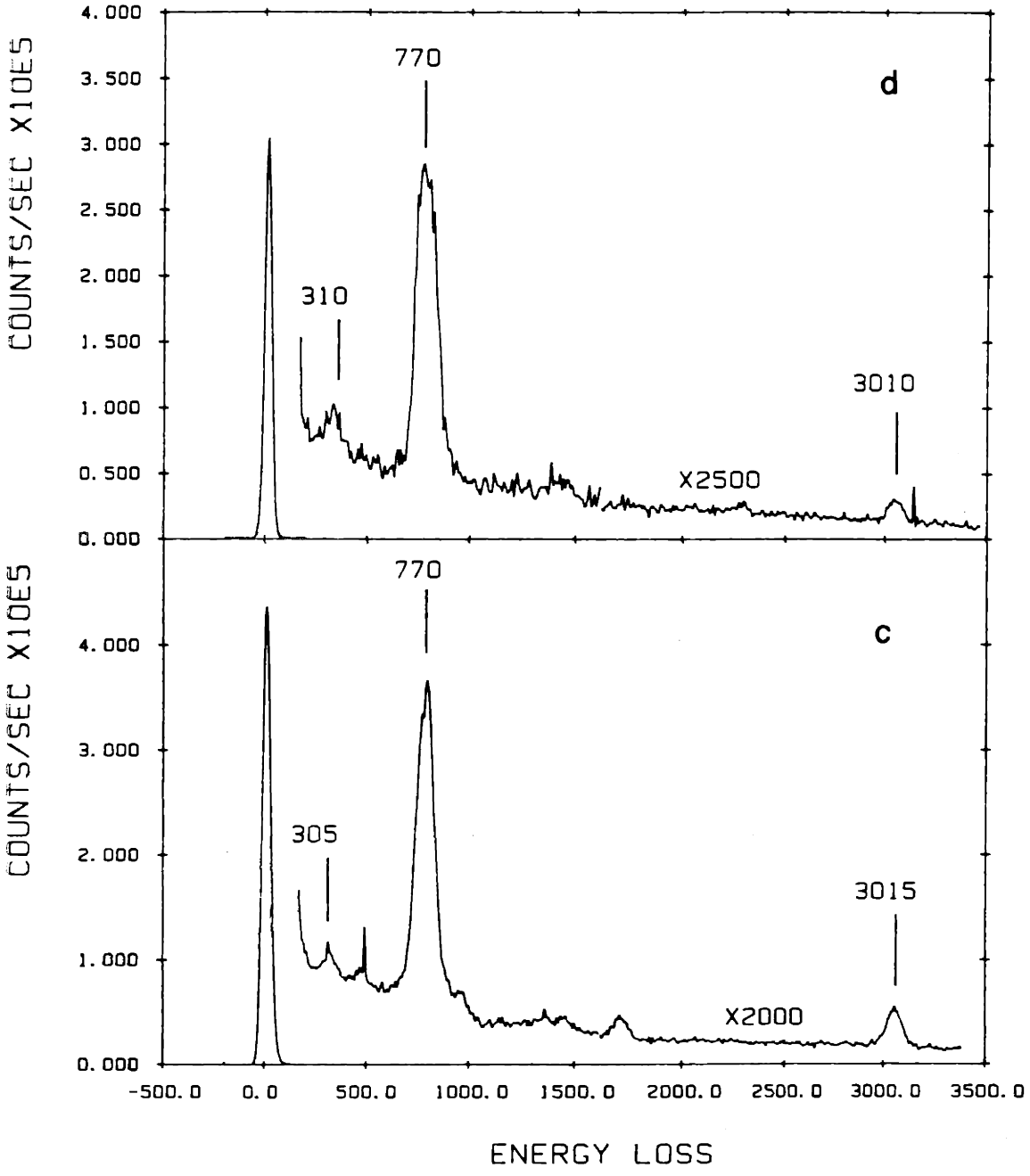
COUNTS/SEC X10E5
4.000
3.500
3.000
2.500
2.000
1.500
1.000
0.500
0.000
770
d
310
3010
X2500
COUNTS/SEC X10E5
770
c
305
3015
X2000
-500.0
0.0
500.0
1000.0
1500.0
2000.0
2500.0
3000.0
3500.0
ENERGY LOSS

observed H_2 desorption must be kinetically limited by the dehydrogenation process on the surface. Figure 18 is a series of vibrational spectra obtained after annealing the surface, initially saturated, to different temperatures. The analysis of these spectra along with the detailed surface chemistry of the remaining C_6H_6 will be the concern of another report [27], but a brief account will be presented in the discussion section. What should be noted in the spectra is the presence of loss features that appear to be at frequencies and of intensities similar to those of the symmetric C-H out-of-plane bending modes of the molecular C_6H_6 on the surface at lower temperatures. In the spectrum taken after annealing the surface at 560 K a single loss at 770 cm^{-1} is observed. The broadness of the loss feature, which is undoubtedly due to inhomogeneous broadening, bears important information on the identities of the surface species. There are also a number of weak loss features in the spectra which will not be discussed except that their presence is an indication of the complexity of the surface species.

IV. Discussion

A. The Ordered Phase

The ordered phase of the C_6H_6 on Ni(111) that gives rise to the observed $(\sqrt{7} \times \sqrt{7})R19°$ LEED pattern has a unit cell with a unit vector 7 times that of the substrate and rotated by 19°. Because there can be two rotations, clockwise and counterclockwise, there are 12 first order diffraction beams [28]. It is straightforward to see that there can be only one C_6H_6 molecule per unit cell provided that C_6H_6 is adsorbed on the surface molecularly and with the ring parallel or nearly parallel to the surface. The assumption is born out in the TDS, LEED and vibrational results that C_6H_6 retains its molecular identity upon adsorption on the surface. Since thermal desorption shows that 40% of the saturated layer desorbs as free C_6H_6 molecules while the LEED result shows that there cannot be two different adsorbates on the surface with a partition of 40% and 60%, the surface layer must be composed of C_6H_6 only. As will be discussed later, the vibrational results can only be interpreted in terms of molecular C_6H_6 with the ring parallel to the surface.

Not only can the unit cell not accommodate more than one C_6H_6 but also the orientation within the plane of the ring is restricted. Benzene cannot adopt a structure with orientation that would give rise to a distance between hydrogens of neighboring molecules smaller than the hydrogen van der Waals diameter which is 2.4 Å . Because the real space lattice is known, the distance between hydrogens of two neighboring C_6H_6 molecules can be calculated, for any given orientation, assuming that the molecular structure is not significantly perturbed and thus the bond length parameters of the gas phase C_6H_6 molecule can be used. Of the two configurations shown in Figure 19 which are rotated with respect to one another by 30° around the C_6 axis of the molecule, only one is allowed as a result of steric restriction. For configuration B, for which the C-H bond is aligned along the $[11\bar{2}]$ direction, the calculated closest distance between hydrogen of neighboring molecules is 1.85 Å . Because the distance is smaller by 0.55 Å than the hydrogen van der Waals diameter, hydrogen would intrude significantly into the space defined by the van der Waals diameter of H on a neighboring molecule and as a result such a configuration can be dismissed. On the other hand, configuration A, for which the C-H bond point along $[\bar{1}10]$ direction, gives a closest and second closest distance of 2.4 and 2.6 Å . Now that neither is smaller than the H van der Waals diameter, this rotational configuration should be considered in the vibrational analysis.

Figure 20 shows benzene adsorbed at three kinds of binding sites, the atop, the bridge and the threefold hollow sites with the two rotational orientations. For adsorption on the atop site, both rotational configurations have C_{6v} symmetry if the interaction between C_6H_6 and the surface is limited to the first layer Ni atoms but is reduced to $C_{3v}(\sigma_v)$ (B) and $C_{3v}(\sigma_d)$ (A) respectively, when the perturbation of the second layer Ni is included. Due to the steric effect discussed above, only configuration A needs to be considered in the vibrational analysis. For the threefold site, the one labeled as configuration D, which corresponds to C_{3v} (σ_v), can be ruled out based on steric arguments while configuration C of $C_{3v}(\sigma_d)$ symmetry needs to be considered. For the same steric reasons only the benzene with C_{2v} (x-y) (E) symmetry on the bridge site needs to be included in the discussion of vibrational assignments. The symmetry

C_{2v} (x-y) reduces to $C_s(\sigma_d)$ when consideration of the effect of the substrate is extended beyond the first Ni layer. It may be asked what happens if all the configurations favored by the steric effect are much less stable than one of the other three, for example the one with the C_{3v} (σ_v) symmetry on the threefold site, without considering the steric effect of the neighboring molecules. The answer is that the $(\sqrt{7} \times \sqrt{7})$R19° ordered phase would probably not have been observed. Thus the LEED result provides important information about the symmetry point group and, combined with the vibrational analysis, the adsorption site.

Figure 19. Two rotational orientations of benzene adsorption in the $(\sqrt{7} \times \sqrt{7})$R19° ordered phase on Ni(111) (a) The distance between two neighboring hydrogen atoms on two molecules in this orientation is 1.85 Å, smaller by 0.55 Å than the hydrogen van der Waals diameter. The two hydrogens intrude into the space of one another defined by the hydrogen van der Waals diameter. (b) The closest distance between the neighboring hydrogen on two molecules in this orientation is 2.4 Å and they do not intrude into the space of one another defined by the van der Waals diameter.

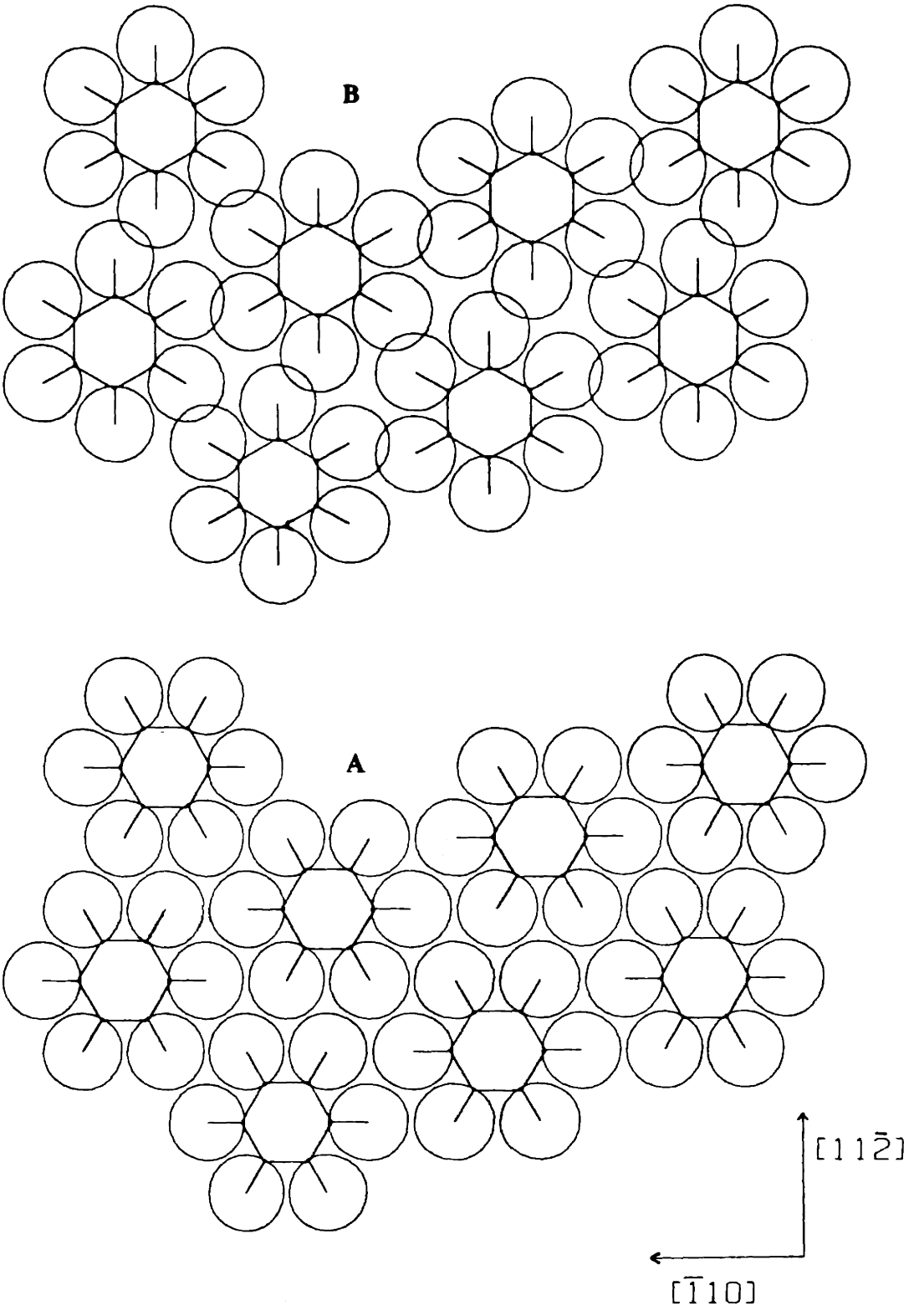
B
A
[11$\bar{2}$]
[$\bar{1}$10]

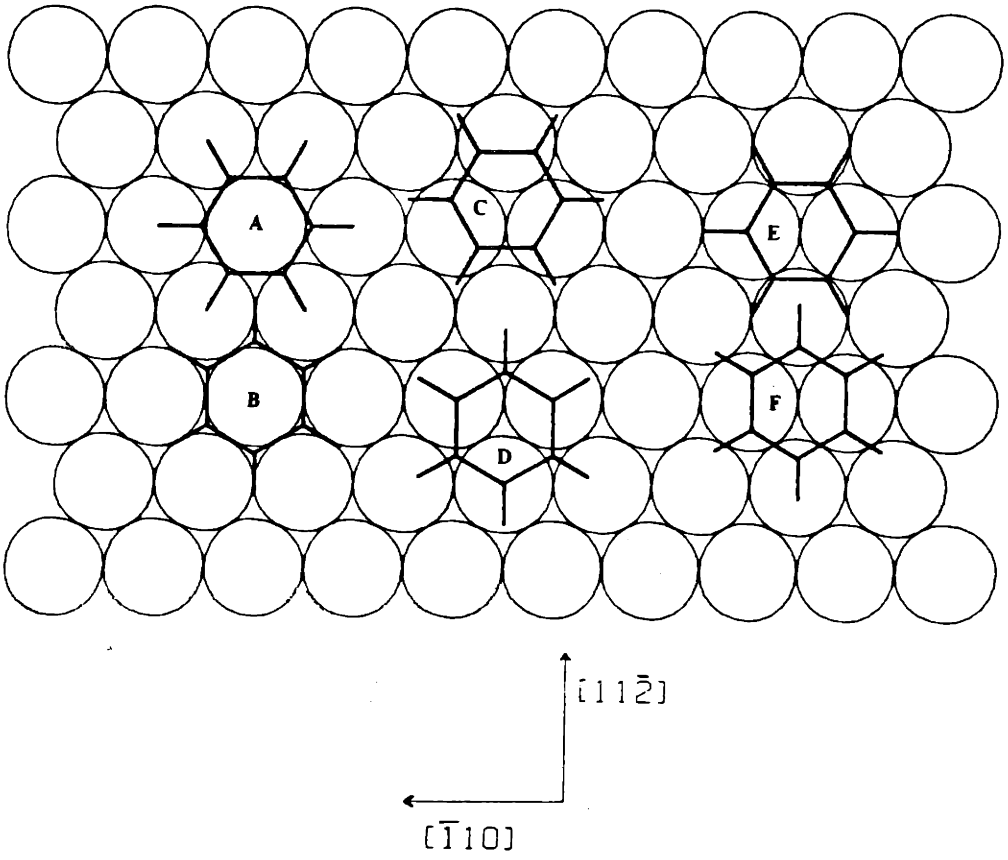

Figure 20. Six possible adsorption orientation-sites of benzene on Ni(111) surface. The symmetry point group is (A) C_{6v}, (B) C_{6v}, (C) $C_{3v}(\sigma_d)$, (D) $C_{3v}(\sigma_v)$, (E) C_{2v}(x-y) and (F) C_{2v}(x-x).

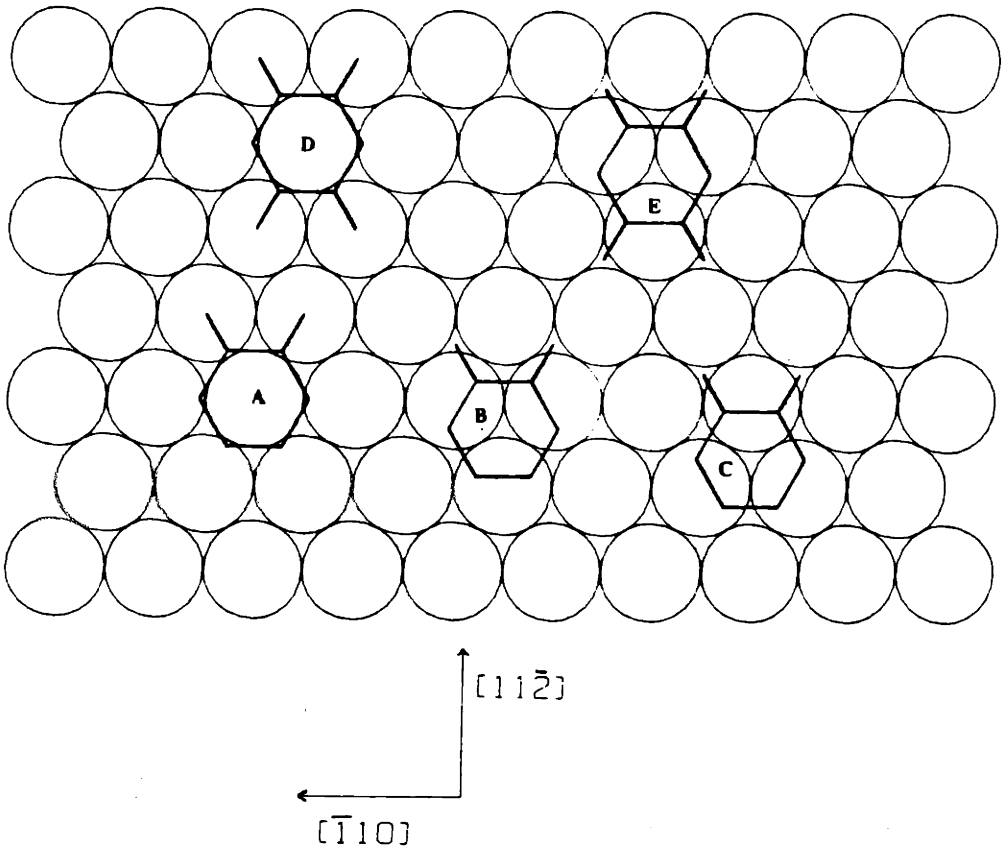

Figure 21. The configurations of (A) 1,2-$C_6H_4D_2$ adsorbed on the atop site with $C_s(\sigma_d)$ symmetry, (B,C) 1,2-$C_6H_4D_2$ adsorbed on the threefold hollow sites with $C_s(\sigma_d)$ symmetry. (D) 1,2,4,5-$C_6H_2D_4$ on the atop with C_{2v}(x-y) symmetry and (E) 1,2,4,5-$C_6H_2D_4$ on the threefold hollow site with $C_s(\sigma_d)$ symmetry.

1. The Assignment of the Vibrational Spectra

Although the LEED result rules out some adsorption configurations, there are still several combinations of sites and configurations that are compatible with the fixed orientation and need to be considered. Benzene may be adsorbed on the surface with the ring parallel to or at a slight angle with respect to the surface and the tilting may be along different directions. The adsorption site may be the atop, the bridge and the threefold. The vibrational analysis may tell what the actual structure of the C_6H_6-surface complex is by determining the symmetry point group of the complex. Because of the LEED result, the following discussion is limited to include only thle point groups, C_{6v} , $C_{3v}(\sigma_d)$, C_{2v}(x-y) and $C_s(\sigma_d)$. The first three correspond to adsorption on the atop, the threefold and the bridge sites which are shown in Figure 20. The point group $C_s(\sigma_d)$ is for adsorption with the ring tilted or with the center of the ring displaced from a high symmetry site. Adsorption leading to C_1 will not be discussed because for C_1 symmetry there should be no nondipole active mode which is contrary to the vibrational results that some of the modes are nondipole active. It should also be noted that the C_{6v} and C_{2v}(x-y) are the symmetry point group for the atop and the bridge site adsorption when only the first layer of the substrate is considered and they would respectively reduce to $C_{3v}(\sigma_d)$ and $C_s(\sigma_d)$ otherwise. Such a reduction in the symmetry will be accompanied by some modes becoming dipole active. However, since the perturbation of the second layer of Ni atoms is expected to be weak, as far as the symmetry point group is concerned, the dynamical dipole moment thus induced will be small and the corresponding loss feature will be weak. Table I [16] is a list of the symmetry of each C_6H_6 mode for all the point groups on a (111) surface for adsorption with the ring parallel or nearly parallel to the surface except C_1. Groups ruled out by the steric effect discussed earlier are also included because they may be needed for the vibrational analysis of the disordered phase for which the steric effect will not be operative. Also listed in Table I are the frequencies of the modes of gas phase $C_6H_6(C_6D_6)$ and frequencies of the observed loss feature of $C_6H_6(C_6D_6)$ on Ni(111) in the ordered phase according to the assignments made in the following discussion.

Table I. Symmetry of benzene vibrational modes and comparison of frequencies on Ni(111) with gas phase values

Mode Number[a]	Symmetry representation[b]							Vibrational frequencies (cm^{-1}) C_6H_6		C_6D_6	
	D_{6h}	C_{6v}	$C_{3v}(\sigma_d)$	$C_{3v}(\sigma_v)$	$C_s(\sigma_d)$	$C_s(\sigma_v)$	C_{2v}	Gas phase[c]	Ni(111)	Gas phase[c]	Ni(111)
ν_1	A_{1g}	A_1	A_1	A_1	A'	A'	A_1	3062	3023	2293	2256
ν_2	"	"	"	"	"	"	"	992	880	943	830
ν_3	A_{2g}	A_2	A_2	A_2	A"	A"	A_2	1326		1037	
ν_4	A_{2u}	A_1	A_1	A_1	A'	A'	A_1	673	755	497	540
ν_5	B_{1u}	B_1	A_2	A_1	A"	A'	B_2	3068		2292	
ν_6	"	"	"	"	"	"	"	1010		969	
ν_7	B_{2g}	B_1	A_2	A_1	A"	A'	B_2	995		827	
ν_8	"	"	"	"	"	"	"	703		601	
ν_9	B_{2u}	B_2	A_1	A_2	A'	A"	B_1	1310	1335	1286	1320
ν_{10}	"	"	"	"	"	"	"	1150		824	
ν_{11}	E_{1g}	E_1	E	E	A'+A"	A"+A'	B_2+B_1	849	850	662	640
ν_{12}	E_{1u}	E_1	E	E	A"+A'	A'+A"	B_1+B_2	3063		2287	
ν_{13}	"	"	"	"	"	"	"	1486	1440	1335	1355
ν_{14}	"	"	"	"	"	"		1038		814	
ν_{15}	E_{2g}	E_2	E	E	A"+A'	A'+A"	B_1+B_2	3047		2265	
ν_{16}	"	"	"	"	"	"	"	1596		1552	
ν_{17}	"	"	"	"	"	"	"	1178	1130	867	830
ν_{18}	"	"	"	"	"	"	"	606	555*	577	
ν_{19}	E_{2u}	E_2	E	E	A"+A'	A"+A'	A_2+A_1	975		795	
ν_{20}	"	"	"	"	"	"	"	410	440	352	406
ν_s^{Ni-C}, T_z	A_{2u}	A_1	A_1	A_1	A'	A'	A_1		330		315
ν_{as}^{Ni-C}, T_x,T_y	E_{1g}	E_1	E	E	A'+A"	A"+A'	B_1+B_2		555*		

*Assignment uncertain. [a]Herzberg notation. [b]Reference 16. [c]Reference 29

The 755 cm^{-1} C_6H_6 loss feature is clearly due to ν_4, the symmetric C-H out-of-plane bending mode which is at 670 cm^{-1} for the gas phase C_6H_6 molecule. The assignment is based on the fact that ν_4 is a C-H bending mode, as required by the isotope ratio of the loss, on the closeness of the frequency of this mode to the ν_4 mode in the gas phase molecule and more importantly on the strong dynamical dipole moment. For the gas phase C_6H_6 molecule there are four strong IR modes: ν_4, polarized perpendicular to the ring and three others, ν_{14} at 1040, ν_{13} at 1490 and ν_{12} at 3063 cm^{-1} [29] polarized parallel to the ring. The fact that the ν_4 mode has the strongest dynamical dipole moment, while the other three appear either as weak loss features or are not observed for adsorbed C_6H_6, indicates that the C_6H_6 adsorbs with the ring parallel or nearly parallel to the surface. If this were not the case, one or more of the other three strong IR modes would have shown up as intense loss features in the HREELS spectra. The 880 cm^{-1} C_6H_6 loss feature must be due to a ring deformation or a ring stretch mode judging by its isotope ratio of 1.06. The loss feature is assigned as ν_2, the symmetric ring stretch or ring breathing mode because its gas phase frequency at 995 cm^{-1} is closest to the frequency of the observed loss feature among the ring deformation or ring stretch modes. The observed decrease in frequency of the ring breathing mode which involves the C-C bond stretch is consistent with the ring parallel or nearly parallel to the surface. Such a structure would maximize the interaction between the surface and the π orbitals of the C_6H_6 molecule. Because the π orbitals are an important part of the C-C bonds, they are weakened as a result of the involvement of the π orbitals in the bonding between the molecule and the surface. The decreased frequency of the mode is an indication of the weakened C-C bonds if it is noted that the frequency of C-C bonds decreases with the bond order [33]. Direct observation of π-d bonding between C_6H_6 and Ni(111) surface has been made using photoemission technique [11]. The interaction may involve the donation of the bonding π orbital electrons to the surface and/or the back-donation of electrons from the surface to the antibonding orbitals. The negative work function change seems to indicate that the former is more important. The 330 cm^{-1} loss feature is obviously due to the symmetric Ni-C stretch. The C-H stretch is observed

at 3025 cm^{-1}. Because of limited resolution and the small separation of about 20 cm^{-1} between the four C-H stretch modes of the gas phase C_6H_6, it is unknown whether the loss feature is composed of more than one peak.

Careful vibrational analysis of the weak loss features at 440, 555, 850, 1130, 1335 and 1440 cm^{-1} for the purpose of determining the symmetry of each corresponding mode is essential to the determination of the symmetry point group and the adsorption site. The C_1 symmetry point group can be rejected regardless of the assignments of these loss features because all modes are dipole active which is in stark disagreement with the observation. The C_6H_6-surface complex must have C_s symmetry or higher. Among the six loss features the only one that is clearly due to a dipole active mode is the one at 1335 cm^{-1} for C_6H_6 and 1320 cm^{-1} for C_6D_6. The isotope ratio dictates that the mode is a ring deformation or ring stretch mode. The loss feature is assigned to ν_9, a ring stretch mode which is at 1310 cm^{-1} with b_{2u} symmetry for the gas phase C_6H_6 molecule. It can be seen in Table I that this mode is dipole active only if the symmetry point group is $C_{3v}(\sigma_d)$ or $C_s(\sigma_d)$. It seems then that adsorption on the atop or the bridge site can be ruled out because the mode symmetry would be b_2 or b_1 for the C_{6v} or the C_{2v}(x-y) group. However, since the intensity of the loss feature is weak, it should be taken into consideration that the dipole moment may be a result of the interaction of the C_6H_6 molecule with the substrate beyond the first layer. With this interaction included, the point group reduces to $C_{3v}(\sigma_d)$ or $C_s(\sigma_d)$ and the mode symmetry to a_1 or a' for the atop or the bridge site, respectively.

The two low frequency loss features at 440 and 555 cm^{-1} must be due to nondipole active modes predominantly involving C motion. The degenerate hindered translations (T_x,T_y), the hindered rotation R_z or the degenerate hindered rotations (R_x,R_y) are among the possibilities. Equally possible are two internal modes which are ν_{20} for the 400 cm^{-1} loss feature and ν_{18} for the one at 555 cm^{-1}. For gas phase C_6H_6 molecule, the ν_{20} mode at 410 cm^{-1} has e_{2u} symmetry and the ν_{18} mode at 600 cm^{-1} has e_{2g}. It is not possible to make unambiguous assignments for the two loss features except neither of the two can be due to the

hindered translation (T_x,T_y) or the hindered rotation R_z because their frequencies should not be higher than about 300 cm^{-1}. The order in frequency among the hindered translations and rotations is expected to be similar to the one among the metal ligand skeletal vibrations of the organometallic complex MR_2 (R=C_6H_6 or C_5H_5) with the metal atom sandwiched between the two ligand rings [30,31]. For these complexes, the frequency range of these modes is well known; the ones analogous to the hindered translation (T_x,T_y) and the hindered rotation R_z are below 300 cm^{-1} while those analogous to the hindered rotation (R_x,R_y) are between 300 and 500 cm^{-1}. The relatively high frequencies of the latter vibrations are because they involve asymmetric M-C stretches. For this reason, the hindered rotation (R_x,R_y) will also be referred to as the asymmetric Ni-C stretch. The assignment of the 440 and 555 cm^{-1} loss features can be reduced to three possible combinations: ν_{20} and ν_{18}, ν_{20} and (R_x,R_y), and (R_x,R_y) and ν_{18}. The higher frequency of ν_{20} compared with the gas phase C_6H_6 molecule, when the 440 cm^{-1} loss is assigned to it, can be explained by the fact that this out-of-plane ring deformation also involves the asymmetric Ni-C stretch vibration of C_6H_6 on the surface.

With possible assignments for the two loss features at 440 and 555 cm^{-1} now made, the point group $C_s(\sigma_d)$ can now be ruled out. Within the C_s symmetry point group, the symmetry is a'+a" for all three modes which means that these modes should show some dipole activity. The significance of the observation that the symmetry point group cannot be C_s is that adsorption of C_6H_6 must be on the atop, the bridge or the threefold site and with the ring parallel to the surface. In other words, adsorption of benzene with the center of the ring displaced from a high symmetry site or with the ring at an angle with respect to the surface can be ruled out. For the C_{2v}(x-y) point group of the bridge site, the symmetry is a'+a" for both ν_{18} and ν_{20}, and is b_1+b_2 for the asymmetric Ni-C stretch (R_x,R_y). The asymmetric Ni-C stretch (R_x,R_y) reduces to a'+a" symmetry when the point group C_{2v}(x-y) reduces to $C_s(\sigma_d)$ when the effect of the second layer Ni atoms is included. Consequently, the observation that the two loss features are due to nondipole active modes opposes the assignment of adsorption site to the bridge site.

Another weak loss feature that must be due to a nondipole active mode is at 1440 cm^{-1} for C_6H_6 and at 1355 cm^{-1} for C_6D_6. Based on the frequency and the isotope ratio, this loss feature is assigned to the ν_{13} mode, a ring stretch and deformation mode which is at 1485 cm^{-1} and with e_{1u} symmetry for the gas phase C_6H_6. The observed nondipole activity of the mode is consistent with the conclusion that the symmetry of the C_6H_6-surface complex does not belong to the point group $C_s(\sigma_d)$ because in this group the ν_{13} mode would be dipole active because its symmetry is a'+a". The observation provides further support for the conclusion that the site is not the bridge site perturbed by the second layer interaction.

The loss feature at 1130 cm^{-1} for C_6H_6 and 830 cm^{-1} for C_6D_6 can be assigned to the ν_{10} or ν_{17} mode judging from the frequency and isotope ratio. For the gas phase C_6H_6, ν_{10} has a frequency of 1150 cm^{-1} and b_{2u} symmetry and ν_{17} has a frequency of 1180 cm^{-1} and e_{2g} symmetry. The latter assignment is preferred because the loss feature at 1130 cm^{-1} displays a different dipole activity from the ν_9 mode at 1335 cm^{-1}. If the feature at 1130 cm^{-1} could be properly assigned to ν_{10}, then this feature and the ν_9 mode should exhibit the same dipole activity because the ν_9 and ν_{10} modes are of the same symmetry. In addition, the two loss features at 1130 and 1335 cm^{-1} for the disordered phase also show different dipole activity although their dipole activity is reversed from what it is in the ordered phase. Once again, point group $C_s(\sigma_d)$ and adsorption on other than a high symmetry site or with the ring tilted with respect to the surface can be ruled out because for a C_s group both the ν_{10} and ν_{17} modes are dipole active. The bridge site, however, is consistent with the assignment of the loss feature to ν_{10} except it has to be assumed that the mode is unaffected by the second layer substrate, unlike ν_9 although they have the same symmetry. Adsorption on the bridge site is, however, contradicted for the preferred assignment of the loss feature to ν_{17} which could be a_1+a_2 symmetry and dipole active for $C_{2v}(x\text{-}y)$ point group.

The remaining loss feature is at 850 cm^{-1} for C_6H_6 and 640 cm^{-1} for C_6D_6 which can be assigned to ν_{11}, a C-H out-of-plane bending mode at 850 cm^{-1} and with e_{1g} symemtry for the gas phase C_6H_6. The angular distribution of the intensity of the loss feature of C_6D_6 at 640

cm^{-1} shows a small dipole lobe (2% of the C_6D_6 loss feature at 540 cm^{-1} that has been assigned to the ν_4 mode). A similar dipole lobe has also been observed for the corresponding $C_6H_2D_4$ mode. This mode of the gas phase $C_6H_2D_4$molecule of D_{2h} symmetry has a frequency of 662 cm^{-1} and b_2 symmetry. There are two possible explanations for the observed dipole lobes of the loss features of C_6D_6 and $C_6H_2D_4$. The first explanation is that the adsorption is on the bridge site and when the second layer interaction is included, the corresponding mode becomes dipole active for both C_6D_6 and $C_6H_2D_4$. The symmetry of C_6H_6 on a bridge site is $C_{2v}(x\text{-}y)$ without and $C_s(\sigma_d)$ with the second layer substrate interaction included. Similarly the symmetry of $C_6H_2D_4$ on a bridge site is, depending on the azimuthal orientation, $C_{2v}(x\text{-}y)$ or $C_s(\sigma_d)$ without and C_2 or C_1 with the second layer interaction included. It seems then that the observation of the dipole lobes of the C_6D_6 ν_{11} mode and the corresponding $C_6H_2D_4$ mode supports adsorption on the bridge site. However, adsorption on the bridge site is very unlikely from the analysis of the other loss features given above.

Thus a second explanation is proposed as the appropriate one that the observed dipole lobe of the loss feature at 640 cm^{-1} for C_6D_6 is the result of some disordering in the ordered layer. In other words, should C_6D_6 form a perfect $(\sqrt{7}x\sqrt{7})R19^o$ ordered structure, the dipole lobe of the 640 cm^{-1} loss feature would not be observed becaue the ν_{11} mode of C_6D_6 whose point group is at least threefold in this ordered phase is nondipole active. However, in reality the C_6D_6 layer is not perfect or there is some disordering in the ordered phase. As a result, a small percentage of the molecules are adsorbed on other sites, specifically on the sites that are populated in the disordered phase which will be discussed later, whose symmetry is such that the ν_{11} mode is dipole active. The dipole scattering of these molecules is responsible for the observed dipole lobe of the loss feature at 640 cm^{-1} for C_6D_6 in the ordered phase. As will be shown, there are two different adsorption sites in the disordered phase and the ν_{11} mode is dipole active with an appreciable dipole moment for $C_6H_6(C_6D_6)$ on one of the adsorption sites. Consequently, the contribution of the C_6D_6 molecules adsorbed on this site

to the intensity of the loss feature at 640 cm^{-1} causes the appearance of the observed dipole lobe for this feature.

The extent of disordering in the ordered phase is estimated to be such that no higher than 12% of the molecules are adsorbed on the sites that are populated in the disordered phase. The estimate is based on the observed relative intensities of the dipole lobes for the loss features at 540 and 640 cm^{-1} for C_6D_6. Assuming that the dynamical dipole moment of the ν_4 mode for $C_6H_6(C_6D_6)$ on different sites is the same, the ratio of the intensities of the loss features for the ν_4 modes of $C_6H_6(C_6D_6)$ on any two sites would be the ratio of the number of molecules on the two sites. As will be discussed later, for the C_6D_6 on the site of the disordered phase whose ν_{11} is dipole active and responsible for the observed dipole lobe of the feature at 640 cm^{-1} in the ordered phase, the intensity of the loss feature for the ν_{11} mode is about one third that of the ν_4 mode. Thus in the ordered phase the ratio in intensity of the ν_4 mode of C_6D_6 on the site of the disordered phase to the ν_4 mode of C_6D_6 on the site of the ordered phase should be 6% since the intensity of the ν_{11} mode of the former is 2% of the ν_4 mode of the latter. It should be noted, though, the loss features of the ν_4 modes of C_6D_6 on the two sites are not resolved in the spectra of the ordered phase shown in Figure 6. Consequently, in the ordered phase the ratio of the number of molecules on the two sites, the site of the disordered phase versus the site of the ordered phase, is 6%. Since there are two different adsorption sites of the disordered phase and the one whose ν_{11} is dipole active is more populated at 80 K, it is assumed that in the ordered phase, the ratio of the number of molecules on the other site of the disordered phase and the site of the ordered phase is also 6%. Thus in the ordered phase, the ratio of the number of molecules on the two sites of the disordered phase and on the site of the ordered phase is 12% which is a measure of the extent of disordering. Similarly, the estimate of the extent of disordering applies to the $C_6H_2D_4$ ordered layer.

It is very likely for the layer to have some disordering for the following reason. At the temperature (260 K) at which the surface is exposed to benzene and held for a short period (1-3

minutes) in order for the background gas to be pumped out for both HREELS and TDS measurements, some desorption may have already taken place although the leading edge of the thermal desorption curve for the ordered phase shown in Figure 2 is at 270 K. The leading edge of the thermal desorption curve (not shown) is observed at 250 K when the surface is exposed to C_6D_6 at 190 K. In other words the starting thermal desorption temperature is probably lower than 260 K at which the surface is exposed to benzene gas. As a result the coverage is slightly lower than that of the perfect $(\sqrt{7} \times \sqrt{7})R19^o$ ordered layer which is 0.14 ML. It is proposed that the slightly lower coverage than that for a perfect ordered phase causes some disordering in the ordered layer resulting in the observation of the small dipole lobes for both the C_6D_6 feature at 640 cm^{-1} and the $C_6H_2D_4$ feature at 640 cm^{-1}. The corresponding mode of the molecules on the site of the ordered phase is consequently nondipole active which is consistent with adsorption on the atop or threefold site.

From the above vibrational analysis, it is clear that the symmetry point group of the C_6H_6-surface complex cannot be $C_s(\sigma_d)$ because all of the observed loss features that have been assigned to nondipole active modes should have been dipole active if the symmetry point group were $C_s(\sigma_d)$. Adsorption on the threefold site is a likely alternative because all of the observed loss features behave in accordance with their dipole activity of a $C_{3v}(\sigma_d)$ symmetry group. Adsorption on the atop site is just as likely if it can be accepted that the interaction between C_6H_6 and the surface beyond the first layer is sufficient to induce, as the symmetry is lowered from C_{6v} to $C_{3v}(\sigma_d)$, a weak dynamical dipole moment for ν_9 as observed for the loss features at 1335 cm^{-1}. It requires no other assumption because the dipole activity of all of the other modes, for which loss features have been observed, remains the same for C_{6v} to $C_{3v}(\sigma_d)$ group. It is very unlikely, if not impossible, that C_6H_6 is adsorbed on the bridge site. Depending on the exact assignments of the 440 and 555 cm^{-1} loss features, one or the other or both should be dipole active for the C_{2v}(x-y) group of the bridge site adsorption, contrary to what has been observed. Similary, the bridge site adsorption is not supported by the 1130 cm^{-1} loss feature when it is assigned as mode ν_{17}. Finally, for C_6H_6 adsorption to be on the

bridge site, an argument also has to be made that while ν_9 is observed with a dipole moment because of the presence of the second layer substrate, ν_{13} and ν_{10}, which the 1130 cm^{-1} loss feature should likely be assigned), are not. A complete list of the assignments of the observed C_6H_6 and C_6D_6 loss features is given in Table I, except for some very weak features that are not discussed due to the difficulty of correlating C_6H_6 with C_6D_6 features.

2. Adsorption Site of the Ordered Phase.

Now that it is known that C_6H_6 in the ordered phase is adsorbed either on the atop or the threefold site, one would like to know which of the two is the actual adsorption site. Vibrational spectra of partially deuterated benzene should bear information on such an issue. This is the purpose for which the vibrational spectra of 1,2-$C_6H_4D_2$ and 1,2,4,5-$C_6H_2D_4$ were measured. For $C_6H_4D_2$, the point group is C_{2v} for the gas phase molecule and is lowered to $C_s(\sigma_d)$ when adsorbed on the surface either on the atop or on the threefold site. However, there are two different orientations that in principle should show different vibrational spectra for the threefold site while there is only one for the atop site as shown in Figure 21. A vibrational loss feature should split into two if the adsorption is on the threefold site and, in contrast, this would not be the case if the adsorption is on the atop site. If one or more of the loss features are observed clearly to split into two, it can be certain that the adsorption is on the threefold site. On the other hand, if no splitting of any of the loss features is observed, it will be difficult to draw a conclusion. Such an observation agrees with the adsorption being on the atop site, but it is also possible that the splitting is not resolved although the adosorption is on the threefold site. For $C_6H_2D_4$, the symmetry point group of the gas phase molecule is D_{2h} and becomes $C_{2v}(x\text{-}y)$ for the atop site adsorption and $C_s(\sigma_d)$ for the threefold site. A mode may show different symmetry and be dipole active or nondipole active depending whether the adsorption is on the threefold or the atop site. Again, practical difficulty may arise so that the dipole moment of a mode is too small to be observed although it is allowed by symmetry.

The situation becomes more complicated if possible Kekulé distortion [1,3] is included. Such distortion has been reported for C_6H_6 on Pt(111) [1] and Rh(111) [3]. Two C-C bond

lengths at 1.33 and 1.81 Å are determined for the c($2\sqrt{3}$x4) rectangular phase on Rh(111). If Kekulé distortion occurs for C_6H_6 on the atop site (though very unlikely) there would be two different $C_6H_4D_2$, depending whether the C-C bond between the two D atoms is lengthened or shortened. In this case the symmetry point group would become $C_s(\sigma_d)$ for $C_6H_2D_4$. As a result it is not possible to make a distinction between the atop or the threefold site. On the other hand, any significant Kekulé distortion can be ruled out if no splitting for any of the vibrational loss features is observed for $C_6H_4D_2$ and the symmetry point of the $C_6H_2D_4$-surface complex is determined to be C_{2v}(x-y).

Table II is a list of the symmetries and frequencies for some of the $C_6H_4D_2$ modes, both for the gas phase molecule [22-24,26] and on the Ni(111) surface, that may distinguish adsorption on the atop from adsorption on the threefold site. The table also shows how each mode is correlated with the gas phase C_6H_6 mode. The best candidates are the modes involving C-H and C-D out-of-plane bending vibrations, because the frequencies of these modes have been observed to depend on the chemical identity of the surface and to depend also on the adosprion site as observed for C_6H_6 in the ordered and the disordered phases on Ni(111). Furthermore, these modes are also dipole active with appreciable dipole moments so that the experiment is less difficult. The $b_2(\nu_4)$ mode at 580 cm^{-1} and $b_2(\nu_{11})$ at 783 cm^{-1} are two such modes that change to a' symmetry for point group $C_s(\sigma_d)$ of the atop site or the threefold site adsorption. The former correlates with the C_6H_6 ν_4 mode and invovles mainly the C-D out-of-plane bending vibration. The latter is one of the two modes that are correlated with the C_6H_6 ν_{11} mode which splits as a result of the $C_6H_4D_2$ point group being lowered to C_{2v} from the C_6H_6 D_{6h} group.

The two modes are observed at 575 and 755 cm^{-1} shown in Figure 8 as the two most intense loss features and neither shows a clear splitting in the vibrational spectrum. The slightly larger width (by less than 10 cm^{-1}) of the 755 cm^{-1} loss feature compared with the elastic peak

Table II

Correlation of vibrational frequencies of gas phase and adsorbed 1,2-$C_6H_4D_2$ with C_6H_6

C_6H_6 Gas Phase	1,2,4,5-$C_6H_2D_4$			
	Gas phase[a], D_{2h}		Ni(111), $C_{2v}(x\text{-}y)/C_s(s_d)$	
ν_2, a_{1g}	a_1	947	a'	870
ν_4, a_{2u}	b_2	580	a'	574
ν_{11}, e_{1g}	a_2	775	a"	
	b_2	783	a'	755
ν_{20}, e_{2u}	a_2	373	a"	
	b_2	391	a'	430
ν_s(Ni-C)			a'	330

[a] Ref. 22-24, 26

may be due to a homogeneous broadening. The asymmetry of the 575 cm^{-1} loss feature is probably due to the presence of another loss feature at about 555 cm^{-1}. For C_6H_6, a loss feature at 555 cm^{-1} has been assigned as the ν_{18} mode or the asymmetric Ni-C stretch (R_x,R_y) and the corresponding mode for $C_6H_4D_2$ should split into one dipole active mode and one nondipole active mode with frequencies slightly lower than the C_6H_6 mode. Thus the $C_6H_4D_2$ vibrational results favors adsorption on the atop site. The result also opposes any significant Kekulé distortion. The assignments for the other loss features observed are 330 cm^{-1} to the symmetric Ni-C stretch, 430 cm^{-1} to ν_{20} or the asymmetric Ni-C stretch (R_x,R_y) and 870 cm^{-1} to the ring breathing mode (ν_2).

The purpose of the experiment with $C_6H_2D_4$, whose point group is D_{2h} in the gas phase, is to tell whether the point group of the adsorbed molecule is C_{2v}(x-y) corresponding to adsorption on the atop site or $C_s(\sigma_d)$ corresponding to adsorption on the threefold hollow site. The frequencies and the symmetries for some of the $C_6H_2D_4$ modes for the gas phase molecule are listed in Table III [22-26]. The observed frequencies as well as possible symmetries of $C_6H_2D_4$ on Ni(111) are also given in the table. The intensity of the loss feature corresponding to the gas phase mode at 662 cm^{-1} with b_2 symmetry should be different depending on whether the mode is dipole allowed in the C_s point group or not allowed in the C_{2v} point group. The mode involves C-H and C-D out-of-plane bending vibrations so that an appreciable dipole moment may be expected if dipole allowed. The symmetry of the mode is b_1 in the C_{2v}(x-y) group and is a' in the $C_s(\sigma_d)$ group. If the loss feature appears as one with a fairly strong dipole moment, one can be certain that the adsorption is on the threefold site. Otherwise the mode should be nondipole active for adsorption on the atop site provided that there is no significant Kekulé distortion to the molecule. The distinction also requires that the second layer of substrate does not interact with the moelcule strongly enough to induce a significant dipole

Table III

Correlation of vibrational frequencies of gas phase and adsorbed 1,2,4,5-$C_6H_2D_4$ with C_6H_6

C_6H_6 Gas Phase	1,2,4,5-$C_6H_2D_4$ Gas phase[a], D_{2h}		Ni(111), $C_{2v}(x\text{-}y)/C_s(\sigma_d)$	
ν_2, a_{1g}	a_g	979	a_1/a'	853
ν_4, a_{2u}	b_{1u}	545	a_1/a'	568
ν_{11}, e_{1g}	b_{3g}	759	b_2/a''	
	b_{2g}	662	b_1/a'	640
ν_{20}, e_{2u}	a_u	346	a_2/a''	
	b_{1u}	377	a_1/a'	425
ν_{19}, e_{2u}	a_u	804	a_2/a''	
	b_{1u}	925	a_1/a''	810
ν_s(Ni-C)			a_1a'	325

a. Ref. 22–26

moment in the case of the atop adsorption. The observed vibrational result is consistent with the conclusion from the $C_6H_4D_2$ results that the adsorption site is the atop site and that there is little Kekulé distortion. The mode under consideration is observed at 640 cm^{-1} with an intensity of only about 2% of that for ν_4, the most intense loss feature at 570 cm^{-1} as shown in Figure 9.

As discussed earlier even this minimal intensity measures not the dipole moment but the slight disordering of the ordered phase. The result should be taken as stronger evidence than the evidence from the $C_6H_4D_2$ results to support the conclusion that the adsorption is on the atop site and there is no significant Kekulé distortion. Although not impossible, it is very unlikely that the loss feature would appear with a dipole moment as small as observed if the adsorption were on the threefold site.

The 325 cm^{-1} and 853cm^{-1} loss features are assigned to the symmetric Ni-C stretch and the ring breathing mode, respectively. The 810 cm^{-1} loss feature can only be assigned as the $b_{1u}(\nu_{19})$. It is surprising that the mode shifts down by 115 cm^{-1} from the frequency at 925 cm^{-1} of the gas phase molecule. The loss feature is assigned to $b_{1u}(\nu_{19})$ because there is no other loss feature with an intensity that can be appropriately assigned as this mode which shows an IR intensity about one fifth of the ν_4 mode for the free molecule [25]. As for other isomers, the loss feature at 425 cm^{-1} may be assigned to ν_{20} or the asymmetric Ni-C stretch (R_x,R_y). However, the loss feature cannot be due to the asymmetric Ni-C stretch (R_x,R_y) if the adsorption is on the atop site because the mode symmetry is b_1+b_2, nondipole active for the C_{2v}(x-y) point group of the atop site adsorption. The asymmetric Ni-C stretch still cannot appear as strong as observed, even if the interaction between the molecule and the substrate beyond the first layer is included. In that case, the symmetry of the mode changes to a'+a" as the point group changes to $C_{s(}\sigma_d)$ but the induced dipole moment should be very small because the interaction is expected to be weak. It follows that the adsorption woud be definitely on the threefold site if it can be proved that the loss feature at about 400 cm^{-1} for the various isomers is due to the asymmetric Ni-C stretch. In the present analysis, however, the loss feature is

assigned to the ν_{20} mode in accordance with adsorption on the atop site. It should be noted that the assignment of the loss feature to ν_{20} does not rule against the threefold site adsorption.

To sum up the vibrational analysis of the four benzene isomers of the $(\sqrt{7} \times \sqrt{7})R19^{o}$ ordered phase, the concluded adsorption site is the atop site. The formation of the $(\sqrt{7} \times \sqrt{7})R19^{o}$ LEED pattern below room temperature dictates that the azimuthal orientation of benzene in the ordered phase is restricted so that only the σ_d plane of the gas phase molecule is preserved. Based on the angular distribution measurements of the intensities of the loss features, the dipole activity of the vibrational modes is determined. It is concluded that adsorption is either on the atop site with C_{6v} symmetry which reduced to $C_{3v}(\sigma_d)$ when the interaction with the second layer of the substrate is included or on the threefold hollow site with $C_{3v}(\sigma_d)$ symmetry because the ν_{20}, ν_{18} (or the asymmetric Ni-C stretch), ν_{11}, ν_{17} and ν_{13} modes are observed to be nondipole active. The adsorption on the atop site instead of the threefold site is concluded from the vibrational results which show that there is only one $C_6H_4D_2$ azimuthal orientation and that the symmetry point group of $C_6H_2D_4$ is C_{2v}(x-y). The vibrational results with the two partially deuterated benzene also indicates that the structure of the molecule on the surface shows no Kekulé distortion because the point group can be characterized as C_{6v} that is only slightly reduced to $C_{3v}(\sigma_d)$. There is only a weak interaction between the molecule and the substrate beyond the first layer as far as the moelcular symmetry is concerned.

3. Comparison to Previous Results

The result clearly shows that there is only one C_6H_6 site for the ordered phase. Whether there are one or two C_6H_6 adsorption sites on Ni(111) has been a controversy between two previous studies [5-7]. One study [5] shows that there are two different C_6H_6 sites while another [6,7] seems to show that there is only one C_6H_6 site. From the discussion given above and in the next section it is clear that the number of C_6H_6 adsorption sites depends on the coverage. Different conclusions were drawn in the two previous studies because the coverage was different in these studies. The result of Ref. 5 shows two C_6H_6 sites because

the coverage was in the range for the disordered phase for which the present result also shows that there are two different C_6H_6 adsorption sites, as will be discussed in the next section. There appears to be one C_6H_6 adsorption for the result of Ref. 6 because the coverage is close to the saturation coverage. This can be seen from the similarity between the vibrational spectra of Ref. 6 and the present study. The coverage difference between the two previous studies has not been noted probably because it was not known then that the saturation coverage is sensitive to the surface temperature around room temperature as can be seen from the thermal desorption measurement. The problem may have been further complicated by the high sticking probability of C_6H_6 on metal surface which may cause a variation of local pressure in a UHV chamber and the real exposure on the sample surface different from the ion gauge reading.

Benzene adsorption on other transition metal surfaces has been observed to show similar behavior [8-10]. Benzene is adsorbed on the surface molecularly and with the ring parallel to the surface. Vibrational loss features are observed at very similar frequencies to the gas phase molecule except for ν_4, the symmetric C-H out-of-plane bending mode which varies by about 200 cm^{-1} among different metal surfaces. This is the case even for the surface such as Rh(111) on which C_6H_6 structure shows significant Kekulé distortion.

B. The Disordered Phase

1. The Adsorption Sites

It has been shown that for the ordered phase benzene is adsorbed on a single site of point group $C_{3v}(\sigma_d)$. The results on the partially deuterated benzene indicate that the adsorption is on the atop site. The rotational orientaiton of the benzene molecule around its C_6 axis, which preserves the σ_d plane instead of the σ_v plane, is the only rotational orientation allowed by the steric effect between neighboring molecules. However, if the steric effect is eliminated by lowering the coverage, the C_6H_6-surface complex structure can change. It cannot be assumed that C_6H_6 in the disordered phase has the same orientation or is adsorbed on the same site as in the ordered phase. It is therefore necessary to carry out detailed vibrational

analysis for the disordered phase in order to determine the C_6H_6 adsorption site and the C_6H_6-surface complex structure.

The situation, however, is more complicated because there are two different C_6H_6 sites for the disordered phase at coverages below the saturation coverage of 0.14 ML of the $(\sqrt{7}x\sqrt{7})R19°$ ordered phase. The main evidnece to support the two site model [5] is the observation of the two intense loss features at 720 and 810 cm^{-1} at 0.07 ML coverage shown in Figure 10. The relative intensities of the two loss features exhibit a dramatic temperature dependence indicating that the population distribution bewteen the two adsorption sites is a function of the surface temperature as a result of the difference in the binding energy. It is apparent from the intensities of the two loss features that they must be due to ν_4, the symmetric C-H out-of-pane bending modes of the C_6H_6 on the two adsorption sites. The 810 cm^{-1} loss feature is associated with the C_6H_6 adsorbed on the higher binding energy site and the 720 cm^{-1} loss feature with the lower binding energy site. This can be seen from the change in the relative intensity of the two loss features from 80 K to room temperature shown in Figures 10 and 11. For C_6H_6, the two corresponding loss features are observed at 515 and 560 cm^{-1}. The temperature dependence of the two C_6D_6 loss features indicates that the one at 515 cm^{-1} is related to the 720 cm^{-1} C_6H_6 loss feature and the one at 560 cm^{-1} is associated with the 810 cm^{-1} C_6H_6 loss feature. It is not clear why the mode of the C_6H_6 on the higher binding energy site shows an isotope ratio as high as 1.45 but possible explanations will be discussed later.

Another piece of evidence to support the two site proposal is the observation of a frequency shift in the symmetric Ni-C stretch loss feature. The shift from 320 cm^{-1} at 80 K to 300 cm^{-1} at room temperature is caused by the change in the intensities of the symmetric Ni-C stretch modes of C_6H_6 on the two sites. The intensity of the Ni-C stretch of the C_6H_6 on the lower binding energy site increases while the one for the C_6H_6 on the higher binding energy site decreases from 80 K to room temperature. Because the frequenies of the two Ni-C stretches are slightly different, a single loss feature is observed that shifts in frequency. The observed downward frequency shift from 80 K to room temperature indicates that the C_6H_6

on the lower binding energy site is one with a lower Ni-C stretch frequency. A good estimate of the difference between the two Ni-C stretch frequencies would be about 30 cm^{-1}. The change of the intensities of the other C_6H_6 and C_6D_6 loss features from 80 K to room temperature is additional evidence to support the idea that there are two different C_6H_6 adsorption sites.

Except for the ν_4 and symmetric Ni-C stretch modes, no frequency difference is observed between the vibrational modes of C_6H_6 on the two different sites in the disordered phase. The mode assignments for these loss features are assumed to be the same as for the C_6H_6 in the ordered phase since the same frequencies are observed. However, the dipole activity for some of the modes does seem to be different indicating that the symmetry point group is different among the C_6H_6 in the ordered phase and the two C_6H_6 in the disordered phase. For the higher binding energy site in the disordered phase, as most evident by the intensity of the C_6D_6 loss feature at 625 cm^{-1} in the spectra measured at 80 K shown in Figures 12 and 14, the ν_{11} mode becomes dipole active. According to Table I for the ν_{11} mode to be dipole active the point group must be C_s for which the ν_{11} mode symmetry is a'+a". For C_s group, all of the modes that are doubly degenerate for the gas phase C_6H_6 molecule, as well as the asymmetric Ni-C stretch (R_x,R_y), belong to the same symmetry a'+a" as shown in Table I. The observation that the loss features at 440, 555, 1130 and 1440 cm^{-1} are each associated with a dipole lobe as shown in Figure 15 indicates that the corresponding modes (ν_{20}, ν_{18} (or R_x,R_y), ν_{17} and ν_{13}) become dipole active for the C_6H_6 adsorbed on the higher binding energy site. The observed dipole activity of these modes is consistent with the assignment of the point group to C_s for the higher energy binding site. The distinction between $C_s(\sigma_d)$ and $C_s(\sigma_v)$ is made based on the observed dipole activity of the ν_9 mode at 1335 cm^{-1}. The angular distribution of the intensity of the loss feature at 1335 cm^{-1} in Figure 15 clearly shows that the corresponding mode (ν_9) is nondipole active for the higher binding energy site. Based on this observation it is concluded that the symmetry point group of the higher binding energy site is $C_s(\sigma_d)$. Although it is made based on the observed dipole activity of a single mode, the

conclusion is quite unambiguous because of the strong supporting evidence that the ν_9 mode is clearly observed bo be nondipole active.

For the C_6H_6 on the lower binding energy site the symmetry point group $C_{3v}(\sigma_v)$ can be concluded. The substantial decrease in the dipole lobe of the angular distributions of the intensity of the loss features at 440 and 555 cm^{-1} from 80 K to 300 K shown in Figures 15 and 16 clearly shows that the corresponding modes (ν_{20} and ν_{18}(or R_x,R_y)) modes become nondipole active for the lower binding energy site. Consequently, the group must be a threefold one according to Table I. Again, the distinction between the two C_{3v} groups, $C_{3v}(\sigma_d)$ and $C_{3v}(\sigma_v)$ is made based on the observed dipole activity of the ν_9 mode. From the angular distribution of the intensity of the loss feature at 1335 cm^{-1} measured at room temperature shown in Figure 16, the ν_9 mode is concluded to be nondipole active and the symmetry point group is concluded to be $C_{3v}(\sigma_v)$ for the lower binding energysite

Now that the symmetry point groups of the two C_6H_6 adsorption sites have been determined, the following statements about the adsorption sites can be made. From the $C_{3v}(\sigma_v)$ symmetry point group, the adsorption site for the lower binding energy C_6H_6 molecule is concluded to be either the atop site or the threefold site. For the higher binding energy C_6H_6 molecule very little can be said about the adsorption site because the $C_s(\sigma_v)$ can be achieved by adsorption on any of the high symmetry sites by tilting the ring plane with respect to the surface or by adsorption away from a high symmetry site so long as one of the three σ_v planes of the C_6H_6 molecule is preserved. For a C_6H_6 on Ni(111) to preserve the σ_v plane instead of the σ_d plane, as is the case for C_6H_6 adsorbed on both the higher and lower binding energy sites, the rotational orientation of the molecule has to be such that the C-H bond is pointed along $[11\bar{2}]$ direction. This is the rotational orientation that is rotated by 30^o from that of the C_6H_6 in the ordered phase. It is significant that C_6H_6 adsorbed on both the higher and the lower binding energy sites in the disordered phase have the same rotational orientation that is different from that of the ordered phase C_6H_6. It is proposed based on this observation that

the steric effect between neighboring C_6H_6 molecules is responsible for the rotational orientation observed in the ordered phase.

The C_6H_6 on the higher binding energy site is the one with C_s symmetry and also the one that displays an unusually high isotope ratio of 1.45 for the ν_4 mode. It may be asked whether the two characteristics are somehow related. For C_6H_6 of C_s symmetry the number of dipole active modes is very large including all of the internal modes, their combination bands and the ones for the hindered motions of the molecule as a whole. Given the large number of modes that belong to the same symmetry, a', there is a greater possibility that the ν_4 mode of either the C_6H_6 or the C_6D_6 molecule is involved in Fermi resonance with another mode and as a result is pushed upwards or downwards in frequency so that the isotope ratio is higher than 1.4. The combination band of the symmetric Ni-C stretch and ν_{20} at about 770 cm^{-1} is at a frequency such that it may be in Fermi resonance with the C_6H_6 ν_4 mode. If this were true, the frequency of the ν_4 mode in $^{13}C_6H_6$ should shift downwards by an appreciable amount from the frequency of the vvmode in $^{12}C_6H_6$ because the ^{13}C isotope substituted molecule should be free of Fermi resonance between ν_4 and the combination band because the combination band in $^{13}C_6H_6$ should be about 30 cm^{-1} lower in frequency than that in $^{12}C_6H_6$. The shift in the frequency for the ν_4 mode in $^{13}C_6H_6$ from the ν_4 mode of $^{12}C_6H_6$ should be about 30 cm^{-1} which is estimated from the frequency of the ν_4 mode at 540 cm^{-1} of the C_6D_6 adsorbed on the same site and the isotope ratio of 1.4 for the ν_4 modes of the C_6H_6 adsorbed on the lower binding energy site in the disordered phase and the C_6H_6 in the ordered phase. Although the frequency of the ν_4 mode of $^{13}C_6H_6$ is observed to shift down, it is only about 10 cm^{-1}, which is too small to account for the high isotope ratio. Other reasons must exist that would explain the anomalous isotope ratio including Fermi resonance involving other C_6H_6 or the C_6D_6 ν_4 mode. Further study is necessary to understand the high isotope ratio of the higher binding energy C_6H_6 ν_4 mode

2. Comparison to Previous Results

There has been a debate on whether there are two. different C_6H_6 sites, or just one, on the Ni(111) surface. The two site model for C_6H_6 [5] was challenged [10] for the following three reasons. One is that in the original report in which the two site model is proposed [5], no corresponding C_6D_6 vibrational spectrum is published. The second is that it was not known before the present experiment that the number of C_6H_6 sites on Ni(111) depends on the coverage. The third is that around room temperature the saturation coverage may vary substantially for a temperature difference of 20-30 K. In a different study [6,7] the vibrational spectra are explained in terms of a single C_6H_6 site on Ni(111). This conclusion is also correct because these spectra [6,7] are very similar to those measured in the present experiment for the ordered phase. For example, two loss features observed at 845 and 750 cm^{-1} for C_6H_6 and at 645 and 540 cm^{-1} for C_6D_6 with the lower frequency loss feature dominating in intensity are very similar to what have been observed for the ordered phase C_6H_6 and C_6D_6 in the present work. The intensity at specular angle of the loss feature at 845 cm^{-1} is higher in the previous study [6,7] probably because there is a greater degree of disordering and the spectrometer angular aperture is larger which is shown by the lower resolution. The loss feature at 845(645) cm^{-1} is also assigned to the $C_6H_6(C_6D_6)$ ν_{11} mode. Later, the two site model is questioned [10] based on the assumption that the 820 cm^{-1} loss feature of Ref. 5 and the one at 845 cm^{-1} of Ref. 6 result form the same mode, ν_{11}. The two loss features, however, do not arise form the same mode. The 845 cm^{-1} loss feature of Ref. 6 is due to the ν_{11} mode of the C_6H_6 in the ordered phase while the 820 cm^{-1} loss feature of Ref. 5 is due to the ν_4 mode of C_6H_6 on one of the two sites in the disordered phase. The conclusions on the number of C_6H_6 sites on Ni(111) of the two previous studies are both correct because the two studies were carried out at different coverages. It is apparent that the coverages are different in the two studies upon comparison of the spectra of this work to those in each of the two previous reports [5,7]. Although in Ref. 5 it is implied that the two site picture applies to the saturation coverage, the coverage in this previous study actually corresponds to a disordered phase because the

temperature of 310 K used in that experiment is too high for the ordered phase to form, as shown in this study. The one or two site model controversy would have been avoided if it had been known 1) that the coverage is sensitive to the surface temperature around room temperature, 2) that the ordered phase can only be obtained below room temperature, 3) that there is a difference between the vibrational spectra below room temperature saturation coverage and lower coverages, and 4) if the C_6D_6 vibrational spectra had been published in Ref. 5 and appropriate correlation between C_6H_6 and C_6D_6 loss features, particularly for the 820 cm^{-1} loss feature had been made.

Although in one of the previous studies [5] it is correctly concluded that there are two different C_6H_6 species in the disordered phase, the suggested symmetry point groups for the C_6H_6 on the two sites are questionable. The symmetry point group for C_6H_6 on both adsorption sites was concluded to be $C_{3v}(\sigma_d)$ and the adsorption sites are the atop, the fcc threefold hollow or the hcp threefold hollow sites. The point groups in this previous study are probably incorrect because they are not based on detailed angular distribution measurement of loss intensities. As discussed earlier, one of the adsorption sites is the atop or the threefold site but the rotational orientation is different from that concluded previously. The symmetry point group for the C_6H_6 on this site is $C_{3v}(\sigma_v)$ instead of $C_{3v}(\sigma_d)$. For the C_6H_6 on the other site in the disordered phase, it cannot even be said that the adsorption site is necessarily the atop or the threefold site as concluded previously, although neither can be ruled out. Again, in this case the rotational orientation is to preserve the σ_v instead of the σ_d plane.

C. The Dehydrogenation of C_6H_6 at Higher Temperatures

This brief discussion on the higher temperature species will focus on the intense loss feature at 770 cm^{-1} in the vibrational spectrum after the surface temperature is raised to 560 K and shown in Figure 18. The same spectra have been observed when a C_2H_2 or C_2H_4 layer adsorbed on Ni(111) is annealed to a similar temperature [32]. Similar vibrational spectra have also been seen on other transition metal surfaces [15,34,35] when either a C_6H_6 or C_2H_2 adsorbed layer is annealed to higher temperatures. The loss feature at 770 cm^{-1} was first

assigned to the C-H bending mode of a CH group, produced as the C_2H_2 dissociation product on Ni(111) when a layer of C_2H_2 was annealed to higher temperatures [32]. Following the example on Ni(111), CH has been proposed for other surfaces [15,34,35] based on the observation of an intense loss feature in the range of 700-850 cm^{-1} which is assigned as a C-H bending mode. However, the broadness of the 770 cm^{-1} loss feature in the spectra shown in Figure 18 is very difficult to explain by a simple species such as CH. The width estimated to be about 60 cm^{-1} can only be due to an inhomogeneous broadening since it is unlikely that any vibrational mode would have such a homogeneous width. A simple molecule like CH cannot possibly display the observed inhomogeneous broadening. In fact, the vibrational spectrum of the dissociation product of the adsorbed CH_3 on Ni(111) has been conclusively assigned to an adsorbed CH group in Chapter II of this thesis and elsewhere [37] and this vibrational spectrum is strikingly different from the ones under consideration here. In addition a series of reactions has been observed on Ni(111) [36,37], $CH_4(g) \rightarrow CH_3 \rightarrow (CH_2) \rightarrow CH \rightarrow C_2H_2 \rightarrow C_6H_6$. Based on these observations it can be concluded that the loss feature at 770 cm^{-1} cannot be due to a CH group. Later, the C-H bend of a C_2H group on Rh(111) was proposed [15] as the origin of the intense loss feature between 700 and 850 cm^{-1}. This assignment is also suspect since there have been observations of species that are more appropriately assigned as C_2H on Ni(110) [38] and Pd(110) [39] whose vibrational spectra do not resemble the ones observed after annealing the adsorbed C_6H_6 to higher temperatures.

Judging by the frequency and the intensity of the 770 cm^{-1} loss feature in the spectrum shown in Figure 18, it can be said that the bonding of the hydrogen to the carbon strongly resembles the C-H bonding in adsorbed C_6H_6. The correlation between the intensity and frequency of this loss feature and those of the ν_4 mode of C_6H_6 are striking on several metal surfaces. For example, on Pd(111) [10] and Ru(001) [9], the ν_4 mode of C_6H_6 is observed at 720 and 760 cm^{-1}, respectively, while the intense loss feature for the higher temperature species is observed at 762 cm^{-1} [35] and 810 cm^{-1} [34]. Based on these correlations, it is proposed that the intense loss feature at 780 cm^{-1} is due to the C-H out-of-plane bending

modes of a series of molecules produced when C_6H_6 dehydrogenates and polymerizes. The main pathway of the C_6H_6 chemistry on Ni(111) up to the temperature at which the 770 cm^{-1} loss feature disappears involves no C-C bond breaking based on the following observation. Similar broad loss features in the region from 1100 to 1400 cm^{-1} in the spectra measured in the off-specular direction are observed after annealing both C_6H_6 and C_6D_6 to higher temperatures. As will be discussed in another report [27], the vibrational features in this region are similar to the benzene C-C stretch and deformation modes which indicates that the benzene ring is preserved in the reactions at higher temperatures. A series of homologs is formed on the surface that are different only in the number of C_6 rings and the extent of dehydrogenation. For these homologs the C atoms, to which the H atoms are bonded, are similar to the ones of molecular C_6H_6 on the surface so that the C-H bonds are parallel to the surface and as a result the C-H out-of-plane bending modes show similar frequencies and intensities to those of a molecular C_6H_6 on the surface. The proposed surface reactions are consistent with the irregular H_2 thermal desorption curve shown in Figure 3. The dehydrogenation of the proposed homologs happens continuously as the surface temperature is raised. To summarize, the main conclusion on the higher temperature species is that the broad loss feature at 770 cm^{-1} cannot be due to a CH or a C_2H group but is due to the C-H out-of-plane bending modes of a series of molecules formed when C_6H_6 dehydrogenates and polymerizes. A detailed study of the surface chemistry at C_6H_6 on Ni(111) at higher temperature will be reported elsewhere [27].

V. Conclusions

Benzene is adsorbed on Ni(111) molecularly below room temperature. A well ordered $(\sqrt{7}x\sqrt{7})R19°$ phase forms when the surface is saturated at 0.14 ML coverage at slightly below room temperature. Vibrational results show that there is only one C_6H_6 site on the surface for the ordered phase. The structure of the C_6H_6 molecule on the surface is only slightly perturbed from that of the gas phase molecule. The symmetry point group is determined to be $C_{3v}(\sigma_d)$ but very close to C_{6v}. Results on the partially deuterated benzene

1,2-$C_6H_4D_2$ and 1,2,4,5-$C_6H_2D_4$ favors the atop over the threefold site as the adsorption site. The presence of an interaction between the C_6H_6 and the substrate beyond the first layer may be responsible for the very small distortion of the C_6H_6 symmetry from C_{6v} to $C_{3v}(\sigma_d)$. The results rule out any significant Kekulé distortion for the C_6H_6 molecule as observed on some other surfaces. The C_6H_6 ring is strictly parallel to the surface. The orientation in the ring plane is observed to preserve the σ_d instead of the σ_v planes. A steric effect between the neighboring molecules may be responsible for the observed rotational orientation.

At lower coverages below the saturation coverage of 0.14 ML for the $(\sqrt{7}\times\sqrt{7})R19^\circ$ ordered phase, the surface layer of C_6H_6 is disordered. The detailed vibrational study at 0.07 ML coverage indicates that there are two different C_6H_6 adsorption sites in the disordered phase. The relative population between the two C_6H_6 adsorption sites changes dramatically from 80 K to room temperature as a result of their binding energy difference. It is certain that the symmetry point group is $C_s(\sigma_v)$ for the C_6H_6 on the higher binding energy site and $C_{3v}(\sigma_v)$ for the C_6H_6 on the lower binding energy site. The higher binding energy adsorption site is undetermined, while the lower binding energy site is either the atop or the threefold site. The rotational orientation around the C_6 axis for C_6H_6 on both adsorption sites in the disordered phase is different and rotated by 30° from that for the C_6H_6 in the ordered phase.

The adsorption is partially reversible and about 40% of the saturation coverage desorbs as free C_6H_6 molecules in the temperature range from 260 to 480 K. The remaining C_6H_6 dehydrogenates and polymerizes in the temperature range between 400 and 700 to produce homologous molecules in which the original C_6 rings are preserved.

References Chapter III

1. H. Ohtani, M. A. Van Hove and G. A. Somorjai in: *Proc. ICSOS II,* Amsterdam, June 1987, eds. J.F. van der Veen and M.A. van Hove (Springer, Berlin, 1988).

2. J. C. Bertolini and J. Massardier, *The Chemical Physics of Solid Surfaces and Heteregenous Catalysis*, Vol. III B, eds. D. A. King and D. P. Woodruff (Elsevier, New York, 1984.)

3. M. A. Van Hove, R. F. Lin and G. A. Somorjai, J. Am. Chem. Soc. **108**, 2532 (1986).

4. C. M. Mate and G. A. Somorjai, Surf. Sci. **160**, 542 (1985).

5. S. Lehwald, H. Ibach and J. E. Demuth, Surf. Sci. **78**, 577 (1978).

6. J. C. Bertolini and J. Rousseau, Surf. Sci. **89**, 467 (1979).

7. H. Jobic, B. Tardy and J. C. Bertolini, J. Elec. Spec. Relat. Phenom. **38**, 55 (1986).

8. B. E. Koel, J. E. Crowell, C. E. Mate and G. A. Somorjai, J. Phys. Chem. **88**, 1988 (1984).

9. P. Jakob and D. Menzel, Surf. Sci. **201**, 503 (1988).

10. G. D. Waddill and L. L. Kesmodel, Phys. Rev. B **31**, 4940 (1985).

11. J. E. Demuth and D. E. Eastman, Phys. Rev. Lett. **32**, 1123 (1974).

12. C. M. Friend and E. L. Muetterties, J. Am. Chem. Soc. **103**, 773 (1981).

13. A. K. Myers, G. R. Schoofs and J. B. Benziger, J. Phys. Chem. **91**, 2230 (1987).

14. P. M. Blass, S. Akhter and J. M. White, Surf. Sci. **191**, 406 (1987).

15. B. E. Koel, J. E. Crowell, B. E. Bent, C. M. Mate and G. A. Somorjai, J. Phys. Chem. **90**, 2949 (1986).

16. H. Ibach and D. L. Mills, *Electron Energy Loss Spectroscopy and Surface Vibrations* , (Academic, New York, 1982).

17. J. C. Bertolini, G. Dalmai-Imelik and J. Rousseau, Surf. Sci. **67**, 478 (1977).

18. S. L. Tang, Ph.D. Thesis, Massachusetts Institute of Technology, 1985.

19. J. D. Beckerle, Ph. D. Thesis, Massachusetts Institute of Technology, 1988.

20. M. B. Lee, Ph. D. Thesis, Massachusettes Institute of Technology, 1987.

21. S. L. Tang, M. B. Lee, Q. Y. Yang, J. D. Beckerle and S. T. Ceyer, J. Chem. Phys. **84**, 18767 (1986).

22. D. H. Whiffen, Phil. Trans. Roy. Soc. London Ser. A **248**, 131 (1955).

23. F. A. Miller and B. L. Crowford, Jr., J. Chem. Phys. **14**, 282 (1946).

24. G. C. Nieman, J. Chem. Phys. **50**, 1660 (1969).

25. M. Akiyama, J. Mol. Spectr. **84**, 49 (1980).

26. A. G. Ozkabak and L. Goodman, J. Chem. Phys. **87**, 2564 (1987).

27. K. J. Maynard, A. D. Johnson, Q. Y. Yang and S. T. Ceyer, to be published.

28. G. A. Somorjai, *Chemistry in Two Dimensions: Surfaces* (Cornell University Press, Ithaca, 1981).

29. T. Shimanouchi, Natl. Stand. Ref. Data Ser., Natl. Bur. Stand., No.*39*; J. Chem. Ref. Data **6**, 993 (1977).

30. K. Nakamoto, *Infrared and Raman Spectra of Inorganic and Compounds* (Wiley, New York, 1978).

31. Aleksanyan, *Vibrational Spectra and Structure* , Vol. 11, ed. J. R. Durig (Elsevier Scientific Publishing Company, New York, 1982).

32. G. Herzbert, *Molecular Spectra and Molecular Structure, II. Infrared and Raman Spectra of Polyatomic Molecules* (Van Nostrand-Reinhold, New York, 1945).

33. J. E. Demuth and H. Ibach, Surf. Sci.**78**, L238 (1978).

34. M. M. Hills, J. E. Parmeter, C. B. Mullins and W. H. Weinberg, J. Am. Chem. Soc. **108**, 3554 (1986); J. E. Parmeter, M. M. Hills and W. H. Weinberg, J. Am. Chem. Soc. **108**, 3563 (1986).

35. J. A. Gates and L. L. Kesmodel, Surf. Sci.**124**, 68 (1983).

36. Q. Y. Yang, Ph.D. Thesis, MIT, 1989.

37. Q. Y. Yang, A. D. Johnson and S. T. Ceyer, to be published

38. J. A. Stroscia, S. R. Bare and W. Ho, Surf. Sci. **148**, 499 (1984).

39. M. Nishijima, J. Yoshinobu, S. Sekitani and M. Onchi, J. Chem. Phys. **90**, 5114 (1989).

Chapter IV

Vibrational Spectroscopy of Hydrogen on Ni(111)

I. Introduction

Hydrogen adsorption on transition metal surfaces is a very interesting and important subject on which extensive research efforts have been focused [1]. This is so for the reason that hydrogen adsorption on transition metal surfaces is involved in many important practical processes such as heterogeneous catalytic reactions, metal embrittlement and energy storage of hydrogen in solution in metals. From a fundamental point of view, the importance of hydrogen on metal surfaces lies in its simplicity and it serves as a model for adsorption. High resolution electron energy loss spectroscopy (HREELS) as a surface vibrational spectroscopic technique [2] has been widely used and shown to be one of the most powerful tools in the study of adsorbate structure, binding site and chemisorption geometry. In the case of hydrogen on transition metal surfaces HREELS has been successful when combined with calculations in the determination of H binding sites. Recent results [3-7] have shown that HREELS is capable of providing more detailed information regarding dynamical coupling between H vibrations and this will help to understand one of the more subtle aspects of chemisorption, mutual interaction between adsorbates which may be direct or substrate mediated.

A variety of surface science techniques including thermal desorption spectroscopy (TDS), LEED, HREELS, UPS and work function measurement [18] have been applied to the study of hydrogen on Ni(111). It is well established that H_2 adsorbs dissociatively on Ni(111). Hydrogen on Ni(111) shows a single desorption feature (β_2) in TDS at coverages up to one half monolayer and is interpreted to be adsorbed on a single site. A second desorption feature (β_1) at a lower temperature as the coverage is increased above one half monolayer has been attributed to the increased mutual interaction instead of adsorption onto a new site [8,15]. Hydrogen on Ni(111) at one half monolayer gives rise to a (2x2) LEED pattern below room temperature. A dynamical LEED study [8] concluded that hydrogen forms a (2x2)2H ordered structure as shown in Figure 1 with the H adsorbed on the threefold hollow sites and arranged in a graphite-like structure. Of the threefold hollow sites there are two different kinds, fcc and

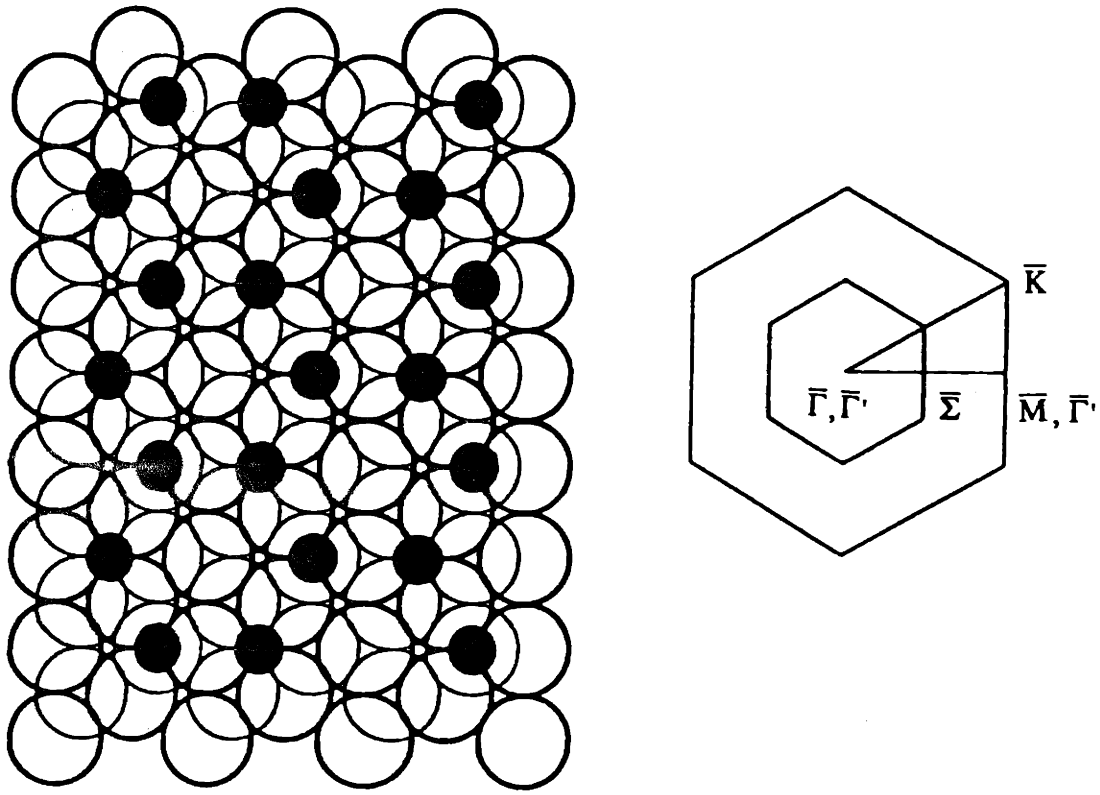

Figure 1. The (2x2)2H structure of hydrogen on Ni(111) that forms at one half monolayer below room temperature and the two dimensional Brillouin zones for both the substrate and overlayer. The substrate zone is four times the overlayer zone and $\overline{M}$ of the substrate zone becomes the $\overline{\Gamma}$ of the overlayer zone.

hcp and they are occupied with an equal population. A recent study [11] using transmission channelling, an ion beam technique, showed that at one half monolayer, hydrogen occupies the two different threefold hollow sites with an equal population and therefore supported the (2x2)2H ordered structure proposed previously. The same experiment also showed that hydrogen is adsorbed on the threefold site as the coverages is increased above one half monolayer until saturation. The same conclusion that hydrogen is adsorbed on the threefold site at all coverages was also arrived at in another recent experiment [12] using the second harmonic generation technique. The binding energy of hydrogen on Ni(111) has been determined experimentally to be about 2.7 eV [8,18]. There have been calculations [19,22] based on different methods that concluded the threefold site to be most stable with the calculated binding energy being very close to the experimental value.

There has been only one experimental study of H vibrations on a Ni(111) surface [13]. In this study employing HREELS, two broad loss features were observed at 1120(730) and 710(540) cm^{-1} for H(D). The assignment of these loss features was discussed, but no definitive conclusion was drawn. The frequency of the symmetric Ni-H stretch or the perpendicular mode for hydrogen adsorbed on the threefold site has been calculated [19-22] and it was between 1050 and 1200 cm^{-1} depending on the theory used. If a comparison is made between the frequencies of the two observed loss features in the previous HREELS study and the calculated symmetric Ni-H stretch frequencies, the 1120 cm^{-1} loss would be assigned to the symmetric Ni-H stretch. However, there are still other questions concerning H vibrations on Ni(111) that remain to be resolved. For example the assignment of the second loss feature at 710 cm^{-1} is not clear. It could be a different mode, such as the asymmetric Ni-H stretch or the same mode as that at 1120 cm^{-1}, however, associated with hydrogen on a different threefold site. Both experiments and calculations have shown that hydrogen on the two different threefold sites have the same bond length and binding energy. In particular, the calculated symmetric Ni-H stretch frequencies for H on the two sites are also the same, except in two calculations [21,22] where the two frequencies are calculated to be different by slightly

more than 100 cm^{-1}. Therefore, it seems that the 710 cm^{-1} loss feature should be assigned to the asymmetric Ni-H stretch. However, it is necessary to show experimentally that this is the case and, if assignments are made such as this, the vibrational spectra from this previous study does not show that there are two different hydrogen adsorption sites on the surface. Whether the second desorption feature (β_1) above one half monolayer is due to an increased mutual interaction or adsorption onto a new site may be answered by monitoring the change in vibrational spectra. Therefore, another HREELS study of H vibrations on Ni(111) is warranted.

II. Experimental

The experiments are carried out in a molecular beam-UHV apparatus that has been described in detail previously [23-25]. The molecular beam source is not described here because the supersonic beam is not essential to these experiments. A 10" liquid nitrogen trapped diffusion pump pumps the UHV chamber resulting in a typical base pressure of $4x10^{-11}$ torr. The chamber is equipped with a high resolution electron energy loss spectrometer (HREELS), a cylindrical mirror analyzer (CMA) with a coaxial electron gun for Auger spectroscopy, a rearview low energy electron diffraction (LEED) apparatus, an ion sputter gun, a Bayard-Alpert type ionization gauge and a leak valve. In addition there is a quadrupole mass spectrometer which is used for residual gas analysis and the detection of species desorbed from the crystal surface in a thermal desorption measurement.

The crystal is mounted on the end of a cryostat that can be cooled with cold air, liquid nittrogen or liquid helium. The cryostat is bolted to a manipulator composed of a rotatable feedthrough seated on a X-Y-Z translational state. The manipulator is mounted eccentrically on a 36 cm diameter differentially pumped, Teflon sealed rotatable flange. The rotation of the flange provides horizontal translation of the crystall necessary to position the crystal in front of each surface analytical instrument. The crystal is spot-welded to two tungsten rods that are clamped into two copper rods extending from the base of the cryostat. The high thermal conductivity between the crystal and the bottom of the cryostat ensures a stable crystal

temperature of no higher than 80 K with liquid nitrogen as a coolant and a cooling time of no more than 2 minutes to reach 80 K after flashing the crystal to 1100 K. The sample heating is by radiation or electron-beam bombardment from a tungsten filament behind the crystal. In the case of electron-beam heating, the sample is biased by a DC voltage variable between 0 and 600 V. The temperature is monitored with a type E (chromel-constantan) thermocouple spot-welded to the top of the crystal. A heating rate of as high as 20 K/sec may be achieved by controlling the filament emission power supply. The cryostat and crystal heating and cooling have been described in detail previously [25]. The Ni crystal is oriented to within 0.2 degrees of the (111) plane. The absence of contaminants on the crystal surface is verified by Auger spectroscopy and HREELS. Since the numerous cleaning cycles have removed most of the bulk impurities of the crystal, only occasional sputtering is necessary to remove small amounts of S, C and O contaminants.

The HREELS spectrometer is composed of two single-pass 127 degree cylindrical deflector electron energy analyzers with a nominal incident and scattering angle of 60 degrees from the crystal normal. A typical count rate of 10^6 cps with a 50 cm^{-1} resolution is achieved routinely for the beam elastically scattered from the clean crystal. The electron energy can be measured at an off-specular angle by the rotation of the monochromator away from the 60 degree angle of incidence. The electron impact energy is varied by the bias on the crystal. The impact energy is precisely determined by the difference between the current cut-off bias, which is the bias at which the current at sample arising from the primary electrons incident normal to the surface drops to zero, and the bias at which a spectrum is measured. The data acquisition is achieved through a dual timer/counter interfaced to a PDP-11/03 which also controls the DAC that supplies the linear ramp for scanning the voltage on the electron energy analyzer. Typically HREELS spectra are measured with a width of 1 mv per channel.

The gases used in the experiment are H_2 from MG Industries with a 99.9999% purity and D_2 of 99.0% isotope purity from Matheson. They are used as delivered with no further purification. The crystal is exposed to H_2 or D_2 by backfilling the UHV chamber with $H_2(D_2)$

gas through the leak valve while the sample is held at 80 K. The coverage was determined by the magnitude of the $H_2(D_2)$ thermal desorption signal compared to that from the (2x2)2H ordered phase known to be 0.5 H per Ni atom. All the spectra were measured at 80 K. The off-specular spectra were collected after rotating the crystal away from the 60 degree angle of incidence.

III. Results

A. The (2x2)2H Ordered Phase

The main interest of this report is the ordered phase at one half monolayer coverage that gives rise to a (2x2) LEED pattern to which the following results and discussion refer unless stated otherwise. The exposure to reach this coverage was determined by the observation of the (2x2) LEED pattern and was used subsequently for HREELS measurement. To achieve a well-ordered overlayer, the crystal was flashed to 273 K after its exposure to H_2 gas at 80 K. However, no difference in the HREELS spectra or LEED pattern was noted. In Figures 2 and 3, spectra measured at the specular angle and at an off-specular angle of 10^o and at a 5.5 eV impact energy are shown for H(D). The intensity of the elastically scattered electron beam measured at the specular angle is about $1.5x10^6$ counts/sec with a resolution of 35 cm^{-1} given by the full width at half maximum. There are a total of seven(six) loss features observed for H(D) and the frequencies of these loss features, averaged over 5 to 10 spectra, are marked in the spectra and listed in Table I. The significant isotope shift upon deuterium substitution demonstrates that these loss features are associated with H(D) vibrations.

The observation of seven(six) loss features is in stark contrast to the two loss features observed for both H and D adsorbed on Ni(111) in a previous study [13]. In that study, broad features at 710 and at 1120 cm^{-1} were observed. However, as a result of the imporved resolution (50 cm^{-1} or better) and increased incident electron intensity in the present study, it became apparent that the two features centered at 710 and 1120 cm^{-1} are each composed of two loss features and that three additional loss features of low intensity are present at 1260(1020), 1400(1080) and 2180(1600) cm^{-1} for H(D). The splitting of the 710 cm^{-1} feature into two loss

Table I

Assignments of the vibrational frequencies for H and D adsorbed on Ni(111).

Vib. Mode	Ni-H	Ni-D
ν_{as}	745 790	560 580
ν_{s}	1080 1105	800 800
$\nu_{as}^{(2)}$	1260 1400	1020 1080
$\nu_{s}^{(2)}$	2180	1600

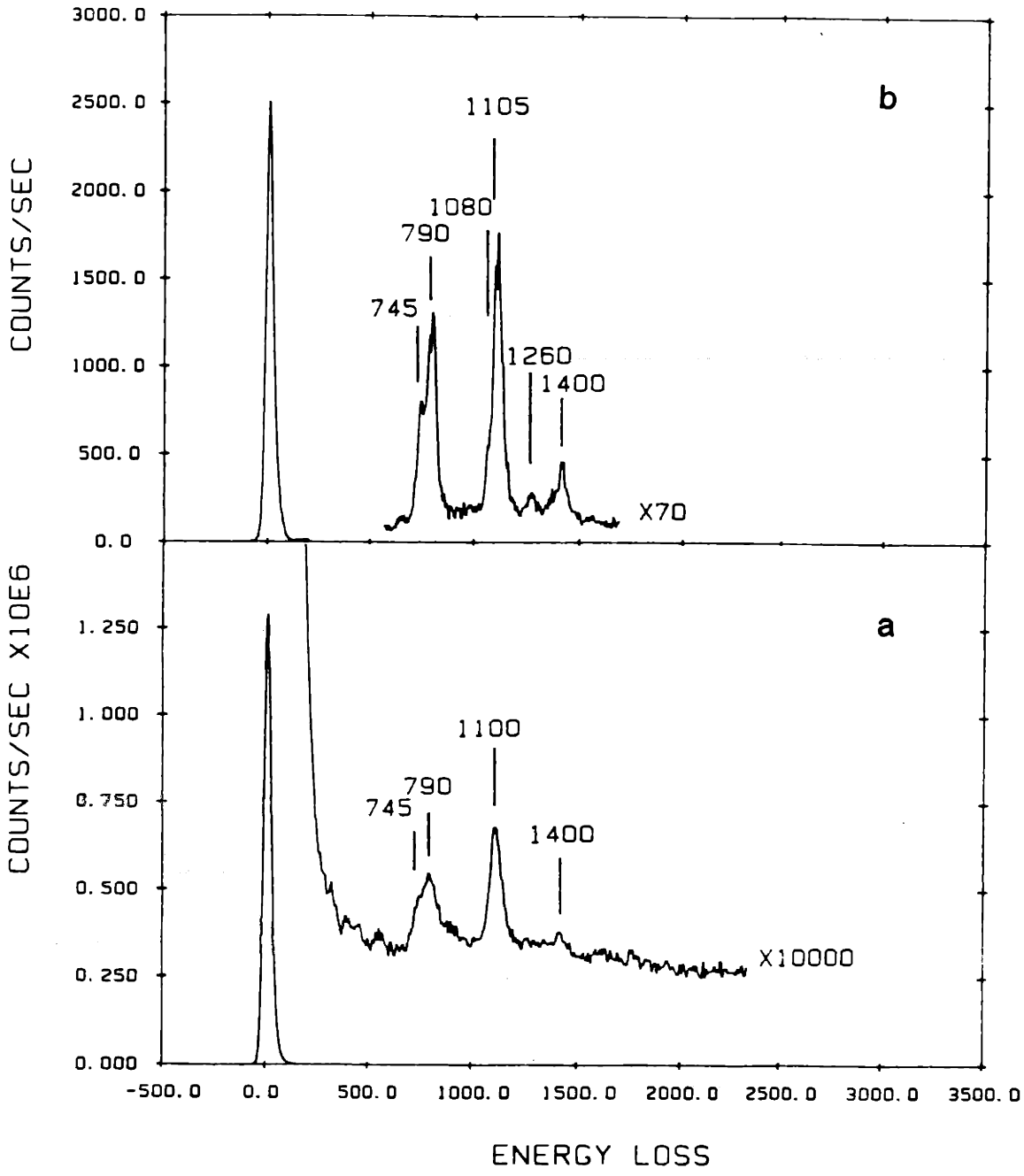

Figure 2. HREEL spectra of the Ni(111)(2x2)2H ordered phase of hydrogen measured (a) in the specular direction at 6.0 eV impact energy and (b) in the 10° off-specular direction at 5.5 eV impact energy after 15 L (not corrected for the ionization cross section) exposure at 80 K.

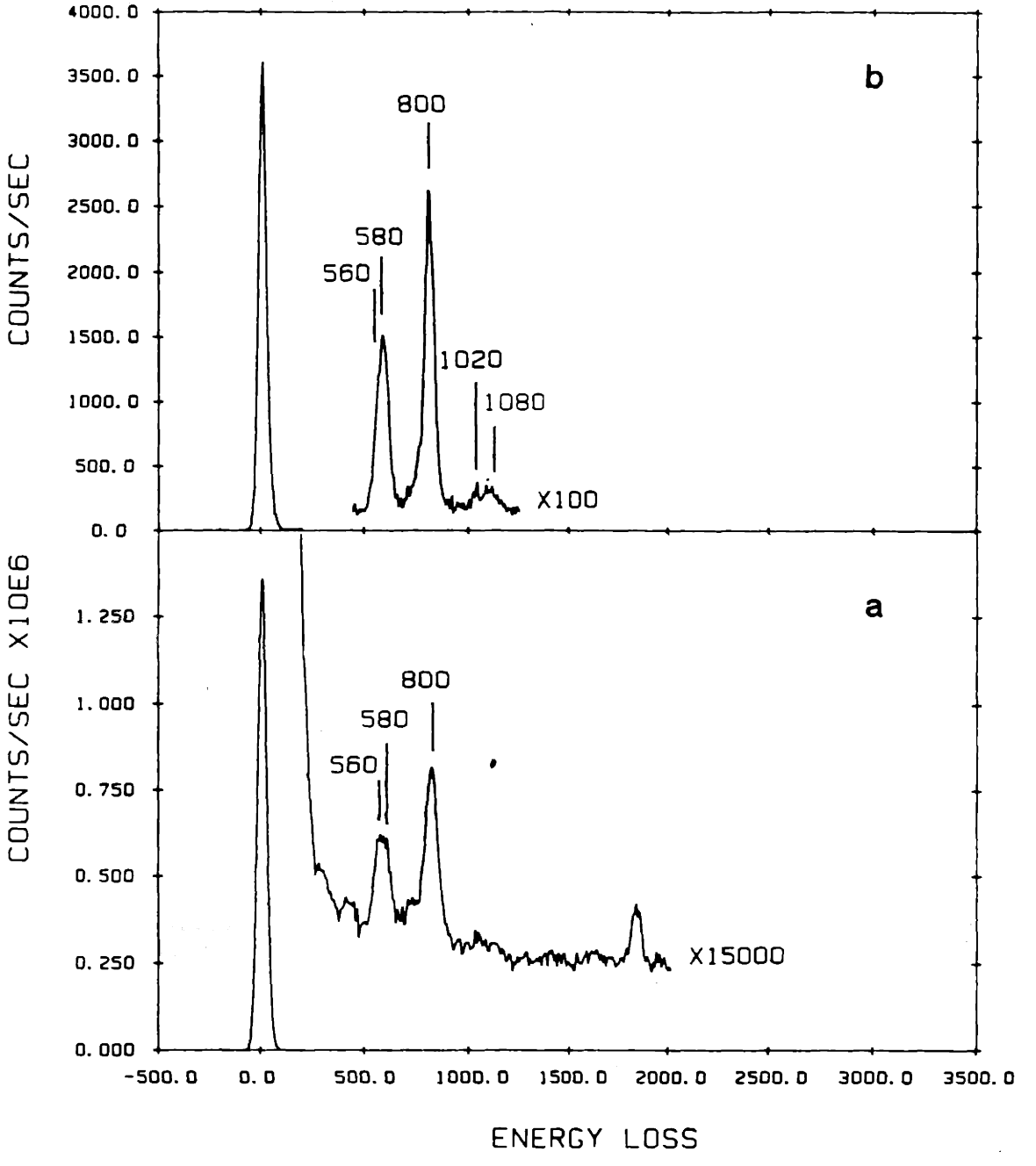

Figure 3. HREEL spectra of the Ni(111)(2x2)2D ordered phase of deuterium measured in the (a) specular and (b) 10^{o} off-specular direction at 5.5 eV impact energy after 15 L (not corrected for the ionization cross section) exposure at 80 K.

features at 745 and 790 cm^{-1} and the splitting of the 1120 cm^{-1} feature into two features at 1080 and 1105 cm^{-1} is most clear by comparing spectra measured at different impact energies at an angle 10 degrees away from the specular angle as shown in Figure 4. At 3.5 eV impact energy, only the low frequency feature at 745 cm^{-1} of the pair at 745 and 790 cm^{-1} is observable while both features of the high frequency pair at the 1080 and 1105 cm^{-1} are present with a comparable intensity. At 5 eV impact energy, both features of the pair at 745 cm^{-1} and 790 cm^{-1} are observed but with the 790 cm^{-1} feature more intense while the higher frequency loss feature of the pair at 1080 and 1105 cm^{-1} is observed to dominate. At 7.5 eV, the relative intensity of the two features at 745 and 790 cm^{-1} reverses so that the feature at 745 is much more intense while both features at 1080 and 1105 cm^{-1} are observed with the 1105 cm^{-1} feature slightly more intense. The two deuterium loss features that correspond to the 745 and 790 cm^{-1} loss features of hydrogen are observed at 560 and 580 cm^{-1}. The observation of the splitting between and the determination of the frequencies of the two D loss features are possible only because their intensities show a very different dependence on the impact energy. In the spectra shown in Figure 5, only the feature at 560 cm^{-1} is observed at 3.5 eV impact energy. At 5.5 eV the superposition of the two features at 560 and 580 cm^{-1} appears at 580 cm^{-1}. At 7.5 eV the superposition of the two features appears at 560 cm^{-1}. Only one loss feature is observed at 800 cm^{-1} as a superposition of two features that correspond to the two H loss features at 1080 and 1105 cm^{-1}.

The different dependence of the intensities of these features on impact energy is the key to resolving the two H loss features at 1080 and 1105 cm^{-1} and the two D features at 560 and 580 cm^{-1} as the separation between each two loss features is slightly less than the resolution of the spectrometer. On Pd(111) and Pd(110), H vibrational loss features have been observed to show strong enhancement within a narrow range of impact energy [26]. The impact energies at which resonant enhancement of loss features are observed have been shown to be coincident with those of surface states. However, in that study, different H vibrational modes were observed to have also different impact energy dependence.

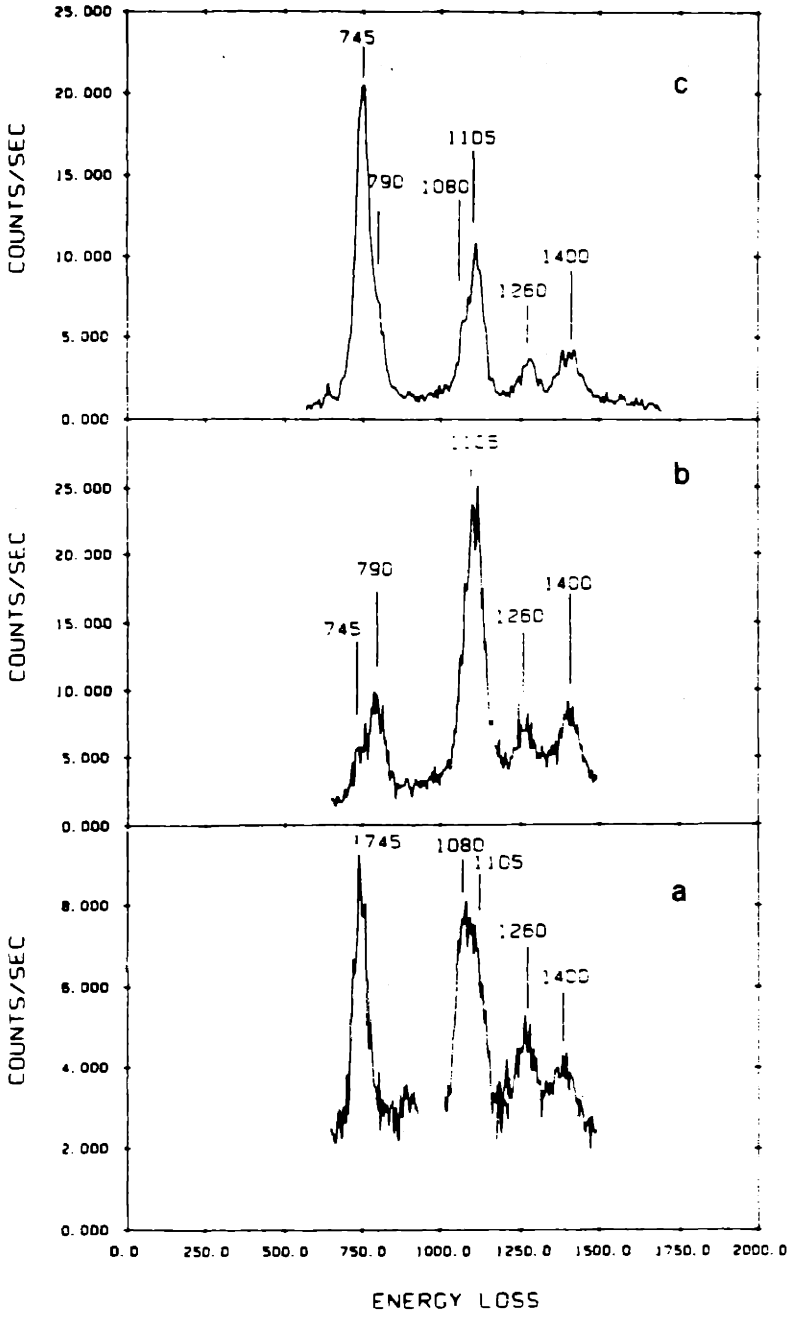

Figure 4. HREEL spectra of the Ni(111)(2x2)2H ordered phase of hydrogen measured at 80 K at 10° off-specular angle at an impact energy of (a) 3.5, (b) 5.0 and (c) 7.5 eV with a full width at half maximum of the elastically scattered feature of 40 cm^{-1}.

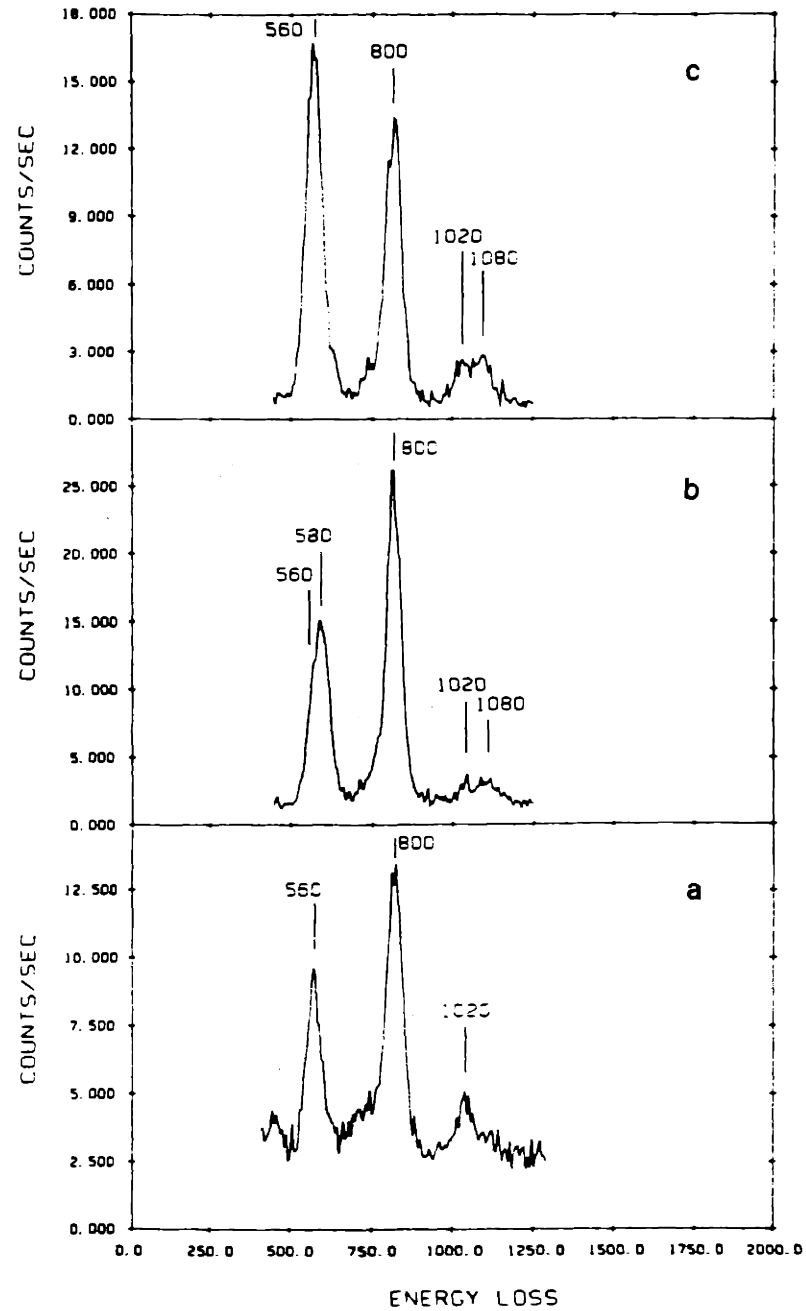

Figure 5. HREEL spectra of the Ni(111)(2x2)2D ordered phase of deuterium measured at 80 K at 10° off-specular angle at an impact energy of (a) 3.5, (b) 5.5 and (c) 7.5 eV with a full width at half maximum of the elastically scattered feature of 40 cm^{-1}.

coupling depends on the vibrational mode and the surface state involved. The different impact energy dependence of the vibrational loss features is likely due to the same effect.

The inelastic scattering occurs predominantly by an impact scattering mechanism as evidenced by the angular distribution of the loss intensities. This is consistent with a small dynamical dipole moment for H vibrations as on other transition metal surfaces [1]. Figure 6a shows the angular profiles of the intensities of the D vibrational loss features at 560/580 and 800 cm^{-1} measured at 4.5 eV impact energy. At this impact energy, the intensities of two H loss features at 745 and 790 cm^{-1} are about the same. The angular distribution of the D loss feature at 560/580 cm^{-1} is the superpositon of the loss features of two different vibrations. The angular distribuiton of the Ni-D loss feature at 800 cm^{-1} is similarly a superposition of two unresolved loss features because the two corresponding H loss features at 1080 and 1105 cm^{-1} are both observed at this impact energy although the higher frequency one of the two features is more intense. The strong peaking of the intensity of the D vibrational loss feature at 800 cm^{-1} in the specular direction indicates that at least one of the two vibrations, observed as a superposition, is dipole active. In contrast, the superposition of the two loss features at 560 and 580 cm^{-1} is observed to exhibit an isotropic angular distribution. As a result, the two vibrational features are concluded to be due to nondipole active modes. In terms of H vibrations, the angular distribution results indicate that, while at least one of the two loss features at 1080 and 1105 cm^{-1} is observable by dipole scattering, neither of the two features at 745 and 790 cm^{-1} is. As will be shown in the discussion, these results are important evidence which, along with other evidence, based on which he vibrational assignments are made.

The angular profile of the 800 cm^{-1} loss feature shown in Figure 6a is much more sharply peaked in the specular direction than the corresponding feature at 1120 cm^{-1} in the earlier study [13]. There are two reasons for this. First, the previous measurement at 6 eV impact energy is 1.5 eV higher in energy than the present experiment [2]. Since the dipole contribution decreases smoothly as the impact energy is increased, a less peaked angular distribution is expected at a higher impact energy. Second, the angular aperture in the previous

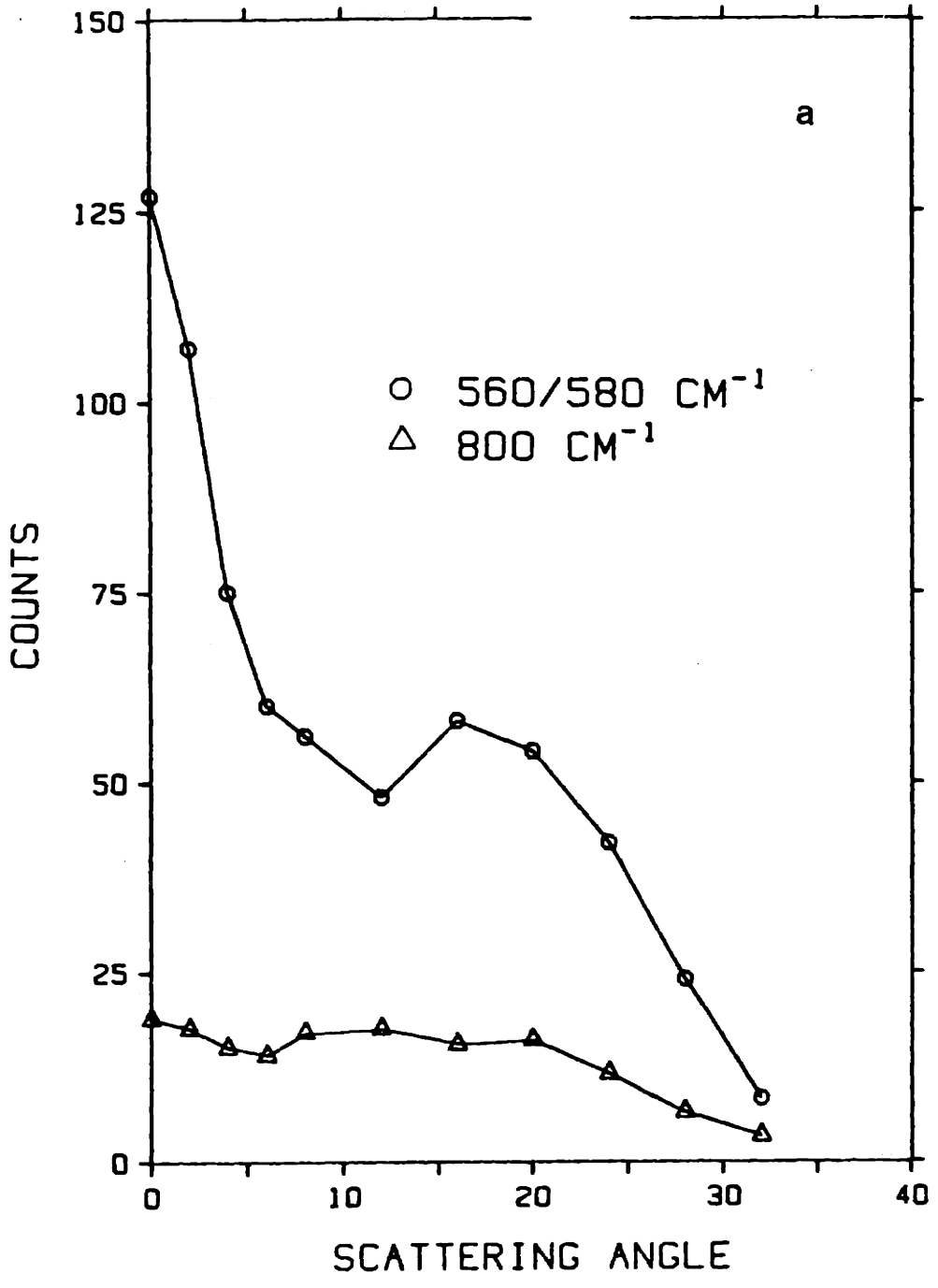

Figure 6. Intensity of the (a) deuterium vibraional loss features at 560/580 $cm^{-1}$and 800 cm^{-1} measured at 4.5 eV impact energy and (b) hydrogen loss features at 1260 $cm^{-1}$and 1400 cm^{-1} measured at 4.0 eV impact energyas a function of scattering angle for the (2x2)2H ordered phase .

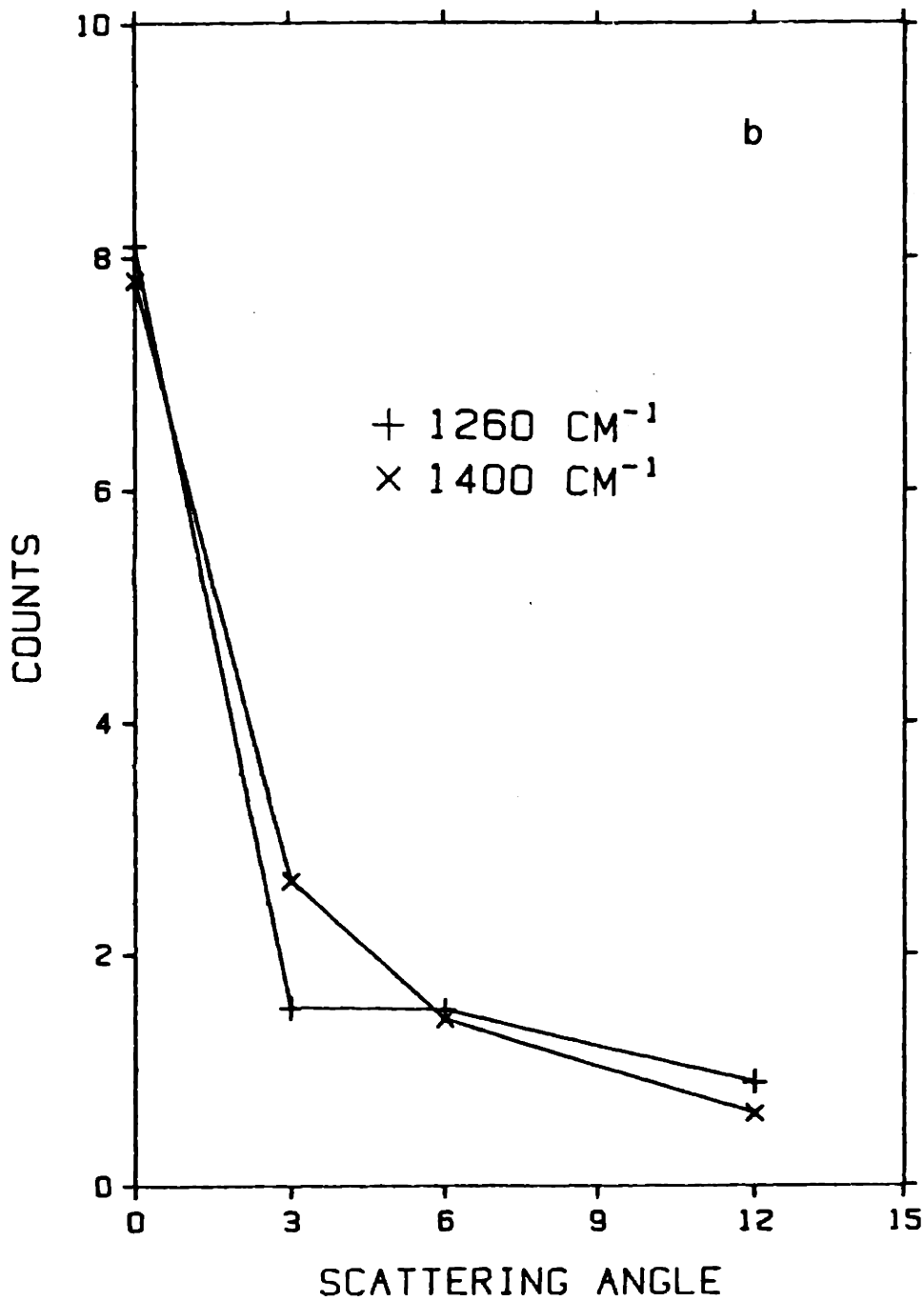
b
+ 1260 CM⁻¹
× 1400 CM⁻¹
COUNTS
SCATTERING ANGLE
0
2
4
6
8
10
0
3
6
9
12
15

experiment is much larger than the one used here which results in a broadening of the angular distribuiton of the inelastically scattered electrons. The difference between the angular apertures with which the spectra were measured in the two experiments can be seen from the different widths of the elastically scattered electron energy distributions measured in the two experiments.

During the analysis of the vibrational results it became necessary to measure the angular distributions of the H loss features at 1260 and 1400 cm^{-1} in order to assign not only these two but also the other vibrational loss features and to interpret the vibrational spectra of hydrogen on Ni(111). The angular distributions of the H vibrational loss features at 1260 and 1400 cm^{-1} measured at 4.0 eV impact energy are shown in Figure 6b. Although the two loss features are weak and therefore the uncertainty of the intensities at each scattering angle is higher in comparison to other loss features, both angular distributions are observed with a dipole lobe. As will be shown in the discussion, the two loss features are observable by dipole scattering not because the vibrational modes involved are totally symmetric but because they are due to transitions to overtone states that are totally symmetric.

For a two dimensional lattice such as the ordered phase of H on Ni(111) at one half monolayer, vibrational dispersion due to dynamical coupling must be considered. However, it is very difficult to measure the frequencies of the vibrational features at larger scattering angles and higher impact energies where vibrations away from the center ($\bar{\Gamma}$) of the two dimensional Brillouin zone are probed. The Brillouin zone for the previously proposed (2x2)2H structure of H on Ni(111) at one half monolayer is also shown in Figure 1. All the vibrational spectra that have been shown so far including those measured at 10 degrees away from specular angle correspond effectively to vibrations at the center ($\bar{\Gamma}$) of the Brillouin zone and are measured with the scattering plane aligned along $\overline{\Gamma K}$ of the Brillouin zone. As will be shown in the discussion, for the Ni(111) (2x2)2H phase, the importance of dynamical coupling effect on the vibrational frequencies can be estimated by comparing the splitting between the H vibrational features at 745 and 790 cm^{-1} at $\bar{\Gamma}$ and that between the two corresponding features at $\bar{\Sigma}$ of the

Brillouin zone. This requires the plane to be aligned with scattering $\overline{\Gamma M}$ of the Brillouin zone which is the $[1\bar{1}2]$ direction. For this purpose, the crystal sample is rotated by 30° around the normal so that the $[1\bar{1}2]$ direction of the crystal is alinged in the scattering plane of the spectrometer. Figure 7 shows two spectra measured under identical conditions that correspond to $\bar{\Gamma}$ and $\bar{\Sigma}$ of the Brillouin zone of the substrate. They were both measured at 15 eV impact energy. The spectrum at 6 degrees scattering angle correspond to $\bar{\Gamma}$ and the one at 32 degrees scattering angle corresponds to $\bar{\Sigma}$. The two loss features at 745 and 790 cm^{-1} in the spectrum at $\bar{\Gamma}$ appear at the same frequencies in the specturm at $\bar{\Sigma}$. No frequency shift for either of the two loss features can be resolved within the resolution of this experiment.

B. Hyrdogen Coverage Above 0.5 Monolayer

Figure 8 is a set of spectra measured at hydrogen coverages between one half and one monolayer. At one monolayer coverage two vibrational loss features are observed at 955(710) and 1160(835) cm^{-1} in place of the features at one half monolayer. The spectrum that was measured at a coverage higher than one half but lower than one monolayer is a superposition of the spectra at one half and one monolayer coverages. The implication of the change in the vibrational spectra as the coverage is increased above one half monolayer is that a new species of hydrogen on the surface appears at coverages above one half monolayer. The superposition of the two sets of loss features indicates that not only does the additional hydrogen adsorb as a new species but also the species present at low coverage converts into the new one. Only the new species remains at one monolayer saturation coverage. The thermal desorption spectra measured in previous experiments [8,15] and in this experiment (not shown) show that there are two different thermal desorption features ($\beta_1 + \beta_2$) of hydrogen on Ni(111). For coverages up to one half monolayer, a single desorption feature is observed (β_2) which is at 375 K at one half monolayer coverage. As the coverage is increased above one half monolayer, another thermal desorption feature (β_1) appears at slightly lower temperature in addition to the one observed for lower coverages. At one monolayer coverage, the two thermal desorpiton features ($\beta_1 + \beta_2$) are observed at 330 and 375 K. The determination of the difference between

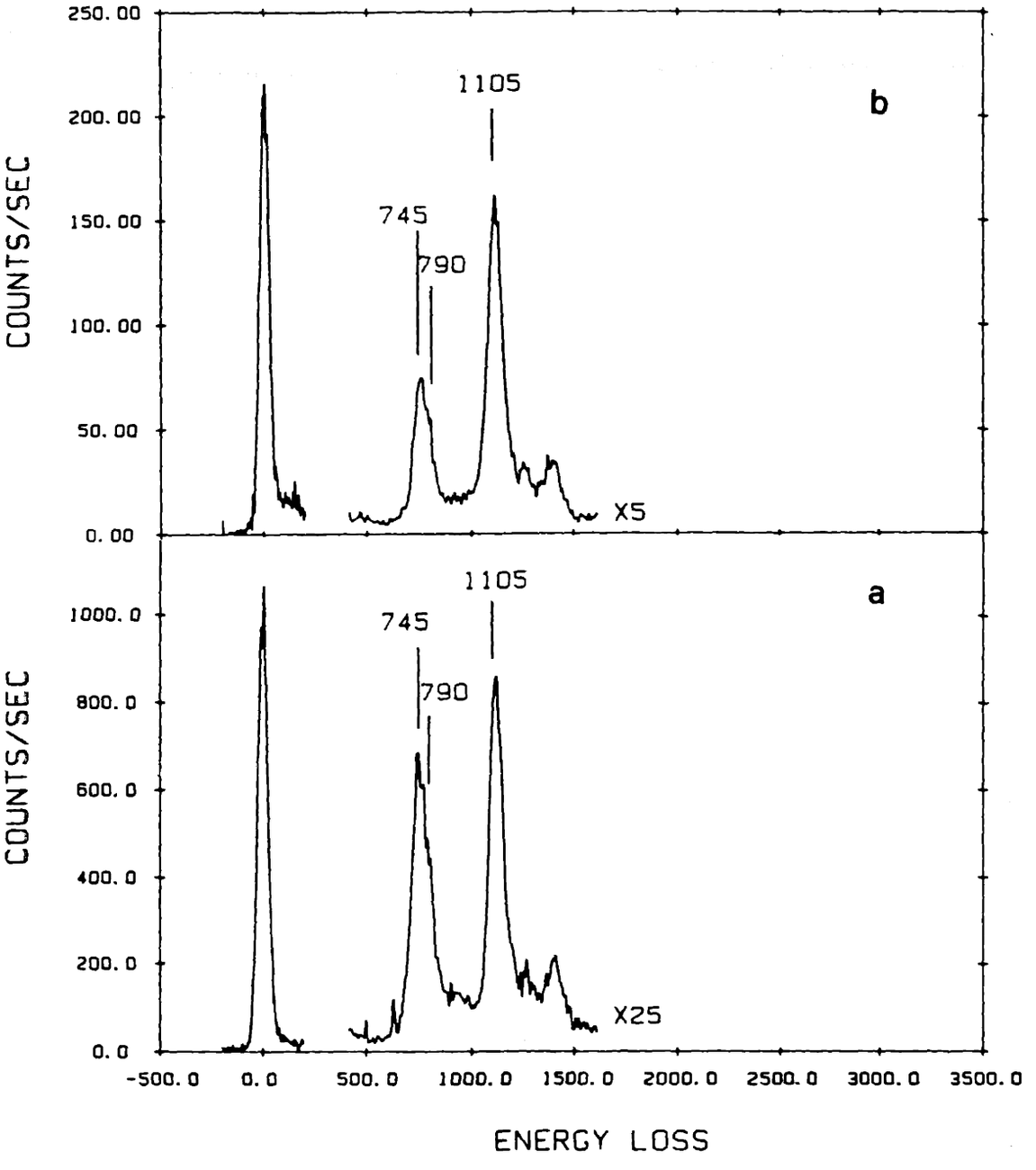

Figure 7. HREEL spectra of the (2x2)2H phase of hydrogen at 80 K. The spectra are measured at 15 eV impact energy and with (a) θ_i=54° and θ_s=60° and (b) θ_i=39° and θ_s=75° that corresonds to scattering at (a) $\bar{\Gamma}$ and (b) $\bar{\Sigma}$ of the two dimensional Brilluoin zone.

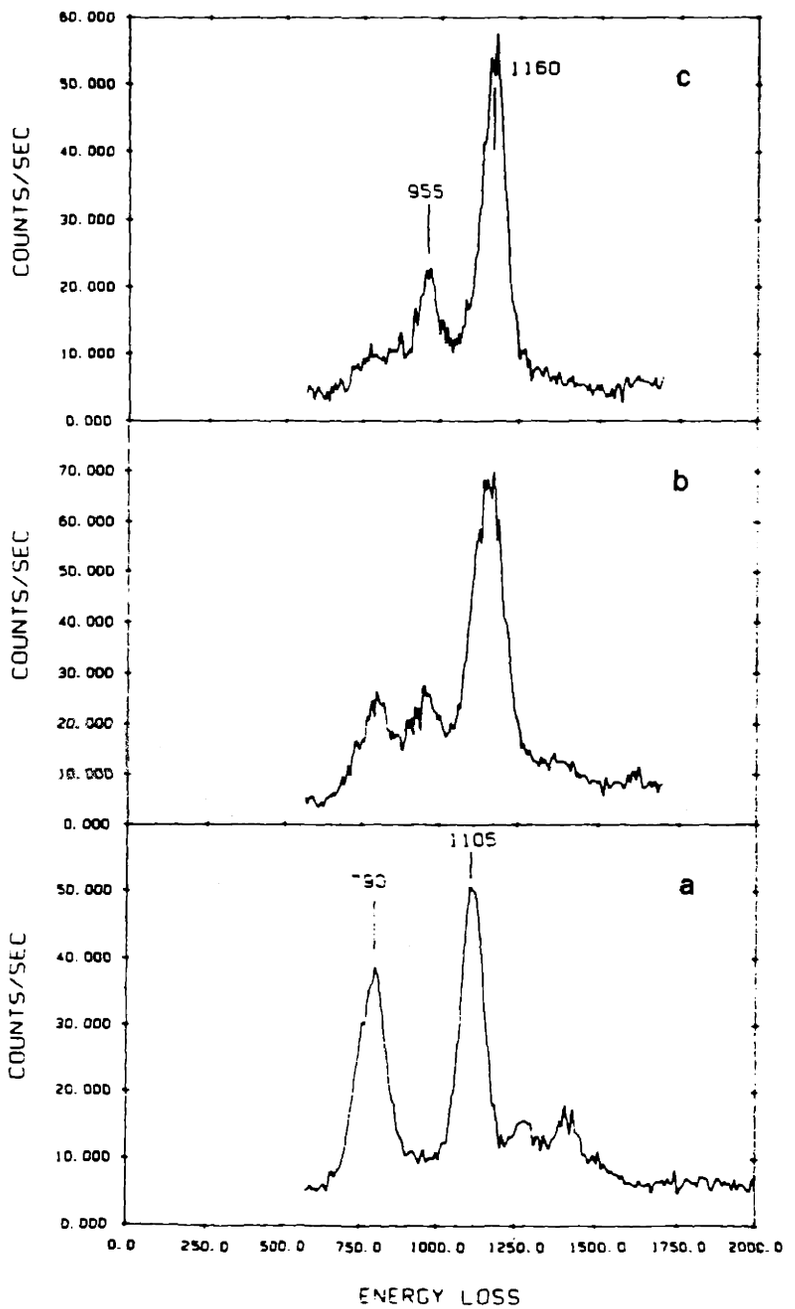

Figure 8. HREEL spectra of hydrogen on Ni(111) at 80 K with coverage (a) θ =0.5 ML, (b) θ = 0.7 ML and (c) θ =1.0 ML measured in the 10° off-specular direction at 4.5 eV impact energy.

hydrogen adsorption, in terms of adsorption sites, above and below one half monolayer coverage may reveal the origin of the observation of two desorption features, i.e. whether it is due to adsorption on different sites or mutual interaction between hydrogen on the surface.

IV. Discussion

A. The (2x2)2H Ordered Phase

1. Assignment of the Vibrational Sepctra

The (2x2) LEED pattern of hydrogen on Ni(111) at one half monolayer was first determined to correspond to a (2x2)2H ordered structure shown in Figure 1 by a dynamical LEED study [8]. For this (2x2) ordered structure, the unit cell of the two dimensional lattice contains two hydrogen atoms that occupy the two, hcp and fcc, threefold sites. Subsequent experiments using other techniques [11,12] support the proposed structure by concluding that hydrogen is adsorbed on the two threefold sites with an equal population.

There are three vibrational modes to a hydrogen atom on a metal surface, one symmetric M-H stretch with the vibrational vector polarized perpendicular to the surface and two asymmetric M-H stretches polarized parallel to the surface. For a hydrogen adsorbed on a threefold site such as the (2x2)2H phase on Ni(111), the symmetry point group is C_{3v} so that the two asymmetric Ni-H stretches are degenerate. The symmetric Ni-H stretch is expected to show negligible anharmonicity because the H-substrate potential well in the direction perpendicular to the surface is several electron volts deep, e.g. 2.8 eV for hydrogen on Ni(111) [8.18], so that low lying vibrational states are harmonic. As a result, the first overtone frequency should not deviate significantly from twice the fundamental. In contrast, the H-substrate potential well in the direction parallel to the surface is much shallower. The potential shows only a smooth corrugation parallel to the surface. This is the reason for the high mobility of hydrogen on metal surfaces. Various estimates of the potential well depth of hydrogen on Ni(111) parallel to the surface place it at a few tenths of an electron volt [1,8]. The asymmetric Ni-H stretch is expected to be very anharmonic so that the first overtone should appear substantially below twice the frequency of the fundamental. Consequently the

symmetric and the asymmetric Ni-H stretch vibrations can be distinguished based on the frequencies of the overtones relative to the fundamentals if the overtones are observed. The symmetric and the asymmetric Ni-H stretch vibrations are also different in another respect. For H on a threefold site such as in the Ni(111) (2x2)2H phase, the symmetric Ni-H stretch of A_1 symmetry is dipole active because the vibration is totally symmetric while the asymmetric Ni-H stretch should be nondipole active because the vibration is E symmetry. Although it is known that the dynamical dipole moment of hydrogen vibration on a metal surface is small, a fundamental vibrational loss feature of hydrogen on Ni(111) can only be assigned to the symmetric Ni-H stretch if the angular distribuiton of the vibrational loss intensity is measured to show a dipole lobe.

A total of seven vibrational loss features have been observed for hydrogen on Ni(111) at one half monolayer coverage. Since the loss signal is mostly due to impact scattering it is possible that some of the loss features are due to overtone transitions [2]. The assignments, based on the arguments to follow, are that the vibrational loss features at 1080(800), 1105(800), and 2180(1600) cm^{-1} are due to vibrations involving the symmetric Ni-H(Ni-D) stretch with the one at 2180(1600) cm^{-1} as the first overtone. The loss features at 745(560), 790(580), 1260(1020) and 1400(1100) cm^{-1} are due to the vibrations involving the asymmetric Ni-H stretch with the two features of higher frequency as the overtones The specific assignment of each member of the pair of fundamental vibrational loss features is more complicated because the pairs of fundamentals arises from the presence of two hydrogen atoms in the unit cell of the Ni(111)(2x2)2H phase. The assignments will be presented in the discussion below.

The observation of vibrational loss features that can be assigned as overtones is important information for the interpretation of the spectra. The fact that the 2180 cm^{-1} loss feature is at about twice the frequency of the ones at 1080 and 1105 cm^{-1} but with much lower intensity is a clear indication that the feature at 2180 cm^{-1} is an overtone of the two features at 1080 and 1105 cm^{-1} and all three features are associated with the vibrations that involve the

symmetric Ni-H stretch. It should be noted that the 2180 cm^{-1} loss feature cannot be a double loss due to its negligible intensity because the scattering probability of a double loss is the square of that of the corresponding single loss and the scattering probabililty of the loss features at 1080 and 1105 cm^{-1} is less than 10^{-3}. As has been mentioned, the potential energy surface of hydrogen on Ni(111) in the direction perpendicular to the surface has a well depth of 2.8 eV [8,18] and vibrations polarized in this direction, the ones that involve the symmetric Ni-H stretch, can be described as those of harmonic oscillators.

These assignments are consistent with the measured angular distributions of the intensity of the two deuterium vibrational loss features at 560/580 and 800 cm^{-1}. The vibrations that involve the symmetric Ni-H stretch should be dipole active. A dipole lobe in the angular distribuiton of the intensity of the 800 cm^{-1} deuterium loss feature indicates that it is due to a vibration that is dipole active. The corresponding hydrogen loss features at 1080 and 1105 cm^{-1}, are therefore also dipole active. Their dipole activity is consistent with their assignment to symmetric Ni-H stretch mode.

The remaining loss features are due to vibrations that involve the asymmetric Ni-H stretch, polarized parallel to the surface. The two loss features at 1260(1020) and 1400(1100) cm^{-1} of hydrogen(deuterium) are clearly due to overtones because of the weak intensity and their small isotope ratio (1.24 and 1.27). For an anharmonic vibration the isotope ratio decreases as the level of vibrational excitation increases. The two vibrational loss features at 745 and 790 cm^{-1} are assigned as the fundamentals of these vibrations. The small isotope ratio of the overtones at 1260 and 1400 cm^{-1} and the fact that their frequencies are much lower than twice the fundamentals at 745 and 790 cm^{-1} can only be explained by vibrations that involve the asymmetric Ni-H stretch with parallel polarization where the potential energy surface shows strong anharmonicity. The isotropic angular distribution of the intensity of the 560/580 cm^{-1} loss features that are the equivalent of the hydrogen vibrational loss features at 745 and 790 cm^{-1} shows that neither of the two vibrations is dipole active. This observation is consistent

with the assignment of the 560/580 cm^{-1} deuterium features and the 745 and 790 cm^{-1} hydrogen loss features to the asymmetric Ni-H (Ni-D) stretch modes.

Because hydrogen occupies two different threefold sites in the Ni(111)(2x2)2H phase and there are two vibrational modes for each hydrogen on a threefold site, a symmetric and an asymmetric Ni-H stretch, four fundamental vibrational loss features are expected in HREELS spectra. This is in agreement with the total number of fundamentals, as well as with the number of fundamentals for each polarization, perpendicular or parallel to the surface, observed. The conclusion seems then that each pair of vibrations involving the symmetric and asymmetric Ni-H stretches are associated with hydrogen on one of the two threefold sites. The frequency difference between the two vibrations of the same polarization arises from the different potential energy surface at each site between one of the two adsorption sites.

2. The Complication of Dynamical Coupling.

However, it is true that each vibration is associated with one site only if the vibrations of hydrogen on neighboring sites are not coupled. In the case that there is dynamical coupling between vibrations of hydrogen on different sites, it is necessary to describe the vibrations in terms of modes that are composed of coherent motions of hydrogen on all sites, or delocalized vibrations [2]. For an ordered phase the frequencies of delocalized vibrations show dispersion across the two dimensional Brillouin zone. At the center ($\overline{\Gamma}$) of the Brillouin zone of the (2x2)2H phase of hydrogen on Ni(111) which is also shown in Figure 1, there are three vibrations, one perpendicular which involves the symmetric Ni-H stretch and two parallel to the surface which involve the asymmetric Ni-H stretch. The motion of the neighboring hydrogens in each of the three vibrations are all in phase. The two in-phase vibrations parallel to the surface are degenerate because the symmetry at $\overline{\Gamma}$ for a p3m1 space group is C_{3v} [27]. At $\overline{M}$ of the substrate Brillouin zone there are three vibrations with the same polarizations as the ones at $\overline{\Gamma}$, but the vibrational motions of two hydrogen atoms in a unit cell are 180° out of phase. Because the symmetry at $\overline{M}$ can be described as C_{2v}, the two out-of-phase vibrations parallel to the surface are no longer degenerate,one of B_1 and the other of B_2 symmetry. These

vibrations at $\overline{\Gamma}$ and $\overline{M}$ have zero momentum and are probed when a HREEL spectrum is measured in the specular direction. The possibility that the observed vibrational loss features in the spectra in Figure 2-5 are due to delocalized vibrations needs to be considered, now that five vibrations, three parallel and two perpendicular to the surface, are derived without the premise that the potential energy surface is different for hydrogen on the two threefold sites. In other words, it is possible that the observed splitting between the vibrations of the same polarization is mainly due to the effect of dynamical coupling so that one corresponds to the in-phase and the other to the out-of-phase vibration.

The purpose here is to unravel which of the two effects, difference in the potential energy surface between the two adsorption sites or dynamical coupling between the vibrations of hydrogen, is responsible for the observed splitting of the vibrations of the same polarization in a vibrational spectrum measured at $\overline{\Gamma}$ of the substrate Brillouin zone. The following discussion focuses on the two vibrations at 745 and 790 cm^{-1} which involve the asymmetric Ni-H stretch and are polarized parallel to the surface. If dynamical coupling is responsible for the splitting between the two loss features, one would be due to the in-phase vibration $\overline{\Gamma}$ and the other due to the out-of-phase vibration at $\overline{M}$. Although there are two non-degenerate out-of-phase vibrations at $\overline{M}$ the difference between the frequencies of these two out-of-phase vibrations should be smaller than the difference between each of them and the degenerate in-phase vibrations at $\overline{\Gamma}$. The in-phase and out-of-phase vibrations of the same polarization are actually a part of a dispersion curve along $\overline{\Gamma M}$. The Ni(111)(2x2)2H phase is a two dimensional system whose unit cell contains two different oscillators that are coupled. For such a system a vibrational dispersion curve is smooth except at $\overline{\Sigma}$ which is the edge of the Brillouin zone of the overlayer lattice, on the two sides of which the vibrational frequency is different by an amount that equals the difference between the frequencies of the two oscillators without dynamical coupling. The difference between the vibrational frequencies at $\overline{\Gamma}$ and at $\overline{\Sigma}$ when approached from $\overline{\Gamma}$ is a measure of the dynamical coupling strength. Similarly the

difference between the vibrational frequencies at $\overline{M}$ and at $\overline{\Sigma}$ when approached from $\overline{M}$ is a measure of the dynamical coupling strength.

Consequently the difference between the frequencies at $\overline{\Gamma}$ and $\overline{M}$ is composed of two contributions, the difference between the two local oscillator frequencies and the dispersion due to dynamical coupling between the two oscillators. The vibrational wave functions are also different on the two sides of $\overline{\Sigma}$. From $\overline{\Gamma}$ to $\overline{\Sigma}$ the vibrations of the two oscillators in a unit cell are in phase with unequal vibrational amplitudes. In contrast, from $\overline{M}$ to $\overline{\Sigma}$ the vibrations of the two oscillators in a unit cell are 180° out of phase with unequal vibrational amplitude but the oscillator that has a smaller amplitude is the oscillator which had the larger amplitude for $\overline{\Gamma}$ to $\overline{\Sigma}$. In the limit of weak coupling where the difference between the local oscillator frequencies dominates the frequency difference between the two vibrations at $\overline{\Gamma}$, and $\overline{M}$ splitting between the vibrations immediately to the two sides of $\overline{\Sigma}$, is the same as the difference between the vibrations at $\overline{\Gamma}$ and $\overline{M}$. In this case the vibrational amplitude of one of the oscillators goes to zero for the in-phase vibration while the amplitude of the other oscillator goes to zero for the out-of-phase vibration so that vibrations reduce to localized oscillators. In other words, there is no dispersion in frequency across the Brillouin zone. In the limit of strong coupling, the difference between the two vibrations at $\overline{\Sigma}$ is negligible. In between the two limits, the splitting between the two vibrations at $\overline{\Sigma}$ is different from that between the vibrations at $\overline{\Gamma}$ and at $\overline{M}$.

Consequently, a comparison of a vibrational spectrum of the Ni(111)(2x2)2H phase measured at $\overline{\Sigma}$, to that measured at $\overline{\Gamma}$, can distinguish between the two possible origins, local potential difference or dynamical coupling, for the splitting of the vibrational features to 745 and 790 cm^{-1} as observed in the specular direction in Figures 2 and 3. It should be noted that there are three dispersion curves along $\overline{\Gamma}\overline{M}$, one polarized in the $[\bar{1}10]$ direction, one polarized in the $[11\bar{2}]$ direction and one perpendicular to the surface. The first two involve the asymmetric Ni-H stretch and the third involves the symmetric Ni-H stretch. Since the frequency of the vibrations polarized along $[11\bar{2}]$ and $[\bar{1}10]$ are expected to be close, two

vibrations split in frequency similar to the splitting between the two loss features at 745 and 790 cm^{-1} may be observed at $\bar{\Sigma}$ even though each dispersion curve is perfectly smooth. Thus it seems not possible to distinguish between the two possible origins for the observed splitting between the two loss features at 745 and 790 cm^{-1}. Fortunately, a selection rule for impact scattering is in operation that forbids the vibration polarized along $[\bar{1}10]$. This is not only true for $\bar{\Sigma}$ but also at any point along $\overline{\Gamma M}$. This is a consequence of a selection rule for impact scattering [2] which says that the scattering amplitude for any scattered wave vector in the scattering plane must vanish when a mode is odd under a reflection operation if the surface is symmetric under reflection and the scattering plane is aligned parallel to the mirror plane. The vibration polarized along the $[\bar{1}10]$ direction at any point along $\overline{\Gamma M}$ that can only be probed by aligning the scattering plane along the $[11\bar{2}]$ direction would be forbidden because the two dimensional lattice of the Ni(111)(2x2)2H phase is symmetric with respect to a mirror plane parallel to $[11\bar{2}]$. As a result, a comparison between the vibrational spectrum measured at $\bar{\Gamma}$ and the one measured at $\bar{\Sigma}$ can still resolve the issue on the origin of the observed splitting between the two vibrational loss features at 745 and 790 cm^{-1}

The vibrational spectrum measured at $\bar{\Sigma}$ is shown in Figure 5a ($Q_{\|}$= 0.78 $Å^{-1}$, E_i=15 eV, θ_i=39°, θ_s = 75°). This spectrum shows no observable difference from that measured at $\bar{\Gamma}$ which is shown in Figure 5b ($Q_{\|}$=0.1 $Å^{-1}$, E_i=15 eV, θ_i=54° , θ_s = 60°). It can be concluded based on this observation that the observed splitting for the two vibrational loss features at 745 and 790 cm^{-1} is mainly due to the difference between the potential eneryg surface of the two adsorption sites. Although the two threefold sites are very similar, a difference of 45 cm^{-1} between the frequencies of the asymmetric Ni-H stretch vibrations for the hydrogen atoms adsorbed on the two different sites and a difference of 25 cm^{-1} for the symmetric Ni-H stretch vibrations of hydrogen on the two sites are certainly reasonable. There have been two recent calculations [21,22] that show a difference of more than 100 cm^{-1} between the symmetric stretch frequencies of hydrogen on the two sites. The symmetric stretch frequencies are calculated to be 1043 and 1176 cm^{-1} in one study [21] and 1093 and

1222 cm^{-1} in another study [22]. The frequencies for the two adsorption sites are observed to be more similar than what the calculations have predicted. Although the Ni(111)(2x2)2H phase has been studied using different techniques [8,18], this is the first observation of any measurable difference in the properties of hydrogen adsorbed on the two threefold sites.

A different ordered structure (2x1)H at one half monolayer coverage [8] can also give rise to the observed (2x2) LEED pattern because in this structure there are three domains that are rotated by 60° from one another. The unit cell contains one hydrogen on a single kind of threefold site. At most three vibrational loss features can be observed in a vibrational spectrum measured in the specular direction because only a single site is occupied. The vibrational result of the present study which clearly shows four fundamental vibrational loss features is in agreement with the conclusion using other techniques [8,11,12] that the (2x2)2H overlayer, instead of the (2x1)H overlayer, is the correct structure.

3. Estimate of Dynamical Coupling

Although the vibrational result indicates that the main contribution to the frequency difference between the two vibrations parallel to the surface is from the difference between the potential energy surface of hydrogen on the two sites, the result does not rule out a minor contribution from dynamical coupling. The result does not exclude a small frequency shift from $\bar{\Gamma}$ or $\bar{M}$ to $\bar{\Sigma}$, within the limited energy resolution. Dynamical coupling of hydrogen vibrations have been observed on Ni(110) [3], W(100) [5] and Ru(100) [7]. For example, for the (2x1) phase of hydrogen on Ni(110), the in-phase and out-of-phase asymmetric Ni-H stretch vibration polarized perpendicular to the trough are observed at 560 and 630 cm^{-1}, a 70 cm^{-1} splitting. Similarly the vibrational dispersion of the other asymmetric Ni-H stretch vibrations is observed though only part of the dispersion curve can be measured. Different from the Ni(111)(2x2)2H phase, the two hydrogen atoms in a unit cell in the Ni(110)(2x1)H phase are adsorbed on the same site. Two oscillators can couple better when their frequencies are the same than when their frequencies are different for a given interaction between the two oscillators. Oscillators of different frequencies do not couple well because the oscillators are

not in tune. It is possible that the nature of the vibrational coupling between hydrogen is the same on the two surfaces, Ni(110) and Ni(111). However, the vibrational dispersion is small, and it is therefore not resolved on Ni(111) because the vibrational frequencies of hydrogen on the two sites without dynamical coupling are different .

There is one feature of the vibrational spectra that can not be explained simply by adsorption of hydrogen on different sites. For the pair of vibrational loss features at 745 and 790 cm^{-1}, it is obvious that their intensities show dramatically different impact energy dependence as shown in Figure 4. The two vibrational loss features at 1080 and 1105 cm^{-1} also show different impact energy dependence in intensity although it is not as dramatic. Different impact energy dependencies have been observed previously for the vibrational loss intensities of the symmetric and the asymmetric M-H stretches of hydrogen on Pd(111) and Pd(100) [26]. The vibrational loss intensities of the two modes show enhancement at different impact energies which have been shown to coincide with those of surface states. That the two modes show enhancement at different impact energies can be explained by a difference in coupling of the two modes to surface states due to their different polarizations or different symmetries. Coupling between H vibrations and the electronic degrees of freedom has been proposed to explain the observed Fano line shape in IRRAS of the overtone of the hydrogen wag mode on Mo(100) and W(110) [4]. A symmetry argument is used to explain why the coupling is only observed for the wag mode. The different impact energy dependence of the intensities of the two vibrational loss features at 745 and 790 cm^{-1} for hydrogen on Ni(111) may be due to the same effect, i.e. vibrations are coupled to surface states. However, if the two vibrational loss features are respectively due to the asymmetric Ni-H stretches of hydrogen on the two threefold sites and therefore they have the same polarization and symmetry, it is difficult to explain why they would couple to surface states differently. Arguing that hydrogen on the two sites would couple to surface states differently contradicts the fact that the two hydrogen on the two sites show similar binding energy, bond length and, more importantly, electronic structure.

On the other hand, if the two vibrational loss features are due to the in-phase and out-of-phase vibrations, the two may couple to surface states differently because the vibrational wave functions of the two are different, the out-of-phase vibration has a node between every two hydrogen atoms while the in-phase vibration does not. Since the vibrational result shows that the frequency difference between the two vibrational loss features at 745 and 790 cm^{-1} is mainly due to the difference in the potential energy surface of hydrogen on the two sites, the wave functions of the coupled vibrations, in-phase and out-of-phase, have unequal amplitudes on the two sites. The two coupled vibrations can still couple to surface states differently because the phase relationship between the two hydrogen in a unit cell is different for the in-phase and out-of-phase vibrations, so that the corresponding vibrational loss features show different impact energy dependence in intensity.

For the purpose of showing that there is dynamical coupling between hydrogen vibrations on the surface but that the dispersion is too small to be observed due to the resolution of the technique, a simple calculation is presented here. It shows that if dynamical coupling between hydrogen vibrations for the Ni(111)(2x2)2H phase is similar to that for the Ni(110)(2x1)H phase, the frequencies of the coupled vibrations shift by only 10 cm^{-1} from those for the vibrations without dynamical coupling. It is a reasonable assumption that dynamical coupling is similar for the two phases on the two surface if it is noted that hydrogen adsorption in Ni(111)(2x2)2H [8] and Ni(110)(2x1)H [28] is similar in the adsorption site, binding energy, Ni-H bond length and, most importantly, the nearest neighbor distance. The nearest neighbor distance for hydrogen on Ni(111) is 1.87 Å. There are two different nearest neighbor distances of 2.81 and 3.35 Å for H on Ni(110).

A simple model is used for this purpose which assumes that the vibration of each hydrogen can be represented by a harmonic oscilator and that there is linear coupling between the nearest neighbor hydrogen. Since only the splitting between the in-phase and out-of-phase vibrations at $\overline{\Gamma}$ and $\overline{M}$ is concerned, instead of the detailed dispersion curve, the eigenvalue

problem of Eq. (5.10) of Ref. 2 needs only to be solved at the center ($\bar{\Gamma}'$) of the overlayer Brillouin zone which simplifies to

$$(\omega^2-\omega_1^2)e_1 - d_{12}e_2 = 0$$
$$(\omega^2-\omega_2^2)e_2 - d_{21}e_1 = 0 \qquad (1)$$

with

$d_{12} = d_{21} = d = 3D$ for Ni(111)(2x2)2H

$d_{12} = d_{21} = 2 = 2D_\alpha + 2D_\beta$ for Ni(110)(2x1)H

In equation (1), e_1 and e_2 are the vibrational wave vector and ω_1 and ω_2 are the vibrational frequencies when there is no coupling between the two hydrogen atoms in the unit cell. The effective coupling between the vibrations of two hydrogen atoms, d_{12} and d_{21}, are rewritten as d since they are necessarily equal. This effective coupling constant, d, the sum of the coupling (D or D_α, D_β) between one hydrogen and its nearest neighbors of which there are three for Ni(111)(2x2)2H and four for Ni(110)(2x1)H, two each of two different kinds. The energies of the in-phase and out-of-phase vibrations for the lattice of coupled harmonic oscillators can be solved as

$$\omega_\pm = \omega_o\left(1 \pm \frac{1}{4}\left(\left(\frac{\Delta}{\omega}\right)^4 + \left(\frac{W}{\omega_o}\right)^4\right)^{1/2}\right) \qquad (2)$$

with

$$\omega_o = \frac{1}{2}(\omega_1^2 + \omega_2^2)$$

$$\Delta^2 = |\omega_1^2 - \omega_2^2|$$

$$\omega^2 = 2d$$

and with

$$\Delta^2 << \omega_0^2, \quad W^2 << \omega_0^2$$

It is apparent that the splitting between the in-phase and out-of-phase vibrations is a combination of two independent contributions: one is Δ^2 which reflects the difference between the potential energy surface of the two sites and the other is W^2 which is a measure of the coupling strength.

For the Ni(110)(2x1)H phase where $\Delta^2=0$ since the two sites are the same, $W^2_{(110)}$ can be calculated ($W^2_{(110)}$ and $W^2_{(111)}$ are used as W^2 for Ni(110)(2x1)H and Ni(111)(2x2)2H, respectively) from the measured frequencies of the in-phase and out-of-phase vibrations. There are two pairs of in-phase and out-of phase vibrations that involve asymmetric Ni-H stretch motion because of the symmetry of the Ni(110)(2x1) H phase. The coupling strength for hydrogen on Ni(111) is asssumed to be the same as that of hydrogen on Ni(110) reflected by the pair of in-phase and out-of-phase vibrations at 630 and 560 cm^{-1}. The other pair are not used because their frequencies can only be estimated by extrapolation [3]. From

$$\omega_{\pm} = \omega_0\left(1 \pm \frac{1}{4}\frac{W^2_{(110)}}{\omega_0^2}\right)$$

since $\Delta^2=0$ and

$$\omega_+=630\ cm^{-1} \qquad \omega_-=560\ cm^{-1}$$

$W^2_{(110)}$ can be calculated

$$W_{(110)} = 8.33 \times 10^4\ (cm^{-1})^2.$$

For the assumption that dynamical coupling between nearest neighbors is the same for the hydrogen atoms on the two surfaces or

$$D = D_\alpha = D_\beta$$

the parameter $W^2_{(111)}$ for Ni(111)(2x2)2H can be calculated,

$$W^2_{(111)} = W^2_{(110)} \bullet \left(\frac{3}{4}\right)$$

The factor 3/4 is needed because there are three nearest neighbors for Ni(111)(2x2)2H while there are four for Ni(110)(2x1)H. Since from the measured vibrational spectrum at $\bar{\Gamma}$ and $\bar{\Sigma}$,

it is known that the major contribution to the observed splitting between the loss features at 745 and 790 cm^{-1} is from the difference between the potential energy surface of the two threefold site, the splitting is first assumed to be totally due to this effect so that Δ^2 can be calculated. The additional splitting due to dynamical coupling is then calculated using $W^2_{(111)}$ calculated above. From $\Delta^2 = 6.9x10^4(cm^{-1})2$ and $W^2_{(111)} = 6.23x10^4$ $(cm^{-1})^2$ calculated earlier, the frequencies of the two coupled vibrations are calculated from equation (2)

$$\omega_+ = 798 \text{ cm}^{-1}, \omega_- = 738 \text{ cm}^{-1}.$$

The dynamical coupling effect, therefore, shifts the vibrational frequencies to 738 and 798 cm^{-1} from 745 and 790 cm^{-1}, respectively, or causes an additional splitting of 15 cm^{-1}. A change of 15 cm^{-1} in the splitting of these two loss features from $\bar{\Gamma}$ to $\bar{\Sigma}$ is below the limit of detectability for the resolution of the present experiment. Consequently, it is possible that there is dynamical coupling between the hydrogen vibrations for the Ni(111)(2x2)2H phase comparable to that for the Ni(110)(2x1)H. However, the additional splitting is only 15 cm^{-1} because the frequencies of the two oscillators are different or not in resonance. If it is assumed that the frequencies of the two oscillators are the same, then the frequencies of the two coupled vibrations for the coupling constant would be at 748 and 788 cm^{-1}, resulting in a splitting of 40 cm^{-1} due to dynamical coupling alone. Although the effect of dynamical coupling on the frequencies is small for Ni(111)(2x2)2H because hydrogen is adsorbed on different sites, it is still true that the wave functions of the in-phase and out-of-phase vibrations show different phase relationship between the two sites. They may couple to surface states differrently so that their vibrational loss intensities show different impact energy dependence.

4. The Overtones - Localized vs. Delocalized

Although there may also be some coupling between the vibrations of hydrogen on different sites in the first excited state, the second excited state can be viewed as excitation localized on a single site. For a system of coupled oscillators, a two-quantum transition may be to a delocalized vibrational state or to a bound overtone state whose vibrational amplitude is localized on a small number of oscillators [7,29-32]. The existence of a bound overtone state

is determined by $\omega_0\chi/|\omega_+ - \omega_-|$, the ratio of the anharmonicity of the local potential energy surface to the dispersion width of the fundamental transition [7,29-31]. In the case where the potential energy surface is strongly anharmonic and dynamical coupling is relatively weak, the vibrations of neighboring oscillators do not couple well, particularly for excited states so that localized excited state or bound overtone states can exist. Such bound overtone states have been proposed to explain the observed obertone vibrational loss features of hydrogen on Rh(111) [7]. As discussed earlier, for hydrogen on Ni(111) the vibrations involving asymmetric Ni-H stretch are strongly anharmonic and show relatively weak dynamical coupling. These facts, plus the fact that the neighboring sites are different so that it is more difficult for neighboring oscillators to couple, are sufficient to label the overtone excitations for the Ni(111)(2x2)2H phase as localized. Based on these considerations, it is concluded that the two overtone vibrational loss features at 1260 and 1400 cm^{-1} are due to transitions to the second excited states of the asymmetric Ni-H stretch vibrations of hydrogen on the two threefold sites, respectively.

The angular distribution of the intensities of the two overtone features shown in Figure 6b is consistent with this interpretion. The second excited state of the asymmetric Ni-H stretch vibration of E symmetry in a C_{3v} point group has two components, $A_1 + E$ [33]. Indeed both overtone loss features are observed to show dipole scattering indicating that the two corrresponding excited states have the same symmetry and that they are due to excitations of the two different adsorption sites. This observation supports the conclusion that the two fundamental loss features at 745 and 790 cm^{-1} are mainly determined by the local potential energy surface of the two adsorption sites. However, suppose that the potential energy surface of the two sites were the same and the splitting between the two fundamental loss features were caused mainly by dynamical coupling. In this case the two overtone loss features could only be assigned as the two components (A_1+E) of the split overtone vibration which is the same for both sites. Since the excited states responsible for the two observed overtone loss features must be the same symmetry type as shown by the angular distribution measurements, this

interpretation can be rejected. Thus the observation of the two overtone loss features at 1260 and 1400 cm^{-1} being dipole active supports that the observed splitting between the two fundamental loss features at 745 and 790 cm^{-1} is mainly due to the difference between the potential energy surface of the two sites.

5. Comparison to a Morse Oscillator

Now that two transitions are observed for the asymmetric Ni-H stretch vibrations of each site, an estimate of the zero order frequency and the anharmonicity may be obtained assuming that the asymmetric Ni-H vibration can be described as a Morse oscillator. For a Morse oscillator the two parameters are related to the frequencies by

$$\hbar\omega^{(n)} = \hbar\omega_0\left(\left(n+\frac{1}{2}\right)^2 + \chi\left(n+\frac{1}{2}\right)^2\right)$$

and both parameters should show an isotope ratio 1.4,

$$\frac{\omega_0^H}{\omega_0^D} = \frac{\chi^H}{\chi^D} = \sqrt{2}$$

The extracted parameters, ω_0 and χ of H(D) and their isotope ratios are 985(670) cm^{-1}, 0.120(0.08), 1.47 and 1.50 when the two H(D) loss features at 745(560) and 1260(1020) cm^{-1} are paired together as the fundamental and overtone. The corresponding values for ω_0 and χ are 980(660) cm^{-1} and 0.10(0.06) and 1.48 and 1.57 for the isotope ratios of the two parameters when the H(D) loss features at 790(580), 1400(1080) cm^{-1} are paired, respectively. The large anharmonicity factors of 0.12 and 0.10 for the asymmetric Ni-H stretch vibrations of hydrogen in the two threefold sites are the result of the shallow potential wells. The isotope ratios for both ω_0, the zero order frequencies and χ, the anharmonicity factors are in reasonable agreement with an ideal Morse oscillator. However, the isotope ratios on both sites are higher than those of an ideal Morse oscillator. This indicates that the potential energy surface parallel to the surface can not be accurately described by a Morse potential.

6. Conclusions

The observation of four fundamental loss features of which two at 1080(800) and 1105(800) cm^{-1} involve the symmetric Ni-H(Ni-D) stretch vibration and two at 745(560) and 790(580) cm^{-1} involve the asymmetric Ni-H(Ni-D) stretch vibration, supports the (2x2)2H ordered structure proposed previously [8]. The observation of the overtone loss features as well as the angular distribution measurements of the loss intensities allows an unambiguous assignment of the loss features to the vibrations of the symmetric and asymmetric Ni-H(Ni-D) stretches. The observed splitting between the frequencies of the two vibrational loss features of the same polarization are mainly due to the difference in the potential energy surface between the two adsorption sites, the fcc and the hcp threefold hollow sites. This is the first experimental observation of different vibrational frequencies for hydrogen adsorbed on the two different threefold sites of a (111) surface of a fcc crystal. Dynamical coupling between vibrations of hydrogen on neighboring sites may also contribute to the observed frequency splitting between the loss features at 745 and 790 cm^{-1}, but is too small to be detected by HREELS. However, such coupling may effect the vibrational wave functions so that the observed vibrations couple to surface states differently resulting in the observed different impact energy dependence of the loss features.

B. Hydrogen Vibrations at Coverages Above One Half Monolayer

The change in HREELS spectra as the coverage is increased above one half monolayer correlates with the appearance of the second desorption feature (β_1) above one half monolayer. The spectra at coverages between one half and one monolayer show that there are two different hydrogen species on the surface. In addition to the one observed below one half monolayer coverage, another hydrogen species appears with which the two new loss features at 955(710) and 1160(835) cm^{-1} for H(D) are associated. The relative population of the two species changes as a function of coverage. The population of the new species increases as the coverage is increased such that at the saturation coverage of one monolayer, the low coverage species disappears completely.

The inelastic neutron scattering (INS) results [9,10] show that the vibrational frequencies of H(D) on Raney Ni, at coverages from as low as 10% of the saturation to the saturation, are also at 1140(840) and 945(690) cm^{-1}. Hydrogen adsorption on Rainey Ni was concluded to be on the threefold site and the vibrational features at 1140 cm^{-1} and at 940 cm^{-1} have been assigned to the symmetric and asymmetric Ni-H stretch modes, respectively [9]. Because of the similarity of the vibrational frequencies, the same assignments are made for the two vibrational loss features at 1160 and 945 cm^{-1} of the hydrogen species observed in this study at coverages above one half monolayer on Ni(111) single crystal surface. Therefore the adsorption site for hydrogen on Ni(111) at one monolayer coverage is concluded to be a threefold site. The same conclusion for the binding site hydrogen on Ni(111) at high coverage have been reached previously in studies using other techniques [11,12]. It was proposed in a study using ion channeling technique [11] that at one monolayer coverage, hydrogen forms a (1x1) ordered phase. The only way to attain a (1x1) ordered phase is to arrange all hydrogen on the same site at one monolayer. Because hydrogen is adsorbed on a single site, only one symmetric and asymmetric Ni-H stretch vibration is observed. The shift in frequencies of the asymmetric Ni-H stretch from 745 and 790 cm^{-1} at one half monolayer to 955 cm^{-1}at one monolayer is due to interactions between hydrogen atoms since hydrogen is adsorbed on the threefold site at both coverages. Similar interactions are responsible for the shift in frequency of the symmetric Ni-H stretch from 1080 and 1105 cm^{-1} at one half monolayer to 1160 cm^{-1} at one monolayer. The observation of the additional, low temperature thermal desorption feature (β_1) at coverages above one half monolayer is also a result of interaction between hydrogen atoms.

References Chapter IV

1. K. Christmann, Surf. Sci. Reports **9**, 1 (1988).

2. H. Ibach and D. L. Mills, *Electron Energy Loss Spectroscopy and Surface Vibrations* , (Academic, New York, 1982).

3. B. Voihtländer, S. Lehwald and H. Ibach, Surf. Sci. **208**, 113 (1989).

4. J. E. Reutt, Y. J. Chabal and S. B. Christman, Phys. Rev. B **38**, 3112 (1988).

5. J. P. Woods, A. D. Kulkarni, J. L. Erskine and F. W. de Wette, Phys. Rev. B **36**, 5848 (1987).

6. P. -A. Karlsson, A.-S. Martensson, S. Andersson and P. Nordlander, Surf. Sci. **175**, L759 (1986).

7. L. J. Richter, T. A. Germer, J. P. Sethna and W. Ho, Phys. Rev. B **38**, 10403 (1988).

8. K. Christmann, R. J. Behm, G. Ertl, M. A. Van Hove and W. H. Weinberg, J. Chem. Phys. **70**, 4168 (1979).

9. R. R. Cavanagh, R. D. Kelley and J. J. Rush, J. Chem. Phys. **77**, 1540 (1982).

10. D. Graham, J. Howard and T. C. Waddington, J. Chem. Soc., Faraday Trans. 1, **79**, 1281 (1982).

11. K. Mortensen, F. Besenbacher, I. Stensgaard and W. R. Wampler, Surf. Sci. **205**, 433 (1988).

12. R. J. M. Anderson and J. C. Hamilton, Phys. Rev. B. **38**, 8451 (1988).

13. W. Ho, N. J. DeNardo and E. W. Plummer, J. Vac. Sci. Technol. **17**, 134 (1980).

14. H. P. Steinrück, A. Winkler and K. D. Rendulic, Surf. Sci. **152/153**, 323 (1985).

15. J. N. Russell, Jr., I. Chorkendoff, A.-M. Lanzillotto, M. D. Alvey and J. T. Yates, Jr. J. Chem. Phys. **85**, 6186 (1985).

16. G. Comsa, R. David and B.-J. Schumacher, Surf. Sci. **85**, 45 (1979).

17. F. Greuter, I. Strathy and E. W. Plummer, Phys. Rev. B **33**, 736 (1986).

18. K. Christmann, O. Schober, G. Ertl and M. Neumann, J. Chem. Phys. **60**, 4528 (1974).

19. T. H. Upton and W. A. Goddard, III, Phys. Rev. Lett. **42**, 473 (1979).

20. J. K. Norskov, Phys., Rev. Lett. **48**, 1620 (1982).

21. H. Yang and J. H. L. Whitten, to be published.

22. T. N. Truong, D. G. Truhlar and B. C. Garrett, to be published.

23. J. D. Beckerle, A. D. Johnson, Q. Y. Yang and S. T. Ceyer, to be published.

24. S. T. Ceyer, J. D. Beckerle, M. B. Lee, S. L. Tang, Q. Y. Yang and M. A. Hines, J. Vac. Sci. Tech. **A5**, 501 (1987).

25. J. D. Beckerle, Q. Y. Yang, a. D. Johnson and S. T. Ceyer, Surf. Sci. **195**, 77 (1988).

26. H. Conrad, M. E. Kordesch, W. Stenzel, M. Sunjic and B. Trninic-Radja, Surf. Sci. **178**, 578 (1986).

27. A. P. Cracknell, Thin Solid Films **21**, 107 (1974).

28. W. Reimer, V. Penka, M. Skottke, R. J. Behm, G. Ertl and W. Moritz, Surf. Sci. **186**, 45 (1987).

29. J. C. Ariyasu and D. L. Mills, Phys. Rev. B **28**, 2389 (1983).

30. T. Holstein, R. Orbach and S. Alexander, Phys. Rev. B **26**, 4721 (1982).

31. J. Jortner and S. A. Rice, Phys. Rev. B **26**, 4727 (1982).

32. J. C. Kimball, C. Y. Fong and Y. R. Shen, Phys. Rev. B **23**, 4946 (1981).

33. G. Herzberg, *Molecular Spectra and Molecular Structure II. Infrared and Raman Spectra of Polyatomic Molecules* (Van Norstrand Reinhold, New York, 1945).